One base pair resolution histone H1-nucleosomal DNA interaction mapping and 3D organization of H1 containing nucleosome

Sajad Hussain Syed

Université Joseph Fourier-Grenoble 1
Chimie et Science du Vivant
(Arrêtés ministériels du 5 juillet 1984 et du 30 mars 1992)

THÈSE

Pour obtenir le titre de
Docteur de l'Université Joseph Fourier
Discipline Biologie

Présentée et soutenue publiquement par
SYED Sajad Hussain
Le 03 Decembre 2009

One base pair resolution histone H1-nucleosomal DNA interaction mapping and 3D organization of H1 containing nucleosome

Jury

Dr. Didier TROUCHE	Rapporteur
Dr. Francesca PALLADINO	Rapporteur
Pr. Hans GEISELMANN	Examinateur
Dr. Dimitar ANGELOV	Co Directeur de thèse
Dr. Stefan DIMITROV	Directeur de thèse

Thèse préparée au sein du laboratoire
Biologie Molécularie et Cellulaire de la Differenciation
Unite INSERM U823
Institut Albert Bonniot
Universite Joseph Fourier-Grenoble 1
France

A mountain is composed of tiny grains of earth. The ocean is made up of tiny drops of water. Even so, life is but an endless series of little details, actions, speeches, and thoughts. And the consequences whether good or bad of even the least of them are far-reaching.

Swami Sivananda Saraswati

Dedicated to

"Abba and Khala"

who made the difference!!!

ACKNOWLEDGEMENTS

The journey of my doctoral studies may not have been so pleasant and full of joy without the help of colleagues and collaborators, both at the Ecole Normale Supérieure de Lyon and Université Joseph Fourier - Grenoble I, coordinated admirably by my mentor Dr. Stefan Dimitrov. I am highly thankful to him for his kind support and involving me in fruitful collaborative works with people from different fields which will have an everlasting influence on my scientific temperament. His enthusiastic, knowledgeable and friendly scientific discussions are the keys to the success of my thesis research, and are deeply appreciated. I am indebted for the personal care he took all along the way.

I'm also very grateful to my thesis co-supervisor, Dr. Dimitar Angelov for providing a congenial lab atmosphere and teaching me the chromatin biochemistry. His tireless scientific discussions, tit bits for experimental optimization and thorough result interpretations were essentials for the timely completion of the work. A specials thanks for all his efforts and support, and has been a pleasure to work with him personally as well as scientifically.

I would like to thank Prof. Hans Geiselmann, Dr. Didier Trouche and Dr. Francessca Palladino for their time and efforts to evaluate the thesis.

I take this opportunity to express my debt of gratitude to Dr. Namita Surolia for her contribution in teaching me the protein biochemistry in the beginning of my research life.

I was very lucky to meet Prof. Philippe Bouvet, who actually introduced me to the team of Dr. Stefan Dimitrov and supported me all the way. Thank you very much.

Special thanks to the patience and expertise of Dr. Jan Bednar for the long dark room experimental sessions for the Cryo-electron microscopy and the beautiful image galleries.

I would also like to thank Dr. Nils Becker, Dr. Ralf Everaers and Sam Meyer for their help in mathematical modeling experiments.

I also wish to thank Dr. Cendrine Moskalenko for the Atomic Force Microscopy experiments, Dr. Andrew Travers, Dr. Mathieu Boulard, Dr. Thierry Gautier, Dr. Manu Shukla and Damien Goutte-Gatat for their help in some of my experiments.

Manu, Imtiaz and Richi are "not to forget" persons for the wonderful times spent in the lab especially while writing this manuscript.

Hats off to all the people of Joliot Curie Laboratory especially Marie-Jo, Fabien Mongelard, Hervé, Fabien Montel, Elsa and Zofia for providing the scientifically vibrant and homely environment. I will miss those afternoon cake parties.

My fellow students have helped me in many different ways. I would like to thank Anu, Farhan, Dinil, Aijaz, Mubarak and Sadaf for their interest, their support and their encouragement.

My deepest gratitude belongs to my family members and relatives for their love and moral support throughout my life.

Finally, I would like to thank the people who actually made the difference. Thanks to Abba (Peer Ghulam Nabi Shah) and Khala (Syeda Hanefa Akhter) for everything.

INDEX

LIST OF TABLES AND FIGURES

CHAPTER I

CHAPTER II

CHAPTER III

CHAPTER IV

RESUME DE LA THESE

(Interaction entre H1 et le nucléosome: cartographie à haute résolution et organisation tri-dimentionnelle du complexe)

La composition et l'organisation de base du nucléosome ont été établies depuis déjà quelques décades (1). La structure de la particule du cœur nucléosomal (NCP) a été résolue à l'échelle atomique par diffraction aux rayons X (2, 3). Cependant, le même type d'information concernant la structure complète du nucléosome, c'est-à-dire la particule du cœur (NCP) contenant de l'ADN de liaison (linker) associée avec l'histone de liaison, n'est pas disponible. Les nombreux efforts investis depuis plus de trente ans pour comprendre le mode d'association de l'histone de liaison avec l'ADN nucléosomal n'ont pas abouti et les données reportées restent controversées.

Dans ce travail, nous avons étudié en détails l'interaction de l'histone H1 avec l'ADN nucléosomal afin de comprendre comment cette interaction conduit à l'organisation en fibre nucléosomale. Nous avons pu résoudre ce problème ancien par l'utilisation de : (i) l'incorporation de H1 par une chaperonne d'histone physiologique, NAP-1, (ii) la reconstitution de nucléosomes parfaitement homogènes sur une matrice d'ADN contenant la séquence 601 fortement positionnante, (iii) une combinaison de cryo-microscopie électronique (EC-M) et de technique d'empreinte aux radicaux OH°, (iv) une modélisation mécanique du polymère ADN de type « coarse-grain ». Notre « cartographie » par empreinte OH° de résolution d'un nucléotide montre que le domaine globulaire de H1 (GH1) interagit à travers le petit sillon avec des « patch » d'ADN de 10 pb de part et d'autre de la dyade du nucléosome. De plus, GH1 organise environ un tour d'hélice d'ADN de chaque ADN de liaison du nucléosome. En même temps, une suite de 7 acides aminés (120-127) de la partie COOH-terminale est requise pour la formation de la structure en tige de l'ADN de liaison.

En utilisant les données expérimentales, nous avons construit un modèle 3D qui explique comment les différents domaines de H1 interagissent avec l'DN nucleosomal et qui prédit la structuration spécifique en tige de l'ADN de liaison. Dans ce modèle, la structure du GH1 est assez large pour occuper l'espace entre l'ADN d'entré-sortie et d'interagir avec environs 10 pb de chaque linker et avec l'ADN nucleosomal à la dyade. L'association de la partie C-terminale de H1, en même temps que du GH1, « pince » efficacement les linkers entrant-sortants de manière à les assembler en structure de tige. Environ 20-30 pb des deux linkers s'associent entre eux à l'extérieure du NCP dans une tige superhélicale à 2 débuts avec

une légère courbure de 100-120 pb. Il est à noter que ce modèle exige l'existence de trois points de contact de GH1 avec l'ADN nucléosomal, donc d'une orientation spécifique des linkers. Selon ce modèle, si l'orientation des ADNs de liaison dans la particule de cœur du nucléosome est perturbée ceci aurait affecté l'association de H1 avec le nucleosome et abolie la possibilité de formation de la structure en tige.

L'incorporation de l'histone variant H2A.Bbd au sein du nucléosome conduit à l'altération de sa structure. Nos images d'AFM (Microscopie à Force Atomique) et de EC-M montrent une grande flexibilité de la structure de la particule variante H2A.Bbd, ou l'angle d'entré-sortie de l'ADN est d'environ 180° (conformation parallèle) par opposition à la forme « V » des nucléosomes conventionnels. La raison de cette déformation de structure réside dans l'existence du domaine d'accrochage (docking) « défectueux ».

Dans ce travail, nous avons caractérisé les propriétés structurales et fonctionnelles du nucléosome contenant un autre variant d'histone de la famille de H2A, H2AL2, qui par analogie à H2A.Bbd présente un domaine d'accrochage « défectueux ». Les trinucléosomes, reconstitués avec H2AL2, présentent une structure de type « collier de perles » très similaires à celle des trinucleosomes H2A.Bbd. De plus, nos données biochimiques et microscopiques démontrent, en accord avec le modèle, que l'histone H1 est incapable de s'associer correctement avec ces deux nucléosomes variant et de former la structure en tige. Des expériences avec des histones chimères contenant les domaines d'accrochage variants et conventionnels intervertis ont montré que la cause est à nouveau le domaine d'accrochage « défectueux » qui contribue à l'ouverture du nucléosome et l'impossibilité d'accommoder et retenir l'histone H1.

SUMMARY OF THE THESIS

The composition and the basic organization of the nucleosomes were established since few decades (1). The structure of the nucleosomal core particle (NCP) was solved with nearly atomic precision by X-ray diffraction (2, 3). However, the same type of information for the structure of a complete nucleosome, i.e. the NCP containing linker DNA with associated linker histone, is not available. The numerous efforts (invested since more than 30 years) to understand the mode of association of the linker histone with the nucleosomal DNA have not led to a successful outcome and the reported data have a controversial character.

In this work we have been able to dissect how histone H1 interacts with the nucleosomal DNA and to understand how this interaction leads to the spatial organization of the nucleosomal templates. We have solved this long-stayed problem in the field thanks to the use of: (i) physiologically relevant linker histone chaperone NAP-1 assisted deposition of histone H1, (ii) 601 DNA sequence for reconstitution of strongly positioned nucleosomes, (iii) a combination of electron cryo-microscopy with OH° footprinting techniques and, (iv) Coarse-grain DNA mechanics. The one base pair resolution mapping by OH° footprinting showed that the globular domain of histone H1 (GH1) interacts, through the minor grove of DNA, with 10 bp localized symmetrically to the nucleosomal dyad. In addition, GH1 organizes ~ one helical turn of DNA from each linker of the nucleosome. A row of seven aminoacids (120-127) of the COOH-terminus of histone H1 was required for the formation of the stem structure of the linker.

A 3D molecular model, based on these data and coarse-grain DNA mechanics, was constructed. The model explains how the different domains of H1 interact with nucleosomal DNA and predicts a specific H1-mediated stem structure of the linker DNA. In this model, the GH1 structure was large enough to fill the space between the exiting and entering DNA and to simultaneously interact with ~10 bp of each linker DNA as well as with the nucleosomal dyad. The binding C-terminus of H1 together with the binding of GH1 efficiently "clamped" the exiting and entering linkers and resulted in the formation of the stem structure. Within the stem, the linkers come together along ~20-30 bases outside the core particle, slightly curving into a two-start superhelical stem with a large pitch of around 100-120 bp. Note that the model requires three contacts of GH1 with nucleosomal DNA and thus, a specific orientation of the linkers. According to the model, if the orientation of the linkers in the core particle is perturbed, this should affect the binding of H1 to the nucleosome and would not allow the formation of a stem.

The incorporation of the histone variant H2A.Bbd within the nucleosome resulted in alteration of its structure. AFM and EC-M images show a highly flexible structure of the H2A.Bbd variant particles where the entry/exit DNA form ~ 180° angle (the linkers are close to parallel) in contrast to the V shape in the conventional nucleosomes. The defective docking domain of H2A.Bbd appeared to be responsible for the altered structure of the H2A.Bbd particles. In this work we have characterized the structural and functional properties of a nucleosome, containing H2AL2, another variant of the H2A family, which, as H2A.Bbd, exhibited a defective docking domain. H2AL2 reconstituted trinucleosomes had a type of a “beads on a string” structure very similar to that of H2A.Bbd ones. Our biochemical and EC-M data demonstrate, in agreement with the model, that histone H1 was unable to bind properly to the variant nucleosomes and to generate a stem structure. Experiments with swapped docking domains of conventional histone H2A and the variant histone H2A.Bbd showed that this is determined by the "defective" docking domain of the these H2A histone variants.

INFORMATION OF THE LABORATORIES IN WHICH THE THESIS WAS PREPARED

a) Main Laboratory

Unité INSERM U823
Institut Albert Bonniot
Domaine de la Merci
38706 La Tronche cedex
France

b) Affiliated laboratory

Laboratoire Joliot Curie
École Normale Supérieure
46 allée d'Italie
69364 Lyon cedex 07
France

LIST OF ABBREVIATIONS

AA:	Aminoacid
ACF:	ATP-utilizing chromatin assembly and remodeling factor
ADP:	Adenosine diphosphate
AFM:	Atomic force microscopy
ARP:	Actin-related proteins
ATM:	Ataxia telangiectasia mutated
ATP:	Adenosine triphosphate
BSA:	Bovine serum Albumin
CBP:	CREB Binding Protein
CENP-A:	Centromeric protein A
CCD:	Charge coupled device
CH:	Carboxy terminal helix
CHD:	Chromodomain
CHRAC:	Chromatin accessibility complex
CL:	Carboxy loop
CTD:	Carboxy terminal domain
DBD:	DNA binding domain
DNA:	Deoxy ribonucleic acid
DNase I:	Deoxy ribonuclease I
DSB:	Double strand break
DTT:	Dithiothreitol
EC-M:	Electron cryomicroscopy
EDTA:	Ethylenediaminetetraacetic acid
FPLC:	Fast protein liquid chromatography
FRAP:	Fluorescence recovery after photo bleaching
FTIR:	Fourier transform infra-red
GD:	Globular domain
GNAT:	Gcn5-related N-acetyltransferase
HAT:	Histone acetyl transferase
HDAC:	Histone deacetylases
HILS1:	H1-like protein in spermatids
HMG:	High Mobility Group
HP1:	Heterochromatin protein 1
HSP:	Heat shock protein
INO80:	Inositol requiring 80
INCENP:	Inner centromere protein
IPTG:	isopropyl-beta-D-thiogalactopyranoside
ISWI:	Imitation SWI
LSD1:	Lysine-specific demethylase 1
MBD:	Methyl CpG-binding domain
MeCP2:	Methyl CpG binding protein 2
Msx1:	msh homeobox 1
NAP-1:	Nucleosome assembly protein
NCP:	Nucleosome core particle
NHR:	Non- Histone Region
NMR:	Nuclear magnetic resonance
NP40:	Nonyl phenoxylpolyethoxylethanol 40
NRL:	Nucleosome repeat length
NURF:	Nucleosome remodeling factor
PAD4:	Peptidylargenine deiminase 4
PAGE:	Polyacrylamide gel electrophoresis
PARP-1:	Poly-ADP ribose polymerase1
PCR:	Polymerase chain reaction
PHD:	Plant Homeo Domain
PRMT:	Protein arginine methytransferases
PTM:	Post translational modification
RNA:	Ribonucleic acid
RNAPII:	RNA polymerase II
RSC:	Chromatin Structure remodeling
RT-PCR:	Reverse transcription polymerase chain reaction
SAXS:	Small-angle X-ray scattering
SDS-PAGE:	Sodium dodecyl sulfate PAGE
SWI/SNF:	SWItch/Sucrose NonFermentable
TAF:	Tata associating factor
TCA:	Trichloroacetic acid
TFE:	2, 2, 2-trifluoroethanol
UV:	Ultraviolet
Xist:	X-inactive-specific trascript
3D:	Three dimension
4WJ:	Four way junction

CHAPITRE I: CHAPITRE D'INTRODUCTION

Le chapitre est dédié à la présentation de la littérature sur les propriétés structurales et biologiques de la chromatine. Y sont inclus dans l'ordre chronologique les découvertes essentielles dans le domaine. Une attention particulière est portée aux aspects structuraux de la chromatine, plus précisément, comment la molécule d'ADN, d'une longueur de quelques mètres, est repliée dans le noyau de la cellule de dimension de quelques microns. Les histones de liaison jouent un rôle essentiel dans la cascade de repliements de la chromatine, et déterminent la structure de l'ordre supérieur de sa structure. Les histones de liaison ont une structure particulière qui contienne un domaine globulaire central, très conservé, et une partie N-terminale courte et C-terminale longue de compositions d'acides aminés variables. Malgré le rôle clé de l'histone de liaison H1 dans la dynamique de la chromatine, son localisation et interaction avec le nucléosome sont encore des sujets de controverse. En effet, l'existence de plusieurs modèles alternatifs montre l'ambigüité du sujet. Les cellules ont développé trois stratégies majeures pour « ouvrir » la chromatine compactée pour que des processus vitaux pour la cellule puissent s'accomplir. Ce sont le remodelage de la chromatine par des complexes protéiques dépendants de l'ATP, l'incorporation d'histones variant et les modifications post-translationnelles des histones.

CHAPTER I: INTRODUCTION

I .1 Chromatin introduction

The basic thread of life in eukaryotes, containing the genetic information, is a complex of DNA and protein called chromatin housed inside the nucleus of the cell. The word has been derived from the Greek "khroma" meaning colored and “soma" meaning body, based on its stainability with basic dyes (4). Chromatin must be compact enough to accommodate two meters of DNA (6×10^9 bp) in a micron sized (5-10µm) nucleus and at the same time must be rapidly accessible to permit its interaction with protein machineries that regulate the functions of chromatin: replication, transcription, repair and recombination. The dynamic organization of chromatin structure thereby influences, potentially, all functions of the genome.

I .2 Chromatin history

The history of chromatin (Figure 1) can be said to begin in 1880 with the W. Flemming (4, 5), who has suggested the name ‘chromatin’. In 1871, while developing the methods for the isolation of nuclei from pus leukocytes, Miescher reported a strong phosphorus rich acid, which he called nuclein (6). Later he performed additional experiments on sperm heads of the Rhine salmon and fractionated a basic component that he called protamine and an acidic component that was highly similar to the nuclein. In 1884 Albrecht Kossel (7), who continued the work of Miesher in E. Hoppe-Seyler laboratory, described the ‘histone’ in acidic extracts from avian erythrocyte nuclei. In the beginning, Miesher`s work was overshadowed by the more hyped discovery of genetic rules by Austrian monk Gregor Mendel and the theory of evolution by British scientist Charles Darwin. This period continued and more progress was done in the field of genetics. In 1900 Mendelian principles were rediscovered by H. de Vries (8), followed by the development of gene theory and principles of linkage in 1910 by T. H. Morgan (9). Another big achievement in the field was made by Franklin Griffith in 1928 (9) while describing the principle of transformation which lead Oswald Avery, Colin Macleod and Maclyn McCarty in 1944 (10) to demonstrate DNA as the molecule responsible for the process.

Discovery of polytene chromosomes in *Drosophila* and gene localization studies by E. Heitz and H. Bauer (1933), T. Painter (1933) and C. Bridges (1935) (9) inspired D. Mazia (11) to use proteases and nucleases to study salivary gland polytene chromosomes and plant chromosome. Nucleases particularly revolutionized the study in chromatin field. It was then

the April 1953 issue of Nature journal which published three papers describing the famous structure of DNA double helix by Watson & Crick (12), Wilkins, Stokes & Wilson (13) and Franklin and Gosling (14) .

Using biophysical approach to study the chromatin structure was made possible by the studies of G. Zubay`s laboratory in 1959 (15) when they were able to prepare the soluble chromatin. In the meanwhile, histone proteins were fractionated by the group of E. Johns (16-18).

Electron micrography was introduced in the chromatin field in 1970 by H. Davies (19) who has observed chromatin threads of 30nm in the chicken erythrocyte nuclei. Such fibers were seen subsequently in purified chromatin preparations by the group of Klug, A in 1976 (20). 'Beads on the thread' were visualized by two independent groups: Olins and Olins in 1974 (21), who named them as v (nu) bodies, and C.L.F. Woodcock 1976 (22).

In 1974 R. Kornberg, in collaboration with J. Thomas (23) postulated a model of chromatin structure describing it a repeat of ~200 base pairs of DNA in complex with core histone octamer, which in itself is made up of a Histone H3-H4 tetramer and two H2A-H2B dimers. This chromatin subunit was named as 'Nucleosome' by P. Chambon in 1975 (24). Linker histones were reported to link the nucleosome core particles in chromatin (23, 25). The organization of DNA and histones in nucleosome was borne out by X-ray crystallographic studies of the histone octamer and the core particle by the groups of Moudrianakis, E.N (1991) (26) and Richmond, T.J (1997) (2), respectively. However, there have been many controversial reports about the precise location of linker histones in chromatin (27, 28). This will be discussed in detail, in the later chapters of this thesis.

In vitro studies of chromatin fiber have led to two main models of the higher order chromatin structure, namely zigzag model (29-32) and solenoid model (33, 34). Despite many refined and compelling studies, the structure of the 30-nm chromatin fiber remains open question.

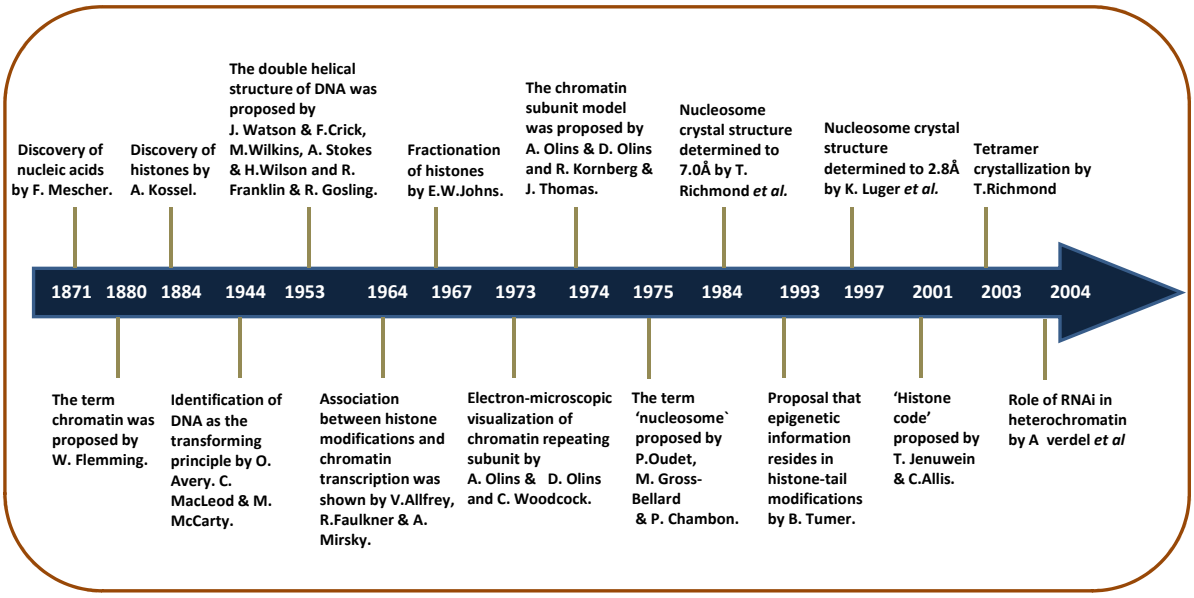

Figure 1: Diagram representing the hallmarks in the history of chromatin studies.

I .2.1 Nobel Prize related to chromatin

Owing to their commendable and unprecedented contribution to the field of chromatin, many scientists were conferred the prestigious Nobel Prize (Table 1).

Year	Who	Award
1910	Albrecht Kossel (University of Heidelberg)	Nobel Prize in Physiology or Medicine "in recognition of the contributions to our knowledge of cell chemistry made through his work on proteins, including the nucleic substances"
1933	Thomas Hunt Morgan (California Institute of Technology)	Nobel Prize in Physiology or Medicine "for his discoveries concerning the role played by the chromosome in heredity"
1962	Francis Crick, James Watson and Maurice Wilkins (MRC Laboratory of Molecular Biology, Harvard University and London University respectively)	Nobel Prize in Physiology or Medicine "for their discoveries concerning the molecular structure of nucleic acids and its significance for information transfer in living material"
1982	Aaron Klug (MRC Laboratory of Molecular Biology)	Nobel Prize in Chemistry "for his development of crystallographic electron microscopy and his structural elucidation of biologically important nucleic acid-protein complexes"
1993	Roberts and Sharp	Nobel Prize in Physiology "for their independent discoveries of split genes"
2006	Roger Kornberg (Stanford University)	Nobel Prize in Chemistry "for his studies of the molecular basis of eukaryotic transcription"

Table 1: Showing Noble prizes awarded related to chromatin

I .3 Chromatin structure

Chromatin exhibits a repeating structure. The basal repeating unit of chromatin, termed the nucleosome, is formed upon wrapping of two superhelical turns of DNA around an octamer of core histones (two of each H2A, H2B, H3 and H4). This structure provides the first level of compaction of DNA into the nucleus. Interconnected by linker DNA, nucleosomes form 10 nm "beads-on-a-string" filament. Upon addition of linker histones, the "beads-on-a-string" structure coils, in turn, into a 30 nm diameter structure known as the 30nm fiber. Chromatin is organized into functional territories (35) within an interphase nucleus. Long range fiber-fiber interactions finally compact the chromatin to highly condensed metaphase chromosome (Figure 2).

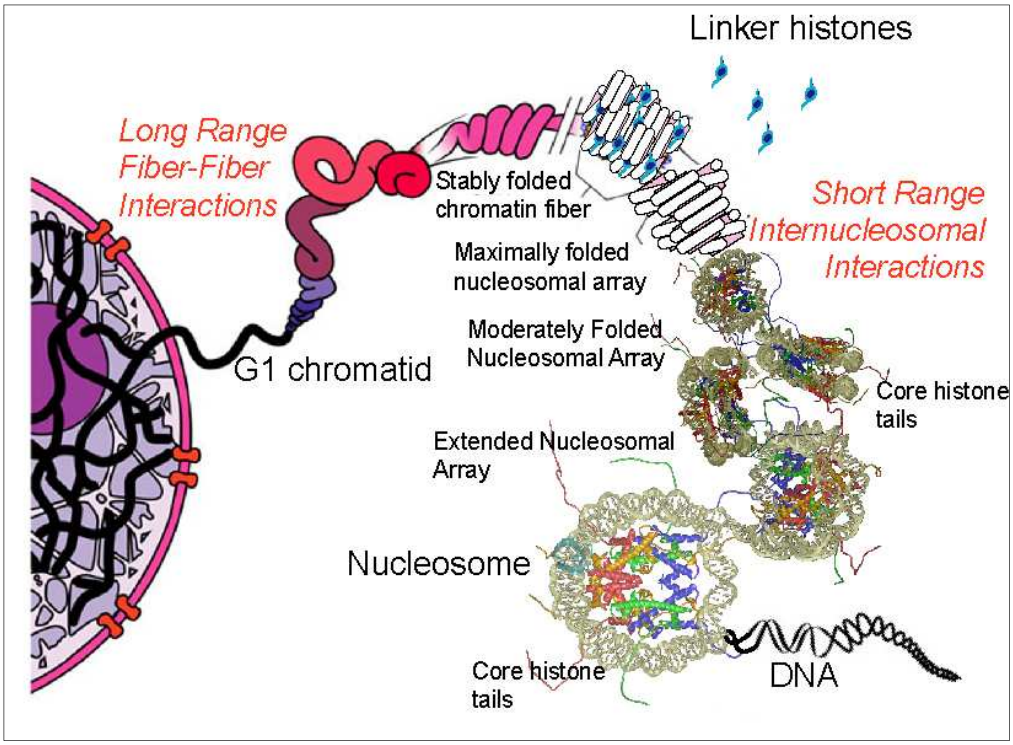

Figure 2: Organization of eukaryotic chromatin fibers. The fundamental unit of chromatin is defined as nucleosome that forms the "beads-on-a-string" chromatin structure. Internucleosomal interactions, linker histones and non-histone proteins mediate the further condensation of chromatin into 30nm fibers and higher order structures. Adapted from (36)

Structurally and functionally chromosome has been divided into two distinct domains. Chromosomal regions that do not undergo postmitotic decondensation were termed as heterochromatin by the German botanist Emil Heit in 1928, whereas fractions of the chromosome that decondense and spread out diffusely in the interphase nucleus were referred to as euchromatin (37).

I .3.1 DNA

In most living organisms (except for some viruses), genetic information is stored and transferred from a parent to its offspring by the molecule deoxyribose nucleic acid, called DNA for short. Regions of DNA which have the information encoded for giving rise to diffusible products (protein or RNA) are called the Genes. The process of transmitting the information from DNA to form protein via RNA is called central dogma of molecular biology. The proteins that are produced have functional roles in just about every aspect of a living cell. Some proteins play a structural role and others serve as enzymes that regulate many biochemical pathways (anabolic and catabolic) in living organisms.

DNA molecule has a right handed double-stranded helical structure in which the two strands run opposite and intertwined to each other (12). Each helix is a polymer of four basic nucleotides. The polymer backbone is composed of the alternating sugar (deoxyribose)-phosphate units, attached to which are four types of heterocyclic nitrogenous bases namely Adenine, Thymine, Guanine and Cytosine, which hold the two strands together. Adenine from one strand forms two hydrogen bonds with Thymine form the other stand, while as Guanine forms three hydrogen bonds with the Cytosine from the opposite strand. The DNA double helix also has two different-sized "grooves": a major groove and a minor groove (Figure 3). These grooves are binding sites for a wide variety of molecules that affect DNA at the molecular level such as proteins that control such functions as gene expression, regulation, replication and transcription. DNA double helical structure has been classified into three types namely B-DNA, A-DNA and Z-DNA. B-DNA is the most abundant form of DNA commonly found under physiological conditions in a cell. In this structure, the helix makes a turn every 3.4 nm, and the distance between two neighboring base pairs is 0.34 nm. Hence, there are about 10 pairs per turn. In a solution with higher salt concentrations or with alcohol added, the DNA structure may change to an A form, which is still right-handed, but every 2.3 nm makes a turn and there are 11 base pairs per turn. A-DNA forms are present under some biological conditions that are not yet well understood. Another DNA structure is called the Z form, because its bases seem to zigzag. Z-DNA is left-handed and also narrower than the other two types of DNA. One turn spans 4.6 nm, comprising 12 base pairs. The DNA molecule with alternating G-C sequences in alcohol or high salt solution tends to have such structure. Z-DNA has been found in synthetic short segments of DNA.

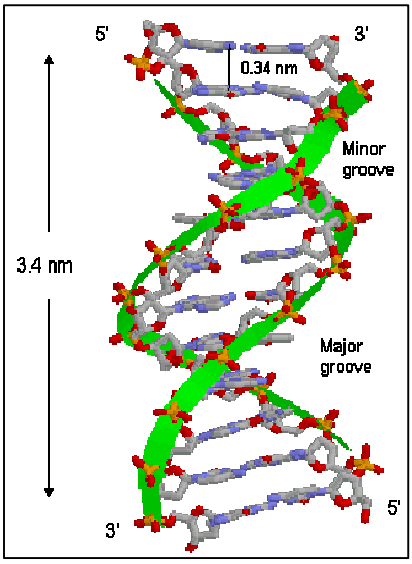

Figure 3: A cartoon of DNA double helix showing DNA major and minor groove.

I .3.2 Nucleosome

Historically, the periodic nature of chromatin was identified by biochemical and electron microscopic studies. The partial digestion of chromatin, isolated from rat liver nuclei, generated fragments of 180-200 base pairs in length which were resolved by electrophoretic migration (38, 39). This regularity of chromatin structure was later confirmed by electron microscope analysis that revealed chromatin as regularly spaced particles or "beads on a string" (21, 24). In parallel, chemical cross-linking analysis permitted the precise determination of the stoichiometry of DNA and histones in the nucleosome to be 1/1 based on their mass (23). Together these observations led to the proposition that the nucleosome was the fundamental unit of chromatin. Pierre Chambon's laboratory was the first to use the term "nucleosome" (24).

Nucleosome is the basic repeating unit of the chromatin, composed of a core particle and a linker region (or inter-nucleosomal region) that joins adjacent core particles. The length of the linker region, however, varies between species and cell type. Therefore, the total length of DNA in the nucleosome can vary with species from 160 to 241 base pairs (40-44). Two copies of each of histone protein H2A, H2B, H3 and H4 are assembled into an octamer that has 146-147 bp of DNA wrapped in 1.65 left-handed super helical turns around it to form a nucleosome core particle (NCP) (26). A complete histone octamer is composed of a central $(H3\text{-}H4)_2$ tetramer flanked by two H2A-H2B dimers. The four core histones are small basic proteins (11 to 16 kDa), which are highly conserved through evolution. Histones induce the structural bending in the major and minor grooves of DNA in a way to compress and narrow

them down when they face the octamer and expand the ones facing outside (45). The nucleosome is stabilized by histone-DNA interactions which occur about once every 10 base pairs, resulting in impressive distortion of the DNA helix, and the final structure is stabilized by 116 direct histone-DNA and 358 water-bridged histone-DNA stabilizing interactions (46). The connections between DNA and histones are mainly non-specific and include non-polar interactions with the pentose groups in the DNA, hydrogen bonds to the phosphate groups of DNA, and electrostatic interactions between the positively charged aminogroups of the histones and the negatively charged DNA phosphate backbone (47).

The association of one molecule of linker histone H1 with the NCP yields 167 bp of DNA and thus protects approximately 20 bp of DNA from micrococcal digestion. This structure was originally termed the chromatosome (48). Nucleosomes are connected with one another to form what are called nucleosomal arrays which further fold into less understood 30nm fiber and higher order chromatin structures.

The function of the nucleosome is paradoxical, requiring it to play two opposite roles simultaneously. On one hand, nucleosomes must be stable, forming tight, sheltering structures that compact the DNA and protect it from harm. On the other hand, nucleosomes must be labile enough to allow the information in the DNA to be used. Chromatin modification enzymes must be allowed access to the DNA for functions like replication, repair and transcription. The method by which nucleosomes solve these opposed needs is not well understood, but may involve a partial unfolding of the DNA from around the nucleosome.

I .3.2.1 Nucleosome core particle

The nucleosome core particle (Figure 4) is the crystallizable substructure of the canonical nucleosome (49), defined by the DNA protection pattern of histone octamer in nuclease digestion of chromatin. The 205 kDa NCP contains two copies of each core histones H2A, H2B, H3 and H4 and 146 base pairs of DNA wrapped in about 1.65 superhelical turns around the histone core. Neutron scattering (50) and low resolution X-ray crystallographic studies (7Å) (51-53) demonstrated the disc shape to the NCP. However the more fine and high resolution structural details were possible only after the solution of 3.1Å structure of the histone core of the nucleosome (26) and 2.8 Å structure of NCP (2), using 146bp X chromosome α-satellite palindromic DNA and heavy atom labeled recombinant histone proteins. A refined structure of NCP using 146 bp α-satellite palindromic DNA and native

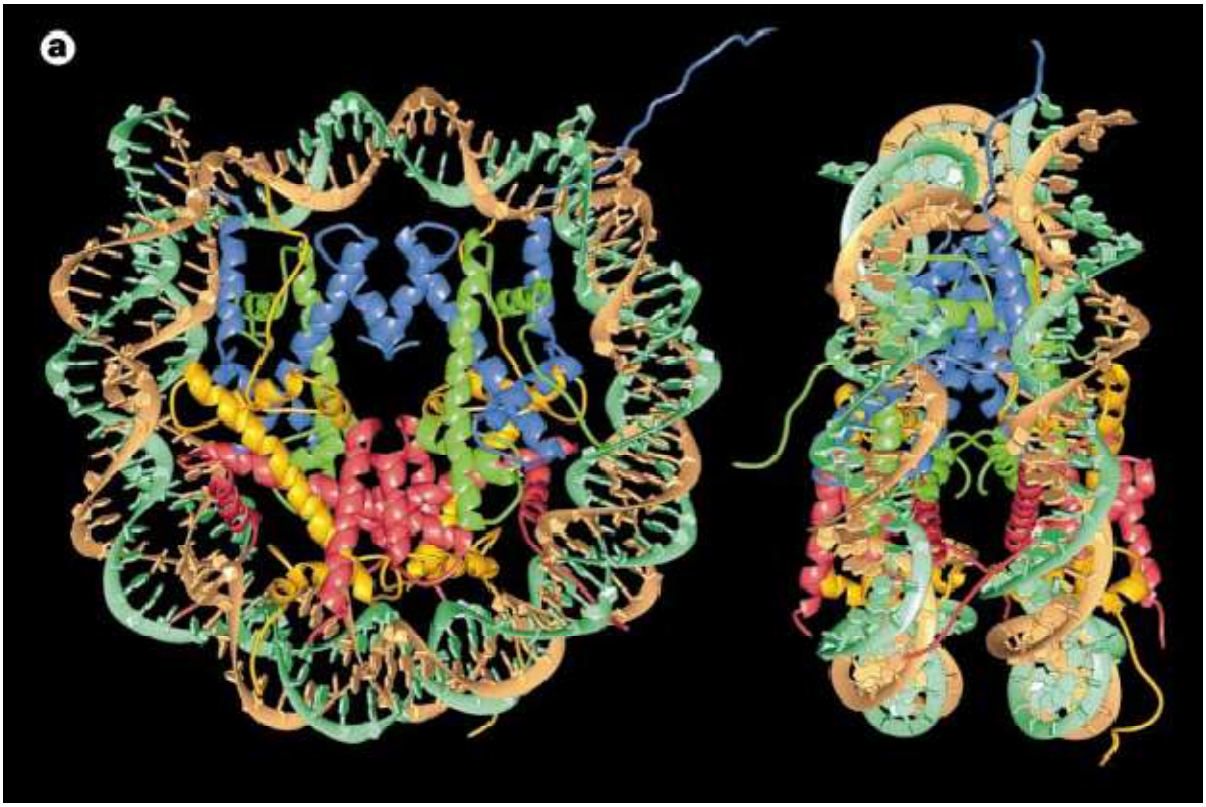

Figure 4: Nucleosome core particle: ribbon traces for the 146-bp DNA phosphodiester backbones (brown and turquoise) and eight histone protein main chains (blue: H3; green: H4; yellow: H2A; red: H2B. The views are down the DNA superhelix axis for the left particle and perpendicular to it for the right particle. For both particles, the pseudo-twofold axis is aligned vertically with the DNA centre at the top. Image adapted from (54)

chicken histone octamer cores demonstrated the asymmetries in the nucleosome core particle at 2.5 Å resolution (49).

The histone octamer looks like a tripartite assembly, when looking straight into the dyad axis, with a central V-shaped $(H3\text{-}H4)_2$ tetramer flanked by two flattened balls, the H2A-H2B dimers. The octamer surface has several grooves and ridges, which are set to incorporate the left handed superhelix of the DNA double helix. Individual core histones of the octamer share a common feature of having a symmetrically duplicated (evolutionary) helix-turn-helix motif called 'histone fold' motif (Figure 5A), consisting of three helices: a short helix on the N-terminal side of the symmetry center of the fold (NH), the long median helix (mH) and a short helix on the C-terminal side (CH). The helices are joined by loop NL between the NH helix and the mH helix, and loop CL between the median helix and the CH helix. Histone folds mediate histone-histone as well as histone-DNA interactions and account directly for the organization of 147 bp DNA, each fold pair associating with 27-28 bp DNA primarily binding to the phosphodiester backbone as they face the protein.

Histones assemble in pairs of heterodimers, in which the two monomers are intimately associated in a head-to-tail manner in a so called "handshake motif' (2, 26) and are stabilized largely through hydrophobic interactions. The short terminal helices are folded back and rotated over the median helix, which lead to interdigitation of the terminal helices and overlapping of the central helices (Figure 5B). This type of structure is stabilized by extensive hydrophobic interactions between the helices. Also there are some other interactions within the heterodimers, which lead to the formation of β bridges between the CL loop of H2A and the NL loop of H2B and between the CL loop of H3 and the NL loop of H4. These bridges form the primary DNA docking sites on the histone surface.

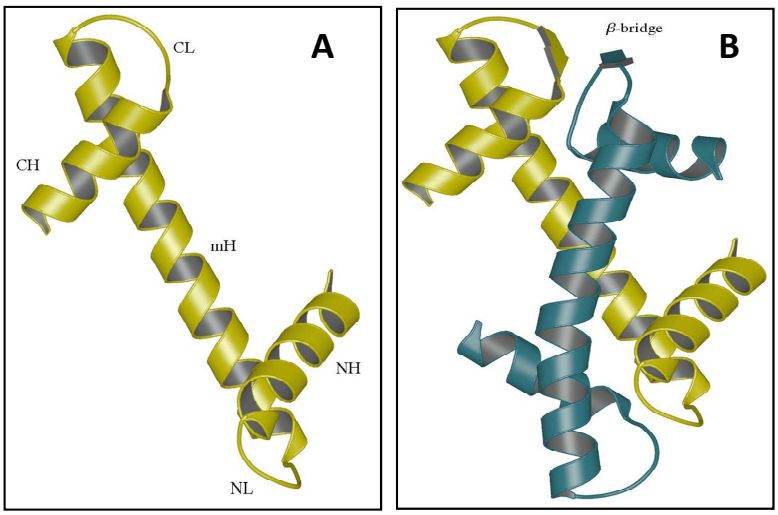

Figure 5: Showing the structure of the histone fold motif of H3 (A), H3-H4 heterodimer showing the two histones interdigitated in a handshake motif (B) Image adapted from (49)

Long median and C-terminal side helices of two H3 from two H3-H4 dimers interact to form a four-helix bundle, which assists the formation of heterotetramer $(H3\text{-}H4)_2$. The tetramer shape resembles a twisted open horseshoe (2, 26, 55) and determines the nucleosome positioning. Tetramer exists as soluble complex at physiological ionic strength solutions and interacts more strongly to the DNA than the H2A-H2B dimer. To complete the octamer two H2A-H2B dimers bind to the two opposite sides of the tetramer to form the tripartite structure.

Histones also have a highly basic unstructured amino-terminal domain (‘tail’), which extends from the surface of the nucleosome (56, 57). These histone tails are targets for post-translational modifications, and are important for higher order chromatin structure. These tails, pass through DNA gyres, assume definite conformation once bound to DNA and are reported to be involved in interparticle and linker DNA interactions (58).

Histone octamer construction favors the placement of the arginine side chains of the core histones at the places which can fit in the minor grooves of the B-DNA to form a left-handed superhelical ramp with the minor grooves spaced more or less evenly along the ramp.

I .4 Linker histone

Linker histones are the arginine rich, highly diverse group of histones which lack the proper histone fold domain unlike the other core histones. They bind to linker DNA between the NCPs and help to compact and stabilize the higher order chromatin structure. They are constituted of a particular three domain structure: an unstructured N-terminus, relatively conserved central globular winged-helix domain and an unfolded lysine rich C-terminus (59). The linker histone family is highly diverse with at least 11 tissue, stage and species-specific variants (60-62), which differ in molecular weight, amino acid sequence, biochemical/biophysical and immunochemical properties (63).

The Linker histone function was studied by several groups. Fan and coworkers have systematically deleted linker-histone genes in mouse embryonic stem cells and generated mice null for H1°, H1a, H1c, H1d, H1e, or H1t, as well as several double mutants of H1 variants. Surprisingly, mice lacking any one of these subtypes develop normally (64-66), whereas the disruption of multiple H1 isoforms leads to embryonic lethality. These results suggest that the lack of a phenotype in single null mice is due to compensation by the remaining subtypes. Careful examination, however, revealed only limited functional redundancy of the variants, since the knockouts of histone H1d (H1.3) or H1e (H1.4) affected age dependent regulation of globin expression (67).

Tetrahymena thermophila has a single linker histone and the Knockout histone H1 strains grow at normal rates (68, 69) and reach near-normal cell densities, arguing that H1 in this organism is not essential for cell survival. However, it is believed that *Tetrahymena* histone H1 is not the real linker histone as it lacks a globular domain in its structure. On the contrary yeast *Saccharomyces cerevisiae* has a linker histone, Hho1p, (70) which contains two globular domains, without N and C terminal tails. The Hho1p knockout cell line is viable, although there are detectable alterations in gene regulation. A recent report has also shown Hho1p essential for chromatin compaction in stationary phase of yeast cell cycle (71). Other studies suggest that the linker histone subtypes play differential roles in the control of gene expression (67). Apart from being the main architectural protein of the chromatin and maintaining the chromatin structure, linker histone H1 has been reported to regulate core

histone acetylation *in vivo* (72) and some variants of H1 induce chromatin repression in a tissue specific manner (73). Recently, Konishi and his colleagues demonstrated a role for the linker histone H1c or H1.2 in triggering apoptosis in response to DNA damage (74).

I .4.1 Location of Globular domain on nucleosome

The central conserved winged-helix globular domain (GD) of the linker histone appeared to be internally located in the 30 nm chromatin fiber (75, 76), but its exact position within the nucleosome remains the major controversy in the available data (for review see (77-81). Several models have been postulated in the past 30 years (Figure 6) to explain exact location of globular domain on either native or reconstituted nucleosomal substrate. The very first model was postulated by Allan in 1980 (82), according to which GD binds 10bps

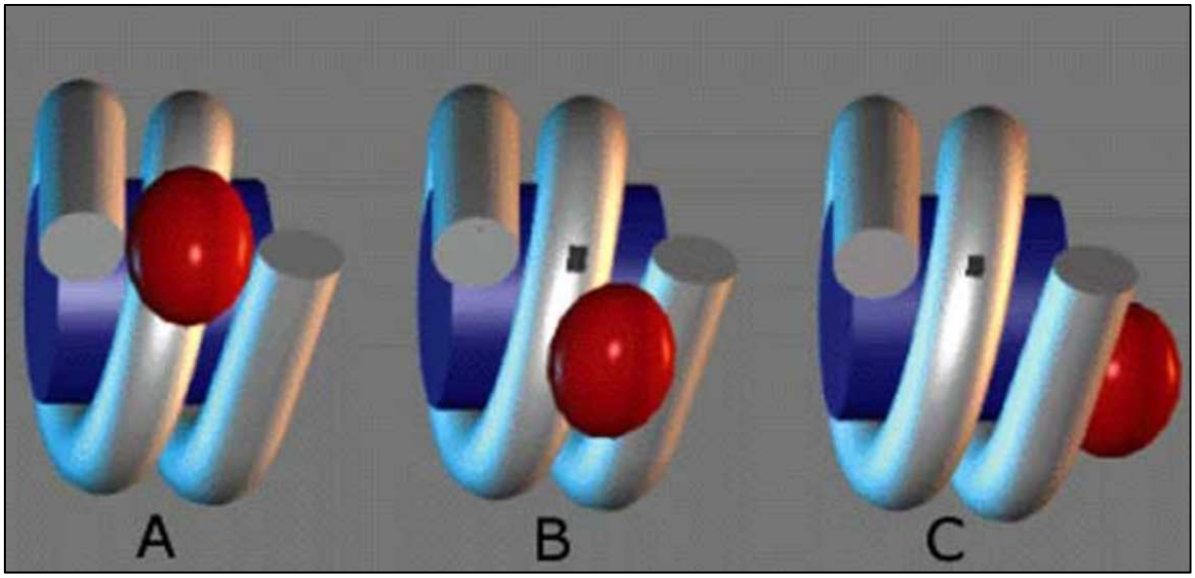

Figure 6: Different models of Globular domain localization on the nucleosome A. Symmetrical model (83), B. Bridging model (84) and C. Unsymmetrical model of (85).

entering and 10bps exiting DNA (linker DNA) of the nucleosome in such a way that it is placed at nearly dyad axis in a symmetrical manner. The model was validated by the GD specific DNase I footprint on nucleosomal dyad (86). This view was however challenged by the asymmetrical GD binding model of An W. and colleagues (87), which proposed that GD protects 20bp of either entering or exiting DNA. This pattern, in turn, probably can lead to directionality or polarity of the chromatin fiber. The polarity of H1 binding to nucleosome may be due to the presence of certain marker sequences found at one end of bulk chromatosomes (88) or due to a conformational change in the NCP (89).

Another study utilized the nucleosome positioning sequence 5S RNA from *Xenopus borealis* and cross-linked the nucleosomal DNA to the GH5 and proposed a still much debated model for GH5 binding. According to the findings of this group the GD binds asymmetrically to the nucleosome inside the gyres of DNA at a distance of ~ 65 bp from the dyad (90) and protects 15bp of DNA from one side and 5bp from other side of NCP (85). This model was objected by the "bridging model" of Zhou et al. (84), according to which GH5 interacts with the dyad and with only one (either the exiting or entering) of the free DNA arms. This model was supported by the findings of *in vivo* photobleacing experiments and subsequent modeling (28). Fluorescence recovery after photobleaching (FRAP) studies suggested the presence of only two DNA binding sites in globular domain. One of the two binding sites fit within major groove close to the dyad axis and the other within minor groove on the linker DNA in proximity of the NCP (28).

Recently Fan & Roberts (91) described the three binding site model for GH5 binding using the exhaustive rigid molecular docking programs (note that no experimental data were presented in (89)). This model favors the symmetrical binding model for GH5, in which one of the three binding sites contact the nucleosome at the dyad and two others bind symmetrically to the entering and exiting linker DNA (Figure 7).

Several reasons could explain the controversial character of the reported data. The above *in vitro* studies used salt dialysis to deposit histone H1 to the nucleosomes. This would lead to improper assembly of histone H1 (92). In addition, the reconstitution on 5S DNA would result in the formation of nucleosomes exhibiting several translational positioning, which, in turn, would interfere with the mapping of histone H1:nucleosomal DNA contacts (93). The *in vivo* photobleaching studies could be viewed as indicative for the mapping of H1:nucleosomal DNA interactions, as they provide indirect information .

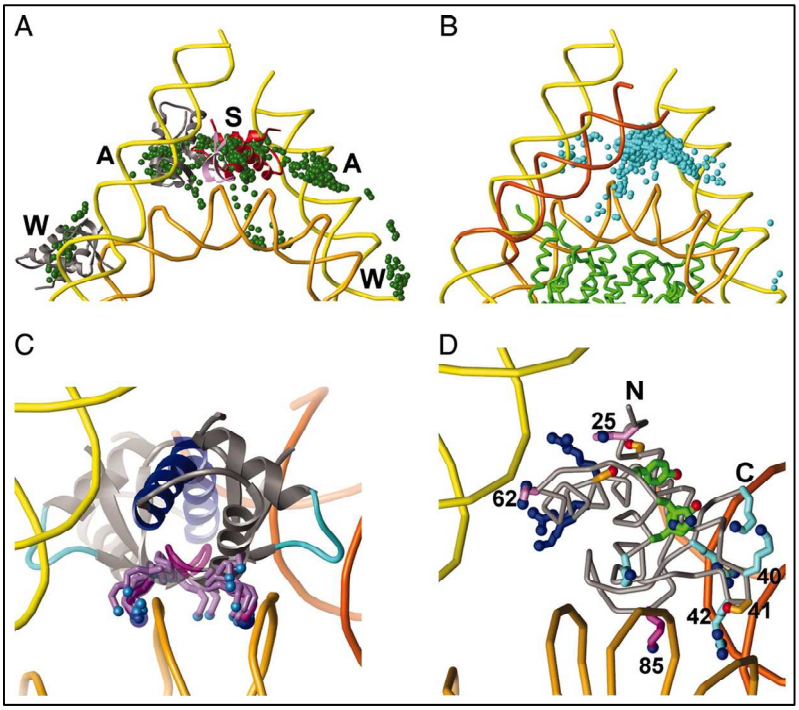

Figure 7: GH5 docked to the nucleosome. (A) Different possibilities to dock GH5 on the nucleosome, which include dockings far from the nucleosome dyad axis, near the dyad axis but contacting only one arm and over the dyad axis. (B) Nucleosome model with one DNA arm bent (orange). The 1,000 top-ranked GH5 solutions are concentrated over the dyad axis. (C) Lys-85 lies in the DNA minor groove at the dyad axis in 27 of the 30 top-ranked solutions or slightly to one side of the phosphate backbone at the dyad axis. (D) Interactions of GH5 side chains with the nucleosome. The top-ranked GH5 solution has Lys-69, Arg-73, and Arg-74 (blue) from helix H3, site I, contacting one arm, with His-25 and His-62 (lavender) and Ser-29 and Ser-71 (gold with red OG) nearby. Lys-85 (magenta) and its wing (site II) are centered in the DNA minor groove at the dyad axis; and Arg-40, Lys-42, Arg-94, and Lys-97 (light blue, right, site III) contact the other DNA arm. The Ser-41 side chain (gold, lower right) extends toward DNA at the dyad axis. The N and C termini of GH5 are indicated. Figure adapted from (91)

I .4.2 Role of the Carboxy terminus of Histone H1

Histone H1 is characterized by a long unstructured C-terminus (~100 aminoacid residues), which has been shown very important for the H1 induced chromatin condensation (82). The C terminus is highly rich in lysine, proline and alanine aminoacids (94). H1 N-terminal deletion protein can stabilize chromatin folding to the same extent as the full-length H1s. However, neither the globular domain alone nor the globular domain plus the N-terminus could facilitate chromatin folding (82, 83). These studies indicate that the ability of linker histones to stabilize chromatin folding resides in the C-terminal domain (CTD) of the protein, and the C-terminal performs its function by shielding negative charges on the DNA backbone. However, simple charge neutralization role of the CTD has been questioned in many studies where deletion of most of the C- terminal did not drastically interfere with the H1 induced fiber condensation (95). In fact specific sub domains have been identified in the CTD which

mainly control its functions (95). The main function of CTD, i.e. linker DNA conformation and stabilization and self association of nucleosomal array, has been assigned mainly to the first 25 aminoacids flanking the globular domain.

The sequence of CTD varies among various sub-types of H1 and exhibits different *in vitro* DNA and chromatin (96, 97) condensation properties, which do not depend on their length and charge distribution.

Unstructured in solution (98), CTD can adopt a segmental α-helical conformation upon DNA binding (99). Due to the intrinsic spectroscopic properties of DNA, the structure of the C-terminal bound to DNA cannot be resolved either by CD spectroscopy or Fourier transform infra-red (FTIR) spectroscopy. However organic solvent 2, 2, 2-trifluoroethanol (TFE) has been used (reported to be a genuine replacement for the DNA (100)) to study the secondary structure formation in the truncated C-terminal peptides. Such studies proved the induction of alpha helical structure in these unstructured peptides in TFE. Other studies also suggest CTD peptides acquire α-helical structure in both high salt solutions (101-103) and in presence of DNA (101, 102). CTD of some of the H1 variants also possesses one or more β-turn motif sequence S/TPKK (99-103) which has been reported to bind DNA minor groove and mediate condensation of naked DNA (104-106). The presence of three imperfect octapeptide repeats containing S/TPKK motif in H1d linker histone make it a better DNA condensing linker histone than H1t isotype which completely lack such motifs (97). The DNA compacting ability of H1d was found reduced by 1/3 upon deleting these three imperfect octapeptide repeats (107).

Interestingly the DNA compaction ability was reduced by 70% even if a stretch of 10 aminoacids between two of the repeats was deleted, suggesting that a specific secondary structure motifs in the C-termini is responsible for linker histone dependent DNA compaction (97, 107).

Studies (above described) suggest that there is strong circumstantial evidence that the CTD of H1 might assume a segmented α-helical conformation upon binding to DNA, which in turn will track the phosphate backbone, kinking around the linker DNA by virtue of proline-induced bends or breaks in the helix, following one or other of the grooves (possibly the major rather than the minor groove, since early studies revealed no protection of the minor groove from chemical modification (108)). Alternatively, helical segments of the CTD may lie on the face of the DNA, binding across rather than in the groove, but still kinking around the DNA (99).

I .4.3 Molecular dynamics of Histone H1

Recent *in vivo* photo bleaching experiments describe the binding of H1 to nucleosome as a reversible process. The residence time (1-2 min) was found higher (109) compared to transcription factors and other chromatin binding proteins (HMG proteins) (25 seconds), but lower when compared to core histones (30min) (110-112). A typical Fluorescence recovery after photobleaching (FRAP) curve for H1 binding to chromatin suggests three populations of Histone H1: a rapidly diffusing fraction, a weakly bound fraction and a strongly bound pool (Figure 8).

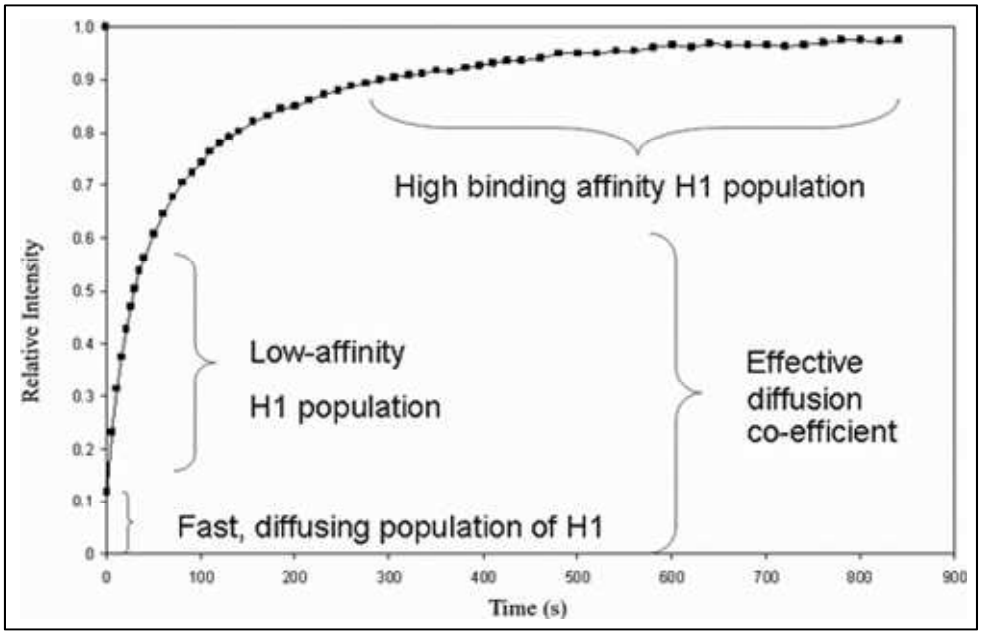

Figure 8: A typical FRAP curve for H1 binding to chromatin showing multiple populations. Figure adapted from (111)

Additionally the recovery pattern looks biphasic suggesting the existence of a low affinity H1 population and a relatively strongly bound H1. Efforts have been put to explain the H1 binding dynamics from this curve (113) and three different models proposed. Brown and colleagues (28) propose a two step process of H1 binding in which unstructured CTD make the initial contact with the linker DNA helping the globular domain to properly position the aminoacids at their specific position on the nucleosome (model I, Figure 9). This binding will in turn induce the formation of secondary structures in the CTD. This implies CTD binding would be responsible for the low affinity H1 population and the globular domain binding represent the high affinity binding. In other words, if the CTD fails to interact with linker DNA, further binding of H1 to the nucleosome will be compromised.

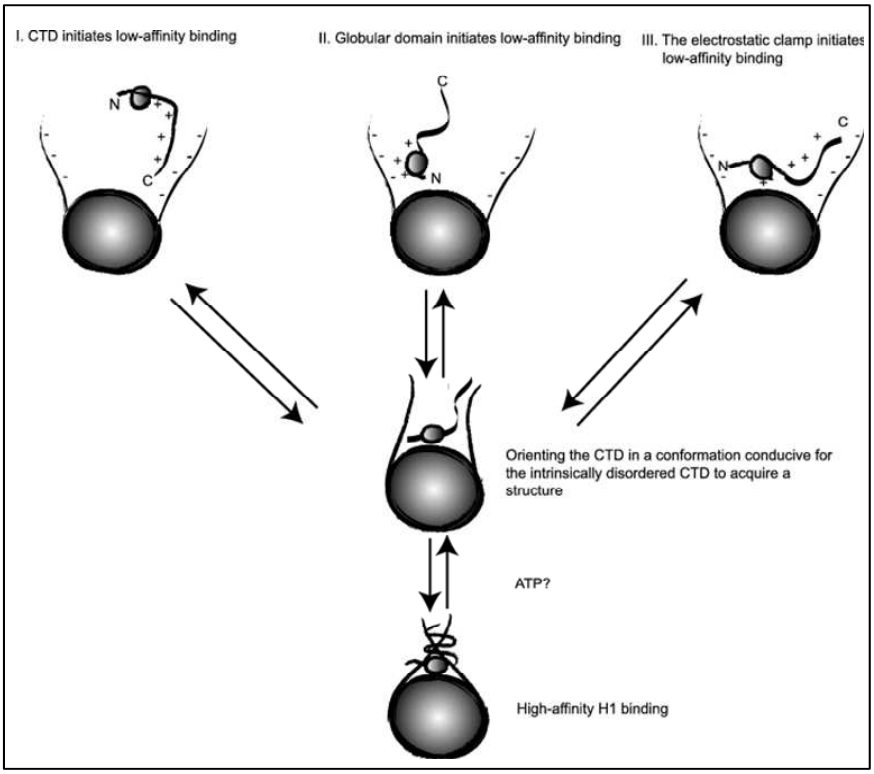

Figure 9: Alternative models for the reversible association of histone H1 with the nucleosome. In model I, the C-terminal domain (CTD) associates nonspecifically through electrostatic interactions with the linker DNA. In model II, the globular domain initiates a low-affinity binding interaction between the linker DNA and histone H1. In model III, both the globular domain and the CTD associate with the linker DNA to form an electrostatic clamp. Figure adapted from (111)

Another model (model II, Figure 9) suggests that GD initially interacts non-specifically with the nucleosome (low affinity binding population). This event in turn induce the three dimensional structure in the CTD, which accounts for the high affinity binding of H1 to the nucleosome. This model was suggested from the FRAP studies of CTD point mutants (28, 104, 107, 114) in which single lysine substitutions at either Thr152 or Ser183 leads to increased affinity of the linker histone to the nucleosome. Surprisingly a double mutant, where both the residues were substituted with lysine, showed a lower binding affinity, making this model questionable. In addition, this model cannot explain why only GD can initiate the nonspecific binding and not CTD.

Studies on swapped-domain mutants of different H1 subtypes, having different FRAP profiles, suggest that perhaps both the globular domain and the CTD of H1 are responsible for the low affinity binding. The DNA binding sites of globular domain and the positively charged CTD could act as an electrostatic clamp that positions H1 at the binding site (model III, Figure 9), consequently the CTD acquires a three dimensional structure necessary for high affinity binding.

I .4.4 Linker histone isoforms

Linker histone family is the most divergent class of histones, composed of related proteins with distinct species, tissue and developmental specificity. Figure 10 shows an overview of the number of currently characterized H1 variants in selected organisms (115) in an evolutionary tree. There are at least eleven different subtypes in human beings, classified on the basis of their discovery and the method of purification. There are at least 12 different systems of naming the histone variants (116, 117), which complicates their systematic study. In this thesis, for convenience, we will follow the Albig and Doenecke (118) way of nomenclature for human H1 variants and for mouse that of Seyedin and Kistler (119).

Linker histone variants differ in their timing of synthesis, rate of synthesis, turnover rates, phosphorylation status and ability to compact chromatin. Broadly they can be classified into three groups based on their expression pattern: histones expressed during S phase of the cell division (H1.1 to H1.5), histones with variant mode of expression in somatic cells (H1.0 and H1x) and germ cell specific histones (H1t, H1T2, H1LS1 and H1oo).

The genes of linker histones have been found to exist either clustered or solitary and their distribution in the genome was found highly conserved between the human, mouse and rat genomes (118, 120-124).

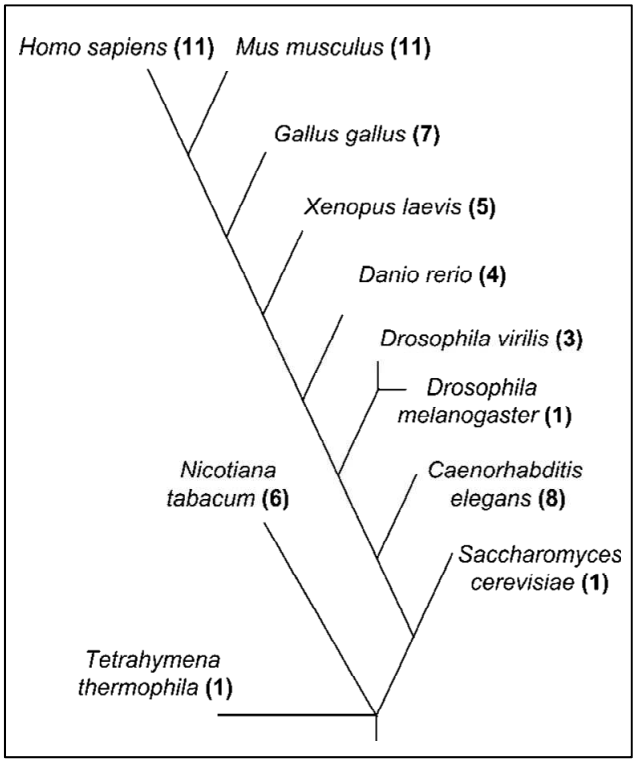

Figure 10: Number of H1 variants in various species. The species are shown on an evolutionary tree; the number of H1 variants is indicated in parentheses. M. musculus and H. sapiens possess two splice variants of H1oo. Image adapted from (115).

I .4.4.1 H1.1 – H1.5

Expressed initially in different tissues in prenatal conditions, H1.1 expression is restricted to thymus, testis, and spleen after birth. H1.1 has the highest turnover among the different variants, with a half-life of five days (125, 126). The studies by Pina group reported that the level of H1.1 decreases from 5% to 0.5% during the post-natal development of cortical neurons in rat brain and is replaced by the H1.4 variant.

Cosmopolitan in expression with highest levels of mRNA of all the somatic variants (127), H1.2 is replaced very slowly and hence has a slower turnover rate compared to H1.1. The expression level of H1.2 and H1.4 has been shown lower in actively transcribed chromatin, in comparison to facultative and constitutive heterochromatin which contains the four somatic main subtypes, H1.2–H1.4 (128). Recently (129), it was shown that H1.2 forms a repressor complex with co-repressor proteins YB1 and PURα. This complex inhibits promoter specific p53-dependent and p300 mediated transcription by a direct interaction of H1.2 with p53, thereby blocking chromatin acetylation. H1.2 has also been found to work in another pathway involving p53. Indeed, Konishi et al (74) have shown that X-ray irradiated cells release all of the H1 isoforms into the cytoplasm in a p53 dependent manner, however only H1.2 activate the apoptosis pathway by inducing the cytochrome C release from mitochondria. In agreement with this, cells from H1.2-deficient mice showed increased resistance to X-ray induced apoptosis. H1.2 is regarded as ‘ground state’ variant, responsible for a basal level of chromatin compaction (128).

H1.3 and H1.4, like H1.2, are also present in both quiescent and non-dividing cells of almost all the tissues and has a low turnover rate (125). Level of H1.3 and H1.4 has been shown to be depleted at active chromatin as well as chromatin poised for transcription (128). Immunofluorescence staining of the human fibroblasts, using specific H1 variant antibodies, show differential nuclear localization, with H1.5 preferentially localized at the nuclear periphery (130) and H1.3 and H1.4 displaying a punctuate staining pattern (128).

H1.4 has been found to participate in Msx1-mediated inhibition of myogenic differentiation. Msx1 (73) interacts *in vivo* with H1.4 and this complex has been found to regulate the activation and expression of MyoD gene during differentiation. This effect of Msx1-mediated inhibition was compromised upon specific H1.4 depletion.

H1.5 has been shown enriched at the heterochromatic regions of chromatin (109) in addition to its preferential localization at the nuclear periphery (130). H1.5 is present in reduced amounts in quiescent cells (60); and its levels decrease after completion of

development and differentiation (125). Moreover, after heat shock induction, H1.5 becomes lost from the activated HSP90 heat shock gene (128).

I .4.4.2 H1°/H5

Expression of H1° is essentially restricted to the specific cell types (131) and was discovered firstly in non dividing cells (132). The expression of this, replication independent expressed, variant of H1 is linked to cessation of DNA synthesis (133). Although having the shortest C-terminal tail, H1° binds to the chromatin with a moderate affinity compared to some others with longer C-terminal (109).

H5 is most similar to the mammalian replacement histone H1°, but a striking difference between the two linker histones is the differential distribution of lysine and arginine residues. Instead of having lysine at more than ten positions in its CTD, chicken and duck H5 carry arginine residues (134).

I .4.4.3 H1x

H1x is the least conserved histone H1 variant showing ubiquitous and replication independent expression. The distribution of H1x protein is non random with a preference in the less accessible regions of the genome (135).

I .4.4.4 Germ line specific linker histone variants

H1.t is a testis-specific variant which is highly divergent in its primary sequence from the other members of the family. Its expression is restricted from pachytene spermatocytes until round to elongated spermatid stages, where it constitutes up to 55% of the total linker histones in chromatin (136, 137). H1.t has a lower DNA condensing capacity than the other H1 subtypes and binds less tightly to oligonucleosomes (97, 138). This feature has been suggested to help maintenance of chromatin in a relatively open state during meiosis, facilitating meiotic events such as recombination (139). However, the H1.t-deficient mice show no specific phenotype and are as fertile as wild-type mice. Two opposite explanations have been suggested to explain this behavior. Some studies show that other H1-subtypes, fully compensate for the absence of this very specific linker histone (65, 140), others report that the other linker histones only partially compensate for H1t in spermatocytes and spermatids (141). In the latter case H1-deficient chromatin containing less linker histones would be like H1t-containing chromatin, less tightly compacted, allowing spermatogenesis to proceed.

A new spermatid-specific H1 variant, HILS1 (H1-like protein in spermatids), has been recently found in mouse and humans (142, 143). In contrast to H1t, mHILS1 is exclusively detected in the nuclei of elongating and condensing spermatids, whereas H1t is essentially detected until the round/elongating stages. This expression pattern highly suggests that HILS1 could replace H1t in elongating spermatids and play a role in the chromatin reorganization occurring in these cells.

H1.oo is the longest linker histone variant which is expressed in oocytes, from the secondary follicle to the two-cell stage embryo (62). The functions of this protein are still not clear. However it may have role in the regulation of specific genes during development.

I .4.5 Linker Histone post translational modifications

Recent proteomics approaches using mass spectrometry for the identification of purified peptides have added a wealth of knowledge to identify the histone post translational modifications. Just like other histones, H1 histones are targets of several post translational modification, in particular phosphorylation. Other modifications found in H1 are acetylation (144), methylation (145), ubiquitination (146) and N-formylation (144, 147). Figure 11 highlights the main residues of different H1 variants, identified till date, targeted for the post translational modifications.

Phosphorylation is the most intensively studied modification of H1 histones and has been suggested to play role in chromosome condensation during mitosis, transcriptional regulation (148), DNA repair, apoptosis and ATP-dependent chromatin remodeling (149-151). The role of H1 phosphorylation is still controversial as far as its role in chromosome condensation is concerned. Some earlier studies ruled out any association of H1 phosphorylation and chromosome condensation (68, 152-154). However dephosphorylation of H1 in mitotically arrested murine cells by kinase inhibitor staurosporine (155) was followed by chromosome decondensation.

H1 phosphorylation has been suggested to play a role in DNA replication (156-158). In fact there is progressive increase in H1 phosphorylation profile during the progress of cell division, existing as unphosphorylated and low-phosphorylated forms during S phase, becoming highly phosphorylated during late G2 and mitosis, till its sharp drop at the end of mitosis in telophase (159-164). In a recent report the replicating DNA and phosphorylated H1 were shown to colocalize (165), suggesting that H1 phosphorylation promotes DNA

decondensation during replication. Also there is an enrichment of phosphorylated H1 in transcriptionally active chromatin (166, 167).

Phosphorylation reduces the electrostatic charge of the linker histones and may interfere with their functions. In addition phosphorylation of specific sites in the CTD has been shown to cause a decrease in the proportion of α-helix and an increase in the β-sheet suggesting a role of phosphorylation through structural alterations (168). Phosphorylation decreases the affinity of H1 for DNA and increases its dynamic exchange within chromatin (169-173). Phosphorylation of H1 has been shown to increase the action of chromatin remodeling complexes in *in vitro* (151) experiments.

Unlike core histones, there is very little literature available for linker histone acetylation and methylation. In fact there are 10 and 2 lysine positions in H1 polypeptide identified as targets for acetylation and methylation respectively. These residues are distributed in the CTD and GD part of H1. The ones in GD have been suggested to play a role in H1 binding with nucleosome (144, 174). Deacetylation or methylation of K26 of H1 has been suggested to be implicated in the formation of facultative heterochromatin and transcriptional repression respectively (175, 176).

$TAF_{II}250$ mediates monoubiquitination of GD and hence may have an effect in DNA binding dynamics. DNA damage in the linker regions have been shown to induce H1 formylation. The exact role of H1 formylation is not clear, however it is speculated that it may have a role in the signaling functions normally associated with acetylation (144, 147).

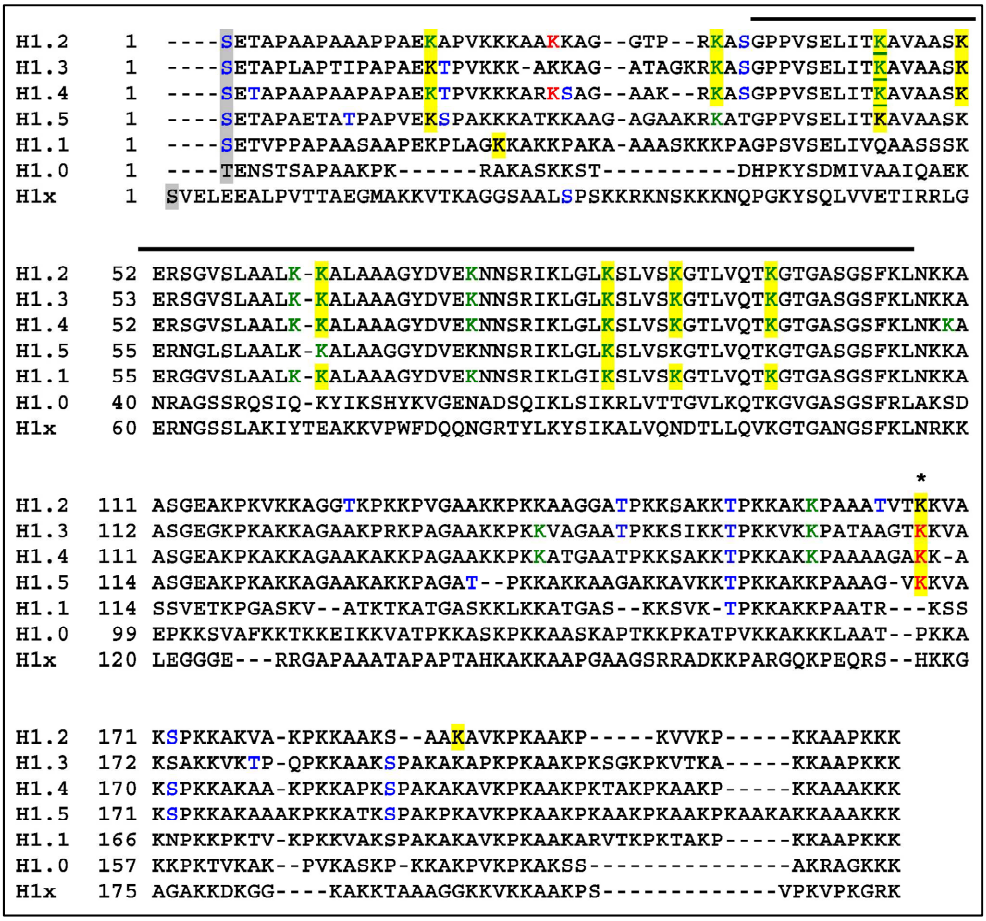

Figure 11: Posttranslational modification sites identified in human H1 isoforms. Residues: blue, phosphorylation; red, methylation; green, formylation; highlighted in yellow, acetylation; highlighted in grey, αN-terminal acetylation; underlined, ubiquitination. The sequence stretch representing the winged helix motif according to (177) is marked with a black bar. *Site of acetylation/methylation has not been assigned exactly: either acetylation of K168 and methylation of K169 or acetylation and methylation of K168 in H1.3 and H1.4 and of K167 and of K168 in H1.5, respectively (144). Image adapted from (178)

I .5 Structure of the 30-nm chromatin fiber

Under conditions of low ionic strength *in vitro*, isolated native chromatin is organized as 11-nm "beads on a string" (24) or "open zig-zag" filament (179), which upon increasing the ionic strength of the solution gets further compact to fibers approximately 30nm in diameter (20, 180). There is a lot of debate on the exact structure of the 30nm fiber. Earlier studies, using the electron microscopy and small-angle X-ray scattering (SAXS) suggested two different models of the chromatin fiber (Figure 12): first the one-start solenoidal helix, in which a linear array of nucleosomes is coiled (20) with bent linker DNA and the consecutive nucleosomes are next to each other (Figure 12A), and second, the two-start helix, in which nucleosomes are assembled in a zigzag with straight linker DNA connecting two adjacent stacks of helically arranged nucleosome cores (31, 181). Coiling or twisting of the two stacks

further divide the fiber models into two subclasses, named the helical/twisted-ribbon model (29, 31) (Figure 12B) and the crossed-linker model (32) (Figure 12C). In twisted-ribbon model linker DNA is oriented at angles varying from 0° to 50° to the fiber axis (29, 31) and in crossed-linker model the linker DNA is oriented approximately perpendicular to the fiber axis (32, 182).

Recent advances in the field came from the use of arrays of 601 nucleosome-positioning DNA (183, 184). A 9-Å crystal structure of a tetramer of nucleosome cores, based on a 167 NRL array without the linker histones (185), (Figure 13B) clearly showed folding of the two-start twisted ribbon type with a diameter of 25 nm. In addition a compaction density of 5–6 nucleosomes per 11 nm was reported and the results were supported by crosslinking experiments (185). To note is that the crystallization studies were carried out at very high salt concentration solutions.

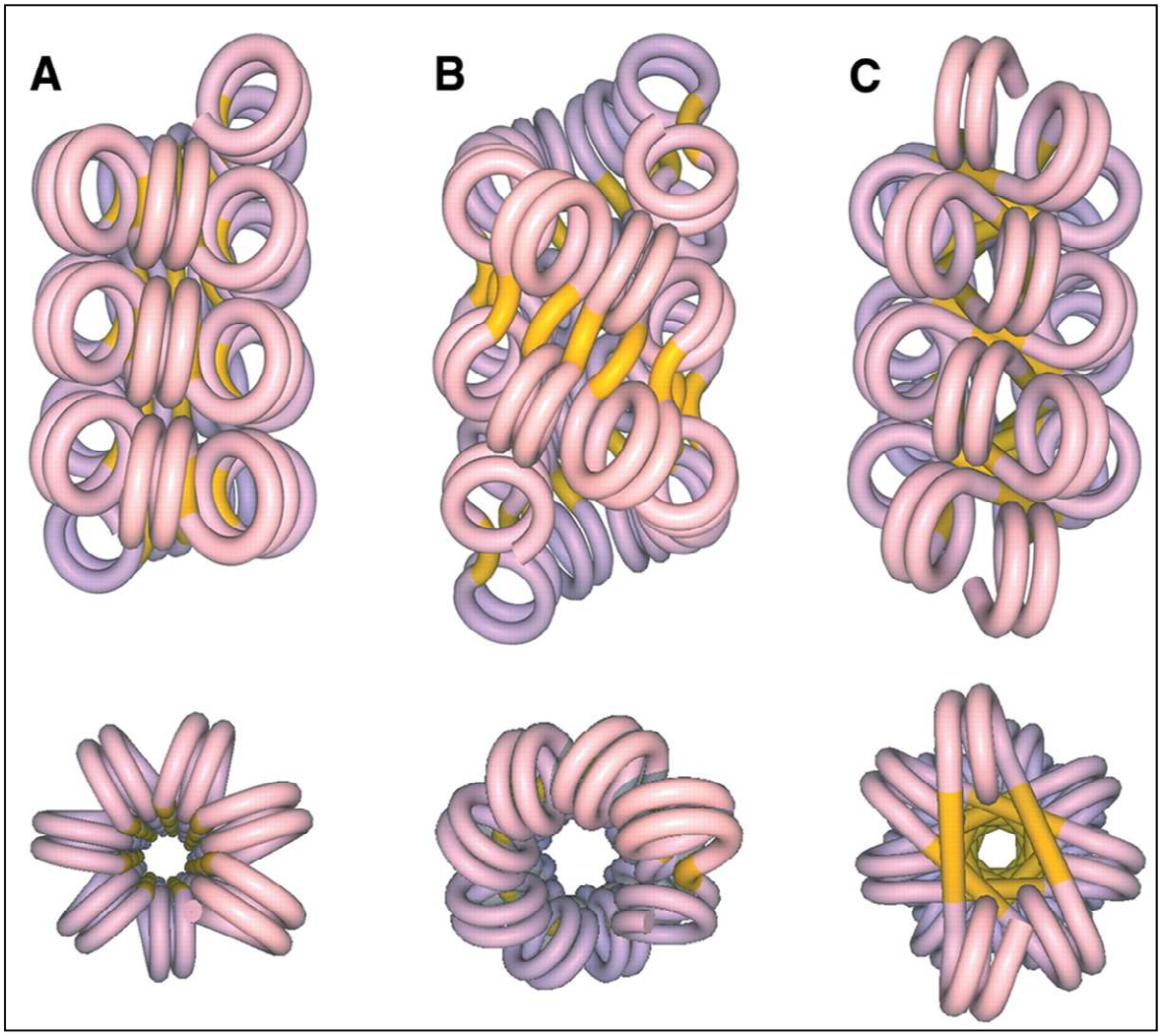

Figure 12: Models for the DNA path in the chromatin fiber. The image shows longitudinal views above and axial views below. (A) Solenoid model. (B) Helical ribbon model. (C) Crossed-linker model Figure adapted from (81, 186)

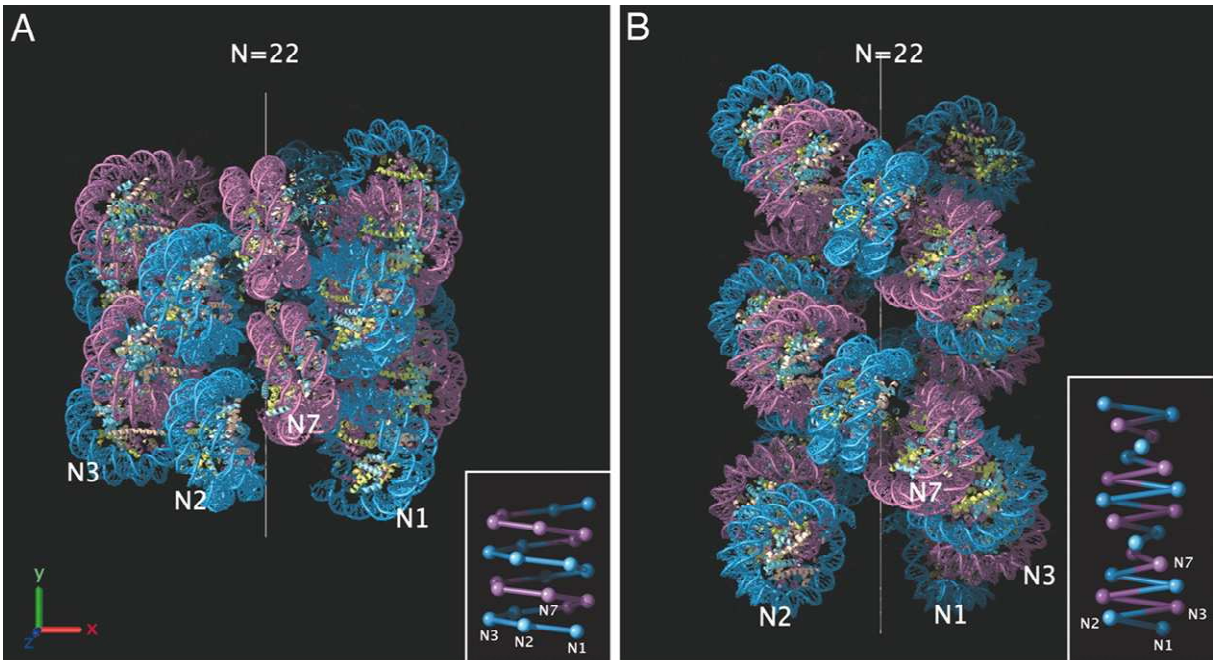

Figure 13: Two widely accepted models of 30nm chromatin fiber (A) Interdigitated one-start helix model (B) Two-start helical crossed linker model. Image adapted from (34)

Using the series of 601 nucleosome-positioning DNA arrays (NRL of 177, 187, 197, 207, 217, 227 and 237 bp) Robinson et al. (34, 184) studied the electron micrograph of the fiber in presence of linker histone at low divalent salt concentrations (1.6 mM $MgCl_2$), which produced a level of compaction corresponding to that obtained in physiological salt conditions. These studies conclude that the diameter of the fiber does not increase linearly with the length of the linker DNA, as expected from the crossed-linker model, but rather there are two distinct structural classes with distinct fiber dimensions and packing ratios. Arrays of NRLs 177–207 bp were shown to form fibers of 33-34nm diameter with a nucleosome packing ratio of ~11 nucleosomes per 11 nm. In contrast arrays with NRLs of 217–237 bp form fibers of 43 nm with a density of ~15 nucleosomes per 11 nm. The study concludes in favor of left-handed one-start helix with 5.4 nucleosomes per helical turn solenoid structure for the short linker arrays (Figure 13A) and suggests the crossed linker structure for long linker arrays (186).

Both of the above studies can be supported from the earlier studies of native and reconstituted fibers reported values of both ~6 and ~12 nucleosomes per 11 nm (187-189) and the ~13 nucleosomes per 11 nm for the native fibers from echinoid spermatozoa which has an average linker length of ~70 nm (190).

From the above described discrepancy it seems the 30 nm fiber, or the study of secondary folding of chromatin, remains an open field of investigation, without definitive proof of the existence of a single structure *in vivo*.

There are evidences that the chromatin fiber is stabilized and condensed by the electrostatic interactions between the nucleosomes. The fact that upon increasing the divalent cations concentration lead the 10nm primary fiber to condense to the 30nm secondary fiber is explained by the notion that these salts actually reduce the repulsive forces between the linker DNA which in turn favour these internucleosomal interactions (191). Crystal structure of the core particle (2) has shown the internucleosomal interactions between the highly basic histone H4 tail and acidic patch on the surface of the H2A-H2B dimer of an adjacent nucleosome. These specific interactions were shown important for the formation of 30nm fiber by indirect experiments like cross linking (185) and H4-N terminal tail (residues 14-19) deletion experiments (185, 192). Further mutational studies show that even a single modification at Lysine 16 of H4 was sufficient to inhibit the formation of the 30 nm fiber (193). On the other hand several histone H2A varaints has been found with altered acidic patch. H2AZ has an extended acidic patch and has been shown to alter the equilibrium dynamics of the 30nm fiber formation from the nucleosomal array and this ability is dependent upon just two amino acid residues in the acidic patch (192). Recently it was demostrated that H2A.Bbd cannot form a regular 30nm fiber (194, 195) and there are just three acidic amino acid residues within the acidic patch, that are required to correct the folding disorder in this varaint (194).

Linker histones influence the degree of chromatin compaction (180), ensure tightly packed fiber (196) and their removal leads to decondensation (197). Linker histone probably induce linker DNA bending (34) and alter the angle of entering and exiting DNA and induce a positive twist (186). Any protein which induce the twist in the fiber would favour folding while, conversely, proteins that bind to the linker and untwist DNA would favour unfolding (198). Linker histones are believed to increase the coiling of the fiber (186), and the process is a highly cooperative process (199). Linker histones like some other chromatin binding proteins (MeCP2) are considered to be the fiber-crosslinking proteins which facilitate and/or stabilze the interdigitation process (200, 201).

Core histone varaints, Linker histone varaints, histone modifications and chromatin remodeling machines are suggested to modulate the fundamental mechanism of opening up and closing the fiber (202).

I .6 Higher order structures of Chromatin beyond the 30 nm fiber

30nm fiber induced 50 fold DNA compaction (1) is not sufficient to fit the ~2 m DNA inside the micron sized nucleus. Cell has developed further, mainly unknown, strategies to

condense the DNA to interphase and metaphase chromosome structures. Several models have been proposed over the years. According to the radial loop model (203), DNA of interphase chromatin is negatively supercoiled into independent domains of ~85kb. Loops can be seen directly when the majority of proteins are extracted from the mitotic chromosomes. The resulting complex consists of the DNA associated with ~8% of the original protein content. As seen in (Figure 14), the protein-depleted chromosomes take the form of a central scaffold surrounded by a halo of DNA. This model suggests a form of organization of mitotic chromosomes in which loops of DNA of ~60kb are anchored in a central proteinaceous scaffold.

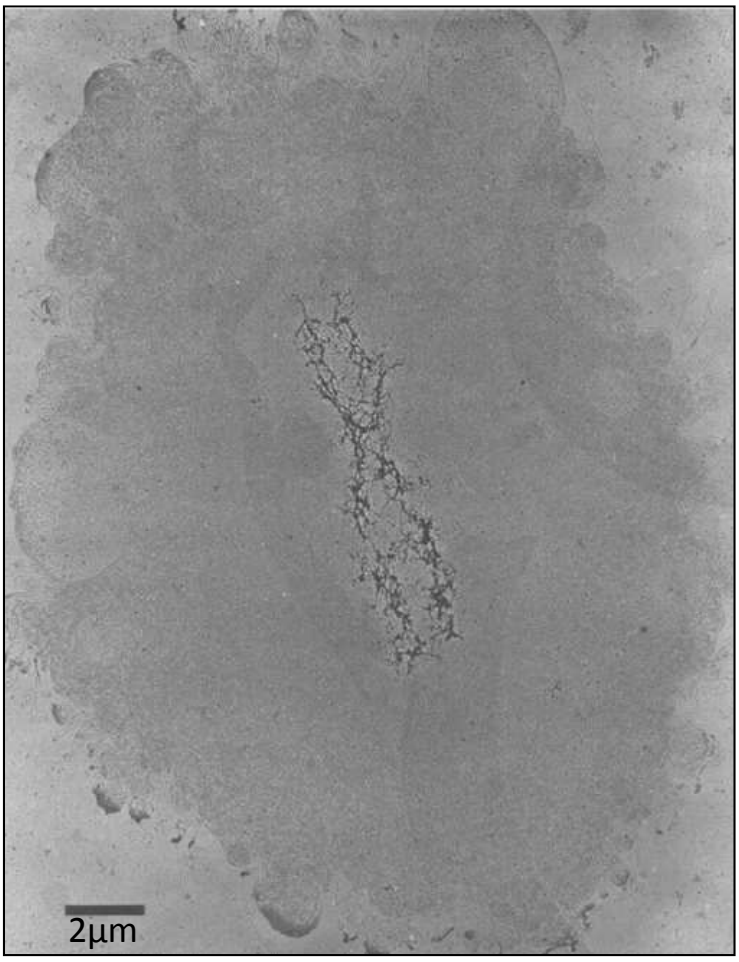

Figure 14: Electron - Micrograph of a Histone-Depleted Metaphase Chromosome from Hela. The chromosome consists of a central, densely staining scaffold or core surrounded by a halo of DNA extending 6-9 µm outward from the scaffold. Image adapted from (203)

In the chromonema model, it is believed that fibers with diameters of 60–80 nm are coiled into 100–130-nm fibers, which are in their turn coiled into the 200–300 nm fibers that constitute the most condensed chromosome structure in metaphase (204). Note that another model suggests the involvement of both loops and helical coils in the organization of metaphase chromosomes (205).

I .7 Chromatin territories

Interphase Chromatin can be distinguished into two domains or territories upon GTG staining (37, 206) (Figure 15); weakly stained regions called Euchromatin and brightly stained regions called Heterochromatin. These domains vary in gene activity, histone modifications, nucleosome packaging (207) and have presumably different higher order packaging (208, 209) and nuclear organization (210).

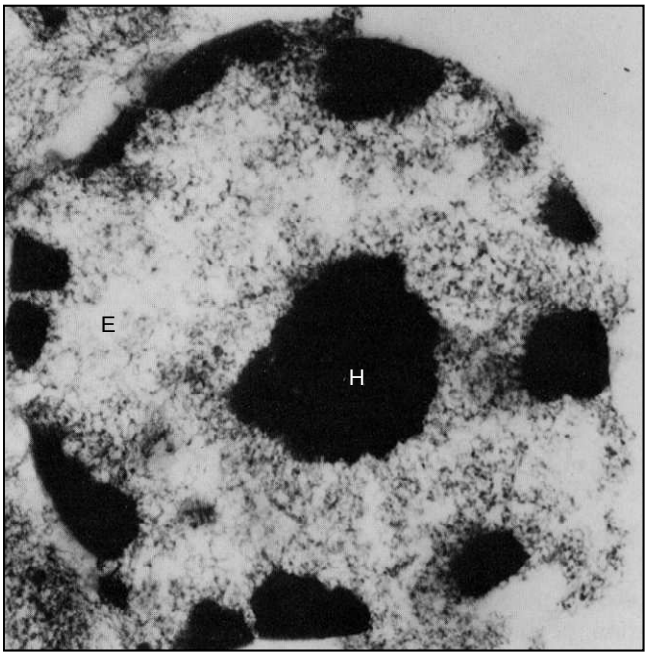

Figure 15: The distribution of Euchromatin (E) and Heterochromatin (H) in a normal thymus lymphocyte. Electron micrograph adapted from (211)

I .7.1 Euchromatin

Euchromatin is a lightly packed form of chromatin that is rich in gene concentration, and is often (but not always) under active transcription. It exists in a relaxed form in interphase, but compact during cell division. This compaction coincides with the cessation of the synthesis of mRNA during mitosis. Replication of these regions occurs during the early S phase. Euchromatin regions are marked by some histone modifications like methylation of lysine 4 of histone H3 (H3K4me) (212), methylation of lysine 36 of histone H3 (H3K36me) (213) and the hyperacetylation of histones H3 and H4 (H3ac, H4ac) (210, 214) (Figure 16).

I .7.2 Heterochromatin

Heterochromatin is generally a gene poor, rich in repetitive sequences, less accessible, condensed and transcriptionally inactive domain of the chromatin. It is spread everywhere in

the chromosome in small parts (215), but occupies predominantly the centric and subtelomeric regions of the chromosome. It is replicated late in the cell cycle (207, 216, 217). Centromeres, telomeres and the Barr body of the inactivated X chromosome are few of the main heterochromatic regions of the genome.

Heterochromatin is thought to play an important role in gene expression particularly during the development and differentiation (217). Repetitive DNA sequence, methylation of histone H3 lysine 9, heterochromatin protein 1 (HP1) and RNAi have been reported to play important roles in generating heterochromatin (217-223). In addition to usual machinery heterochromatin establishment in Drosophila, requires the recruitment of the histone H2Av variant and H4 Lys12 acetylation (224).

Heterochromatin is further divided into facultative heterochromatin and constitutive heterochromatin. Facultative heterochromatin is formed when silencing of genes is required by the cell; it appears during the development of an organism and exhibits varying degrees of condensation. The regions of DNA packaged in facultative heterochromatin will not be consistent between the cell types within a species, and thus a sequence in one cell that is packaged in facultative heterochromatin (and the genes within poorly expressed) may be packaged in euchromatin in another cell (and the genes within no longer silenced). However, the formation of facultative heterochromatin is regulated by proteins like Polycomb-group proteins and non-coding genes such as Xist (225). An example of facultative heterochromatin is X-chromosome inactivation in female mammals: one X chromosome is packaged as facultative heterochromatin and silenced, while the other X chromosome is packaged as euchromatin and expressed.

Constitutive heterochromatin is a permanent structural entity which unlike facultative heterochromatin, can never convert back into euchromatin. The regions of DNA that exist as constitutive heterochromatin will be the same for all cells of a given species. They occurs in certain chromosomal structures, such as at the telomeres, centromeres, and pericentric heterochromatic regions (223, 226).

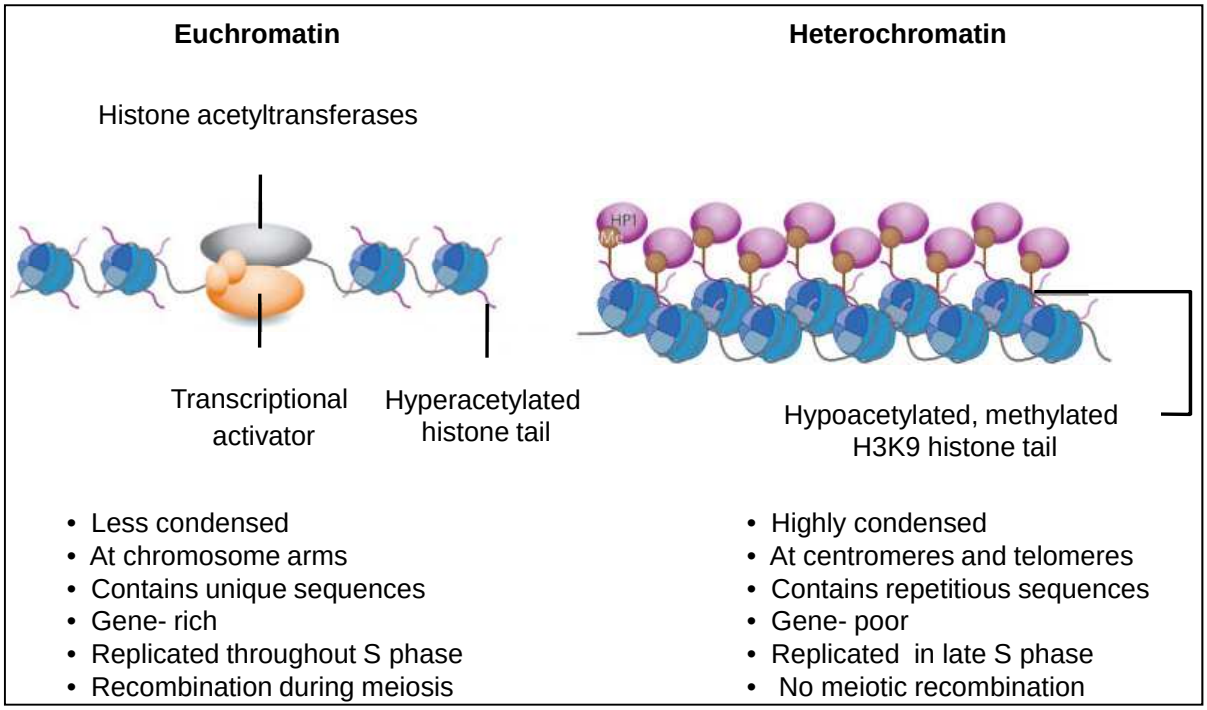

Figure 16: Properties of euchromatic and heterochromatic regions: The decondensed gene-rich euchromatin is permissive to transcription in contrast to highly condensed heterochromatin, which is resistant to gene transcription. Adapted from (210).

I .8 Chromatin Modifications and Their Function

Chromatin compaction creates a relatively inaccessible environment for the binding of regulatory proteins to the DNA template. However chromatin needs to be dynamic to regulate gene expression and other DNA-dependent nuclear processes such as DNA replication, homologous recombination, and DNA repair (227). To increase the dynamicity of the chromatin cell has developed three basic mechanisms to modulate the chromatin structure at molecular level, which are histone post translational modifications, ATP dependent chromatin remodeling and incorporation of histone variants.

I .8.1 Histone post translational modifications

Although discovered quite early (228, 229), covalent posttranslational modifications (PTM) of the core histones gained a lot of importance in the last decade for their suggested role in gene regulation and other DNA-templated processes (230). Histone PTMs have been shown to occur mainly on the flexible N-terminal tails that protrude from the nucleosome, in addition to previously uncharacterized modifications in the central histone-fold domains and C-terminal regions of the Histones (231). PTMs of the tail domain may alter the regulatory capacity of the nucleosome through changes in binding to effector proteins, where as

modifications in the histone-fold domains may directly alter nucleosome structure (232). These modifications serve as targets for protein recognition modules, like the bromodomain, which recognizes acetylated lysine (233, 234), and the chromodomain, which recognizes methylated lysine protein (234, 235). There are at least eight distinct types of modifications found over 60 different residues on histones (Table 2), including acetylation (236, 237), phosphorylation (238), monoubiquitination (239), sumoylation (240), ADP-ribosylation (241), deimination (242, 243) and proline isomerization (244). These modifications are dynamic, mostly reversible and have specific functions in gene regulation and other DNA-templated processes (245-247).

I .8.1.1 Histone Acetylation

Histone acetylation is mediated by histone acetyltransferases (HAT), which catalyze the transfer of acetyl groups from acetyl-CoA to the ε-amino terminal groups of specific lysine residues, mainly in the N-terminal tail of the histones with the exception of a recently discovered yeast protein SPT10 mediated acetylation of H3K56 at the promoters of histone genes (248) (Table 3). Acetyltransferases are divided into three main families, GNAT, MYST, and CBP/p300 (236), which modify more than one lysine but some limited specificity can be detected for some enzymes. The deacetylation process is carried out by other group of molecules called histone deacetylases (HDAC) which have been suggested in most of the cases to function in gene suppression. However histone deacetylation is also described for transcriptional activation in some cases (249-251). Acetylation is almost invariably associated with activation of transcription and has been suggested a role in chromatin assembly, chromosome condensation, DNA repair, apoptosis, VDJ recombination and dosage compensation in Drosophila (230, 252). Histone acetyltransferases can also acetylate non-histone proteins (e.g. the tumor suppressor protein p53 or the transcription factor UBF) and thereby influence their functions (253, 254).

I .8.1.2 Histone methylation

Methylation is a very well characterized PTM to date because of the highly specific nature of methytransferases, which can be broadly divided into Lysine methyl transferases and Arginine methytransferases.

Enzymes that Modify Histones	Residues Modified	Enzymes that Modify Histones	Residues Modified	Enzymes that Modify Histones	Residues Modified
Acetyltransferase		**Lysine Methyltransferase (conti.)**		**Lysine Demethylases (conti.)**	
HAT1	H4 (K5,K12)	MLL4	H3K4	JHDM2a	H3K9
CBP/P300	H3 (K14,K18) H4 (K5, K8) H2A (K5) H2B (K12, K15)	MLL5	H3K4	JHDM2b	H3K9
PCAF/GCN5	H3 (K9, K14, K18)	SET1A	H3K4	JMJD2A/JHDM3A	H3K9, H3K36
TIP60	H4 (K5, K8, K12, K16) H3 K14	SET1B	H3K4	JMJD2B	H3K9
HB01 (ScESA1, SpMST1)	H4 (K5, K8, K12)	ASH1	H3K4	JMJD2C/GASC1	H3K9, H3K36
ScSAS3	H3 (K14, K23)	Sc/Sp SET1	H3K4	JMJD2D	H3K9
ScSAS2 (SpMST2)	H4 K16	SET2 (Sc/Sp SET2)	H3K36	**Arginine Methlytransferases**	
ScRTT109	H3 K56	NSD1	H3K36	CARM1	H3 (R2, R17, R26)
Deacetylases		SYMD2	H3K36	PRMT4	H4R3
SirT2 (ScSir2)	H4 K16	DOT1	H3K79	PRMT5	H3R8, H4R3
Lysine Methyltransferase		Sc/Sp DOT1	H3K79	**Serine/Thrionine Kinases**	
SUV39H1	H3K9	Pr-SET 7/8	H4K20	Haspin	H3T3
SUV39H2	H3K9	SUV4 20H1	H4K20	MSK1	H3S28
G9a	H3K9	SUV420H2	H4K20	MSK2	H3S28
ESET/SETDB1	H3K9	SpSet 9	H4K20	CKII	H4S1
EuHMTase/GLP	H3K9	EZH2	H3K27	Mst1	H2BS14
CLL8	H3K9	RIZ1	H3K9	**Ubiquitilases**	
SpClr4	H3K9	**Lysine Demethylases**		Bmi/Ring1A	H2AK119
MLL1	H3K4	LSD1/BHC110	H3K4	RNF20/RNF40	H2BK120
MLL2	H3K4	JHDM1a	H3K36	**Proline Isomerases**	
MLL3	H3K4	JHDM1b	H3K36	ScFPR4	H3P30, H3P38

Table 2: A detailed list of known histone posttranslational modification enzymes along with the sites they modify. Only enzymes with specificity for one or a few sites have been included. Table modified from (230)

Lysine methytransferases catalyze the transfer of up to three methyl groups from S-adenosyl-methionine to the ε-amino terminal group of a single lysine residues, thereby creating mono-, di- or trimethylated lysines. In contrast the Protein arginine methytransferases (PRMT) generate both mono- or dimethylate arginine residues, either symmetrically or asymmetrically by transferring methyl groups to the guanidine group (255). Although the methylation was discovered 45 years back (256), but it was only in 2004 when first histone demethylase Lysine-specific demethylase 1 (LSD1) was reported to demethylate mono- and dimethylated H3K4, but not the trimethylated form (257). LSD1 has also been observed to remove one or

two methyl groups from H3K9 (258). Furthermore histone demethylase 1 (JHDM1), containing JmjC domain, was recently identified to catalyze the demetylation of mono and dimethylated H3K36 (259). Monomethyl groups of arginine are removed by way of the peptidylargenine deiminase 4 (PAD4), in which methylarginine is converted to citrulline (243).

Methylation has been described to activate as well as suppress transcription in different situations. Methylation of lysine 4, lysine 36 and lysine 79 of histone H3 (212, 260, 261) has been reported to activate gene expression, in contrast to di- and trimethylation of lysine 9 or 27 of histone H3 (262-265) in silenced genes. In fact it is shown that di- and tri methylated form of lysine 9 of histone H3 is a 'docking station' for HP1 (heterochromatin protein 1), and hence suggest a role in the establishment of heterochromatin (266, 267), similarly methylation of lysine 27 of histone H3 facilitates binding of Polycomb (268), a protein involved in maintaining the silencing state of homeotic genes during development.

I .8.1.3 Other covalent histone modifications

Important progress has been made, towards understanding the role of histone phosphorylation in processes such as transcription, DNA repair, apoptosis and chromosome condensation (269, 270). Phosphorylation of serine 10 and serine 28 of histone H3 is well documented in literature to occur during mitosis at metaphase and is important for mitotic chromosome condensation (271). H3 phosphorylation is also known to occur after activation of DNA-damage signaling pathways and has a role to facilitate DNA repair. Phosphorylation is also reported to occur in H2A variant H2A.X upon exposure to DNA-damaging agents (272, 273). Several kinases and phosphatases regulate the phosphorylation state of histones, such as Ipl1/aurora kinase and Glc7/PP1phosphatase (274). Histones can be ubiquitinated as well; a process wherein a 76 aminoacid peptide is added to lysine residues. This is the most recent modification to be linked to DNA repair. UV-induced DNA repair signals ubiquitination of H3 and H4 by the CUL4-DDB-Roc1 complex (275). Monoubiquitylation of H2A is also implicated in UV-induced DNA repair (276). Proline Isomerization enzyme, FPR4, has been identified in budding yeast that can isomerize prolines in the tail of H3 (244). FPR4 isomerizes H3P38 and thereby regulates the levels of methylation at H3K36. Deimination of histones involve the conversion of an arginine to a citrulline. Arginines in H3 and H4 can be converted to citrullines by the PADI4 enzyme (242, 277). The precise function of this process is yet to be known.

I .8.2 Chromatin remodeling

Remodellers are the multisubunit molecular motors which use the energy of ATP hydrolysis to move, destabilize, eject, or restructure nucleosomes to order (chromatin assembly) and/or expose them in a regulated manner for the execution of the DNA templated processes like gene transcription, DNA replication, DNA repair, and DNA recombination (278). Remodellers are currently classified into four different groups which share some similar structural and functional properties in addition to some specialized remodeler specific properties. All the remodelers share some features like having affinity for the nucleosome, possess some histone modification sensor domains, similar catalytic DNA dependent ATPase domain and possess domains and/or protein necessary for regulation of ATPase action and interaction with other chromatin or transcription factors (278, 279). The catalytic subunit is similar to the DEAD/H superfamily of ATP-dependent DNA helicases but is generally devoid of measurable DNA helicase activity. The four families of the multi subunit remodelers (Figure 17), which include SWI/SNF family, ISWI family, CHD family and INO80 family, vary in the type of other subunits other than the similar ATPase domain in their complex (280) (Table 3). All the chromatin-remodeling complexes have been shown to mobilize and relocate nucleosomes on DNA in a manner that requires them to translocate along DNA (281-284).

I .8.2.1 Different Chromatin remodeling Families

I .8.2.1.1 SWI/SNF family remodelers

The SWI/SNF (switching defective/sucrose non-fermenting) family remodelers include many protein complexes which are composed of 8 to 14 subunits (285). Most eukaryotes have two related SWI/SNF family remodelers, like SWI/SNF and RSC in yeast, which have similar catalytic subunits (Table 3). The catalytic ATPase of all the members has an HSA (helicase-SANT), a post-HSA, and a C-terminal bromodomain. In addition a pair of actin-related proteins (ARPs) is present in fungal complexes (286), whereas a dimer of actin and an ARP (hBAF53a/b) are present in higher orthologs (287). Other conserved subunits bear additional conserved domains; examples include hBAF155/170 (SANT, SWIRM), hBAF60 (SwiB) and human polybromo (multiple bromodomains). This family has established

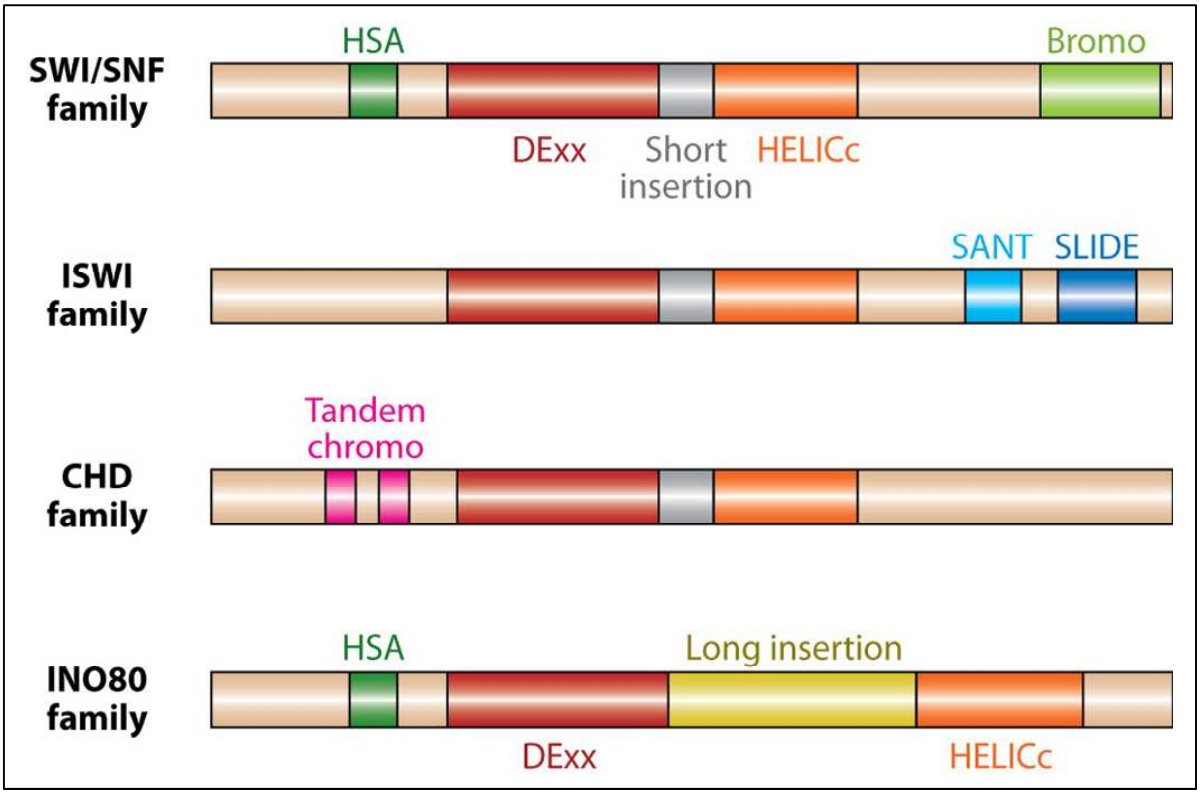

Figure 17: Remodeler Families, defined by their ATPase. All remodeler families contain a SWI2/SNF2-family ATPase subunit characterized by an ATPase domain that is split in two parts: DExx (*red)* and HELICc (*orange*). What distinguishes each family are the unique domains residing within, or adjacent to, the ATPase domain. Remodelers of the SWI/SNF, ISWI, and CHD families each have a distinctive short insertion (gray) within the ATPase domain, whereas remodelers of INO80 family contain a long insertion (yellow). Each family is further defined by the presence of distinct signature distinct combinations of flanking domains: Bromodomain (*light green*) and HSA (helicase-SANT) domain (*dark green*) for SWI/SNF family, SANT-SLIDE module (*blue*) for ISWI family, tandem chromodomains (*magenta*) for the CHD family, and HAS domain (*dark green*) for the INO80 family. Image adapted from (278)

roles in altering nucleosome positioning at promoters, which can regulate transcription either positively or negatively (278, 288, 289).

I .8.2.1.2 ISWI family remodelers

Earlier *in vitro* assays of nucleosome remodeling activity in *Drosophila* embryo extracts (290-293) led to the identification of three members of the ISWI (imitation switch) family named dNURF, dCHRAC, and dACF. ISWI-containing complexes were subsequently identified in many other organisms, including yeast and humans, highlighting the conserved function of this ATPase in chromatin remodeling. This family of remodelers contains 2 to 4 subunits (294) with one or two different catalytic subunits and some accessory subunits. In addition to highly conserved ATPase domains, ISWI contains SANT (ySWI3, yADA2, hNCoR, hTFIIIB) and SLIDE (SANT-like ISWI) domains, which together form a nucleosome

recognition module that binds to an unmodified histone tail and DNA (295). Specialized accessory proteins (Table 3) impart many domains to remodellers, like DNA-binding histone fold motifs (in hCHRAC (296-298)), plant homeodomain (PHD), bromodomains (hBPTF and hACF1) and additional DNA-binding motifs (HMGI(Y) for dNURF301). Many ISWI family complexes (ACF, CHRAC) help in chromatin assembly and nucleosome spacing, which in turn repress transcription (299). However, certain complexes (NURF) work antagonistally and can randomize spacing, which can assist RNAPII activation (300, 301), showing the role of accessory subunits in imparting the diversity to the function of the family.

I .8.2.1.3 CHD family remodelers

The CHD (chromodomain, helicase, DNA binding) family is characterized by two signature sequence motifs: tandem chromodomains (chromatin organization modifier) located in the N-terminal region, and the SNF2-like ATPase domain located in the central region of the protein structure (302, 303). The chromodomain is an evolutionarily conserved sequence motif involved in the remodeling of chromatin structure and the transcriptional regulation of genes (268, 304-306). The member complexes can be as small as monomeric in lower eukaryotes and can be in large complexes in vertebrates (Table 3). The accessory proteins in the complexes often bear DNA-binding domains, PHD, BRK, CR1-3, and SANT domains. Some of the CHD family members can promote transcription by sliding or ejecting nucleosomes while as others have repressive roles, like the vertebrate Mi-2/NuRD (nucleosome remodeling and deacetylase) complex (307), which contains histone deacetylases (HDAC1/2) and methyl CpG-binding domain (MBD) proteins.

I .8.2.1.4 INO80 family remodelers

The INO80 (inositol requiring 80) family (308) is a recently discovered family of remodelers and some of the members contain more than 10 subunits (Table 3). The higher ortholog members of the family like hINO80, hSRCAP (SNF2-related CREB-activator protein) and p400 also have HAT activity. The family is characterized by “split” ATPase domain, with a long insertion present in the middle of the ATPase domain, to which the helicase-related (AAA-ATPase) Rvb1/2 proteins and one ARP protein bind. Both yINO80 and ySWR1 complexes also contain actin and Arp4. INO80 has diverse functions, including promoting transcriptional activation and DNA repair. SWR1 is unique in its ability to

restructure the nucleosome by removing canonical H2A-H2B dimers and replacing them with H2A.Z-H2B dimers, thereby inserting the histone H2A variant H2A.Z.

I .8.2.2 Function of remodelers

A complete up to date reported function of the individual Chromatin remodeling complexes is shown in the form of Table 4 along with the references.

<table>
<tr><td colspan="2" rowspan="2">Family and composition</td><td colspan="12">Model organisms</td></tr>
<tr><td colspan="3">Yeast</td><td colspan="4">Fly</td><td colspan="5">Human</td></tr>
<tr><td rowspan="12">SWI/ SNF</td><td>Complex</td><td colspan="2">SWI/SNF</td><td colspan="2">RSC</td><td colspan="2">BAP</td><td colspan="2">PBAP</td><td colspan="2">BAF</td><td colspan="3">PBAF</td></tr>
<tr><td>ATPase</td><td colspan="2">Swi2/Snf2</td><td colspan="2">Sth1</td><td colspan="4">BRM/Brahma</td><td colspan="2">hBRM or BRG1</td><td colspan="3"></td></tr>
<tr><td rowspan="8">Noncatalytic homologous subunits</td><td colspan="2">Swi1/Adr6</td><td colspan="2"></td><td colspan="2">OSA/ eyelid</td><td colspan="2"></td><td colspan="2">BAF250/ hOSA1</td><td colspan="3"></td></tr>
<tr><td colspan="2"></td><td colspan="2"></td><td colspan="2"></td><td colspan="2">Polybromo BAP170</td><td colspan="2"></td><td colspan="3">BAF180
BAF200</td></tr>
<tr><td colspan="2">Swi3</td><td colspan="2">Rsc8/Swh3</td><td colspan="4">MOR/BAP155</td><td colspan="5">BAF155, BAF170</td></tr>
<tr><td colspan="2">Swp73</td><td colspan="2">Rsc6</td><td colspan="4">BAP60</td><td colspan="5">BAF60a or b or c</td></tr>
<tr><td colspan="2">Snf5</td><td colspan="2">Sfh1</td><td colspan="4">SNR1/BAP45</td><td colspan="5">hSNF5/BAF47/INI1</td></tr>
<tr><td colspan="2"></td><td colspan="2"></td><td colspan="4">BAP111/dalao</td><td colspan="5">BAF57</td></tr>
<tr><td colspan="4" rowspan="2">Arp7, Arp9</td><td colspan="4">BAP55 or BAP47</td><td colspan="5">BAF53a or b</td></tr>
<tr><td colspan="4">Actin</td><td colspan="5">β-actin</td></tr>
<tr><td>Unique</td><td colspan="3">a</td><td>b</td><td colspan="2"></td><td colspan="2"></td><td colspan="2"></td><td colspan="3"></td></tr>
<tr><td rowspan="12">ISWI</td><td>Complex</td><td colspan="2">ISW1a</td><td colspan="2">ISW1b</td><td>ISW2</td><td colspan="2">NURF</td><td>CHRAC</td><td>ACF</td><td colspan="2">NURF</td><td>CHRAC</td><td>ACF</td></tr>
<tr><td>ATPase</td><td colspan="4">Isw1</td><td>Isw2</td><td colspan="4">ISWI</td><td colspan="2">SNF2L</td><td colspan="2">SNF2H [c]</td></tr>
<tr><td rowspan="4">Noncatalytic homologous subunits</td><td colspan="4" rowspan="4"></td><td>Itc1</td><td colspan="2">NURF -301</td><td colspan="2">ACF1</td><td colspan="2">BPTF</td><td colspan="2">hACF1/ WCRF180</td></tr>
<tr><td rowspan="3"></td><td colspan="2" rowspan="3"></td><td>CHRAC -14</td><td rowspan="3"></td><td colspan="2" rowspan="3"></td><td>hCHRAC -17</td><td rowspan="3"></td></tr>
<tr><td>CHRAC -16</td><td>hCHRAC -15</td></tr>
<tr><td>NURF -55/p55</td><td></td><td>RbAp46 or 48</td><td></td></tr>
<tr><td>Unique</td><td colspan="2">Ioc3</td><td colspan="2">Ioc2, Ioc4</td><td></td><td colspan="2">NURF -38</td><td></td><td></td><td colspan="2"></td><td></td><td></td></tr>
</table>

a Swp82, Taf14, Snf6, Snf11.
b Rsc1 or Rsc2, Rsc3-5, 7, 9, 10, 30, Htl1, Ldb7, Rtt102.
c In addition, SNF2H associates respectively with Tip5, RSF1, WSTF to form NoRC, RSF and WICH remodelers.
d Amida, NFRKB, MCRS1, UCH37, FLJ90652, FLJ20309.

(Table 3 continued to next page)

CHD	**Complex**	**CHD1**		**CHD1**	**Mi-2/NuRD**	**CHD1**	**NuRD**	
	ATPase	Chd1		dCHD1	dMi-2	CHD1	Mi-2α/CHD3, Mi-2β/CHD4	
	Noncatalytic homologous subunits				dMBD2/3		MBD3	
					dMTA		MTA1,2,3	
					dRPD3		HDAC1,2	
					p55		RbAp46 or 48	
					p66/68		p66 α, β	
	Unique						DOC-1?	
INO80	**Complex**	**INO80**	**SWR1**	**PhodINO80**	**Tip60**	**INO80**	**SRCAP**	**TRRAP/ Tip60**
	ATPase	Ino80	Swr1	dIno80	Domino	hIno80	SRCAP	p400
	Noncatalytic homologous subunits	Rvb1,2		Reptin, Pontin		RUVBL1,2/Tip49a,b		
		Arp5,8	Arp6	dArp5,8 dActin1	BAP55 Actin87E	BAF53a		
		Arp4, Actin1				Arp5,8	Arp6	Actin
		Taf14	Yaf9		dGAS41		GAS41	
		Ies2,6				hIes2,6		
			Swc4/ Eaf2		dDMAP1		DMAP1	
			Swc2/ Vps72		dYL-1		YL-1	
			Bdf1		dBrd8			Brd8/TRC/p120
			H2AZ, H2B		H2Av,H2B		H2AZ,H2B	
			Swc6/Vps71				ZnF-HIT1	
					dTra1			TRRAP
					dTip60			Tip60
					dMRG15			MRG15 MRGX
					dEaf6			FLJ -11730
					dMRGBP			MRGBP
					E(Pc)			EPC1, EPC-like
					dING3			ING3
	Unique	Ies1, 3-5 Nhp10	Swc3, 5,7	Pho		d		

Table 3: Showing composition of remodeler complexes in different eukaryotes. Adapted from (278)

Family	Complexes	Biological functions	References
SWI/SNF	ySWI/SNF	Replication	(309)
		DNA repair	(310)
		Transcription activation, elongation, and repression	(297, 311-313)
		Targeting by activators, corepressors	(314-317);(313)
		Mitotic gene expression	(318)
	yRSC	DNA repair	(310, 319)
		Targeting by activators	(320)
		RNAPII and RNAPIII regulation	(321-324)
		Cell signaling	(323, 325)
		Spindle assembly checkpoint	(323)
		Chromosome segregation and cohesion	(326-328)
		Cell cycle progression	(329)
	dBAP,	RNAPII regulation and elongation	(330, 331)
	dPBAP	Metamorphosis and immune system function	(332)
	m/hBAF,	Targeting by activators, Transcription elongation	(321, 333-338)
	m/hPBAF	Signaling	(339)
		Differentiation and development	(287, 340-345)
		Tumor suppressor	(346-349)
		Viral integration and expression	(350)
ISWI	yISW1a,b	Transcription activation, elongation, and termination	(351-353)
	yISW2	Replication	(354)
		Transcription repression, repression of antisense transcription	(299, 355, 356)
	dISWI	Maintenance of higher-order chromatin, H1 loading	(300, 357, 358)
	d/hCHRAC	Chromatin assembly	(359-362)
	d/hACF	Replication	(363, 364)
	dNURF	Chromosome organization	(300)
		Transcription activation	(298)(299)(363)(364)(355)
		Embryonic development and differentiation	(300, 301, 365)
	dTRF2	Regulation of TATA-less promoters	(366, 367)
	dRSF	Silent chromatin formation, promoting H2Av replacement	(368)
	x/m/hWICH	Heterochromatin replication	(369)
		Activation of RNAPI transcription	(370)
	hNoRC	Replication, rDNA silencing	(371-374)

(Table 4 continued to next page)

CHD	CHD1	Chromatin assembly, H3.3 loading	(359, 375)
		Replication	(363)
		Transcription regulation, elongation, termination	(331, 351, 376, 377)
	mCHD2	Mammalian development and survival	(378)
	aPICKLE	Repression of seed-specific genes, embryonic to vegetative development	(379)
	dCHD3	Active transcription	(380)
	xCHD4	Control of neuroectoderm/mesoderm boundary	(381)
	m/hCHD5	Tumor suppressor	(382)
	hCHD8	Regional chromatin remodeling	(383, 384)
	NuRD	Transcription repression with deacetylation	(385)
		Regulation of development	(386, 387)
		Cell fate determination and differentiation	(388-390)
	ySHREC	Nucleosome positioning for transcription silencing for heterochromatin	(209)
INO80	SWR1	DNA repair (phospho-H2A recruitment)	(391, 392)
		H2A.Z incorporation	(393-395)
		Regulation of plant development and flowering	(396, 397)
	INO80	Replication	(398, 399)
		DNA repair (phospho-H2A recruitment)	(391, 392, 400-402)
		Core histones removal	(391, 392, 402)
		Homologous recombination	(403)
		Regulation of telomere length	(404)
		Regulation of transcription, RNAPII activation	(403, 405, 406)

Table 4: Summarizing the function of different members of chromatin remodeling family. Adapted from (278)

I .8.2.3 Mechanism of Chromatin remodeling

There have been many studies in the last decade to unravel the still debated molecular mechanism of the chromatin remodeling (407) and the role of different subunits in this process. Earlier studies have suggested that the energy from ATP hydrolysis is used to disrupt histone-DNA interactions within the nucleosome, which reflects in the experimental observations as change in the DNase I digestion pattern, increase in sensitivity of restriction endonuclease digestion, and enhancement in activator binding to nucleosomal DNA both *in vitro* and *in vivo*.

The ATPase and chromatin remodeling activity of different subclasses of the ATP-dependent chromatin remodeling enzymes requires distinct stimulatory factors for the catalytic activity *in vitro*. For instance, both naked DNA and nucleosomal DNA can stimulate the ATPase activity of the Swi2p/Snf2p and INO80 subclasses. However, Mi-2/CHD and ISWI ATPase activity is maximally stimulated by nucleosomal DNA rather than by naked DNA, and the histone H4 N-terminal domain is required for the ATPase activity and nucleosomal sliding activity of ISWI (408, 409).

Two major models have been proposed to explain the molecular events by which the ATP-dependent chromatin remodeling complexes can mobilize nucleosomes or change the nucleosome configuration. The first model “twist-diffusion model” suggests the generation of spontaneous torsional oscillation from the edge of nucleosome (410) which are propagated inside and may cause nucleosome migration one base pair at a time along the DNA (46). Chromatin remodeling enzymes may act as a “molecular ratchet” or a “DNA twistase” that allows the twist defect to exit in one direction and results in DNA twist tension (410). The observed “twist-defects” in the nucleosome crystal structures (411) supported such a mechanism. However, the model could not explain why a DNA nick or gap (loss of up to 10bp), which presumably dissipate the twist tension on DNA, had no effect on ISWI or RSC induced nucleosome remodeling (412-414). In addition, introduction of a DNA branch or hairpin as a barrier did not affect nucleosome remodeling by SWI/SNF and Mi-2 (415, 416). Moreover, ISWI-induced nucleosome sliding was facilitated by nicks in the linker DNA in front of the nucleosome (412).

Compelling evidences have rather favored the second model called “translocation model”. This model implies that the remodeler forms a complex, which has been recently shown stable and processive in ISW2 remodeler (284), with the nucleosome in a way so that the ATPase domain contacts DNA at two turns away from the dyad inside the core particle (Figure 18b, state 1). This then conducts directional DNA translocation by drawing in DNA from the linker and pumping it toward the dyad. This process may occur from the sequential or concerted action of two domains, a DBD that pushes DNA into the nucleosome (Figure 18b, state 1 to 2), creating a small DNA loop on the nucleosome, and a Tr that pumps that DNA toward the nucleosomal dyad (Figure 18b, state 2 to 3). The loop then propagates around the nucleosome by one-dimensional diffusion, breaking histone-DNA contacts at the leading edge of the loop and replacing them at the lagging edge of the loop (Figure 18b, state 3 to 4) (414, 417-420).

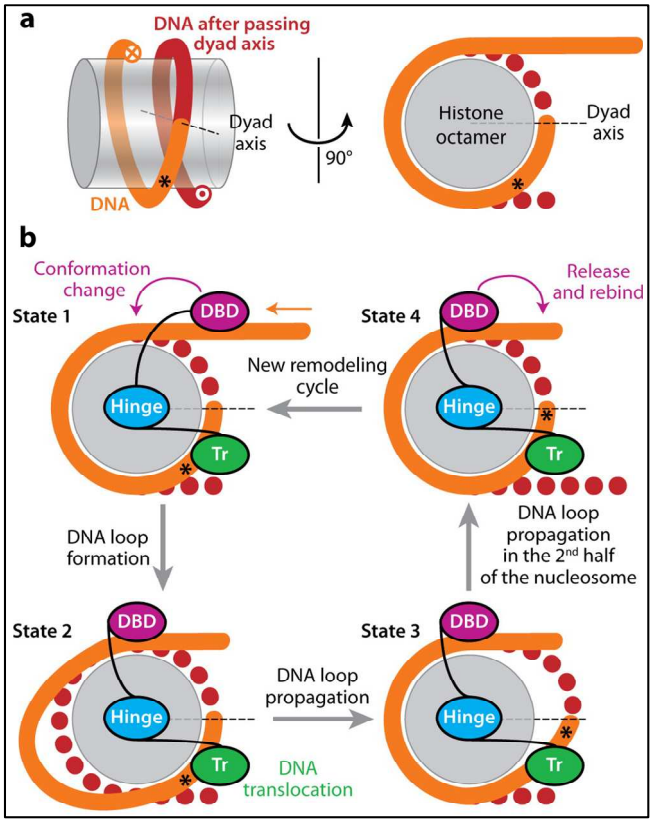

Figure 18: Model of DNA movement during a remodeling event. (a) At left, a nucleosome side view emphasizing the left-handed wrapping of DNA (b) States 1 to 4 represent the successive steps occurring during a remodeling event. The concerted action of a DNA-binding domain (DBD) located on the linker DNA and a translocation domain (Tr) located near the dyad generates a small DNA loop that propagates on the nucleosome surface. The remodeler undergoes a conformational change in its DBD when DNA loop is generated (State 1 to State 2), followed by the translocation of the DNA through the Tr domain, which passes the DNA loop to the dyad (State 2 to State 3). The DNA loop continues its propagation on the second half of the nucleosome surface by one-dimensional diffusion. Loop propagation then resolves into the distal linker, resulting in nucleosome repositioning (State 3 to State 4). The remodeler resets its conformation with original binding contacts, ready for a new remodeling cycle (State 4 to State 1). Figure adapted from (278).

I .8.3 Core histone Variants

Non-allelic isoforms of the conventional histones are called Histone variants which generally have specific expression, localization and species-distribution patterns (421). Discovered as early as in 1969 (1, 422), histone variants have gained a lot of attention in the recent past for their suggested role in the modulation of chromatin structure and dynamics, even though their exact role in such processes is still far from unambigious. Their incorporation into nucleosomes confers novel structural and functional properties of the nucleosome and has been implicated in epigenetic inheritance mechanisms of chromatin markings (423, 424) and shown to play significant roles in gene expression, antisilencing, heterochromatinization and the formation of specialised regions of the chromatin (425-428).

Histone variant genes vary from the conventional histone genes in expression pattern, number of genes and the type of mRNA they synthesize. Expressed generally from a single copy gene throughout the cell cycle, the mRNA of histone variants, in contrast to the conventional histones, is polyadenylated and the longer poly-A tail results in higher transcript stability (429). There are reported histone variant for all the conventional histones, except H4, which vary from the conventional counterparts from almost no aminoacid difference to extremely divergent changes (430).

I .8.3.1 H2A histone variants

The histone variants of H2A form the largest family of identified histone variants, including H2A.Z, MacroH2A, H2A.Bbd, H2A.X, TH2A, H2AL1 and H2AL2 (425, 427, 431, 432). H2A is a unique core histone which has an unstructured C-terminal tail, which makes it more susceptible for divergence in the evolution. This appeared to be related with the weaker interaction of the H2A-H2B dimer with both nucleosomal DNA and H3-H4 tetramer.

I .8.3.1.1 H2A.Z Histone Variant

One of the best studied H2A variants, H2A.Z comprises roughly 5–10% of cellular H2As and is a highly conserved histone variant. H2AZ sequences have been given different names in different organisms like H2A.Z (mammals), H2A.F (birds), H2A.F/Z (sea urchin), H2Av (*Drosophila*), Htz1 (*Saccharomyces cerevisiae*) and hv1 (*Tetrahymena*). H2AZ has been reported non essential in yeast and essential in *Drosophila* and mouse (433-436). X-ray crystallographic structure of the H2AZ nucleosome resembles the conventional nucleosome albeit with some local changes in the variant H2A.Z-H2B dimer and the $(H3\text{-}H4)_2$ tetramer interface. DNase I footprinting analysis also suggested that the structure of the H2A.Z nucleosome in solution closely resembles the conventional core particle (437). There have been contradictory reports about the stability of H2AZ reconstituted nucleosome arrays, some suggesting them less (437) and others report them more stable than the conventional ones (192). It is strongly believed that H2A.Z is important for both heterochromatin assembly and maintenance of higher order chromatin structure. The acidic patch of H2AZ was shown important *in vitro* for heterochromatin protein, HP1α, induced folding of nucleosomal array. *In vivo* suppression of H2A.Z resulted in perturbations in both the structure of constitutive heterochromatin and HP1α–chromatin interactions, which in turn lead to strong mitotic defects (438). H2A.Z is enriched in pericentric heterochromatin in postmeiotic X and Y

chromosomes (439) and also interact with the passenger protein INCENP (440), a member of the Aurora B kinase complex, which plays a crucial role in chromosome segregation and cytokinesis (441).

H2A.Z has been linked to both transcriptional repression and activation and was found to be partially redundant with chromatin remodeling complexes (434, 436, 442). Recent genome-wide high-resolution localization of H2A.Z in yeast (443-446) found that H2A.Z occupied promoters genome-wide, however there was some controversy among the reports about the precise location around the promoters. In addition H2AZ location correlated with both particular transcription factors and particular histone acetylation pattern (445, 447). In *Tetrahymena thermophila* H2AZ localizes to the transcriptionally active macronucleus indicating its role in the activation of gene expression. Chromatin remodeling complex Swr1 was found to aid in exchange the H2A-H2B conventional dimer for the H2A.Z-H2B variant dimer (393).

I .8.3.1.2 H2AX histone variant

Histone H2AX (14 kDa) is a ubiquitous, highly conserved H2A variant which represents up to 25% (depending of cell type and tissue studied) of the mammalian histone H2A family (448). It contains an evolutionary conserved SQ motif at the C-terminus (431). Phosphorylation of Serine 139 within the SQ motif yields a form known as gamma-H2AX (γ-H2AX) in response to double-strand DNA damage and apoptosis (449). γ-H2AX is essential for the efficient recognition and/or repair of DNA double-strand breaks (DSBs). Many molecules, often thousands, of H2AX become rapidly phosphorylated in vicinity of each nascent DSB. Three kinases belonging to the PIKK family, namely ATM, DNA-PK and ATR (450) have been suggested to be involved in the phosphorylation of H2AX and the generation of γ-H2AX. In response to the DNA DSB, chromatin remodeler INO80 is recruited through Nhp10 subunit to γ-H2AX (400) which then opens the DNA for the repair enzyme machinery. Also there are reports of specific interaction of NuA4 HAT complex (involved in the acetylation of histone H4) with γ-H2AX, suggesting that the chromatin acetylation by NuA4 was important for DSB repair (451).

H2A.X knockout in mice results in infertility in the male but not in the female due to failure of meiotic pairing by X and Y chromosomes and has been shown to initiate heterochromatinization in the sex body (452).

I .8.3.1.3 MacroH2A histone variant

MacroH2A, first discovered in rat liver, is an unusual histone H2A variant which is nearly three times the size of conventional H2A histone (42kDa). The N-terminal part of the protein is more like conventional H2A, sharing nearly 64 percent identity, while as the C-terminal domain also called as Non- Histone Region (NHR) or macrodomain resembles a leucine zipper (453) and is characteristic for numerous bacterial, archaebacterial and eukaryotic proteins (454). There is more diversification of macroH2A in humans where two mH2A genes, mH2A1 and mH2A2, were identified, which coded for two distinct, but closely related proteins (455-457). mH2A1, in turn, has two spliced variants, mH2A1.1 and mH2A1.2, which differed only by a short aminoacid sequence in the macrodomain (457).

Several reports in the literature suggest that mH2A could be involved in heterochromatin establishment or maintenance (458-461) and was found enriched in senescence-associated heterochromatic foci which are domains of repressed transcription associated with cell aging (446, 462). mH2A has been also localized to pericentric heterochromatin (463); and found associated with the facultative heterochromatin of the inactive X chromosomes (Xi) in female mammals (458), however immunofluorescence experiments suggest that there is overall higher nucleosome density within the Xi and not an enrichment of mH2A (464). In addition, mH2A is expressed at similar levels in male and female cells (465), suggesting that its function is not restricted to X-chromosome inactivation. Although, recent data illustrate a relatively weak (~1.5 fold) enrichment of mH2A1 all along the inactive X-chromosome (466). Interestingly, constitutive silencing of some autosomal genes, such as the IL-8 gene in B cells was shown mediated by macroH2A. In senescent cells the silent senescence-associated heterochromatin foci (SAHF) were found to be enriched in mH2A (446). In a recent report promoters of numerous genes particularly, the promoters of the inducible *Hsp70.1* and *Hsp70.2* genes, but not that of the constitutively expressed *Hsp70.8*, were shown highly enriched in mH2A1 (467). Macrodomains are reported to bind ADP-ribose with high affinity (468). This fact led to the discovery of a PARP-1-mH2A1.1-nucleosome complex. This interaction was found to be associated with inactivation of PARP-1 enzymatic activity. Heat shock released both mH2A1.1 and PARP-1 from the *Hsp70.1* promoter and activated PARP-1 auto modification activity. The studies suggest that mH2A1.1 recruits PARP-1 to the promoter, thereby inactivating it. Upon heat shock, the *Hsp70.1* promoter-bound PARP-1 is released to activate transcription through ADP-ribosylation of other *Hsp70.1* promoter-bound proteins (467).

Invitro, mH2A was found able to inhibit SWI/SNF nucleosome remodeling and to interfere with initiation of Polymerase II transcription (469, 470) which suggests that mH2A could be involved in transcription repression.

I .8.3.1.4 H2A.Bbd histone variant

Histone H2A.Bbd (Barr body-deficient) was first characterized in humans (471) and shown to be excluded from the female inactive X chromosome, hence named accordingly. The variant was shown to colocalize with the acetylated H4 in the genome suggesting its role in transcriptional activation (471). The protein sequence of the variant is highly divergent, sharing only 48% sequence identity with the conventional H2A and molecular evolutionary analyses have revealed that H2A.Bbd is a quickly evolving hypervariable mammalian histone variant, in striking contrast to all other histones known to date (430, 472). The protein being smaller in size (12.7 kDa) lacks a typical H2A family characteristic C-terminal tail as well as the very last sequence of the docking domain responsible for interactions with H3 in NCP (471, 473). In addition N-terminal tail of H2A.Bbd exhibits a row of six arginines, contains only one lysine residue in its entire aminoacid sequence compared to fourteen in canonical H2A. H2A.Bbd lacks the 'acidic patch' (E69, E100, and E101) (54) in the C terminal tail, which in turn impedes the inter-nucleosomal interactions within the H2A.Bbd nucleosomal array (194). Chromatin fractionation and sedimentation assays have shown histone H2A.Bbd to cofractionate and copurify with core histones (471) suggesting it an integral component of the chromatin. Histone H2A.Bbd can replace the conventional H2A in the *in vitro* nucleosome reconstitutions and form a novel and distinct structure which exhibit numerous structural perturbations compared to the conventional nucleosomes. These perturbations of the nucleosomal structure result in altering its stability, modifying its interaction with transcription factors, repair enzymes and affecting its mobilization by different remodeling complexes like SWI/SNF and ACF (473-479). DNase I footprinting profile showed that the perturbations exist all along the H2A.Bbd nucleosomal DNA (474). Micrococcal nuclease digestion data suggested that the variant octamer, which is stable only in presence of nucleosomal DNA, can organize only 118 base pairs of DNA and the unusual H2A.Bbd docking domain was found responsible for this open structure (473). However micrococcal nuclease digestion experiments in combination with atomic force microscopy (AFM) and electron cryo-microscopy concluded that the H2A.Bbd nucleosome organizes 130 bp of DNA and the entry exit angle of DNA was found to be 180^0 in contrast to the typical V shaped

configuration in the conventional nucleosome. In addition, FRAP and physiochemical experiments pointed to the lower stability of the variant particle (475) and the stability was shown dependent on the docking domain. The structural properties of H2A.Bbd are well characterized, but very few data are available regarding its localization in the nucleus and genome. Its biological role is not known. In humans, H2A.Bbd is detected by northern-blot in the testis by RT-PCR and in some cell lines (471). Recently H2A.Bbd was also detected in the mouse in lower amounts in other tissues (brain, liver, kidney, prostate) (472). The abundance of H2A.Bbd in the testis compared to other tissues where its presence is barely detectable, suggests that this histone is one of many variants involved in chromatin remodeling during spermatogenesis.

I .8.3.1.5 TH2A histone variant

TH2A is a variant of histone H2A, specifically expressed in the rat testis (480, 481). This variant differs from the histone canonical by only eight amino acids. TH2A is actively synthesized and incorporated into the chromatin of primary spermatocytes during the first meiosis. TH2A represents 60% of histone H2A type in pachytene spermatocytes and is suggested to have a role in chromatin organization during spermiogenesis.

I .8.3.1.6 H2AL1 and H2AL2

Chromatin undergoes a dramatic reorganization during spermiogenesis (482), resulting in the replacement of nucleosome based chromatin in round spermatids by highly compact protamine based condensed structure in spermatozoa, which has been shown to retain 10-15% of histones in the human sperm nucleus. The molecular mechanism of this process is still unknown. However global hyperacetylation of several of the core histones and the incorporation of histone variants have been shown involved in this process (483). Recently H2AL1 (H2A Like1) and H2AL2 (H2A Like2) have been identified in the mouse (483). Both variants are specific to mice and no sequence orthologue could be identified in the human genome. H2AL1 and H2AL2 were shown to express in different tissues, but the expression was found to be remarkably strong in testis during spermatogenesis (483). Both of them are expressed in round spermatids, accumulate in elongated spermatids (483) and have been shown to quickly disappear after fertilization in the one cell mouse embryos (484). Both variants were found specifically associated with the major satellite DNA and might be involved in the organization of pericentromeric regions during the late stages of

spermiogenesis (483). When expressed ectopically in somatic cells H2AL1 or H2AL2 has been shown to form dimers with either H2B or a testis specific H2B (TH2B), which are utilized to form the nucleosomes with H3-H4 tetramers. One of the aims of the present study is to analyze the properties of the nucleosomes containing the histone variant H2AL2.

I .8.3.2 H2B histone variants

Unlike H2A there are not many H2B histone variants identified so far. The ones identified are shown to be testis specific (485-488) and their functions are largely unknown. There are two reported H2B variants in humans, Th2B and H2BFWT.

I .8.3.2.1 TH2B histone variant

TH2B variant has been reported and found conserved in human, rat and mouse (489-493). The main differences in sequence between H2B and TH2B are located in the N-terminal tail of the histone, with three additional phosphorylation sites (Ser 12, Thr 23 et Thr 34), and to a lesser extent in the histone-fold domain. The C-terminal parts are completely conserved. Interestingly, most of the differences in the N-ter tail (and also the histone-fold domain) are conserved between the three species, and could be used in a spermatogenesis-specific signalization process (482). It has been shown that TH2B replaces the conventional H2B and remains the major form of H2B in round and elongating spermatids and gradually disappears in humans during the condensation of the spermatid nucleus (490). All this suggests a role in the chromatin reorganization process.

I .8.3.2.2 H2BFWT histone variant

H2BFWT is a recently reported H2B variant which has very low homology (45% identity) with the conventional H2B and presumed to be associated with the telomeric DNA (494). H2BFWT, in contrast to conventional H2B, has been found unable to recruit chromosome condensation factors and to assist in mitotic chromosome assembly. This loss of function is shown to be associated with the highly divergent N-terminal of H2BFWT (495). *In vitro* reconstituted H2BFWT containing nucleosomes showed DNase I footprinting pattern identical to this of the conventional nucleosome, indicating that the variant nucleosome may have very similar solution structure (495). However the exact function of this variant is still unknown.

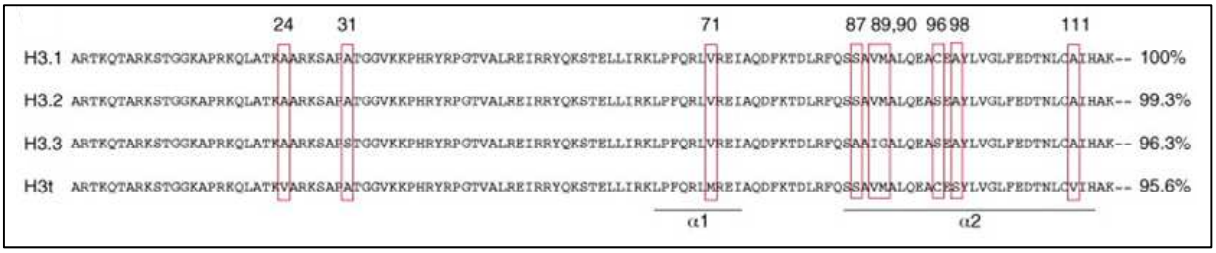

Figure 19: Sequence alignment of the main mammalian histone H3 variants: H3.1, H3.2, H3.3 and H3t. The amino acids that differ among the sequences relative to H3.1 are highlighted. Amino acids 87, 89 and 90 are key to preventing histone H3.1 incorporation into chromatin through the DNA-replication-independent (RI) pathway. The percentage of homology is shown on the right, taking the H3.1 sequence as 100%. The bars labeled α1 and α2 represent the residues that constitute two of the three α helices forming the histone fold domain. Figure adapted from (496)

I .8.3.3 H3 histone variant

Histone H3 variants have special role in the main cellular processes like chromosome segregation and transcriptional activation. Different organisms differ in the number of histone H3 variants and their nomenclature (Table 5). There are four somatic and one testis specific (H3t) (497) histone H3 variants in mammals. Somatic H3 variants H3.1 and H3.2 are the replicative histones expressed during S phase and are 99% identical. H3.3 is the replacement histone expressed throughout the cell cycle and is 96% identical to H3.1, differing at five amino acid residues (Figure 19). Centromeric protein A (CENP-A) is specifically present at centromeres and is highly divergent and shares only 46% identity with H3.1, whereas H3t differs from H3.1 by just four amino acids (496).

Organism	Replication dependent (replicative)	Replication independent (replacement)	Centromere
Saccharomyces cerevisiae	None	Hht1, Hht2 (H3.3-like)	Cse4
Schizosaccharomyces pombe	None	H3 (H3.3-like)	Cnp1 (SpCENP-A)
Neurospora crassa	None	H3 (H3.3-like)	H3v
Caenorhabditis elegans	H3	H3.3	HCP-3
Drosophila melanogaster	H3 (homologous to H3.2)	H3.3	Cid

[a] Owing to a lack of sufficient information at the time of writing, the H3t variant has been omitted from the table.

Table 5: Histone H3 variants in different organisms. Table adapted from (496)

I .8.3.3.1 Centromeric protein A (CENP-A) or CenH3

CenH3 is an essential protein (498), present in all eukaryotes and binds to centromeric DNA by replacing the conventional histone H3 (426, 499, 500). The sequence of histone fold domain is highly conserved while as N-terminal tails of CenH3 proteins are highly divergent among the different species (430). *In vitro* reconstituted CenH3 nucleosomes show a very similar structure as that of the conventional H3 nucleosomes (501). CenH3 interacts directly or indirectly with several kinetochore proteins (502) and is required for the formation of the functional centromeres (498, 503). CenH3 histone fold domain contains the centromere targeting information (504-506) while as the N-terminal domains are required for the binding of other kinetochore proteins.

CenH3 has been suggested to act as a specific epigenetic marker as it is retained in the mature spermatozoa and transmitted through generations. There is still no clearity in the literature about the mechanism of CenH3 deposition in chromatin. Recently a complex of CENH3, histone H4 and the chaperone RbAp48 (507) was isolated from *Drosophila* cells. RbAp48 was shown to promote the assembly of CenH3 nucleosomes *in vitro.* By using tandem affinity purification, a human multiprotein complex (CenH3 NAC) directly recruited by CenH3 nucleosome, was identified (508, 509). The complex was found to carry three new centromere proteins (CENP-M, CENP-N and CENP-T) which were essential for the assembly. Another study (509) reported a complex of transcription implicated protein FACT, histone chaperone nucleophosmin and CenH3 independent of CenH3 NAC.

A recent study in *Drosophila melanogaster*, suggests that the centromeric nucleosomes could contain only one copy of each histone (CenH3, H2A, H2B and H4) forming a tetramer around which would be complexed 120 bp DNA (510).

I .8.3.3.2 H3.3 histone variant

Contrary to the histone H3, variant H3.3 is expressed throughout the cycle cell (511, 512) and incorporated into chromatin independently of replication (513). H3.3 has been found to be the main form of H3 in the non dividing cells like neurons (514) and excess accumulation of H3.3 in nerve cells leads to further severity of Rett syndrome, a common mental disorder directly related to the loss of MeCP2, a methylated CpG binding protein (515). The subtle differences in aminoacid sequence between the histone H3.3 and canonical H3 would not affect the overall structure of the nucleosome. However they are responsible for

the low stability of the H3.3 nucleosomes (516). H3.3 has a serine at position 31, instead of an alanine in H3. The phosphorylation of this serine with unknown function occurs during the prophase in pericentromeric region (517).

H3.3 is highly expressed in dividing cells, and marks euchromatin (513). A good correlation was found in *Drosophila* between the transcriptional gene activity and genome-wide localization of H3.3 (518). In addition the epigenetic markers of H3.3, such as di- and tri-methylation of lysine 4 (K4), acetylation of lysine 9, 18, and 23 and methylation at K79, suggest its important role in the transcriptional activation. Recently a special class of NCPs containing two histone variants, H3.3 and H2A.Z has been found enriched at 'nucleosome-free regions' of active promoters, enhancers and insulator regions. These unstable NCPs could serve as ‘place holders’ to prevent the region from being covered by adjacent quite stable (canonical) NCPs and/or nonspecific factors and at the same time, could more easily be displaced by transcription factors (519)

Histone chaperone HIRA (514, 520) has been found responsible for the deposition of H3.3 in the genome.

OBJECTIVES

Linker histone H1 binds the nucleosome and interacts with an additional 20 bp of DNA as it enters and leaves the nucleosomal core to result in a structure called chromatosome. H1 serves to stabilize a higher order 30 nm diameter chromatin fiber that is fundamental to the structural organization of chromosomes. Structurally Linker histone consists of a globular "winged-helix" central domain flanked by basic NH_2- and COOH-terminal tail domains. Crystal structures of the nucleosome core particle and H1 globular domain have been resolved. However there have been many controversial reports, based on biochemical and imaging data, about where does linker histones bind to the nucleosomal core as the crystal structure of the chromatosome is not yet available. The main reason for these discrepancies in the data is either the undefined starting material (improper deposition of linker histones on nucleosomal template) or the lack of proper resolution in such studies. In addition, the role of long unstructured C-terminal domain of the protein, in chromatin condensation has not been fully addressed. Also there are no studies to show how newly discovered structurally open histone H2A variant nucleosomes, which carry a "disordered docking domain", will interact with the linker histone. By utilising a combination of high resoluition EC-M, OH° radical footprinting and coarse-grain DNA mechanics, we aim to address the following questions in the present thesis:

1 To develop and apply a very specific and physiological method of linker histone H1 deposition on the well positioned *in vitro* reconstituted nucleosomal substrate.

2 To determine the location of globular domain of H1 on the nucleosome and to validate the data with the currently published models.

3 To decipher the role of C-terminal tail in H1 induced "stem structure" of linker DNA and to develop a model, describing the interaction of H1 with the nucleosome.

4 To check the binding of H1 to structurally open histone variant H2A nucleosomes and to decipher the role of H2A docking domain in the process.

RESULTATS: CHAPITRE II

PUBLICATION 1
CARTOGRAPHIE DE L'INTERACTION NUCLEOSOME-H1 ET SON ORGANISATION 3D A LA RESOLUTION D'UNE BASE

Dans ce travail, a l'aide de la technique d'empreinte au radical OH°, nous avons montré que le domaine globulaire de l'histone H1 (GH1) interagit, a travers le petit sillon de l'ADN, avec 10 pb localisées symétriquement a l'axe dyade du nucléosome. En plus, GH1 organise approximativement une tour d'hélice de chaque ADN de liaison du nucléosome. Une série de sept aminoacides (120-127) est requise pour assurer la formation de la structure en tige de l'ADN de liaison. Nous avons construit un modèle mécanique en 3D de type « gros-grain » qui explique comment les diffèrent domaines de H1 interagissent avec l'ADN nucléosomale et qui prédit la génération de la structure spécifique en tige de l'ADN de liaison.

RESULTS:

CHAPTER II: PUBLICATION 1

ONE BASE PAIR RESOLUTION H1-NUCLEOSOME INTERACTION MAPPING AND 3D ORGANIZATION OF H1 CONTAINING NUCLEOSOME

Sajad Hussain Syed[1,3], Damien Goutte-Gatat[1], Nils Becker[2], Sam Meyer[2], Dimitar Angelov[3], Ralf Everaers[2], Jan Bednar[4,5]* and Stefan Dimitrov[1]*

(Manuscript submitted)

[1]Université Joseph Fourier - Grenoble 1; INSERM Institut Albert Bonniot, U823, Site Santé-BP 170, 38042 Grenoble Cedex 9, France

[2]Laboratoire de Physique and Centre Blaise Pascal of the Ecole Normale Supérieure de Lyon, CNRS UMR 5672, Université de Lyon, 46 Allée d'Italie, 69634 Lyon Cedex 07, France

[3]Université de Lyon, Laboratoire de Biologie Moléculaire de la Cellule, CNRS-UMR 5239/INRA 1237/IFR128 Biosciences, Ecole Normale Supérieure de Lyon, 46 Allée d'Italie, 69364 Lyon cedex 07, France

[4]CNRS/UJF, Laboratoire de Spectrométrie Physique, UMR 5588, BP87, 140 Av. de la Physique, 38402 St. Martin d'Hères Cedex, France

[5]Institute of Cellular Biology and Pathology, First Faculty of Medicine, Charles University in Prague and Department of Cell Biology, Institute of Physiology,Academy of Sciences of the Czech Republic, Albertov 4, 128 01 Prague 2, Czech Republic

*Corresponding authors:

e-mail: stefan.dimitrov@ujf-grenoble.fr, phone: +33476549473 ; fax: +33476549595

e-mail: jbednar@spectro.ujf-grenoble.fr, phone:+ 33476514761; fax: +33476635495

Running title: Histone H1 mapping on nucleosome

Keywords: chromatin/hydroxyradical footprinting/nucleosome/cryo-EM

II.1 Abstract

Despite the key role of the linker histone H1 in chromatin dynamics, its location and interactions with nucleosomal DNA are controversial issues. In this work we have used a combination of electron cryo-microscopy (EC-M), hydroxyl radical footprinting and nano-scale modeling to analyze the structure of precisely positioned mono-, di- and trinucleosomes containing physiologically assembled either full-length histone H1 or histone H1 truncated mutants. The one base pair resolution mapping by OH° footprinting showed that the globular domain of histone H1 (GH1) interacts, through the minor grove of DNA, with 10 bp localized symmetrically to the nucleosomal dyad. In addition, GH1 organizes about one helical turn of DNA from each linker of the nucleosome. A row of seven AA (120-127) of the COOH-terminus of histone H1 was required for the formation of the stem structure of the linker. A 3D molecular model, based on these data and coarse-grain DNA mechanics, was constructed. The model explains how the different domains of H1 interact with nucleosomal DNA and predicts a specific H1-mediated stem structure of the linker DNA.

II.2 Introduction

The nucleosome is the fundamental repeating unit of the genomic DNA arrangement in the nucleus of eukaryotic cells. The composition and the basic organization of the nucleosomes were established since few decades (1) and the structure of its dominant part, the nucleosomal core particle (NCP), was solved with nearly atomic precision by X-ray diffraction (3, 54). However, the same type of information for the structure of a complete nucleosome, i.e. the NCP containing linker DNA with associated linker histone, is still missing. Electron microscopy and electron cryo-microscopy (EC-M) imaging shows a relatively low resolution structure of the complete nucleosomes, both native (181) and reconstituted (521) and several important features of the structure remain obscure.

The globular domain of the linker histone appeared to be internally located in the 30 nm chromatin fiber (75, 76), but its exact position within the nucleosome remains the major controversy in the available data (for review see (78, 79, 81, 522-524). The second not yet clearly resolved question concerns the interactions and location of the linker histone C-terminus. These issues have their origin in difficulties related to preparation of well defined nucleosomal samples. The native chromatin has a natural variability both in the content of linker histone and the proportions of linker histone individual somatic subtypes. The preparation of reconstituted chromatin has been significantly facilitated by identification of the strongly positioning sequence 601 (183), which positions the histone octamer with high precision. The last step required for the formation of the complete nucleosome, the linker histone association, proved always to be a very delicate procedure.

The linker histone family is the largest one among other histone families. The linker histones and the core histone NH_2-termini are essential for the maintenance of the chromatin fiber and the mitotic chromosomes (78, 523, 525-527). The linker histones exhibit ~200 AA in length (the numbers vary slightly between species). The vast majority of the linker histone isoforms shares a common structural arrangement; rather short non-structured N-terminus (about 40 AA in length), followed by ~70 AA folded into structured (“globular”) domain, which is fused to about 100 AA long non-structured C-terminus, strongly enriched in lysines (about 40% of all AA). The widely used technique of linker histone association by stepwise salt dialysis does not assure its accurate positioning with the precision required for crystallography and in oligonucleosomal templates it is difficult to achieve native-like

stoichiometry (one linker histone per nucleosome) without at least partial aggregation. The situation can be considerably improved using competitor DNA technique (184).

It was recently shown that in *Xenopus laevis* extracts the embryonic form of linker histone B4 is associated with the histone chaperone NAP-1 (528). This identified NAP-1 as a chaperone for the linker histone B4 (528). It was further demonstrated that NAP-1 could be used to properly incorporate the somatic linker histone H1 as well as B4 in a dinucleosome DNA template containing a tandem repeat of the *Xenopus borealis* 5S RNA gene (92). The DNase I footprinting analysis of the 5S dinucleosome indicated that both B4 and H1 protected linker DNA (92). However, since 5S RNA gene sequence exhibits several translational positions (93), the histone octamers were not precisely positioned on the dinucleosome sequence, and it was difficult to understand how the linker histones interact with nucleosomal DNA in this heterogeneous population of di-nucleosomal templates.

In this study we have analyzed the structure of mono-, di- and trinucleosomes containing either histone H1 or its NH_2- and COOH-terminus truncated mutants. We have used 601 DNA repeats to reconstitute precisely positioned nucleosomal templates. The proper incorporation of histone H1 and its mutants was achieved by using NAP-1. The electron cryo-microscopy data showed that the 3D structure of the reconstituted trinucleosomes particles was indistinguishable from that of the native ones. In all templates studied, the globular domain of histone H1 (GH1) was found to interact specifically with 10 base pairs, localized symmetrically to the dyad axis of the nucleosome. GH1 appears also to organize additional 10 base pairs of DNA from each end of the nucleosome core particle. A stretch of 7 AA at the C-terminus of H1 (located in very close vicinity of the globular domain) was sufficient for both the local and 3D organization of the linker DNA. These data were used to construct a 3D model, which explains how histone H1 binds to the nucleosome and predicts a specific H1-mediated organization of the linker DNA.

II.3 Materials and Methods

II.3.1 Preparation of DNA fragments

The 423 bp dinucleosomal DNA and 623 bp trinucleosomal DNA fragments, containing two and three 601 nucleosome positioning sequences respectively, were sub-cloned from the 33x 200-601 chromatin array DNA (kindly provided by Daniela Rhodes). Prior to reconstitution, the fragments were excised from plasmid either by restriction enzyme EcoRV for cryoEM experiments (610 bp with outer linkers of 35 bp and 27 bp) or by enzymes

XbaI and EcoRI for Klenow radiolabelling. The outer linkers generated were 43 bp and 32 bp while the length of internal linkers was 52 bp in all cases. To probe the binding of globular domain on both strands, named upper strand and lower strand for convenience, of dinucleosomes, the two strands were separately Klenow filled either at EcoRI or XbaI cleaved overhangs respectively. The 255-bp DNA fragment, containing the 601 nucleosome positioning sequence at the middle, was obtained by PCR amplification from plasmid pGem-3Z-601 (kindly provided by J. Widom and B. Bartholomew) using 5` labeled primer for the corresponding lower strand of dinucleosome.

II.3.2 Clone construction and Protein purification

Full length 227 amino acid human H1.5 clone was used to prepare the deletion mutant peptides 1-177, 1-127, 35-127, 35-120 and 40-112 (GH1). The corresponding proteins were expressed by the standard IPTG induction in transformed BL21- RIL bacterial cell line. The soluble proteins were purified first by SP sepharose and later by using 1ml Resource S cation exchange column (Biorad) using FPLC. Mouse NAP-1 (mNAP-1) was also bacterially expressed and purified by Resource Q anion exchange column. Purified proteins were analyzed by 15% SDS-PAGE and stained with coomassie blue. Recombinant *Xenopus laevis* full-length core histones (H2A, H2B, H3 and H4) were produced in bacteria and purified as described (529).

II.3.3 Nucleosome Reconstitution, H1 deposition and footprinting

Mononucleosome, dinucleosome and trinucleosome particles (without linker histone) were reconstituted by the salt dialysis procedure (530). Briefly chicken erythrocyte carrier DNA fragments (150–200 bp) and 50 ng of ^{32}P labeled 601 DNA were mixed with equimolar amount of histone octamer in nucleosome reconstitution buffer (2M NaCl, 10 mM Tris pH 7.4, 1 mM EDTA, 5 mM MeEtOH and 10% glycerol) and serially dialysed to low salt (10 mM NaCl) buffer. Trinucleosome reconstitutions for cryo-EM experiments were carried out without any carrier DNA.

II.3.4 NAP-1 mediated deposition of H1

Full length H1 or its deletion mutants were mixed with mNAP-1 in a 1:2 molar ratio (buffer 20 mM Tris-HCl, pH 7.5/0.5 mM EDTA, 100 mM NaCl, 1 mM DTT/10% glycerol, 0.1 mM PMSF) and incubated at 30°C for 15 minutes. Dinucleosomes were mixed with

different concentrations of linker histones or linker histone/NAP-1 complexes in binding buffer (15 mM Tris-HCl, 0.3 mM EDTA, 0.2 mM DTT, 2% glycerol, 25 mM NaCl) at 30°C for 30 min to find the saturation concentrations. Samples were run on 5% native PAGE in 0.3xTBE. After electrophoresis, the gels were dried and analyzed by autoradiography. Saturated H1 and deletion mutant bound dinucleosomes were used for DNase I footprinting and analyzed on 8% urea denaturing gel as described previously (531).

II.3.5 Hydroxyl radical footprinting

To perform the hydroxyl radical footprinting, the H1 (or H1 deletion mutants) saturated mono, di and trinucleosomes were buffer exchanged (few times using 100 kDa cut off centricons) to be in the final quencher free nucleosomal buffer (5 mM Tris, 5 mM NaCl and 0.25 mM EDTA). Briefly, 15 µl reaction mixture containing 150 ng of full length H1- or H1 deletion mutant bound nucleosomes in nucleosomal buffer were aliquoted at the bottom of an eppendorf tube. Subsequently the hydroxyl radical reaction was carried out by mixing 2.5 µl each of 2 mM $FeAmSO_4$, 4mM EDTA, 0.1 M ascorbate and 0.12% H_2O_2 together in a drop on the side of the reaction tube before mixing it with the reaction solution. The concentration of Fe(II)EDTA in the reaction mixture was varied to achieve different cleavage yields. The reaction was stopped by adding 100 µl stop solution containing 0.1% SDS, 25 mM EDTA, 1% glycerol and 100 mM Tris pH 7.4, and the DNA was phenol/chloroform purified and ethanol/glycogen precipitated.

II.3.6 Cryoelectron microscopy:

Trinucleosome reconstitutions were performed without any carrier DNA. Full length H1 and H1 deletion mutants were deposited in complex with mNAP-1 as described above. The final reaction mixes were concentrated to 200 ng/µl of DNA and buffer exchanged against nucleosomal buffer using 100 kDa cut off centricons. Immediately after the buffer exchange, the samples were prepared for cryo-electron microscopy as described earlier (478). Briefly, 3 µl droplet of the solution was deposited on an electron microscopy grid with home made perforated supporting film with surface treated by successive evaporation of carbon and platinum/carbon layers. The excess of the solution was removed by brief blotting using Whatman No 1 filter paper and the grid immediately plunged into liquid ethan (-183°C). Grid was transferred without re-warming into Tecnai G^2 Sphera 20 electron microscope using Gatan 626 cryotransfer holder. Sample was visualized at 80 kV acceleration voltage using low

dose operation mode with total electron dose not exceeding 15 e/sÅ^2. Images were recorded on Gatan Ultrascan1000 slow scan CCD camera at microscope nominal magnification either 14500x or 25000x (final pixel size 0.7 and 0.4 nm) with 2.5 µm underfocus.

II.3.7 Mathematical analyses and structural model rebuilding

II.3.7.1 Relative accessibilities of nucleosomal DNA to OH°

Raw intensity traces of OH° footprinting gels were processed by automated band counting, band-wise integration and finally rescaling within a moving window (see Supplementary methods). The resulting signal represents the OH° accessibility per nucleotide, corrected for global trends and irregularities in the gel.

II.3.7.2 Visualization

The molecular visualization package Chimera (532) allows rendering of molecular structures using a color code for user-defined atom attributes. This feature was used to present the relative accessibility signals by color coding the deoxyribose C5' atoms. Footprints were measured for one of the strands. Color-coding on both strands of DNA was displayed, by exploiting the two-fold symmetry of the nucleosome. Bases, for which no single nucleotide resolution footprinting was available, were not colored.

II.3.7.3 Structure-derived accessibility profiles

DNA is attacked by OH radicals primarily at the C5' atoms of the backbone sugars (533). Per-C5' unified atom accessible surfaces were calculated with the MSMS program (534) as implemented in the molecular visualization system Chimera (532) (see Supplementary information for detail).

II.3.7.4 Structural model rebuilding

Three structural models (28, 84, 91) for linker histone placement were rebuilt, by manually matching the reported protein α-helix orientations and protein-DNA contact sites. As a molecular model for the linker histone globular domain, an NMR solution structure of H1 was used (535) (see Supplementary methods for details).

II.3.7.5 Restrained energy minimization

We have carried out a restrained energy minimization with the boundary conditions of free linker ends and linker start base-pairs fixed in their nucleosome core particle conformation (54). For energy minimization, we have employed the sequence-dependent rigid base-pair model of DNA elasticity (with the "MP" parameter set, as described in (536, 537). DNA volume exclusion was included by placing purely repulsive Lennard-Jones spheres with 2.05 nm diameter around each base-pair. To enforce contacts between the two DNA linkers at the corresponding maximally protected sites, linear springs were introduced between the C5' atom positions at the minima of the full-H1 accessibility profile. Note that the symmetric construction of the linker protection patterns and the symmetry of the nucleosome structure (which provides the boundary conditions), lead to a stem conformation of the linker with the same two-fold symmetry (see Supplementary methods for details).

II.4 Results

II.4.1 NAP-1 mediated assembly of H1 and its mutants to nucleosomal templates

We have reconstituted strongly positioned mono-, di- and trinucleosomes by using 601 DNA templates. These nucleosomal samples were then used as substrates for binding of full length recombinant linker histone H1 or its truncated mutants (Figure 1). The recombinant proteins were purified to homogeneity (Figure 1B) and allowed to interact with the nucleosomal samples either in the presence or the absence of NAP-1. Then the binding of histone H1 was studied by EMSA (Figure 1C). As seen, in the absence of NAP-1, upon raising the ratio H1:dinucleosomes, the samples begin to aggregate and at higher ratio a smear all along the lane of the gel is observed (Figure 1C, lanes 7-10). This result is in complete agreement with the reported data and reflects the improper association of histone H1 with the dinucleosomes (92, 528). Very similar results were obtained when mononucleosomes were used in the binding reactions (not shown). When NAP-1 was, however, present in the reaction mixture a completely different picture was observed. Indeed, the NAP-1 assisted binding of histone H1 resulted in a sharp band with well defined mobility (Figure 1C, lanes 3-6). Importantly, higher increase of the ratio H1: dinucleosome in the reaction did not change either the shape or the mobility of the band.

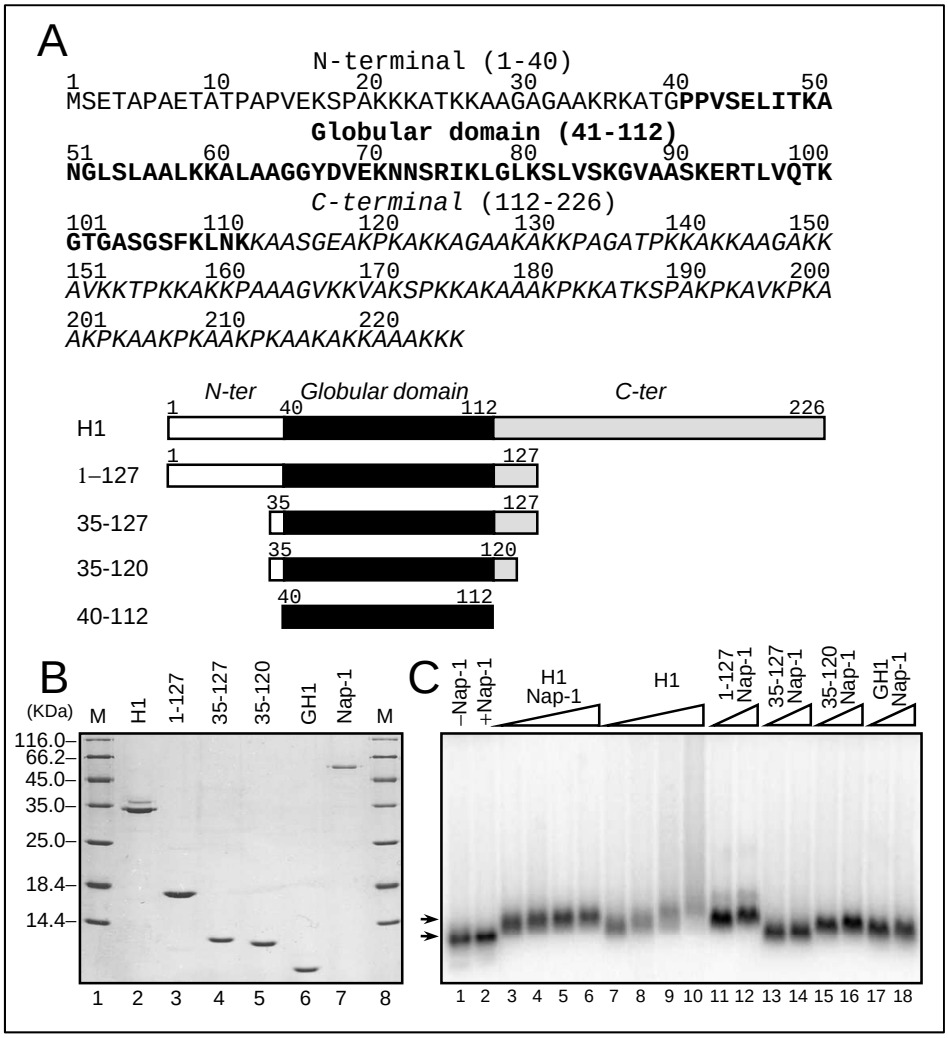

Figure 1: NAP-1 allows the proper incorporation of linker histone H1 and its truncated mutants in 601 dinucleosomal templates. (A) Primary structure of histone H1 (upper panel) and schematics of the different histone H1 mutants (lower panel) used. The globular domain is in bold (upper panel) or in black (lower panel). The beginning and the end of the different mutants are indicated. (B) 15% SDS-PAGE of purified recombinant full length H1, its truncated mutants and NAP-1. M, protein molecular mass markers. The molecular masses of the markers are indicated in the left part of the figure. (C) NAP-1 functions as a chaperone for full length H1 as well as for its truncated mutants. Positioned 601 di-nucleosomes were incubated for 15 min at room temperature with increasing amount of either full length histone H1 alone (lanes 7-10) or with NAP-histone H1 complex (lanes 3-6) or with a complex of NAP-1 with the indicated H1 truncated mutants (lanes 11-18). The samples were then run on 2% agarose gel under native conditions. The positions of both non-associated (-H1) and associated (+H1) with linker histones dinucleosomes are indicated by arrows. Lane 1, control dinucleosomes without H1; lanes 2, dinucleosomes incubated with NAP-1 only. The molar ratio NAP-1: linker histone was 2:1.

These results agree with the literature and illustrate the capacity of NAP-1 to act as a histone H1 chaperone able to properly deposit it in the nucleosome (92, 528). Interestingly, NAP-1 was also able to deposit the different H1 truncated mutants, including the globular domain of histone H1, GH1 (AA 40-112), in the nucleosome (Figure 1C, lanes 11-18). This suggests that the specific association of NAP-1 with H1 is essentially realized through interaction with GH1.

II.4.2 Electron cryo-microscopy imaging of trinucleosomes containing either full length histone H1 or its mutants

In order to evaluate the overall structure of the nucleosomes assembled with the help of NAP-1, we have examined the conformation of trinucleosomes using electron cryo-microscopy. EC-M is the least invasive method for high resolution visualization of such dynamic and flexible structure as chromatin. Indeed, it does not require, contrary to conventional electron microscopy, any fixation and absorption of the material to a supporting film, which may result in structural perturbations (538). Trinucleosomal particles were used in order to best approximate the situation in 30 nm chromatin fiber, where the nucleosomes are surrounded by neighboring ones. The central nucleosome in trinucleosomal particle will thus exhibit behavior similar to this in native chromatin.

Figure 2 shows gallery of trinucleosomes without H1 (Figure 2A) and with NAP-1 associated full length H1 and some H1 truncation mutants (Figure 2B-D). The nucleosomes without H1 adopt open conformation with diverging DNA segments, best visible on the central nucleosome, where DNA is entering and exiting the octamer at different sites (Figure 2A). In case of convenient projection, the short DNA segments on external nucleosomes can be seen. Upon H1 association, the structure of nucleosome closes and the formation of stem structure is clearly visible (Figure 2B, arrowheads). The structural properties of the stem structure are visually identical to these observed in native chromatin (181) (results not shown). We conclude that, by using NAP-1 assisted incorporation of histone H1, we were able to reconstitute native-like chromatin structures.

Intriguingly, the association of the H1 truncated mutants 1-177 or 1-127 (which lack either the last 50 or 100 AA from the H1 C-terminus, see Figure 1A for detail), leads to a structure very similar to this obtained upon the association with full length H1 with the trinucleosome (Figure 2, compare panel B with panel C and supplementary figure S1). In contrast, the 3D organization of the trinucleosomes assembled with the mutant 35-120 (consisting of GH1 and 5 and 8 AA from the NH_2 and COOH-termini of H1, respectively) was close to this of the trinucleosomes without H1 (Figure 2, compare panel A with panel D). We conclude that the H1 globular domain was not, as expected, able to assemble a stem-like structure of the linker DNA.

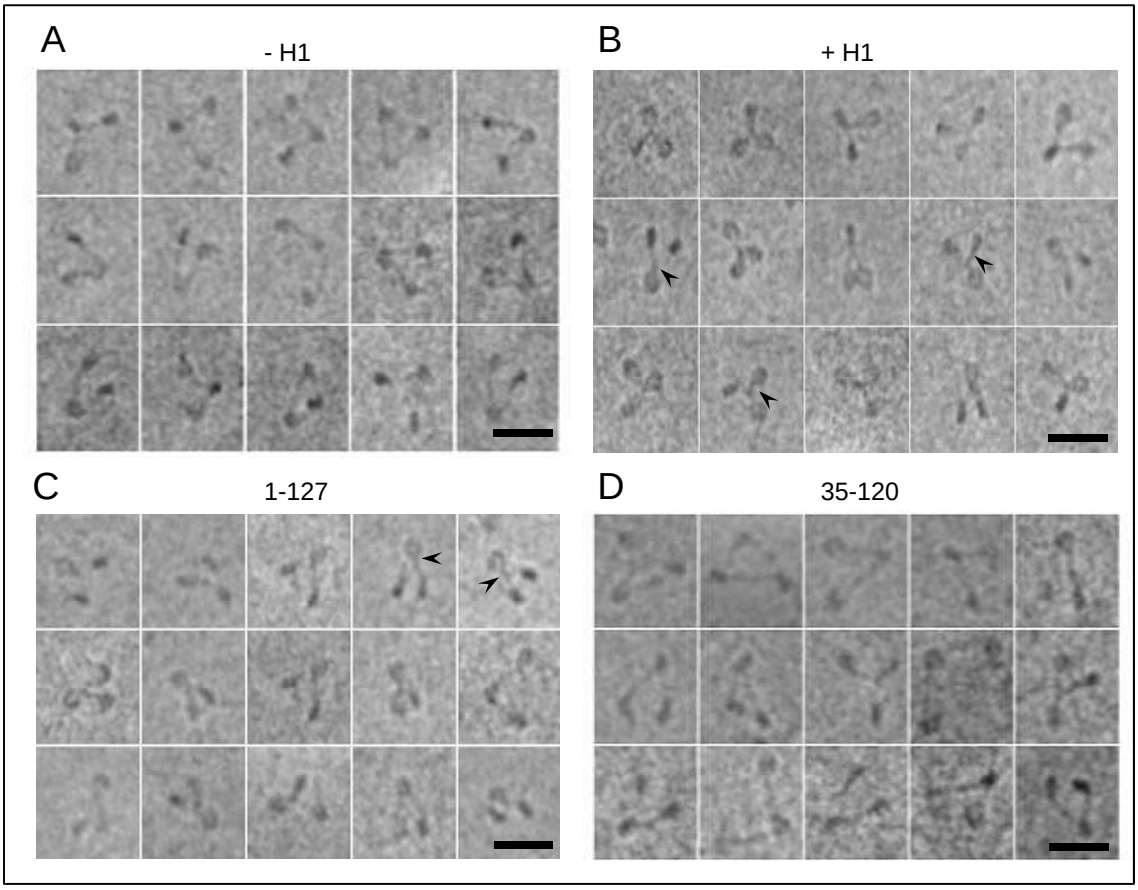

Figure 2: Representative Electron cryo-microscopy images of reconstituted 601 trinucleosomes assembled with full length histone H1 (B), and 1-127 H1 (C) and 35-120 (D), control trinucleosomes without linker histones (A). The arrowheads indicate selected examples of the stem. Bar = 40 nm.

II.4.3 Hydroxyl radical footprinting of chromatin samples assembled with full- length histone H1

EC-M reveals the overall structure and 3D conformation of the nucleosomal particles. To correlate the generation of this structure with the interaction of the different domains of histone H1 with the nucleosomal DNA we have used both DNase I and hydroxyl radical footprinting techniques. Initially we have applied these techniques to study the organization of dinucleosomes. The presence of full-length histone H1, but not of its globular domain, affected the accessibility of the linker DNA to DNase I (Supplementary figure S2). This result is in agreement with the reported data (92, 528) and evidences for an interaction of non-structured NH_2- and COOH termini of histone H1 with linker DNA.

The comparison of the hydroxyl radical cleavage pattern of dinucleosomes without H1 with this of dinucleosomes with H1 provides, however, very interesting information on the interaction of histone H1 with nucleosomal DNA at very high (one base pair) resolution (Figure 3). Each of the two nucleosomes within the dinucleosome without H1 showed a well

defined 10 bp repeat, evidencing for a proper wrapping of the nucleosomal DNA around the histone octamer. The linker DNA exhibited a uniform OH° cleavage pattern. The presence of H1 induces two major alterations in the OH° cleavage pattern of the dinucleosomal DNA (Figure 3 and Figure 4): (i) a strong decrease in the accessibility of DNA at the dyad axis of each individual nucleosome and, (ii) a clear 10 bp repeat of the linker DNA. The data show that 10 base pairs symmetrically located relative to the dyad were protected by histone H1 (see Figure 3C for detail). The protection of each individual DNA strand exhibited some very weak asymmetry (Figure 3 A, B, see dyad and Figure 3C, see scans).

To approach more closely the physiological situation and to correlate the binding of H1 with the 3D organization observed by EC-M we have also carried out OH° footprinting with trinucleosomes without and with H1 (Figure 5). The same types of alterations were observed upon histone H1 incorporation in these particles, namely a very clear footprinting at the dyad of each individual nucleosome and the appearance of a 10 bp repeat of the linker DNA (Figure 5). Note that in this case the central nucleosome has two linkers (the entrance and the exit ones) and each linker exhibited the 10 bp repeat. These types of structural changes resulting from the NAP-1 assisted incorporation of histone H1 were also observed at mononucleosomal level (Supplementary figure S3).

II.4.4 The globular domain of histone H1 protects both 10 bps of DNA located symmetrically to the nucleosome dyad and ~one helical turn of DNA from each linker

Which domain of histone H1 is required for the observed protection of the nucleosome against OH° cleavage? We have first concentrated on the globular domain of histone H1, GH1 (AA 40-112, see Figure 1). As seen (Figure 4), the association of GH1 with dinucleosomes resulted in a clear protection of the dyad. As in the case of full length H1, 10 bps of DNA located symmetrically to the dyad, were protected against OH° cleavage. Note that the binding of the slightly larger (compared to GH1) 35-120 mutant of H1 (comprising additional 5 AA and 8 AA from the H1 NH2- and the COOH-terminus, respectively) resulted in identical footprinting to this of GH1 (Figure 4). Importantly, the association of this mutant with either the mononucleosome (Supplementary figure S3) or the trinucleosome (results not shown) led to the same pattern of protection of the dyad. Therefore, the globular domain of histone H1 interacts specifically with 10 bp of DNA located symmetrically to the nucleosome dyad.

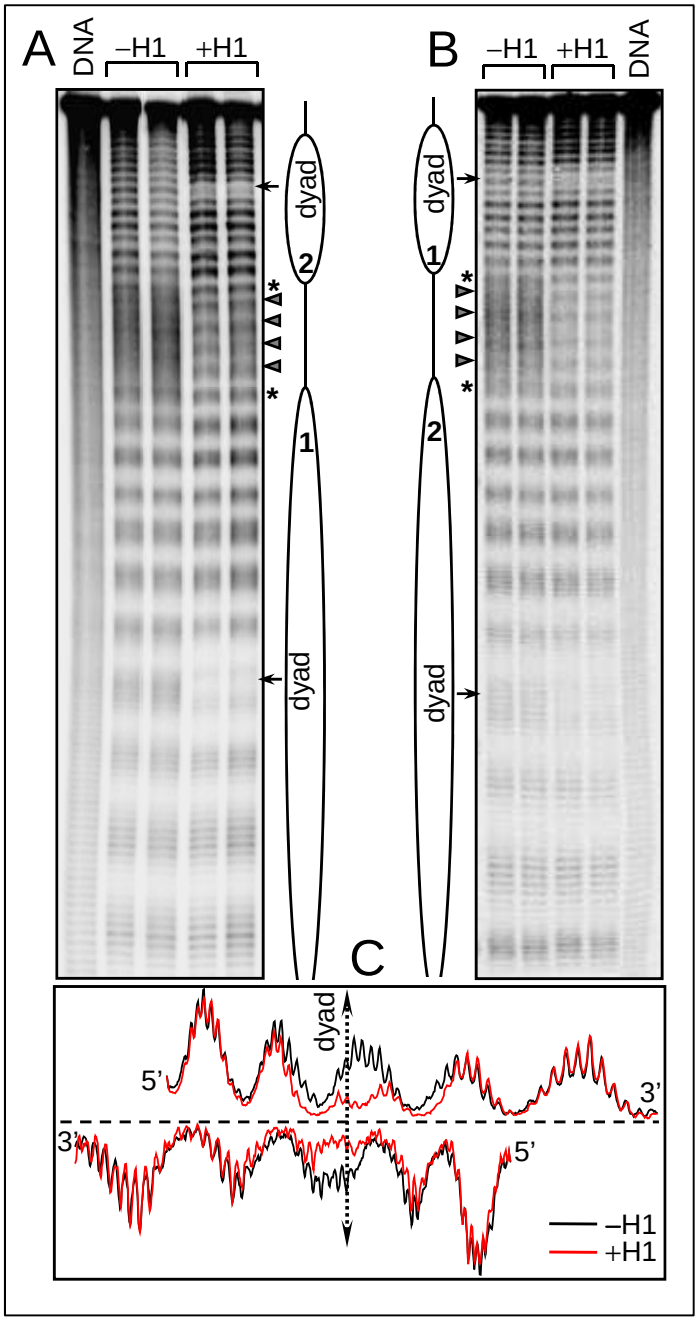

Figure 3: Hydroxyl radical footprinting of control and H1 containing dinucleosomes. Dinucleosomes were reconstituted on a tandem 32P-end labeled 423 bp 601 DNA repeat and NAP-1 was used to deposit histone H1. The samples were then subjected to OH° treatment and the digestion products were run on 8% PAGE under denaturing conditions. (A) OH° cleavage pattern of dinucleosomes reconstituted with 32P-end labeled one of the DNA strands (upper strand for convenience); DNA, OH° cleavage pattern of naked DNA. The arrowheads and the stars show the digestion products of the central part and the ends of the linker DNA, respectively. (B) Same as (A) but for dinucleosomes reconstituted with 32P-end labeled opposite DNA strand (lower strand). The position of the nucleosome dyad is indicated. The arrowheads and the stars designate the digestion products of the central part and the ends of the linker DNA, respectively. In both (A) and (B) schematic drawings of the dinucleosomes are presented. (C) Scans of the OH° digestion pattern in the vicinity of the nucleosome dyad of control (in black) and H1-containing (in red) dinucleosomes. The upper panel shows the scans of the OH° cleavage pattern of the 32P-upper strand end-labeled dinucleosome DNA, while the lower panel shows this of the 32P-lower strand end-labeled dinucleosome DNA. The position of the dyad is indicated.

In addition to the protection to the dyad, the presence of either GH1 (AA 40-112) or 35-120 H1 mutant in the dinucleosome resulted also in a symmetrical 10 bp extension of DNA protection at either ends of the footprint of the core particle (Figure 4, see stars). This additional protection of ~20 bp of linker DNA was also observed in both GH1 and 35-120 H1 mutant associated mononucleosomes (Supplementary figure S3) as well as in trinucleosomes (results not shown). Taken together, the above described data demonstrate a highly specific binding of the globular domain of H1 with 10 bp of DNA located symmetrically to the nucleosome dyad and an additional organization of 20 bp of the linker DNA.

II.4.5 A short aminoacid sequence located between AA 120 and 127 of H1 COOH-terminus is required for the generation of the linker DNA 10 bp repeat upon OH° cleavage

The footprinting of the histone H1 globular domain associated nucleosome samples showed no linker DNA 10 bp repeat, which was otherwise observed in full-length histone H1 bound particles. This suggested that either the NH_2- or the COOH-termini of H1 or both would be implicated in the generation of this repeat. We initially approached this question by studying the OH° cleavage pattern of dinucleosomes containing bound either 1-177 or 1-127 histone H1 C-terminus truncated mutants (see Figure 1 for detail). Both samples exhibited a 10 bp repeat of the linker DNA (Figure 4 and results not shown). Mononucleosomes assembled with either one of these mutants exhibited also the 10 bp repeat of the linker DNA (Supplementary figure S3). This pointed that either the NH_2-terminus or the part of the C-terminus present in the mutants or both are required for the generation of the repeat. To differentiate between these possibilities, we next carried out a OH° footprinting of mono- and dinucleosomes assembled with the 35-127 truncated mutant of histone H1 in which both the main part of the NH_2-terminus (35 AA) and the 100 AA from the COOH-terminus of histone H1 were removed. This has allowed the study of the implication of the histone H1 NH_2-terminus in the structuring of the linker. Both the mono-nucleosomal and di-nucleosomal particles containing the 35-127 mutant showed clear 10 bp repeat of the linker DNA (Figure 4 and supplementary Figure S3). This showed that the NH_2-terminus is not required for the 10 bp repeat of the linker. Since no repeat of the linker was detected in 35-120 H1 mutant associated particles, we conclude that a stretch of only seven AA (AA 121-127) of the COOH terminus of H1 plays a predominant role in the generation of the 10 bp repeat and thus, in the structuring of the linker DNA.

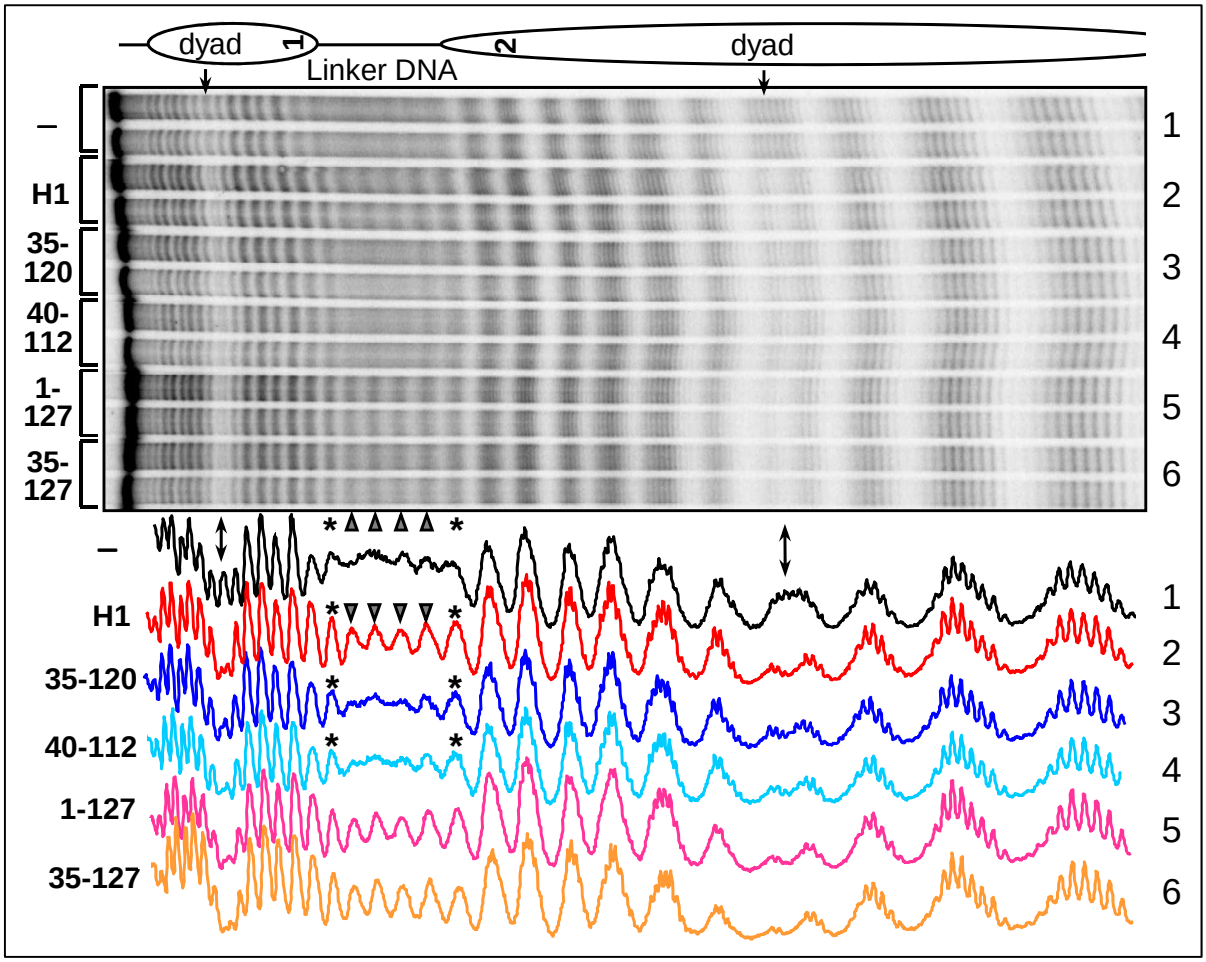

Figure 4: Hydroxyl radical footprinting of control and assembled with full length H1 and its truncated mutants dinucleosomes. Dinucleosomes were reconstituted on a tandem ^{32}P-end labeled 200 bp 601 DNA repeat and NAP-1 was used to deposit either full-length H1 or the individual truncated mutants. The samples were then subjected to OH° treatment and the digestion products were run on 8% PAGE under denaturing conditions. The lower part of the figure shows the scans of the OH° cleavage patterns of the respective samples. The number of the first and the last amino acid residue of the truncated mutants are indicated. (-), control dinucleosomes. (▲), cleavage products corresponding to the central part of the linker DNA; (*), cleavage products corresponding to a DNA fragment at the end of the linker DNA; (↕) designates the footprinting at the nucleosome dyad. A schematic drawing of the dinucleosome is shown at the upper part of the panel. The position of the dyad of each nucleosome as well as this of linker DNA is indicated.

II.5 Discussion

Linker histone is a key player in chromatin dynamics. Despite the numerous studies, the location and the interactions of the different domains of the linker histone with the nucleosomal DNA were and remain a controversial issue. Past studies based on the digestion of native chromatin with micrococcal nuclease and DNase I suggested a symmetrical model of the interaction of the linker histone with the nucleosome (48, 86). According to this model the linker histone interacts with both the dyad and the entering and exiting DNA from the core particle. More recently crosslinking studies of the globular domain (GH5) of the linker histone H5 to nucleosomal DNA pointed to a "bridging model", according to which GH5 interacts with the dyad and with only one (either the exiting or entering) of the free DNA arms (84). Another study, using also a crosslinking of GH5 to DNA, but within reconstituted positioned 5S nucleosomes, led to the proposal of asymmetrical location of GH5 inside the gyres of DNA at a distance of ~ 65 bp from the dyad (90). Recent *in vivo* photobleaching microscopy report supported the existence of two distinct DNA binding sites of the globular domain (GH1°) of the linker histone H1° (28). The data indicated that GH1° interacts with the DNA major groove at about 10 bp apart from the dyad and with one of the free DNA arms adjacent to the nucleosome core (28).

Several reasons could explain the controversial character of the reported data. The above *in vitro* studies used salt dialysis to deposit histone H1 to the nucleosomes. This would lead to improper assembly of histone H1 (92) and this work). In addition, the reconstitution on 5S DNA would result in the formation of nucleosomes exhibiting several translational positioning, which, in turn, would interfere with the mapping of histoneH1:nucleosomal DNA contacts (93). The *in vivo* photobleaching studies could be viewed as indicative for the mapping of H1:nucleosomal DNA interactions, since they are indirect and model derived.

In this work we have overcome the above described problems by using: (i) physiologically relevant linker histone chaperone NAP-1 assisted deposition of histone H1, (ii) 601 DNA sequence for reconstitution and, (iii) a combination of electron cryo-microscopy with OH° footprinting techniques. This has allowed the reconstitution of very precisely positioned nucleosomal templates containing physiologically assembled histone H1 or its truncated mutants, the mapping at one base pair resolution of the histone H1:DNA interactions within mono-, di- and trinucleosomal templates and the dissection of the role of the distinct H1 domains in the 3D organization of the samples.

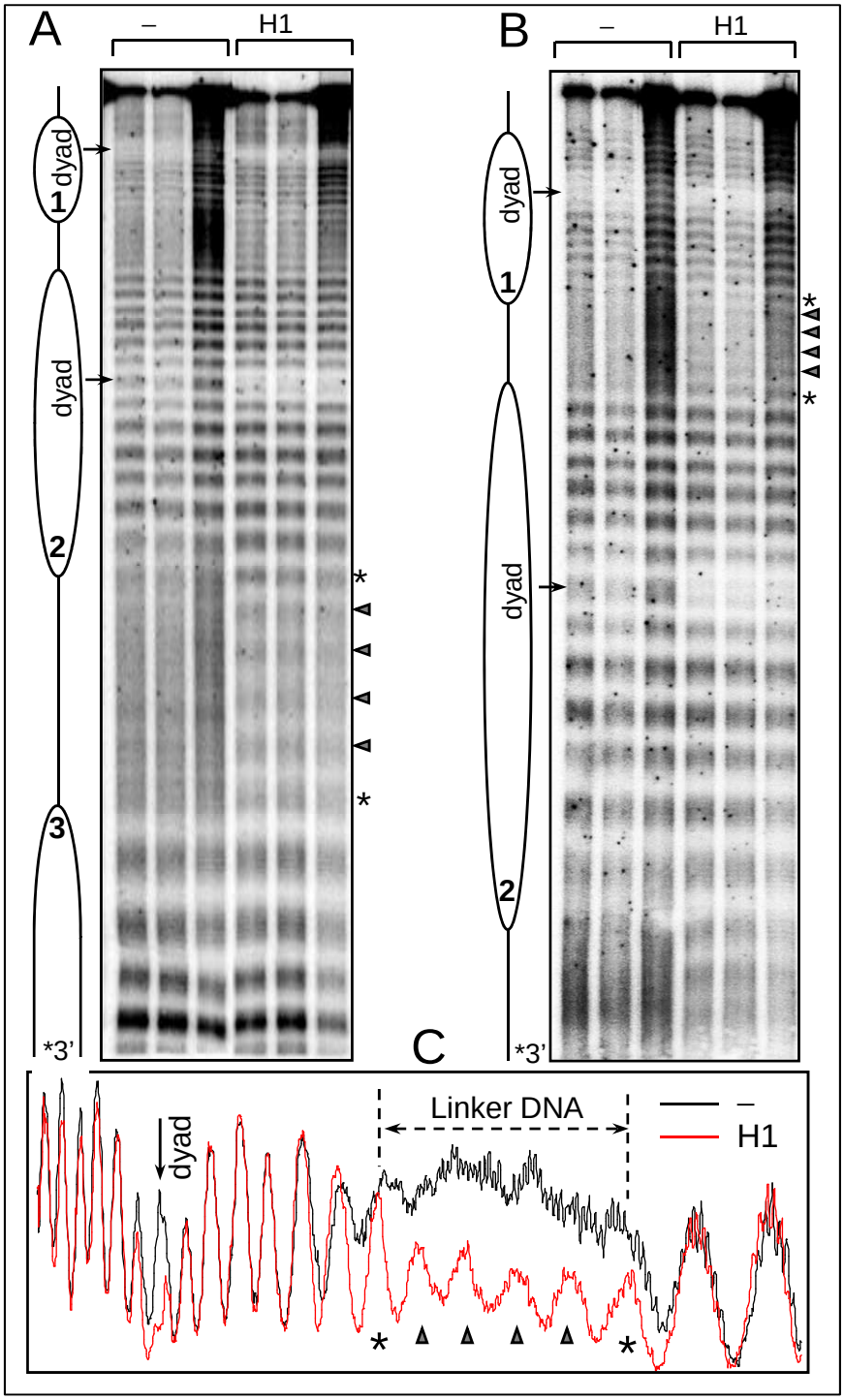

Figure 5: Hydroxyl radical footprinting of trinucleosomes. Trinucleosomes were reconstituted on a ^{32}P-end labeled DNA fragment containing three tandem 200 bp 601 sequences and then H1 was incorporated in the trinucleosome by using NAP-1. The samples were cleaved with OH° and the cleaved trinucleosomal DNA was run on 6.5% denaturing PAGE. Half of the sample was loaded 2 hours after (panel A, less migrated products) the first half (panel B, more migrated products) for better resolution on the same gel. Schematic drawings are presented on the left part of each panel. The positions of the nucleosomes and the dyad in the trinucleosomal templates are indicated. C. Scans of the OH° cleavage pattern of control (in black) and H1-containing (in red) tri-nucleosomes. (▲), cleavage products corresponding to the central part of the linker DNA; (*), cleavage products corresponding to a DNA fragment at the end of the linker DNA. Note the specific protection at the dyad and the structuring of the linker DNA in the H1-containing samples.

The EC-M data demonstrated that the reconstituted H1-containing trinucleosomes were visually indistinguishable from the native trinucleosomes evidencing that the reconstituted samples exhibited a *bona fide* 3D organization. Importantly, the presence of either full-length H1 or its COOH terminus truncated mutant 1-127 led to the generation of characteristic stem structure of the linker DNA observed in native fibers. OH° footprinting of these two samples, but not of samples without H1, showed the appearance of a clear 10 bp repeat in the OH° cleavage pattern of the linker DNA along its entire length. We attributed the generation of this repeat to reflect the structuring (the stem structure) of the linker induced by the binding of H1 or its 1-127 mutant to the nucleosomal DNA. Interestingly, the 10 bp linker DNA repeat was observed in the particles assembled with the NH_2-terminal truncated 35-127 H1 mutant but not in these assembled with the 35-120 mutant. Therefore, the presence of only a short AA sequence (AA 121-127) of the COOH-terminus of H1 appeared to be required for the induction of the 10 bp repeat and thus, for the structuring of the linker DNA.

The second important feature of the OH° cleavage pattern of H1 assembled nucleosomal samples was the protection of the dyad. In mono-, di- and trinucleosomes, 10 bps of DNA located symmetrically to the dyad were protected against OH° cleavage. This highly specific protection was also observed with all samples assembled with GH1. This demonstrates that GH1 interacts with these 10 bps of the dyad. Since OH° cleavage is performed through the minor groove of DNA we conclude that interaction of GH1 with the dyad is realized through the minor groove of DNA. Importantly, GH1, in addition to the protection of the dyad, affected also the footprinting of the linker DNA. Indeed, it protects ~ one additional helical turn from each one of the exiting and entering DNA arms, suggesting a direct interaction with both of them. These data agree with the excellent DNase I footprinting studies published in the past (86).

Model of the nucleosome

The OH°-footprinting data characterize the protection of nucleosomal DNA from OH°-attack at a single base pair resolution. We have used this experimental geometric information, the available crystal structure of the nucleosome core particle (54) in combination with coarse-grain DNA mechanics to construct a 3D model of the nucleosome (see Supplementary methods for detailed description of the whole procedure). Briefly, we first precisely measured the OH° accessibility per nucleotide by processing the gels. We next used the visualization package Chimera (532) to "translate" the relative accessibility signals in 3D

structure of the nucleosomal DNA by color-coding of the C5' carbon atoms of the backbone sugars (OH° primary attacks C5' carbon atoms, (533)). The globular domain of GH1 or the H1 truncated mutant 35-127 were then manually placed in the nucleosome to match the nucleosomal DNA protected sites against OH° attack.

The resulting 3D organization of the nucleosome is presented in Figure 6. As seen (Figure 6A, upper panel and Supplementary movies, movie 1), in nucleosomes without H1, the protected sites (in blue) are located exclusively on the DNA-histone octamer interface, while the outward-facing DNA (including the region around the dyad and the linkers) is freely accessible (in red). This confirms completely the expectation that the molecular contacts are occluding the OH° reactive sites.

Our experimental data show that the presence of GH1 generates a clear protection at the dyad and at both entering and exiting linkers. This suggests that one and the same GH1 molecule could simultaneously interact with three distinct DNA binding sites. Recent extensive computational docking data indicated that the globular domain of the linker histone H5, GH5, exhibits three binding sites and contacts respectively the dyad and both the entering and exiting linker DNA (91). The positively charged chains of GH5, which contact nucleosomal DNA, were found to be conserved among the other linker histones, thus indicating that this mode of interaction would be also applicable for the globular domains of the other linker histones (91). With this in mind, we rebuilt a three-DNA binding site model, by manually matching the GH1 α-helix orientations and the OH° footprint-derived DNA protected sites. We have used very similar (to this described for GH5 (91)) orientation of GH1. The corresponding contacting residues in the resulting structure were the same as these proposed by Fan et al. (Supplementary methods, see Figure *sm-9*). For the matching, an NMR solution structure of GH1 was used ((535) and Supplementary methods). Remarkably, this GH1 structure was large enough to fill the space between the entering and exiting linker DNA and to interact with both linkers and the nucleosome dyad (Figure 6B and Supplementary methods, Figure *sm-9* and Supplementary movies, movie 2). Note that in this three contact GH1-nucleosome model no bending of the linker DNA is observed (compare the upper panels of Figure 6 A and B and Supplementary movies, movie1 and movie 2), i.e. the orientation of both linkers is identical to this for the model of the nucleosome without H1. This is in complete agreement with our experimental EC-M findings, which showed that the presence of GH1 did not affect the orientation of the linker DNA (see Figure 2).

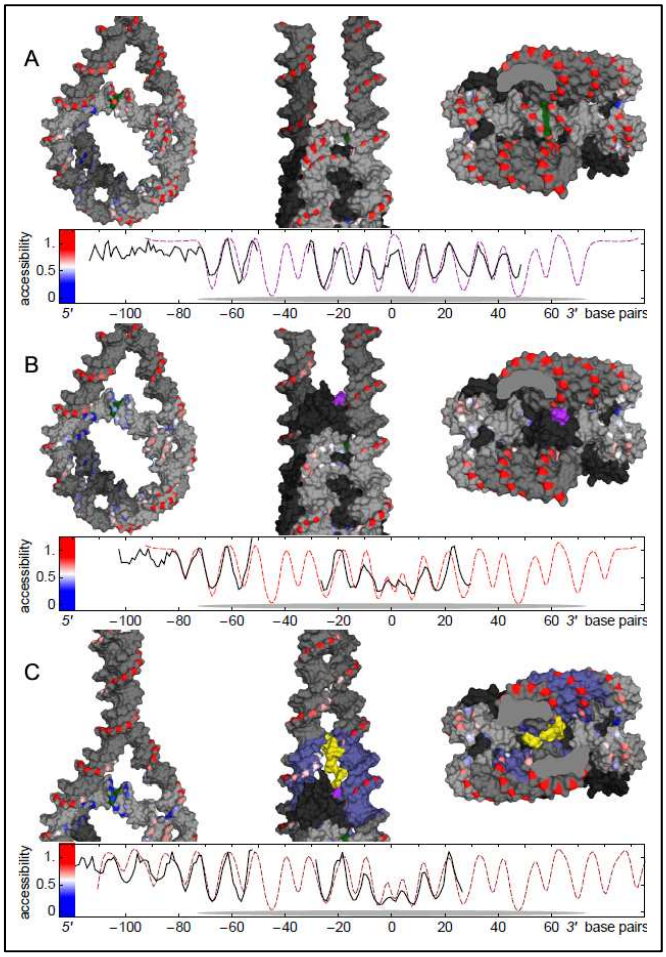

Figure 6: Molecular models for the nucleosome particle. (A) Nucleosome without H1. The experimental relative OH°-accessibility profile (lower panel) is plotted (black, solid). The corresponding structure-derived accessibility profile (dashed, magenta; see text), agrees closely. The upper panel shows the experimental OH°-accessibility profile on the three-dimensional nucleosome structure by color coding the DNA deoxyribose C5' atoms from blue (maximal protection from OH°) over white (partial protection) to red (maximal accessibility to OH°). Protection from OH° attack occurs at the DNA-core histone interface. (B) Nucleosome associated with the globular domain (GH1) of histone H1. The lower panel shows, as in (A), the experimental relative OH°-accessibility profile (black, solid line) and the structure-derived accessibility profile for the GH1 three-contact model (dashed, orange). Note the strong additional protection at the dyad and the additional protection of one helical turn of the linker DNA (left part of the panel). The upper panel illustrates the location of GH1 in the nucleosome in the three-contact model. Note that GH1 protects the dyad and directly interacts with 10 bp of each linker DNA; magenta, the COOH-terminus of GH1. (C) Nucleosome associated with 35-127 H1 mutant. As in (B) the lower panel shows the experimental relative OH°-accessibility profile (black, solid line) and the structure-derived accessibility profile for the 35-127 H1 mutant model (dashed, red). Note the strong protection of the dyad and the presence of the 10 bp repeat within the linker DNA. The upper panel shows the location of the 35-127 H1 mutant and the 3D-organization of the linker DNA stem obtained from constrained DNA elastic relaxation (see text). DNA within a 30 Angstrom radius of the GH1 C-terminus is colored blue. A hypothetical conformation of AA 112-127 is shown in yellow. (A-C) Coloring: DNA C5' atoms without footprinting data and all other DNA shown in gray, the dyad in green. Both strands are color-coded from single-strand data by exploiting two-fold symmetry Protein is shown in black (omitted in the left column). Viewing directions: rotated sideways and up by 30 degrees from the NCP superhelical axis, at right angles with superhelical and dyad axes, and along the dyad axis (from left to right). In the plots, the nucleosome core (in light grey) is schematically presented.

If the above described three contact model reflects the real GH1-nucleosome structure, it should "exhibit" the same accessibility towards OH° than the experimentally found one. To test this, we have developed an approach to calculate the OH° footprinting derived from structural models (a detailed description of the procedure used is presented in Supplementary methods). As seen (Figure 6B, lower panel), the calculated footprinting pattern of the GH1-nucleosome model matches pretty well the experimental one: both the dyad and ~ one helical turn of the linker are strongly protected against OH° cleavage. Note that the predicted accessibility profile for nucleosome without H1 reproduces (Figure 6A, lower panel) also accurately the measured accessibilities (linear correlation coefficient R = 0.79, see Supplementary methods). All this validates our approach for calculating the accessibility profiles from structural models. With this in mind, we next asked if the two contact models proposed for the association of the globular domain of the linker histone with the nucleosomal DNA (28, 84) would exhibit accessibility profiles similar to the experimental ones. Note that in either the model of Zhou et al. (84) or in this Brown et al. (28) the globular domain of the linker histone contact the DNA major groove at a 2 and 5 base pairs distance from the dyad, respectively. Since OH° attacks the DNA backbone through the minor DNA groove, no protection at the dyad should be observed. And indeed, by comparing the predicted (calculated) OH° protection profiles to the experimentally measured accessibilities, we found that both models were incompatible with the strong protection observed at the dyad (see Supplementary movies, movie 3 and movie 4 and data not shown). As for the two contact model of Pruss et al. (90), it predicts a OH° protection by GH5 at ~ 65 bp from the dyad, a protection that we have not experimentally observed. We conclude that the reported in the literature two-contact models were unable to describe the OH° experimentally found accessibilities.

For the linker DNA stem, which is formed with full length H1 or its truncated mutants 1-127 or 35-127, structural models are unavailable. In this case the detailed register of the protected sites along the stem can give valuable structural information. Based on the assumption that the protected sites in the stem arise from DNA-DNA contacts, the linker stem structure may be virtually reconstructed by aligning the linkers in space in a way that their mutual protection reproduces the measured accessibility profile. Such a geometrical reconstruction is giving, however, a whole family of possible stem shapes, corresponding to multiple linker DNA twist profiles. To identify the shape, which would describe closely the real stem structure, we have taken into consideration the mechanical properties of DNA. We reasoned that from all stem structures, which reproduce the experimentally found OH°

cleavage pattern and are compatible with the three contact arrangement of GH1, the most likely structure is that with minimal DNA elastic energy. We have implemented elastic relaxation of the linkers under these constraints (see Supplementary methods for details). The resulting calculated stem structure, which satisfied these requirements, is shown in Figure 6C, upper panel. As expected by construction, the structure-derived accessibility profile matches well the experimental one (Figure 6C, lower panel). In the minimal-energy configuration, the linkers come together along ~20-30 bases outside the core particle, slightly curving into a two-start superhelical stem with a large pitch of around 100-120 bp (Figure 6C, upper panel; see also Supplementary movies, movie 5). This structure has, as the core particle itself, a two-fold symmetry. We have also analyzed the generation of the stem based on the two-contact models (28, 84) and we found that this process was highly energetically unfavorable (results not shown).

The footprinting and EC-M data allowed to predict how the stem structure might be generated and maintained. The short sequence of H1 (AA 121-127), required for the formation of the stem, contained 3 positively charged amino acids residues, namely K122, K124 and K125 (see Figure 1A). These three lysines together with the neighboring lysine K120 would interact with both DNA linkers in the vicinity of the binding site of the COOH-end of GH1 (Figure 6C). The binding of these additional four lysine residues together with the binding of GH1 would be sufficient to efficiently clamp the exiting and entering DNA and to form the stem structure (Figure 6C, upper panel and Supplementary movies, movie 5). We hypothesize that the remaining part of the COOH terminus of H1 (AA 128-227, see Figure 1A) serves to neutralize the DNA phosphates, to stabilize the structure of the chromatin fiber and to assist its condensation.

Alignment of the primary sequences of the different H1 molecules shows that positions of these four lysines were not strictly conserved among different organisms (not shown). Note that the C-terminus of each individual H1 exhibited, however, in vicinity of the GH1 several other rows of lysines, which could play similar role as the 121-127 peptide sequence of the studied H1 molecule. We also speculate that the NH_2-terminus of the core histone H3, which interacts with the linker DNA (539, 540), might be involved in the stem structure formation and maintenance. These open questions remain a challenge for future studies.

II.6 Acknowledgements.

This work was supported by grants from INSERM, CNRS, ANR "EPIVAR" N° 08-BLAN-0320-02 (S.D.), the Association pour la Recherche sur le Cancer (Grant N 4821 to D.A.), the Région Rhône-Alpes (Convention CIBLE 2008 to D.A. and S.D.). S.D. acknowledges La Ligue Nationale contre le Cancer (Equipe labellisée La Ligue) and the Indian-French program ARCUS. J.B. acknowledges the Grant Agency of the Czech Republic (Grant #304/05/2168 to JB), the Ministry of Education, Youth and Sports (Grants MSM0021620806 and LC535 to JB) and the Academy of Sciences of the Czech Republic (541AV0Z50110509 to JB).

II.7 Supplementary figures

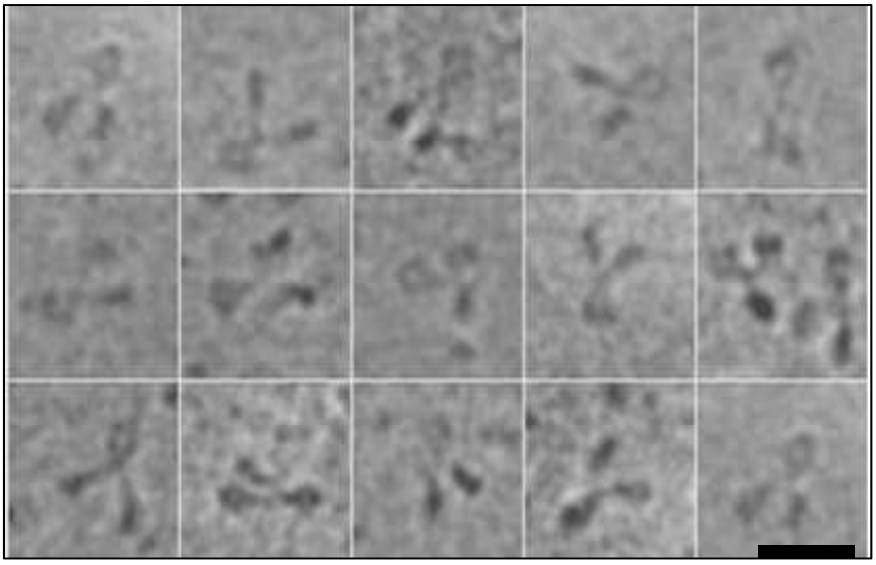

Supplementary figure 1: Representative Electron cryo-microscopy images of reconstituted 601 trinucleosomes assembled with histone H1 truncated mutant 1-177 (in this mutant the last 50 AA from the H1 COOH-terminus were removed). Bar = 40 nm.

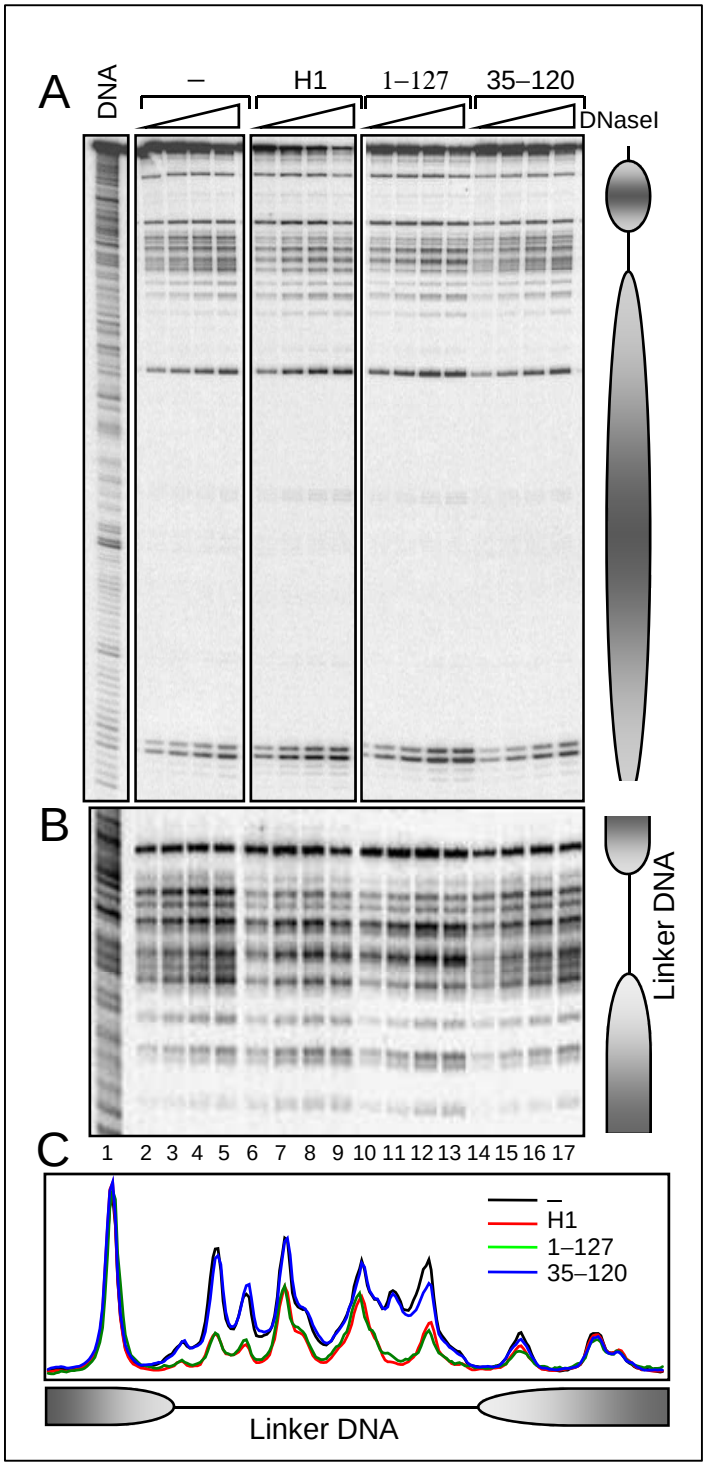

Supplementary figure 2: DNase I footprinting of 601 dinucleosomes containing either full length histone H1 or the truncated mutants 1-127 or 35-120. (A) NAP-1 was used to assemble dinucleosomes with either H1 or its truncated mutants, the samples were digested with DNase I, DNA was isolated from the digested samples and run on an 8% PAGE under denaturing conditions. A schematic drawing of the dinucleosome is shown on the right part of the figure. DNA, DNase I digestion pattern of naked DNA. (B) DNase I footprinting of the linker DNA of the different dinucleosome samples. The part of panel (A), which corresponds to the footprinting of the linker, was presented in an enlarged form to visualize better the differences in the DNase I digestion pattern. In the lower panel are shown the scans of lanes 5,9,13 and 17 corresponding to the DNase I digestion patterns of control (-), H1, and the mutants 35-120 and 1-127, respectively. The positions of the nucleosomes and the linker DNA are indicated in each panel.

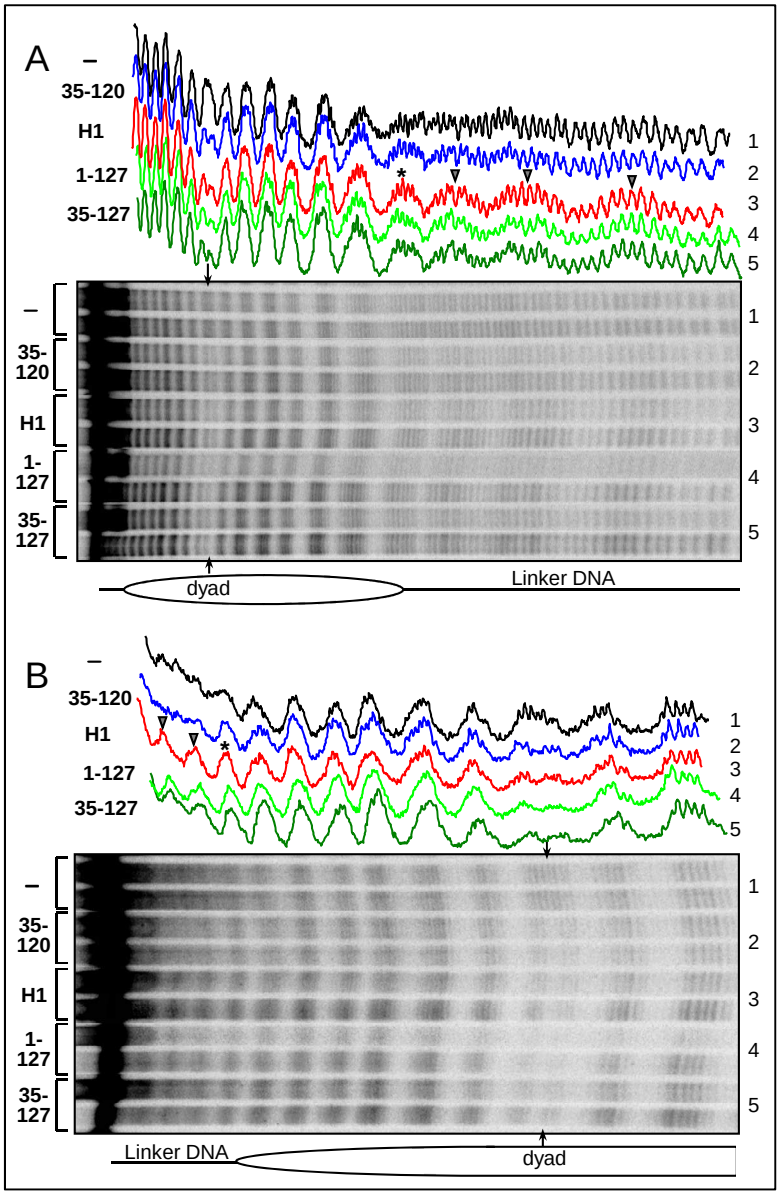

Supplementary figure 3: Hydroxyl radical footprinting of mononucleosomes containing NAP-1 incorporated either full length histone H1 or the indicated histone H1 truncated mutants. Centrally positioned mononucleosomes were reconstituted on ^{32}P-end labeled 255 bp 601 DNA sequence and NAP-1 was used to deposit either full length histone H1 or the indicated H1 mutants. The samples were then treated with OH°, DNA was purified from the digested samples and run on 8% denaturing PAGE. The electrophoresis was carried out for either less time (panel A, less migrated products) or for more time (panel B, more migrated products). In the upper part of each panel are shown the scans of the OH° cleavage patterns of the respective samples. The number of the first and the last amino acid residue of the truncated mutants are indicated. (-), control mononucleosomes. (▼), cleavage products corresponding to the central part of the linker DNA; (*), cleavage products corresponding to a DNA fragment at the end of the linker DNA; (↓) designates the footprinting at the nucleosome dyad. On the lower part of each panel a schematic drawing of the mononucleosome is shown. The position of the dyad of the nucleosome as well as this of linker DNA is indicated. Note the structuring of the linker DNA in the mononucleosomes assembled with full length H1 or with either 35-127 or 1-127 H1 truncated mutants. In contrast to these samples, only one 10 bp linker DNA repeat (designated by *) is observed for the nucleosome assembled with the 35-120 mutant. All the samples assembled with either one of the different H1 truncated mutants, but not the control sample (without H1), show a clear footprinting at the nucleosome dyad.

II.8 Supplementary Methods:

II.8.1 Structural Analysis of OH^o -Footprinting Gels

II.8.1.1 Conversion of gel exposure to relative accessibility signals

Relative accessibility profiles were determined from OH^o footprinting gels of the 'lower' DNA strand of the mononucleosome, in absence of H1 linker histone, with the globular domain of H1 (called GH1 in the following), and with full H1.The typical shape of a gel trace is shown in Figure sm-1. The horizontal axis is the distance in pixels from the (non-migrated) top of the gel, and the vertical axis is the gel exposure intensity, with an arbitrary scale. To illustrate our procedure for converting traces into profiles of relative accessibility per nucleotide we focus on the region highlighted in green in Figure. sm-1. The raw intensity signal shows four main features:

1. The smallest oscillations are single-nucleotide bands. They can be separated reliably only in a region with sufficient contrast, shown in red in Figure sm-1.
2. Oscillations with a period of around 10 bands reflect protection from OH^o - attack.
3. Long-range trends are due to long-range features in the data but also to dilution resulting from logarithmic migration in the gel.
4. The trace contains a constant background exposure level.

The purpose of the accessibility profiles described in the following is to extract the OH-protection signal only, allowing comparisons between different nucleosome complexes and nucleosomal locations.

II.8.1.1.1 Trace adjustment

The varying width of individual bands (7 to 14 pixels in this example) results from a combination of logarithmic migration and irregularities in the gel material. In a first step we determine the nonlinear relation between migrated distance (in pixels) and base number. To determine the positions in pixels x(n) of individual bands (numbered by n), we first de-trended the intensity traces by subtracting a suitable moving average. We then iteratively maximized the correlation between this signal and a modulated cosine function $A(x) \cos [2\pi n(x)]$, where A is slowly varying. In each iteration, the running phase of the cosine is adjusted, $n(x) \rightarrow n(x) + \delta(x)$, to improve the correlation between signal and modulated cosine, in a moving window of 7 bands length.

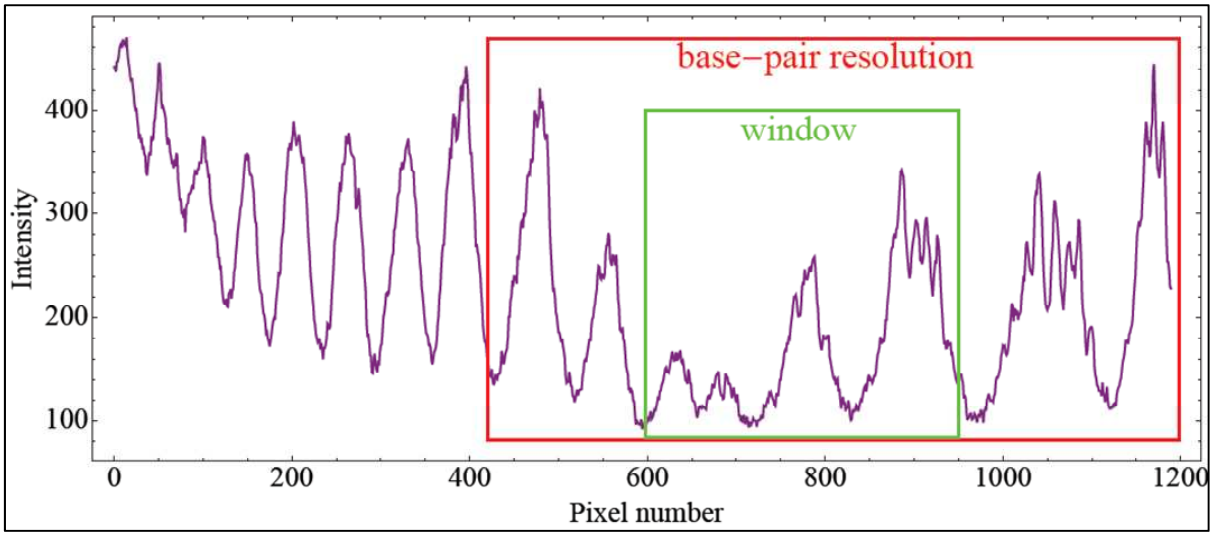

Figure sm-1: Raw intensity trace obtained with a mononucleosome with H1.

The width of the moving window allows to assign bands even in short intermediate regions without sufficient contrast, by using the fact that band widths do not change abruptly, see Figure sm-2. To ensure that no base-pair has been missed, we checked by eye the maximum positions and the final base-pair-pixel correspondence x(n), shown in Figure sm-3. To relate OH^o protected areas to absolute sites on the nucleosome (with the dyad base-pair centered at 0), rather than band numbers only, we identified absolute DNA lengths on the gels by using a combination of molecular weight markers present in the mononucleosome gels, traces of sequence-specific cleavage after UV irradiation, and comparison with absolute positions determined in dinucleosome gels. The unique positioning of the 601 sequence on the nucleosome then allowed us to assign DNA lengths to nucleosomal sites.

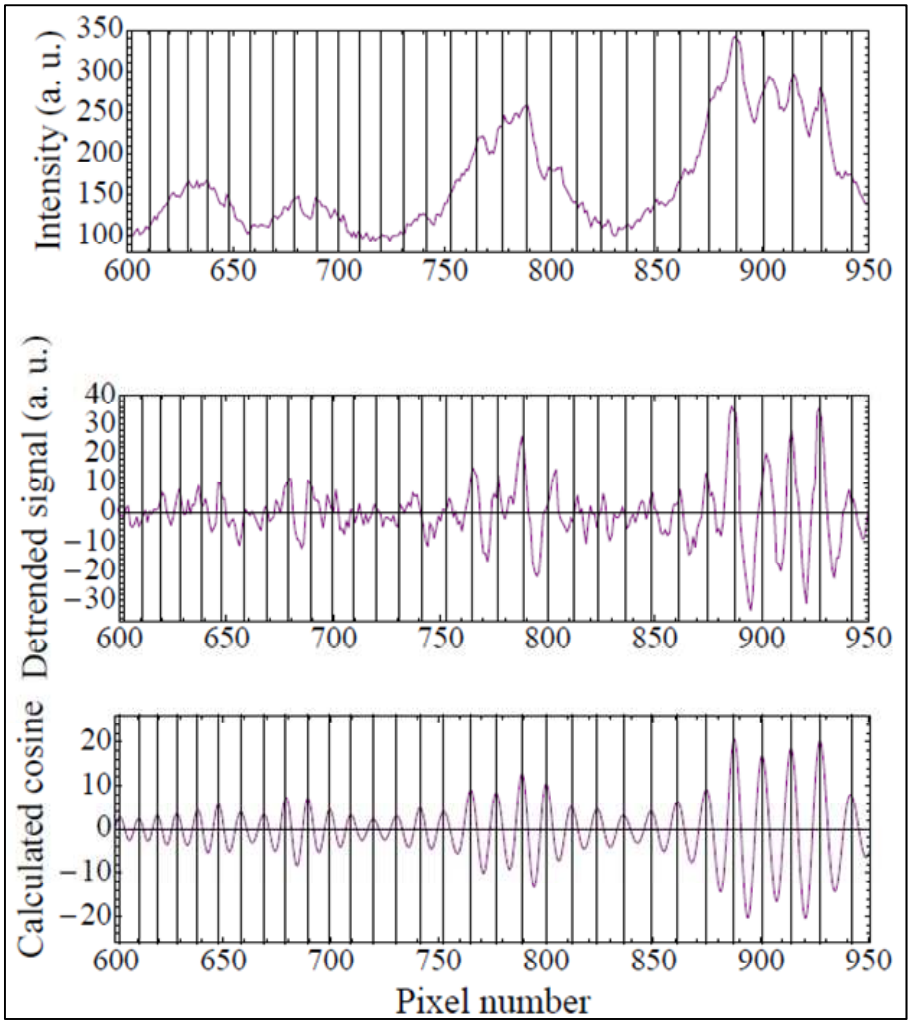

Figure sm-2: Raw intensity trace, de-trended trace and converged sinusoidal fitting function, from top to bottom. Vertical bars indicate the identified band center peaks.

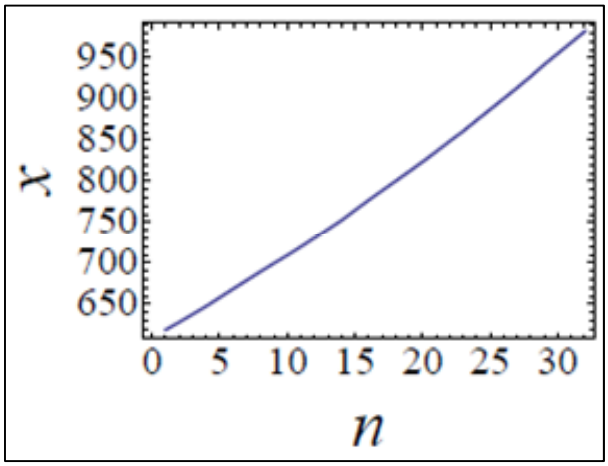

Figure sm-3: Band position x(n) in pixels as a function of band number.

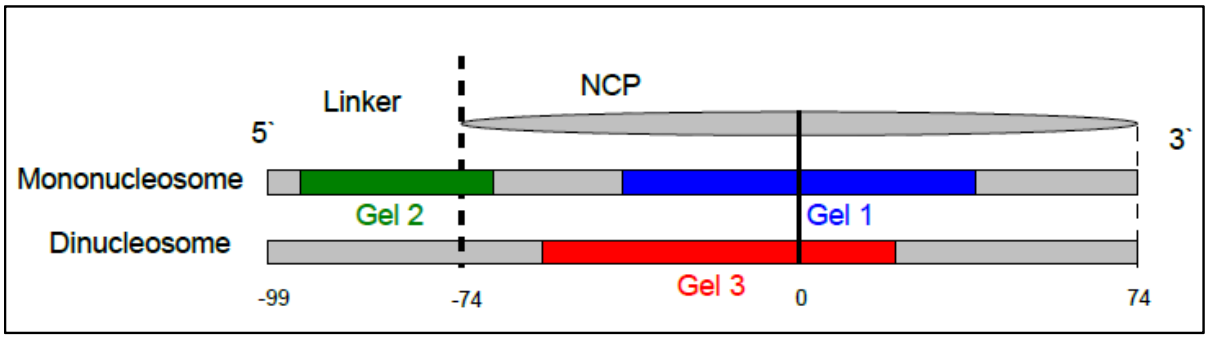

Figure sm-4: Placement of analyzed gels on the nucleosome

II.8.1.1.2 Renormalization

After removing a constant level of background noise, the raw intensity signal measures the amount of DNA of a given molecular weight. By integrating over the width of each band, we obtain the irradiation intensity per band as a function of band number. (Since we consider only regions with well-separated bands, integration instead of fitting of multiple peaks introduces negligible errors.) Per band intensity profiles allow a comparison of corresponding regions in gels with different migration times, see Figures sm-5, sm-6 and sm-7, upper panels. To eliminate the global trends in the trace amplitudes, we then generated a signal which represents the local accessibility of a nucleotide compared to its neighbors. In this final processing step the intensity of each base-pair is divided by the mean of the 3 maximum intensities in a sliding window. The window width was set to a value between 7 and 20 in the presented data. In effect, the ≈10 bp oscillations are rescaled to values roughly between 0 and 1, while respecting the relative protection strengths of different traces in the same region; see Figures sm-5, sm-6 and sm-7, bottom panels. All processing steps were implemented in Mathematica (542).

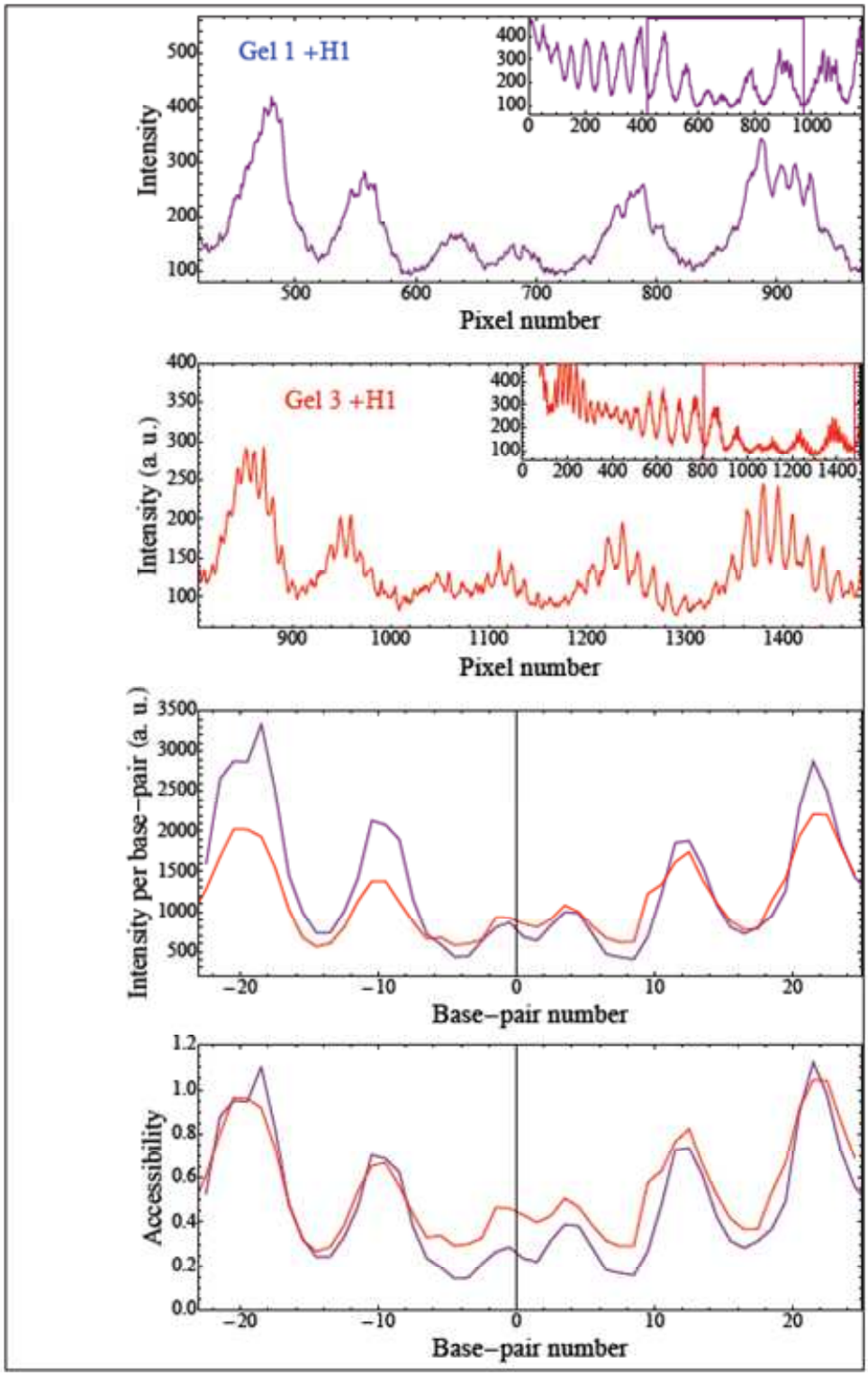

Figure sm-5: Comparison of mononucleosome and dinucleosome accessibilities in the presence of H1. From top to bottom: raw intensity of both gels, superimposed intensities per base-pair and relative accessibilities. See fig. sm-4 for gel numbering.

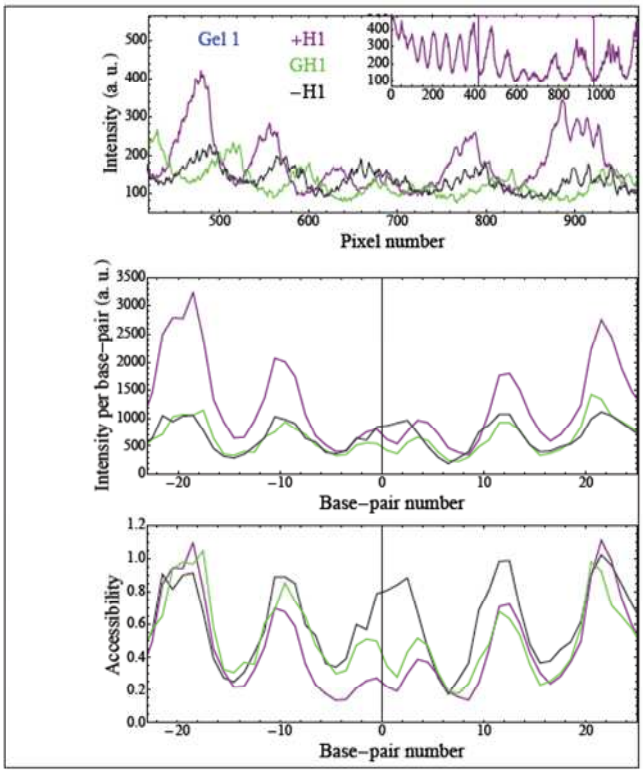

Figure sm-6: Accessibility on the mononucleosome core, without H1 (black), with the globular domain GH1 (light green) and with full-length H1 (purple). From top to bottom: raw intensities, intensity per base-pair and relative accessibility.

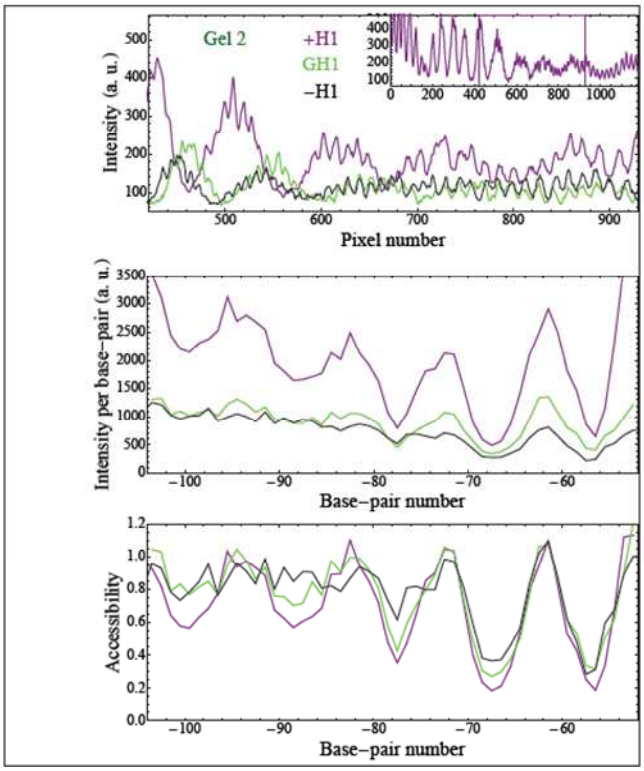

Figure sm-7: Accessibility on the mononucleosome linker, without H1 (black), with the globular domain GH1 (light green) and with full-length H1 (purple). From top to bottom: raw intensities, intensity per base-pair and relative accessibility.

II.8.1.2 OH^o -footprints vs. three-dimensional nucleosome structures

II.8.1.2.1 Exploiting the two-fold symmetry

The mononucleosome accessibility profiles were measured for only one of the two nonequivalent strands, the 'lower' strand. However, the nucleosome structure has an approximate two-fold symmetry axis, which allows to deduce an accessibility profile for the complementary strand, as follows: The 147-bp nucleosome core particle structure NCP147 (3) shows that the two-fold (dyad) axis traverses the central base-pair. Thus by rotating the DNA loop by a half turn around the dyad axis while keeping the histone core in place, one generates two alternative, approximately symmetric conformations in which the two strands change roles. We make the hypothesis that these two conformations are equally represented in our experiments and take the accessibility profile of the complementary 'upper' strand equal to that of the 'lower' strand (both read from 5' to 3'). This hypothesis is supported by the co-localization of protected sites from both strands (see Figures sm-8), and by the close agreement between accessibility traces in the dinucleosome gels where both were measured.

II.8.1.2.2 Three-dimensional rendering of relative accessibilities

The molecular visualization package Chimera (532) allows to render molecular structures using a color code for user-defined atom attributes. We have used this feature to facilitate the geometric interpretation of measured OH^o-radical protection patterns, Figures. sm-6 and sm-7, bottom panels. We depict the local accessibility signal by a color code, ranging from blue (least accessible) over white to red (most accessible). Since DNA is attacked by OH^o radicals primarily at the C5' backbone atoms (533), we choose this subset of atoms for color-coding. This coloring scheme is used to show the protection pattern of H1-less nucleosomes on straight DNA in Figure. sm-8. This '3D-gel' shows directly that the ≈10.5-base periodicity of the experimental accessibility signal places all protected sites on one side of the double helix. As expected, in the nucleosome without H1, linker DNA is not protected, see also the traces in Figure sm-7. In order to display accessibility profiles directly on the nucleosome, we rebuilt several nucleosomal DNA conformations. These were first constructed using a purpose-built Mathematica library for rigid base-pair DNA manipulations, and then translated into pseudo-atomistic structures using the 3DNA program (543). All nucleosomal models presented in the article contain model base-pairs of the 601 sequence used in the experiments, threaded onto the rigid base-pair path DNA from the NCP147

nucleosome structure (3). Linker DNA was added in straight regular B-DNA conformation or in bent conformation, depending on the particular nucleosome model (see below).

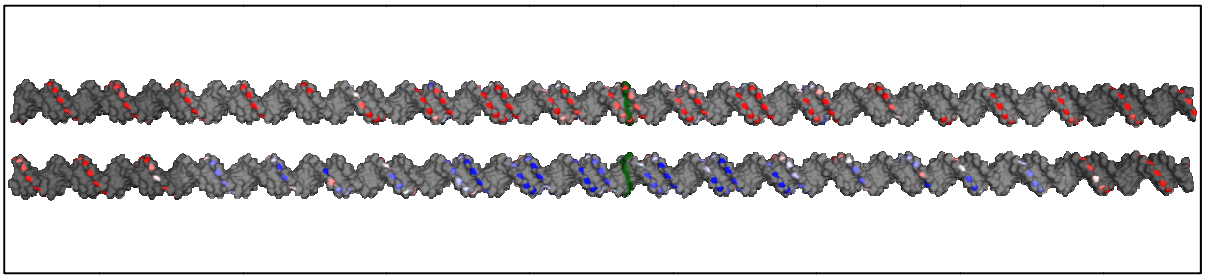

Figure sm-8: Experimental accessibility profile for nucleosomes without histone H1 shown on straight regular B-form DNA, top and bottom views. Only one half, from the dyad base-pair (green), is shown; linker base-pairs outside the 147 core base-pairs are shown in dark gray. C5' atoms not covered in single base-pair resolution are not colored.

II.8.1.2.3 Qualitative test of structural models for H1 placement

Addition of the globular domain GH1 induces additional protected sites on the core DNA and at the entering and exiting linkers (see Figures. sm-6, sm-7 and main text). We addressed the question whether existing models of linker histone placement are compatible with the observed protection patterns. Three specific models were considered: a three-contact model (91) where the linker histone is placed between and contacting both the entry and exit linker DNA and the dyad. Alternatively, in the two-contact models A (84) and B (28), the linker histone is placed between one linker and a site on core DNA, contacting only a single linker.

II.8.1.2.4 Three-contact model

The three-contact structure was proposed by Fan et al. (91) as a result of exhaustive rigid molecular docking for given DNA linker configuration. We rebuilt their structure manually by matching the orientations of the protein alpha-helices and the protein-DNA contacts for each of the three contact sites. Deviating from the choice (91) of using a GH5 X-ray structure (544), we considered the solution NMR structure ensemble of GH1 (535) since it corresponds to our experimental system, has sufficient resolution for the present purpose, and allows to assess the structural variability of the protein. Specifically, while the protein fold is stable, the protein loop regions and lysine side chain orientations are highly variable; we chose conformer 8 in the ensemble (PDB code 1ghc) since it accommodates the predicted contacts well.. At the same time, its relatively extended loop conformation does not necessitate inward bending of the DNA linkers to establish three contacts, in contrast to the

somewhat more compact GH5 conformation (6). Note that corresponding residues numbers in GH1 are offset by 22 AA from those in GH5

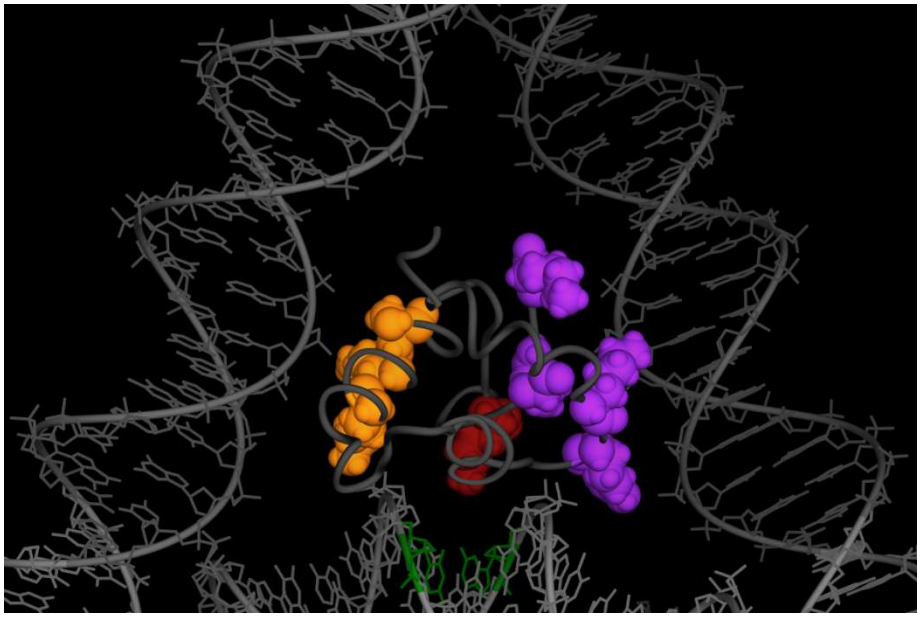

Figure sm-9: Three-contact nucleosome configuration. The contacting residues are Lys47, Lys51 and Ser52 (site I, orange); Lys63 (site II, red); and Lys18, Arg20, Arg72 and the C-terminal Arg75 (site III, purple). They correspond to the contacts proposed in Fan et al. (6). The viewing direction is the superhelical axis, but rotated by 30^0 around the dyad axis.

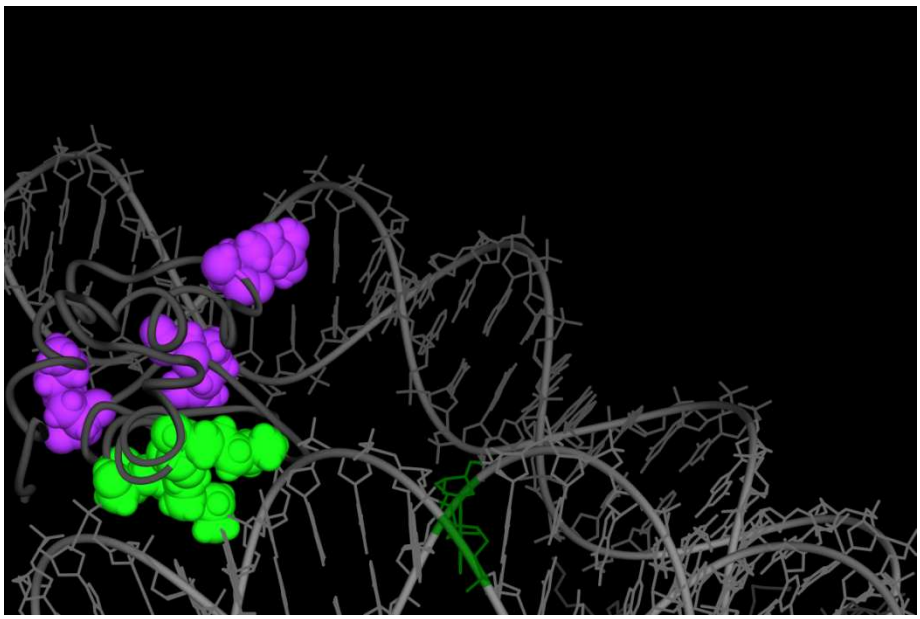

Figure sm-10: Two-contact nucleosome configuration A. Contact is established with core DNA at 1-4 bp from the dyad, and with one DNA linker (the other linker is not shown). The GH1 _-helices I (cyan), II (purple) and III (magenta) are colored as in (7); the C-terminal Lys75 is shown in purple, Lys63 is shown in red, contacting linker DNA. The residues Ser7, 19, 49 mutated in (7) are shown in orange. The viewing direction is the superhelical axis.

II.8.1.2.5 Two-contact models

Zhou et al. (84) proposed an arrangement of linker histone onto the nucleosome based on cross-linking experiments with mutated GH5. In this model (two contact model A) the linker histone globular domain contacts core DNA from the major groove, at around 2 bp distance from the dyad. It also contacts one of the DNA linkers. The spatial arrangement was rebuilt by deforming one of the linkers in the DNA model, and matching the location and helix orientations of the docking solution shown in (545) manually. We used the same molecular model (1ghc, conformer 8) for the H1 globular domain as for the three-contact model, whose shape gives close-fitting molecular contacts also in this arrangement, see Figure. sm-10. Brown et al. proposed molecular model for linker histone placement refined by rigid docking (two-contact model B) (28). Here the linker histone globular domain contacts core DNA from the major groove, at around 5 bp distance from the dyad, and one DNA linker. Note that globular domain positions in the two models A, B are on opposite sides of the dyad. Again the docking solution was reproduced manually by matching the reported helix orientations (different from model A) and contact residues; it is shown in sm-11.

Both two-contact models should be interpreted as showing one of two symmetric coexisting configurations, forming a contact with either of the linkers.

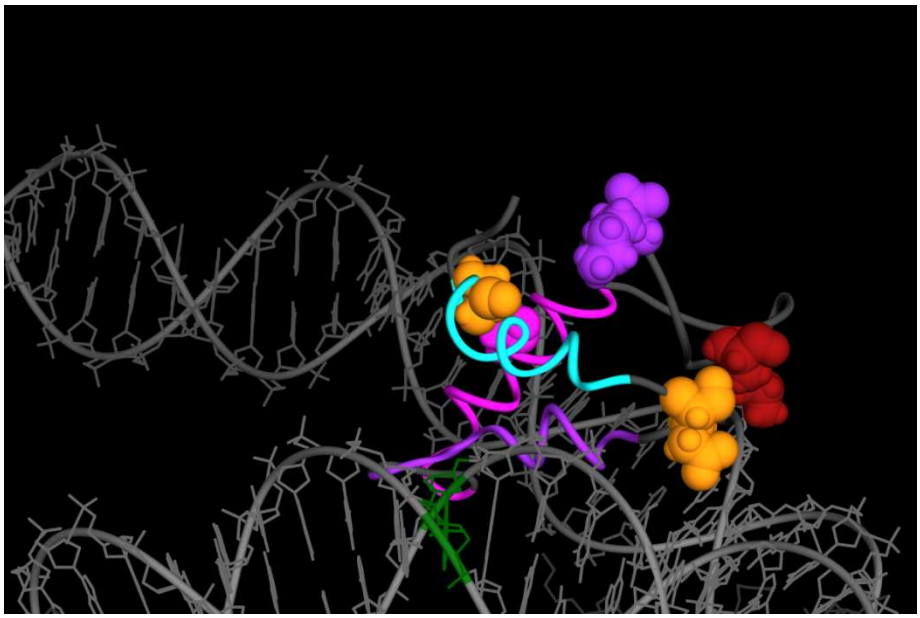

Figure sm-11: Two-contact nucleosome configuration B. Residues contacting core DNA about 5 bp away from the dyad are Lys47, Lys51 and Ser52 are colored light green; residues contacting one DNA linker are Arg20, Arg72 and Lys75 (leftmost) are colored purpl

II.8.1.2.6 Comparison

Figure sm-12 shows a comparison of the two- and three-contact models with the protection pattern observed for mononucleosomes containing the globular domain of H1. Clearly, two-contact model B leaves the dyad base-pair unprotected and thus cannot account for the observed dyad OH^o footprint. While two-contact model A places GH1 closer to the dyad, it does not cover the minor groove, making it unclear if this would produce sufficient protection of the DNA backbone from OH^o attack (see discussion in the next section). In contrast, in the three-contact model, protection from OH^o attack by occlusion due to protein contact is compatible with all three observed protected patches. These observations are unchanged when the symmetry-related configurations are taken into account. For a better impression of the spatial arrangement of GH1 in these models, see supplementary movies 2, 3 and 4.

II.8.1.3 OH^o-Footprinting predictions derived from structural models

II.8.1.3.1 Semi-quantitative OH^o footprinting predictions from structural models.

To establish a more quantitative relation between structural models and OH^o footprints, we calculated footprint predictions for different structural models. It has been shown that the C5'-H atoms of each deoxyribose on the DNA backbone are the most important sites of attack for OH^o radicals, and that the reactivity of attack sites is determined by their respective solvent accessible surface areas (4). The variations of surface accessible areas due to DNA conformation and to contacts formed with protein side-chains have been used successfully to predict the position-dependent relative accessibilities observed in OH^o-footprints (546, 547). Here, the solvent accessible surface is computed by rolling a 1.4 Å sphere representing water, or the similar-sized OH^o radical, over van der Waals spheres of the atoms in the molecular model. As a result, the solvent-accessible area of each atom can be extracted from a structural model (this area vanishes for interior atoms) (548). Lacking the resolution of single protons in our models, we somewhat simplified the procedure, considering solvent accessible surface areas of C5' atoms directly, and using 'unified vanderWaals radii' (549) to account implicitly for the hydrogens. To mimic the smoothing effect of thermal fluctuations, we increased the probe radius to 3Å. Accessible surfaces were calculated with the MSMS program (534) as implemented in the molecular visualization system Chimera (3).

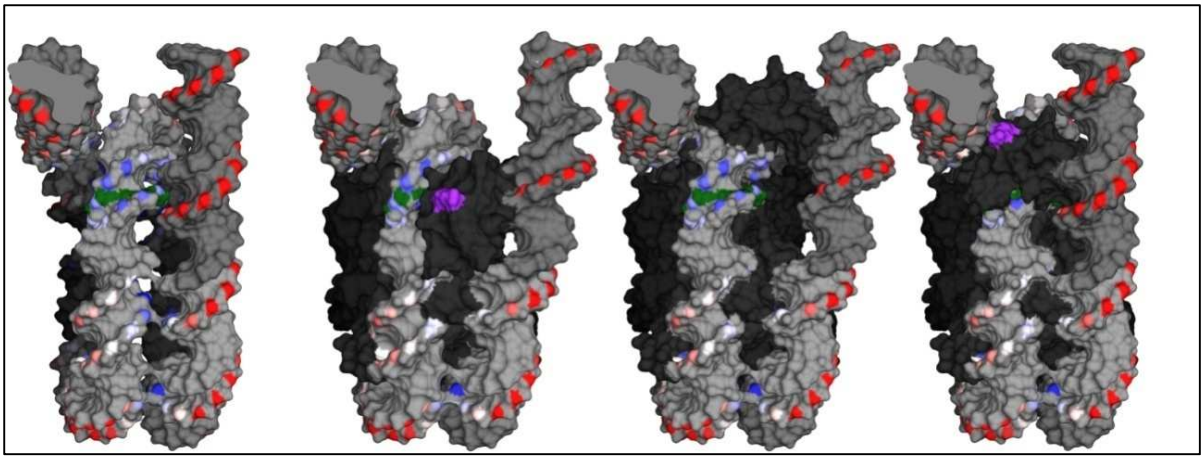

Figure sm-12: Experimental GH1 protection pattern shown color coded on a nucleosomal DNA loop (leftmost panel). The other panels add GH1 according to, from left to right, two-contact models A and B, and the three-contact model. All structures are viewed down one (unbent) linker. See also supplementary movies 2, 3 and 4.

After a moving average over the resulting trace with a 3 bp window, predicted accessibility patterns for the two strands in each complex were averaged to account for the strand-exchange symmetry observed in experimental footprints. These simplifications appear reasonable since we focus on the positions of protected sites, and aim for a semi-quantitative measure for relative protection. They are justified a posteriori by the good correlation between predicted and measured accessibility profiles along the nucleosome without H1, see Figure 6 A in the main text.

II.8.1.3.2 Structure-derived footprints for the two- and three-contact models

Figure sm-13 confronts the measured and the structure-derived accessibility profiles of two- and three-contact GH1 models. The two-contact model B fails to reproduce protection at the dyad. It also incorrectly predicts stronger protection at bp -90 than at -80. Since the contacts between H1 and the core DNA at about 10 bp distance from the dyad are in the major groove, they do not protect the DNA backbone C5' atoms from OH^o attack. As a result, there is no footprint of two-contact model B on core DNA at all. The two-contact model A gives better predictions for linker DNA, generating a protected site at bp -80. However it fails to reproduce the strong protection pattern at the dyad, despite the proximity; here again, protein contacts in the major groove cannot generate sufficient OH^o protection. In contrast, the three-contact model is compatible with the experimentally observed protection pattern, reproducing both the characteristic double-peak dyad protection at bp 2 and the protected site at bp -80.

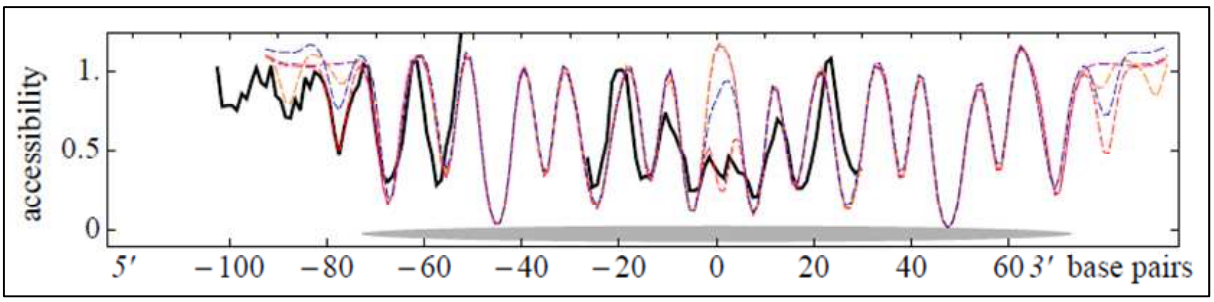

Figure sm-13: Structure-derived relative accessibility for mononucleosomes with globular H1, based on pure mononucleosome (magenta), and on the GH1 placement models: two-contact A (blue) and B (orange), and three-contact (red). The predictions differ in the protection at the dyad where the two-contact models show no or very weak protection, and at the entry/exit linkers. The measured relative accessibility for GH1 is shown in black.

II.8.1 4 Structure refinement based on DNA nano-mechanics

II.8.1.4.1 Geometric and mechanical constraints on the stem conformation

Proposed stem structures need to be compatible with the observed protection pattern on DNA linkers. Clearly, an arbitrarily chosen stem structure with juxtaposed DNA entry and exit linkers would not bring them into contact exactly at the observed sites of maximal protection. This already excludes many otherwise reasonable stem arrangements, see Figure sm-14. However, any nucleosome stem model with contacting linkers can be modified to bring the protection patterns on both linkers to face each other, just by suitably twisting DNA while keeping the linker center-lines in shape. It is thus impossible to conclude on a particular shape of the linker DNA center-lines purely on the basis of the geometric arrangement of protection patterns. On the other hand, twist deformations would imply locally varying torsional stress in the DNA linkers, which seems unlikely. To make this intuition quantitative, we considered the nanoscale mechanics of the linkers, using the rigid base-pair model of double-helical DNA (536, 550). We identify the most likely linker structure as the conformation with the lowest mechanical energy, under the constraint of reproducing the experimentally observed OH^{o}-radical protection pattern, and allowing a three-contact placement of GH1. When applied to the nucleosome without H1 or with GH1 this prescription reproduces the conformations shown in Figure 6 A and B, respectively, since straight linkers minimize the elastic energy. (Sequence dependent effects are a minor correction). For the 35-127 H1 mononucleosome, we carried out a restrained DNA elastic energy minimization which leads to the structure shown in Figure 6C, see below.

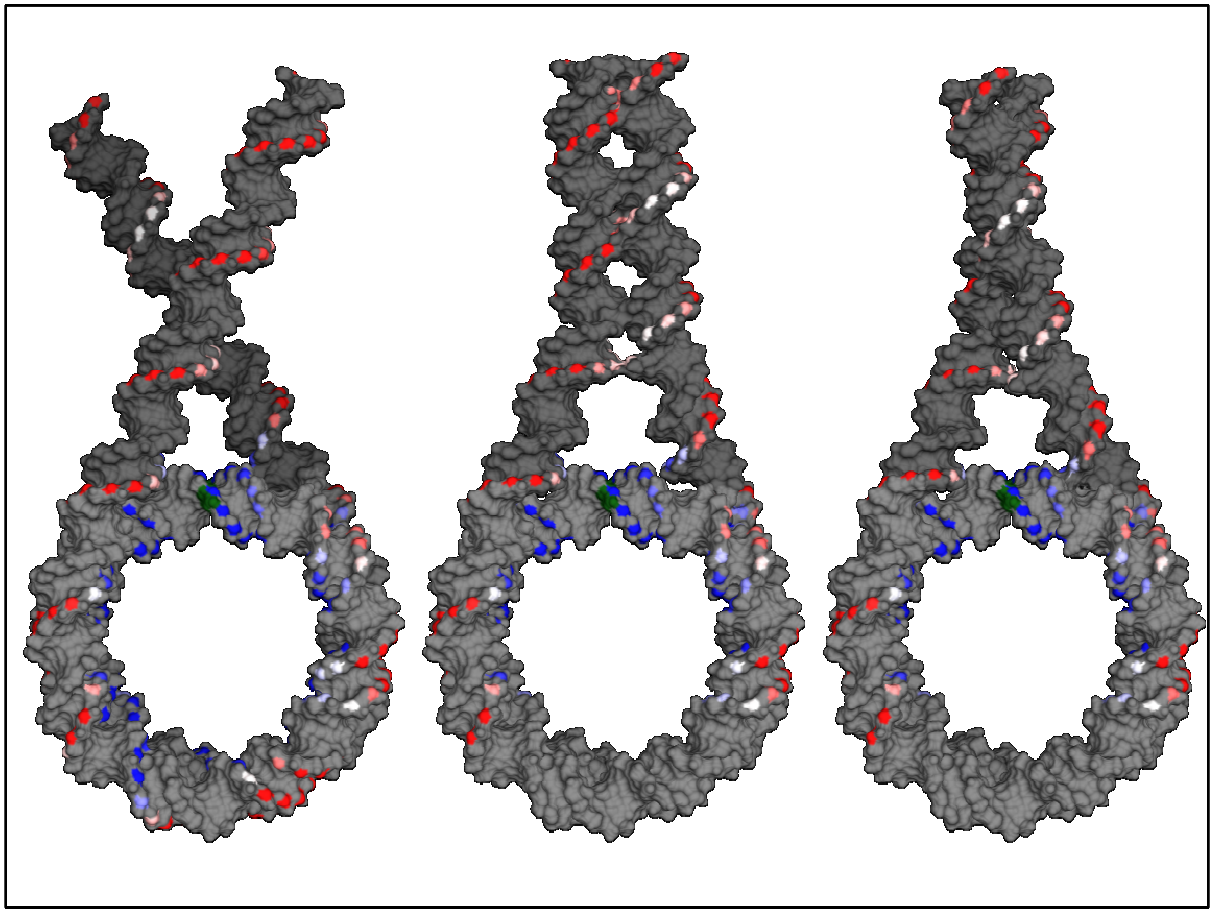

Figure sm-14: Experimental relative accessibility pattern for full-length H1 shown on a mononucleosomal loop (left). Note the extended protection sites on the inside-facing linker DNA surfaces. Two geometric models placing the DNA linkers side-by-side (middle), or with a counter-clockwise twist (right), fail to explain the observed protection pattern.

II.8.1.4.2 DNA elastic energy minimization

For energy minimization, we employed the sequence-dependent rigid base-pair model of DNA elasticity (with the 'MP' parameter set as described in (18)(537)); DNA volume exclusion was included by placing purely repulsive, truncated Lennard-Jones spheres with 2.05 nm diameter around each base pair. To enforce contacts between the two DNA linkers at corresponding maximally protected sites, linear springs were introduced between the C5' atom positions at the maxima of the accessibility profile. The positions were at distances 88.5 bp, 99.5 bp and 109.5 bp on each side of the dyad. The springs had 0 rest length, except for the one connecting positions ±88.5 bp, where the rest length was set to 0.7 nm to allow for insertion of lysines from the H1 C-terminal region. An alternative model where this rest length was set to 0 showed only slightly different global conformations. An additional spring enforced unchanged linker separation at the height of the globular domain of H1 (±80.5 bp from the dyad), and was given a rest length corresponding to the three-contact model (see

Figure. sm-9). The initial configuration was chosen with straight linkers (as in sm-14, left panel), and a conjugate gradient descent was carried out until convergence, keeping only the linker-core junction base-pairs fixed.

II.9 Movies of the Chapter are presented in the compact disc, attached physically to the thesis.

II.9.1 Movie 1: Nucleosome without histone H1

II.9.2 Movie 2: Three-contact model for a nucleosome associated with the globular domain (GH1) of histone H1.

II.9.3 Movie 3: Two-contact model (84) of a nucleosome with the globular domain (GH1) of histone H1.

II.9.4 Movie 4: Two-contact model (28) of a nucleosome with the globular domain (GH1) of histone H1.

II.9.5 Movie 5: Three-contact model for a nucleosome associated with the 40-127 mutant of histone H1.

CHAPITRE III

PUBLICATION 2

L'INCORPORATION DE LA NOUVELLE HISTONE VARIANT H2AL2 CONFER AUX NUCLEOSOMES UNE STRUCTURE INHABITUELLE AINSI DE NOUVELLES PROPRIÉTÉS FONCTIONNELLES

Dans ce travail nous avons étudies les propriétés de la nouvelle histone variant du souris H2AL2. Nous avons utilise l'H2AL2 recombinante pour reconstituer des nucleosomes et étudier leur propriétés structurales et fonctionnelles par une combinaison d'approches biochimiques et microscopiques, comme microscopie de champs de force (AFM) et cryo-microscopie électronique (EC-M). Les empreintes à la DNase I et à la nucléase microcroccocal et l'exonucléase III ont montré une structure altérée du nucléosome H2AL2 a travers toute la longueur de l'ADN nucléosomale. Les expériences de l'accessibilité a la nucléase de restriction ont montre aussi que les interactions entre l'octamer d'histones et les extrémités de l'ADN nucléosomale sont très perturbés. Les images par AFM ont montré que l'octamer d'histones H2AL2 enroule □130 pb de DNA au lieu de 147 pb. En outre, les trinucléosomes reconstitués avec H2AL2 possèdent une structure en « collier de perles » très différente de la conformation en « triangle équilatéral » des trinucléosomes conventionnels. Finalement, la présence de H2AL2 affecte le remodelage et la mobilisation de la particule variante par les facteurs de remodelage RSC et SWI/SNF. Ces propriétés inhabituelles du nucléosome variant H2AL2 suggèrent un rôle spécifique dans la spermiogenèse.

CHAPTER III: PUBLICATION 2

THE INCORPORATION OF THE NOVEL HISTONE VARIANT H2AL2 CONFERS UNUSUAL STRUCTURAL AND FUNCTIONAL PROPERTIES OF THE NUCLEOSOME

Sajad Hussain Syed[1], Mathieu Boulard[1,2], Manu Shukla[1], Thierry Gautier[1], Andrew Travers[3], Jan Bednar[4,5], Cendrine Faivre-Moskalenko[6], Stefan Dimitrov[1]* and Dimitar Angelov[2]*

(Published in Nucleic Acids Research, 2009 Aug, Vol. 37(14):4684-95)

[1]Université Joseph Fourier - Grenoble 1; INSERM Institut Albert Bonniot, U823, Site Santé-BP 170, 38042 Grenoble Cedex 9, France

[2]Université de Lyon, Laboratoire de Biologie Moléculaire de la Cellule, CNRS-UMR 5239/INRA 1237/IFR128 Biosciences, Ecole Normale Supérieure de Lyon, 46 Allée d'Italie, 69364 Lyon cedex 07, France

[3]MRC Laboratory of Molecular Biology, Hills Road, Cambridge CB2 2QH, UK

[4]CNRS/UJF, Laboratoire de Spectrométrie Physique, UMR 5588, BP87, 140 Av. de la Physique, 38402 St. Martin d'Hères Cedex, France

[5]Institute of CellularBiology and Pathology, First Faculty of Medicine, Charles University in Prague and Department of Cell Biology, Institute of Physiology,Academy of Sciences of the Czech Republic, Albertov 4, 128 01 Prague 2, Czech Republic

[6]Université de Lyon, Laboratoire de Physique, CNRS UMR 5672, Ecole Normale Supérieure de Lyon, 46 Allée d'Italie, 69007 Lyon, France

*Corresponding authors:

e-mail : dimitar.anguelov@ens-lyon.fr, phone: +33472728898 ; fax: +33472728080

e-mail : stefan.dimitrov@ujf-grenoble.fr, phone: +33476549473 ; fax: +33476549595

Running title: Histone variant H2AL2

Keywords: chromatin/chromatin remodeling/histone variant/nucleosome/AFM

III.1 Abstract

In this work we have studied the properties of the novel mouse histone variant H2AL2. H2AL2 was used to reconstitute nucleosomes and the structural and functional properties of these particles were studied by a combination of biochemical approaches, atomic force microscopy (AFM) and electron cryo-microscopy (EC-M). DNase I and hydroxyl radical footprinting as well as micrococcal and exonuclease III digestion demonstrated an altered structure of the H2AL2 nucleosomes all over the nucleosomal DNA length. Restriction nuclease accessibility experiments revealed that the interactions of the H2AL2 histone octamer with the ends of the nucleosomal DNA are highly perturbed. AFM imaging showed that the H2AL2 histone octamer was complexed with only ~130 bp of DNA. H2AL2 reconstituted trinucleosomes exhibited a type of a “beads on a string” structure, which was quite different from the equilateral triangle 3D organization of conventional H2A trinucleosomes. The presence of H2AL2 affected both the RSC and SWI/SNF remodeling and mobilization of the variant particles. These unusual properties of the H2AL2 nucleosomes suggest a specific role of H2AL2 during mouse spermiogenesis.

III.2 Introduction

Chromatin exhibits a repeating structure. The basal repeating unit of chromatin, the nucleosome, is formed upon wrapping of two superhelical turns of DNA around an octamer of core histones (two of each H2A, H2B, H3 and H4). The structures of the histone octamer and the nucleosome were solved by X-ray crystallography (2, 26, 56). The histones within both the nucleosome and the histone octamer are constituted of structured histone fold domains and unstructured N-termini (2, 56). The individual nucleosomes are connected by linker DNA and formed in this way the chromatin filament. A fifth histone, termed linker histone, is associated with the linker DNA and it assists the folding of the chromatin filament into the 30 nm chromatin fiber (34, 184, 199, 551, 552).

The nucleosome is a repressive structure. It interferes with the cellular processes, which need access to naked DNA. The cell uses three main strategies to overcome the nucleosome barrier, namely posttranslational histone modifications, chromatin remodeling by ATP-consuming chromatin remodeling machines and histone variants.

The N-termini of the histones play an essential role in the organization of both the chromatin fiber (553, 554) and the mitotic chromosomes (525, 527). The histone posttranslational modifications are essentially located at the non-structured N-termini of the histones. They can affect both the compaction of the chromatin fiber and the ability of remodeling machines to mobilize nucleosomes (for a recent review see(555)). A typical example for such role of the histone modifications is the acetylation of the core histones (556, 557) and in particular the acetylation of histone H4 at K16 (193). Histone modifications serve also as marks. These marks are recognized by specific protein factors, which in turn have important functional consequences (148, 555).

The chromatin remodelers are high molecular multiprotein complexes, which are able, at the expenses of ATP hydrolysis, to mobilize the nucleosomes. The chromatin remodelers are required for several vital cellular processes, including transcription, replication and DNA repair. They are grouped in four distinct families: SWI2/SNF2, ISWI, CHD and INO80 (280). SWI/SNF and RSC (both belonging to the SWI2/SNF2 family), in addition to their capacity to mobilize the nucleosomes, are also able to alter significantly the structure of the nucleosomal particle and even to evict the histone octamers (558, 559).

Histone variants are non-allelic isoforms of conventional histones (422). They show a variable degree of homology with their conventional counterparts (for a recent review see (421)). All core histones, with the exception of H4, have histone variants. The H2A histone

variants form the largest family of histone variants, including macroH2A, H2A.Z, H2A.X, H2A.Bbd, etc. Recently, a novel histone mouse variant, H2AL2, belonging to the H2A family, was described (483). PCR experiments showed that H2AL2 is expressed in different tissues, but its expression was found to be remarkably strong during spermatogenesis (483).

The incorporation of some of the histone variants within the nucleosomes resulted in alterations of its structure, which, in turn, affected its functional properties (194, 469, 478, 516). The most striking example is H2A.Bbd. H2A.Bbd nucleosomes exhibited strong perturbations all over the nucleosomal DNA, these perturbations being stronger around the dyad axis (473, 474, 478). H2A.Bbd histone octamer was able to wrap only ~130 bp of DNA and H2A.Bbd nucleosomes exhibited very low stability both *in vitro* (194, 473, 474, 478) and *in vivo* (475). In addition, the remodeling complexes SWI/SNF and ACF were unable to both remodel and mobilize the H2A.Bbd nucleosomes. Polymerase II activated transcription was more efficient from H2A.Bbd nucleosomal arrays than from conventional H2A templates (194, 474). The unusual docking domain of H2A.Bbd was important in determining these particular properties of the H2A.Bbd chromatin (194, 474).

In this work we have focused on the recently identified histone H2AL2. We confirmed the reported data that H2AL2 is expressed exclusively in testis and we have studied the structural and functional properties of the H2AL2 reconstituted nucleosomes. We show that the incorporation of this sperm specific histone variant within the nucleosomes altered dramatically its structural properties. These structural perturbations affected both the remodeling and the relocation of the H2AL2 nucleosomes induced by either SWI/SNF or RSC chromatin remodelers.

III.3 Materials and methods

III.3.1 H2AL2 cloning and preparation of DNA fragments

The H2AL2 coding sequence was amplified by PCR by using the EST IMAGE clone 6774311 cDNA and the primers 5’-TTTTCCTGGCCATATGGCCAGGAAAAGGCAAAGG -3’ (forward) and 5’-TGAGGATCCTCAGTTGTCATCAGGTTCTGGT-3’ (reverse). The PCR product was cloned between the restriction sites Nde I and BamH I in a pET3a vector (Novagen).

The 255 bp DNA fragments, containing the 601 nucleosome positioning sequence at the middle was obtained by polymerase chain reaction (PCR) amplification from plasmid pGem-3Z-601 (Kindly provided by J. Widom and B. Bartholomew). The fragment was

labeled either by incorporating the [α-^{32}P]CTP and [α-^{32}P]TTP to the PCR reaction for micrococcal digestion experiments or by 5` labeling one of the primers for exonuclease and hydroxyl radical footprinting experiments.

For "One Pot Restriction enzyme Assay" a set of eight pGEM-3Z-601.2 mutants were utilized, each containing Hae III site at a different superhelical location, as described before (560). The 5' labeled 147 bp core particle sequences were obtained by PCR amplification similarly. The same fragments were used for DNase I footprinting experiments.

The 200 bp DNA fragment, containing the 601 nucleosome positioning sequence at the end of the fragment was obtained by cutting the 255 bp 601 with Not I. It was labeled with Klenow enzyme with [α-^{32}P]CTP in the presence of 50 μM dGTP. All the labeled probes were gel purified by 5% native acrylamide gel. DNA containing three repeats of the 601 sequence was constructed by using standard methods. The 33x200-601 DNA was produced as reported (184) and nucleosomal array reconstituted by salt-dialysis.

III.3.2 Protein purification and nucleosome reconstitution

Xenopus laevis histone proteins were produced in bacteria and purified as described (529). Recombinant H2AL2 protein was also purified like other histone proteins by usual process of IPTG induction, inclusion body solubilization and ion exchange purification. RSC and SWI/SNF were purified from yeast cells by using a standard TAP tag protocol (561). The activity of both remodelers was normalized by measuring their effect on the sliding of conventional nucleosomes (477). Nucleosome reconstitution was performed by the salt dialysis procedure (525). To demonstrate that both reconstituted conventional and H2AL2 nucleosomes contain a full complement of core histones, 5 μg of the nucleosomes reconstituted on 255 bp 601 sequence were run on a 5% native polyacrylamide gel. After completion of the electrophoresis, the bands corresponding to the nucleosomes were excised, eluted overnight in TE buffer, TCA precipitated and analyzed by 18% SDS–PAGE. The gel was stained by Sypro ruby protein gel staining solution from Invitrogen for better sensitivity.

III.3.3 Exonuclease III mapping, footprinting, micrococcal nuclease digestion

Exonuclease mapping, DNase I and hydroxyl radical footprinting were performed as described previously (469, 470, 562). Micrococcal nuclease digestion was performed at 8 U/ml at 30^{0}C for indicated times as described previously (470).

III.3.4 Nucleosome mobilization and remodeling

Mobilization experiments were carried out using centrally positioned nucleosomes, reconstituted on a 255 bp DNA fragment containing the 601 positioning sequence. The nucleosome samples (5 ng/µl) were incubated in remodeling buffer (10 mM Tris–HCl, pH 7.4, 5% glycerol, 100 µg/ml BSA, 1 mM DTT, 0.02% NP40, 40 mM NaCl, 2.5 mM $MgCl_2$ and 1 mM ATP) with different concentrations of remodelers for 45 min at 30^0 C and loaded on a 5% native PAGE. End positioned nucleosomes reconstituted on a 200 bp 601 DNA fragment (200 ng) were incubated in remodeling buffer with SWI/SNF and RSC as indicated. The reaction was stopped at different time points (aliquoting) by adding 1 µg of plasmid DNA and 0.02 U of apyrase. These aliquots were subsequently digested by the same amount of DNase I. Similar experiment was done using RSC on the centrally positioned nucleosome with end labeled 601 DNA (Figure 8B).

III.3.5 "One pot" restriction enzyme accessibility assay

For "one pot" assay 200 ng of core particle nucleosomes were digested with Hae III with final concentration of 5 U/µl. Aliquots were taken at different time points and the reaction stopped. Phenol chloroform purified and ethanol precipitated DNA fragments were separated on 8% sequencing PAGE and quantified. The accessibility of different superhelical locations was quantified after normalizing the data against the ratio of different probes in the mixture (560).

III.3.6 Xba 1 restriction assay

To confirm the inefficiency of remodeler to slide the H2AL2 nucleosome, an Xba 1 restriction site in the linker DNA was probed for eventual inhibition of restriction by the translocation of nucleosomes. Briefly Conventional and H2AL2 nucleosomes were reconstituted on an end labeled 255 bp centrally positioned 601.2 sequence with 51 bp and 57 bp linkers. The nucleosomes were subjected to RSC remodeling reaction at 30^0 C in remodeling buffer lacking glycerol for 45 minutes and stopped by adding 0.01 units of apyrase. 0.04 Units/µl of Xba 1 were added to the reaction mixture and aliquots were taken at different time points and the reaction stopped. The purified DNA was resolved by 8% sequencing gel. Note that under the buffer condition used the maximum Xba 1 cleavage was below 60%, even on naked DNA.

III.3.7 Atomic Force Microscopy

AFM imaging of conventional and H2AL2 nucleosomes was carried out as described previously (563). APTES-mica surfaces were used to trap the 3D conformations of the nucleosomes (563). The samples were visualized by using a Nanoscope III AFM (Digital Instruments^{TM}, Veeco, Santa Barbara, CA) in Taping mode in air. Automated image analysis was performed using a specially designed Matlab script (The Mathworks, Natick, MA) based on morphological tools, which allowed the precise length measurement for each naked DNA arm from the nucleosome (563).

Centrally positioned nucleosomes, reconstituted on 255 bp 601 sequence, were used in the AFM experiments. The length (L_c) of DNA in complex with the histone octamer was calculated by $L_c = L_{tot} - L_- - L_+$ where L_{tot} is 255 bp, and L_+ and L_- are the long and the short naked DNA arm of the nucleosome, respectively. The position of the nucleosome relative to the center of the DNA was deduced by $\Delta L = (L_+ - L_-)/2$ (563). An 8 bp-sliding box was used for the construction of both L_c and ΔL smooth distributions (563).

To study the effect of remodeler, the nucleosomes were incubated with RSC for 30 minutes at 29°C in a buffer containing 10 mM Tris pH = 7.4, 1.5 mM $MgCl_2$ and 1 mM ATP). A drop of the reaction mixture was diluted and deposited on functionalized mica surface for visualization by AFM. To plot the conventional and variant nucleosome position distribution, only the nucleosomes having their DNA complexed length in the range $<L_c> \pm \sigma L_c$ were selected (where $<L_c>$ and σL_c are respectively the mean and the standard deviation of the complexed length distribution in the absence of RSC.

III.3.8 Electron Cryo-microscopy

Electron cryo-microscopy samples preparation was performed as described (564). Briefly, the film surface of the electron microscopy grids was treated by subsequent evaporation of carbon and carbon-platinium layers. After dissolving the plastic support, 3 µl of either conventional or H2AL2 tri-nucleosome solution were deposited on the grid, the majority of the liquid was removed by Whatman blotting paper and the grid was then immediately plunged into liquid ethane. The grid was transferred without re-warming in Philips Tecnai G2 Sphera microscope equipped with Ultrascan 1000 CCD camera (Gatan).

III.4 Results

III.4.1 Histone H2AL2 is specifically expressed in the testis and could efficiently replace conventional H2A in the nucleosome

H2AL2 is a recently identified mouse H2A histone variant (483). H2AL2 shows only 41% identity with conventional H2A (483). The protein exhibits similar primary sequence to this of H2A.Bbd, a human variant of H2A (see Figure 1A). Indeed, both H2A.Bbd and H2AL2 show an arginine track at their N-termini and shorter docking domain than this of H2A (Figure 1A). H2A.Bbd is mainly expressed in testis, but it was also found in other tissues (472, 565). RT-PCR data have suggested that H2AL2, similarly to H2A.Bbd, was expressed in different tissues, but mainly in testis (483). Since PCR is, however, very sensitive to small contaminations, we have studied the expression of H2AL2 in different mouse tissues by using Northern blot analysis. The data show that, in general agreement with the reported data, H2AL2 is expressed only in testis (see Supplemental Figure 1), suggesting that H2AL2 is a mouse testis-specific histone variant.

H2A.Bbd could be used to reconstitute nucleosomes, but the H2A.Bbd nucleosomes exhibited peculiar properties (194, 470, 472-475). Bearing in mind the primary sequence similarity between H2A.Bbd and H2AL2 one could expect similar behaviour of H2AL2 nucleosomes. To test this we have first reconstituted H2AL2 nucleosomes (Figure 1). We have expressed and purified to homogeneity conventional core histones as well as H2AL2 (Figure 1B) and used them to reconstitute nucleosome core particles by using ^{32}P-end labeled 147 bp 601.2 positioning sequence. The data show (Figure 1C) no presence of free DNA in the reconstituted both conventional and H2AL2 nucleosomes illustrating that, H2AL2, as H2A.Bbd, could efficiently replace conventional H2A in the histone octamer.

To further show that the reconstituted particles contain a full complement of core histones, we have used conventional and H2AL2 histone variant nucleosomes, reconstituted on 255 bp 601 DNA sequence. Both particles were run on 5% native gel (Figure 1D) and the bands corresponding to the respective particles were excised from the gel. Then we eluted the nucleosomes from the gel slices and separated the histones in 18% SDS-PAGE (Figure 1E). As seen, a full complement of core histones is observed in both cases demonstrating that *bona fide* particles are reconstituted under our experimental conditions.

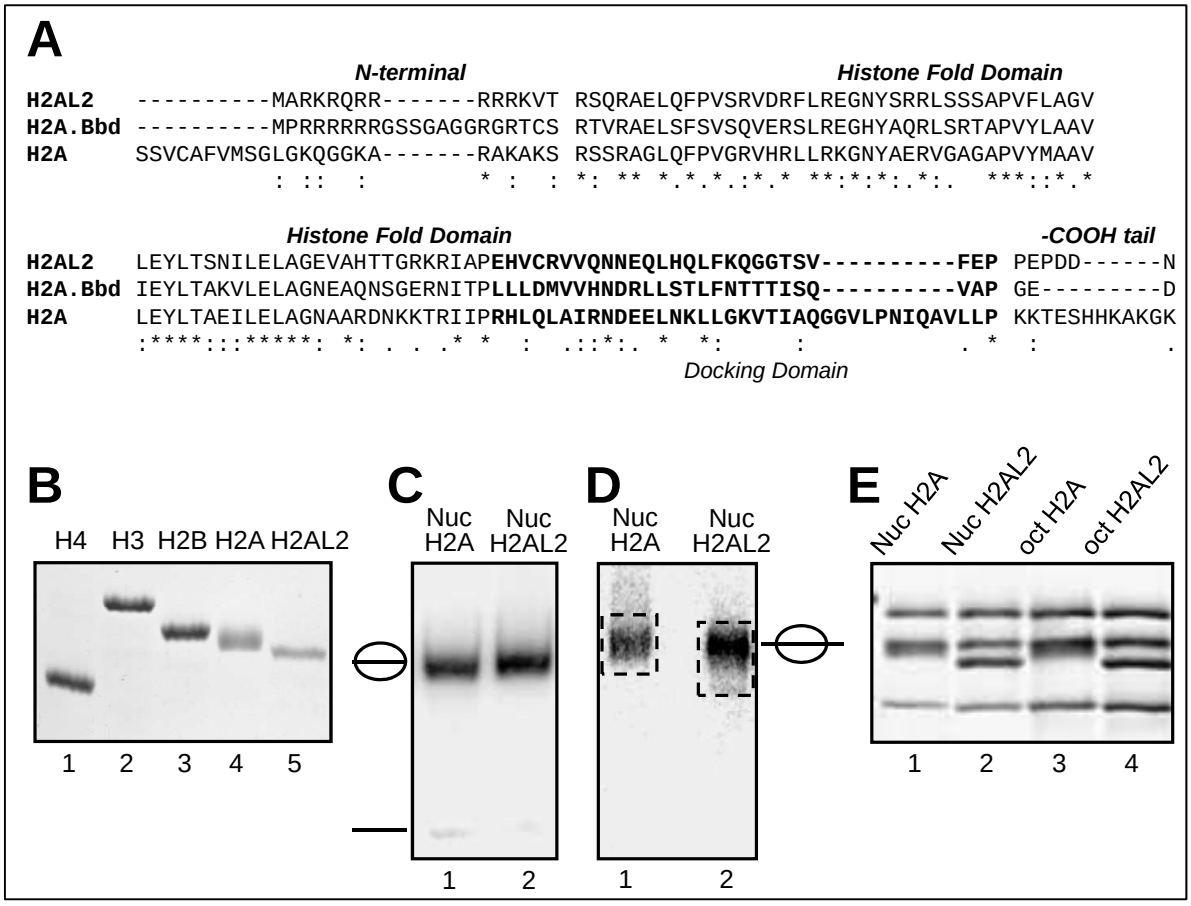

Figure 1: The histone variant H2AL2 can substitute for conventional H2A in the nucleosome. (A) Sequence alignment of mouse H2A.1 and H2AL2 and human H2A.Bbd. The N- and C-termini, the histone-fold domain as well as the docking domain (in bold) are indicated. (B) 18% SDS electrophoresis of the purified recombinant histones used for nucleosome reconstitution. (C) EMSA of reconstituted nucleosome core particles. 32P-end labeled 147 bp 601.2 DNA sequence was used to reconstitute conventional and histone variant H2AL2 core particles. The reconstituted particles were run on 5% PAGE under native conditions. The positions of the core particles and of free DNA are indicated. Note that under the conditions of reconstitution essentially no free DNA was observed. (D) Preparative EMSA of reconstituted nucleosomes. Conventional and H2AL2 nucleosomes, reconstituted on 255 bp 601 DNA sequence, were run on 5% native PAGE, the bands corresponding to the nucleosomes were excised and then the nucleosomes were eluted from the gel. The gel purified nucleosomes were run on SDS electrophoresis. (E) 18% SDS electrophoresis of both conventional and H2AL2 histone octamers (lanes 3 and 4) and gel purified reconstituted nucleosomes (lanes 1 and 2).

III.4.2 DNase I and hydroxyl radical footprinting of H2AL2 histone variant nucleosomes

To study the organization of the nucleosomal DNA in the variant H2AL2 particles we have used both DNase I and hydroxyl radical footprinting (Figure 2). Numerous distinct alterations were observed in the DNase I digestion pattern of the H2AL2 nucleosome core particle (Figure 2A, lanes 2-7) compared to this of the conventional core particle (Figure 2A, lanes 9-14). Indeed, changes in the intensity of many bands corresponding to the DNase I digestion products all over the length of the nucleosomal DNA were clearly detected.

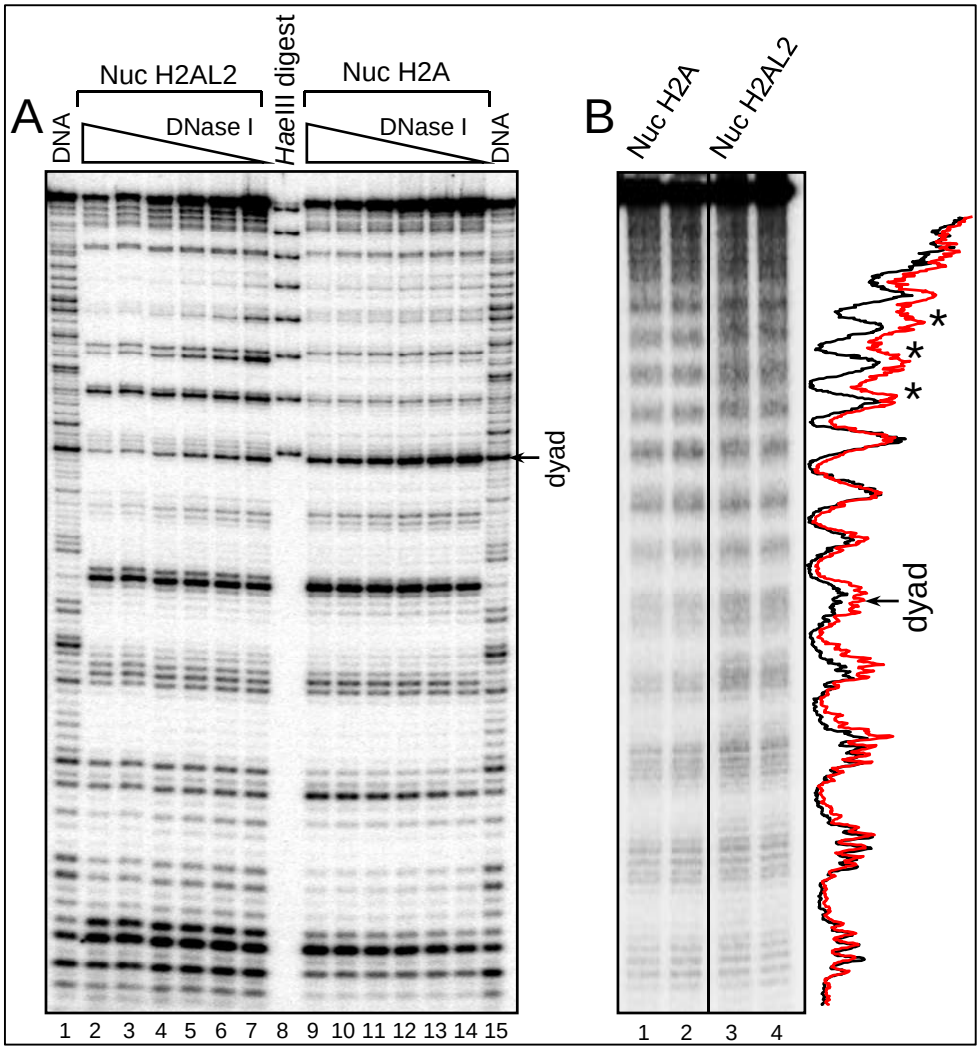

Figure 2: DNase I and hydroxyl radical footprinting show alterations in the structure of the histone variant H2AL2 nucleosome. (A) DNase I footprinting. Conventional (lanes 2-7) and H2AL2 (lanes 9-14) nucleosome core particles were reconstituted by using 32P-radiolabeled 147 bp 601.2 positioning DNA sequence and digested with decreasing amount of DNase I. After purification the cleaved DNA was run on an 8% sequencing PAGE. Lanes 1 and 15 show the DNase I digestion pattern of free DNA. The molecular marker (lane 8), is a Hae III digested mix of the eight 147 bp 601.2 fragments; the band with the highest molecular weight corresponds to 147 bp, and the consecutive bands are separated by 10 bp (see Material and Methods, one pot assay). The position of the nucleosome dyad is indicated at the right part of the figure. (B) Hydroxyl radical footprinting. Centrally positioned conventional and H2AL2 nucleosomes were reconstituted on 32P-radiolabeled 255 bp 601 positioning DNA sequence and subjected to OH° cleavage. The cleaved DNA was purified from the conventional and H2AL2 nucleosomes and run (in duplicate) on 8% PAGE under denaturing conditions. Lanes 1 and 2 were not adjacent to lanes 3 and 4 in the original gel, and they were thus demarked accordingly. The right part of the figure shows the scans of the OH° cleavage patterns of the two samples (red, H2AL2 nucleosomes; black, H2A nucleosomes). The position of the nucleosome dyad is indicated. Note the lower contrast of the cleaved H2AL2 nucleosomal DNA (designated by ∗) towards the end of the nucleosome DNA.

The OH° cleavage pattern of the H2AL2 255 bp nucleosome particle exhibited also some alterations. These alterations were more pronounced towards the end of the DNA complexed with the H2AL2 histone octamer, where the contrast of the bands was clearly decreased (Figure 2B, compare lanes 3 and 4 with lanes 1 and 2). We attributed these changes in the DNase I and OH° cleavage patterns to reflect H2AL2 associated perturbations in the over-all structure of the variant nucleosome.

III.4.3 Micrococcal and Exonuclease III digestion demonstrates a distinct organization of the H2AL2 nucleosome

The structure of the H2AL2 nucleosomes was further investigated by micrococcal nuclease and exonuclease III digestion. For the experiments with micrococcal nuclease, a 255 bp 601 sequence was ^{32}P-body labeled and used for reconstitution of both conventional and H2AL2 nucleosomes. These nucleosomes were centrally positioned leaving two free DNA arms of 52 and 56 bp, respectively. Identical amounts (~ 50 ng) of these two samples were incubated in the presence of 1 μg of naked DNA (the presence of nearly 20 fold excess of naked DNA allows a very precise standardization of the digestion conditions; note that under these conditions the nucleosomes are stable and no transfer of histones to the naked DNA was observed) for the indicated times with 8 units/ml of micrococcal nuclease and after arresting the digestion, DNA was isolated and run on a 10 % PAGE under native conditions (Figure 3A). In the case of conventional particles, the free DNA arms were rapidly digested and a stable digestion intermediate, corresponding to the core particle is generated (Figure 3A, lanes 2-6). Note that even at the longest time of digestion (32 minutes, Figure 3A) a very weak subnucleosomal digestion band was detected. The H2AL2 particles show, however, different digestion pattern (Figure 3A, lanes 8-12). Indeed, a strong band corresponding to the subnucleosomal particle was already observed at 8 minutes of digestion and at the longest time of digestion (32 minutes) essentially only subnucleosomal particles were generated. This demonstrates that the H2AL2 nucleosomal DNA is more accessible to micrococcal nuclease suggesting that its structure is more relaxed compared to this of the conventional particle.

The accessibility of H2AL2 reconstituted nucleosomal arrays to micrococcal nuclease was also investigated and was compared to this of conventional nucleosomal arrays (Figure 3B). The data clearly show that, as in the case of mononucleosomes, the H2AL2 arrays are more rapidly digested than the conventional ones indicated that not only the monosomes but also the nucleosomal H2AL2 arrays, exhibited more relaxed structure.

The accessibility of H2AL2 nucleosomes to exonuclease III was also studied. These experiments use a centrally positioned nucleosome reconstituted on a ^{32}P-5'end labeled 255 bp 601 DNA sequence. This nucleosome bears, as mentioned above, two free DNA "arms" of 52 and 56 bp, respectively. Incubation of the conventional nucleosomes with exonuclease III results into two major stable intermediates: a first one, located at position 200 bp and thus, corresponding to the border of the particle (Figure 3C, lanes 2-5) and a second one at around 185 bp position and reflecting an arrest of the nuclease in the interior of the particle. Small amounts of lower molecular weight intermediates are also generated at longer times of incubation with the enzyme. Upon increasing the time of digestion the amount of the first intermediate decreases, this of the second increases, but even at the longest time of digestion the first intermediate is still present. The exonuclease III digestion profile of the H2AL2 particle was totally different from this of the conventional one, since six distinct digestion products were produced (Figure 3C, lanes 7-10), the molecular masses of the first three higher molecular bands being the same as these of the conventional particles. Increasing the time of digestion leads to the generation of mainly lower molecular mass fragments, corresponding to pauses of the exonuclease deeply in the interior of the H2AL2 particle. The observed ability of exonuclease III to overcome the structural barriers imposed by the H2AL2 particle evidences for weaker histone-DNA interactions and thus, for weaker stability of this particle.

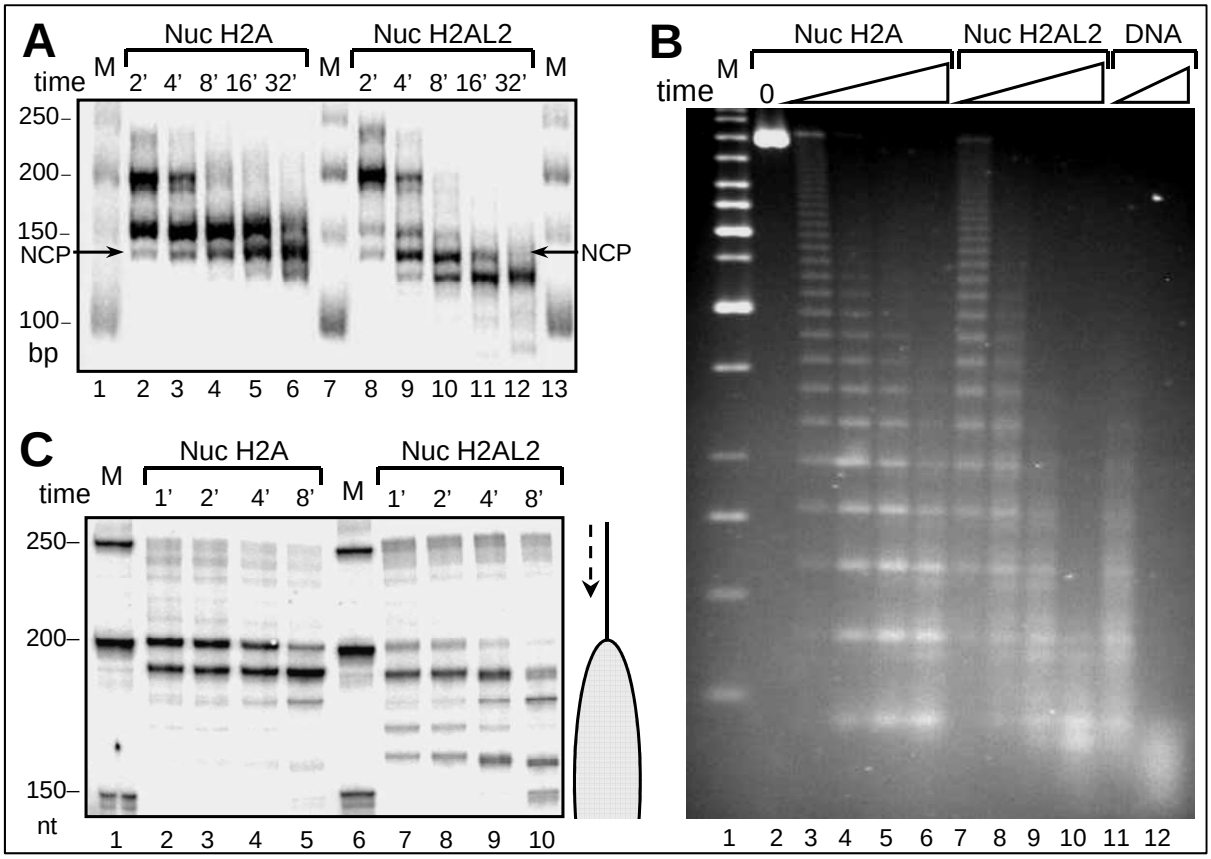

Figure 3: Higher accessibility of H2AL2 mono-nucleosomes and nucleosomal arrays to micrococcal nuclease and exonuclease III digestion. (A) Identical amounts (50 ng) of conventional (Nuc H2A) and H2AL2 (Nuc H2AL2) nucleosomes (reconstituted on a body labeled 255 bp 601 sequence) in a solution of 10 µl were digested (in the presence of 1 µg plasmid DNA) with 8 units/ml of micrococcal nuclease for the indicated times (2 to 32 minutes) at room temperature. After arresting the reaction, the digested DNA was isolated and run on 10% native PAGE. Lanes 1, 7 and 13, DNA molecular mass markers. The lengths (in bp) of the markers are indicated at the left side of the figure. (B) Micrococcal nuclease digestion of conventional H2A and histone variant H2AL2 33X200-601 arrays. 100 ng of fully saturated reconstituted conventional (lanes 2-5), H2AL2 (lanes 7-10) and naked DNA (lanes 11-12) arrays were digested for different time points with micrococcal nuclease. The digested DNA was isolated and run on 1.4 % agarose gel and visualized with SYBR green. Lane 1, 10 kb molecular mass DNA marker. (C) Exonuclease III digestion of conventional and H2AL2 nucleosomes. 50 ng of uniquely 5'-end labeled centrally positioned nucleosomes (reconstituted on a 255 bp 601 sequence) were digested with the same amount of exonuclease III for the times indicated. The reaction was arrested and, after purification, the digestion products were run on an 8% denaturing gel. The lengths of the 50 bp DNA marker (lanes 1 and 6) are indicated at the left site of the figure.

III.4.4 The "one pot assay" shows that the interactions between the histone octamer and the ends of nucleosomal DNA are highly perturbed within the H2AL2 particle

To further study the structure of the H2AL2 histone variant nucleosome we also used a recently described "one pot assay" (560). Briefly, both conventional and H2AL2 147 bp core particles were reconstituted by using eight mutated ^{32}P-end labeled 601.2 DNA sequences. Each individual sequence was mutated in a way to introduce a single Hae III restriction site in it. All restriction sites exhibit the same rotational position with an outward-facing minor groove and are separated by 10 base pairs (560) (for simplicity further in the text the Hae III restriction sites will be designated as d_0 (superhelical position 0) to d_7 (superhelical position 7). Then, the nucleosome samples were incubated with 5 units/μl of Hae III for increasing times. After arresting the reaction, DNA was isolated and run on 8% PAGE under denaturing conditions (Figure 4A) . The quantification of the Hae III cut efficiency at the different sites is shown at Figure 4B. As seen, major differences in the cut efficiencies are observed at d_5 and d_6, i.e. close to the end of the nucleosomal DNA (note that under our experimental conditions we were unable to separate the Hae III d_7 cleavage products from the non-cleaved fragments, which did not allow the calculation of the cleavage efficiency at d_7). Indeed, both the initial cut rate (the slope of the curves) as well as the saturation of the cleavage are much higher for these superhelical positions for the H2AL2 nucleosomes compared to these of the conventional ones.

We conclude that the histone-DNA interactions at the end of the nucleosomal DNA are strongly perturbed within the H2AL2 particle. Note that there are also differences inside the nucleosome, particularly at d_0, d_2 and d_4 consistent with the DNase I digestion data in figure 2.

III.4.5 AFM imaging of conventional and H2AL2 nucleosomes

The described structural alterations in the H2AL2 nucleosomes are similar to these of the H2A.Bbd nucleosomes (478). The length (L_c) of the DNA complexed with the histone octamer was found to be only ~130 bp within the H2A.Bbd nucleosome (478). With this in mind, we next asked whether the H2AL2 variant histone octamer exhibited the same property, i.e. whether it organizes also less DNA than the conventional octamer does (147 bp). To this end we have imaged by AFM both centrally positioned conventional and H2AL2 nucleosomes reconstituted on 255 bp 601 DNA fragment (Figure 5A, B).

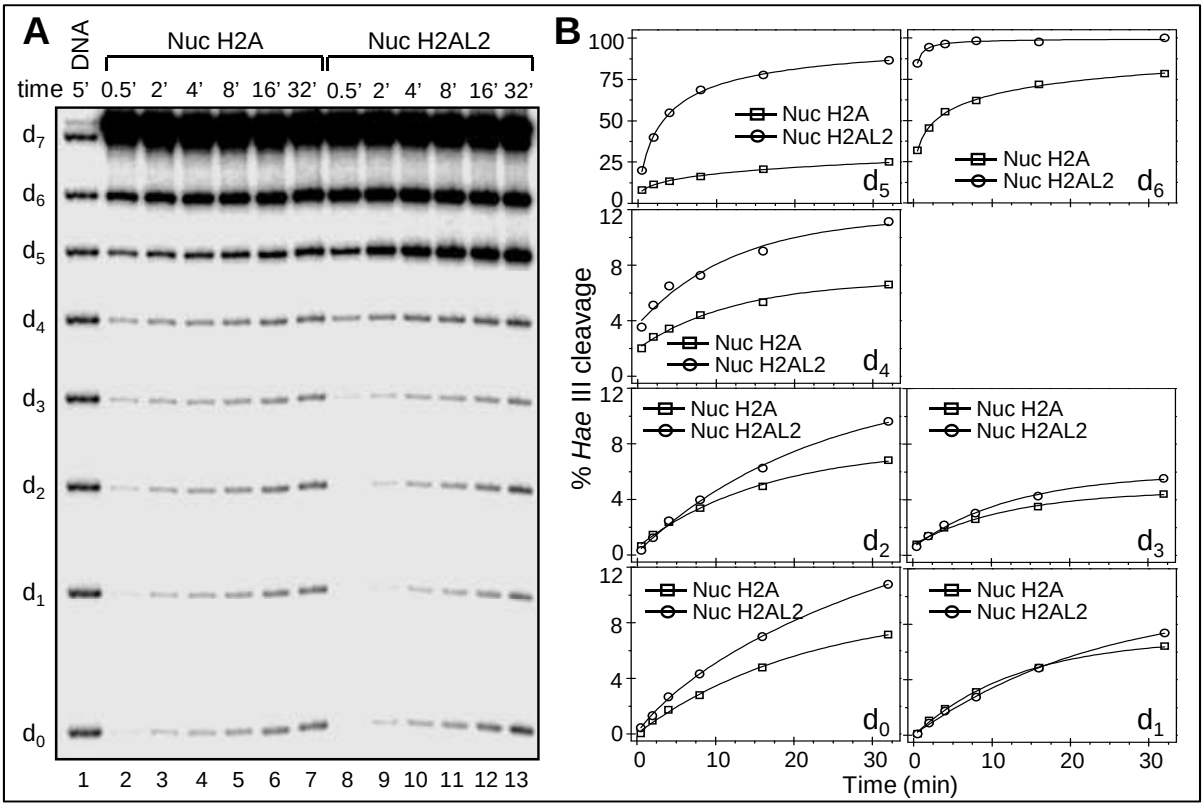

Figure 4: "One pot assay" of conventional and H2AL2 nucleosomes. (A) Kinetics of the Hae III digestion of conventional H2A (Nuc H2A) and variant H2AL2 (Nuc H2AL2) nucleosomes. Identical amounts of both types of nucleosomes were digested with 5 U/µl of Hae III at 30°C for the times indicated. After arresting the digestion, DNA was isolated and run on a 8% denaturing PAGE. Lane 1, naked DNA digested with 5 U/µl for 5 minutes. (B) Quantification of the data presented in (A). Note that the quantification for the accessibility at d_7 is not presented, since the corresponding band is not resolved from the undigested DNA under our conditions (see panel A).

The relatively long free DNA arms present at each end of the nucleosome allowed their precise length measurement by AFM image analysis. This allowed, in turn, the calculation of both the length of the DNA complexed with the histone octamer L_c ($L_c = L_{tot} - L_+ - L_-$, where $L_{tot} = 255$ bp is the length of the 601 fragment used for reconstitution, L_+ and L_- are the lengths of the long and the short DNA arms respectively, as measured by AFM image analysis) and the position of the nucleosome relative DNA template center $\Delta L = (L_+ - L_-)/2$ (Figure 5C, D and (563)). The measurements were performed in a large number of objects (N = 1252 conventional and N = 2805 H2AL2 nucleosomes), which made them statistically relevant. The mean of the length distribution for DNA complexed with the conventional histone octamer was located close to 145 bp and interestingly around 130 bp, for the variant H2AL2 nucleosome (Figure 5C). The position of the nucleosome relative to the DNA center, ΔL, was same for both the particles (Figure 5D).

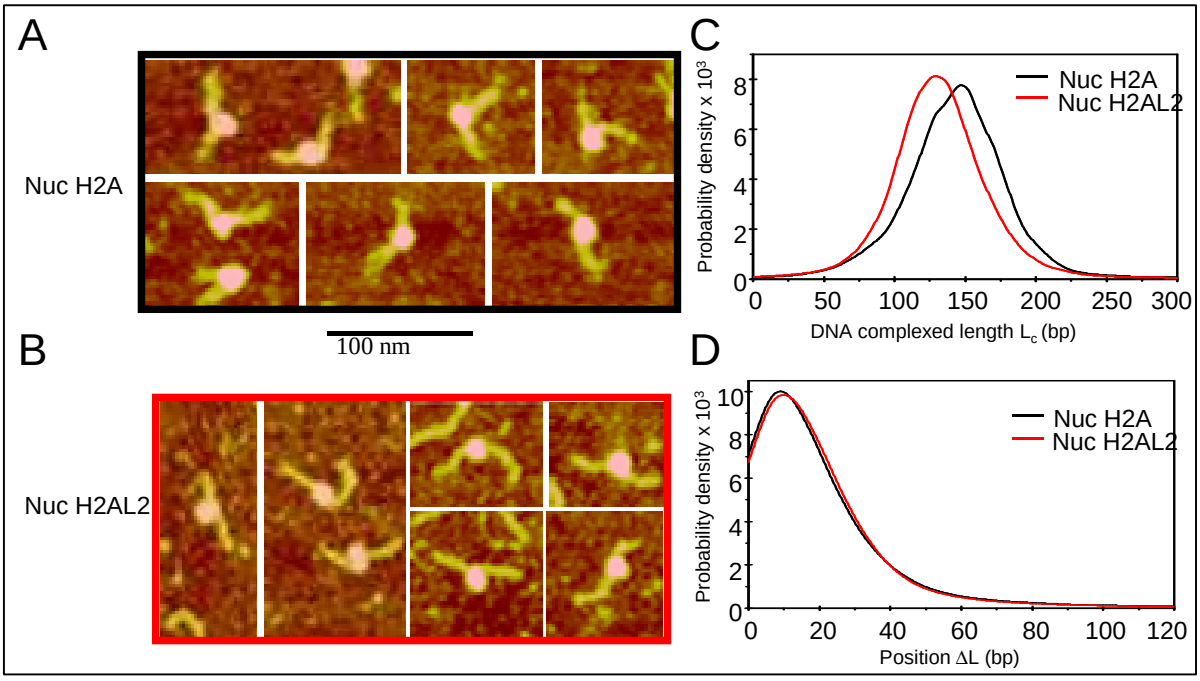

Figure 5: AFM imaging shows that the H2AL2 histone octamer is complexed with ~130 bp of DNA. Centrally positioned conventional and H2AL2 nucleosomes were reconstituted on 255 bp 601 DNA sequence and visualized by AFM. Representative AFM images for the conventional (nuc H2A) and H2AL2 (nuc H2AL2) particles are presented in (A) and (B), respectively. (C) Complexed DNA length (L_c) distribution for conventional and H2AL2 nucleosomes. Note the difference in the peak position in the distribution curves of the two samples. (D) Nucleosome position (ΔL) distribution for conventional and H2AL2 nucleosomes. The numbers of particles used for the calculation of the distributions were N = 1252 and N = 2805 for conventional and H2AL2 nucleosomes, respectively.

III.4.6 Electron cryo-microscopy shows a very open structure of the H2AL2 tri-nucleosomes

The perturbation of the histone-DNA interactions at d_5 - d_6 and the ability of the H2AL2 octamer to organize only ~130 bp may affect the entry/exit angle of the nucleosomal DNA ends. To test this we have used Electron Cryo-Microscopy (EC-M). E-CM experiments are performed in vitrified solutions without the utilization of any contrasting reagents, which allows the visualization of the "native", unperturbed structure of the samples. E-CM was very successfully used for investigating the structure of both reconstituted conventional and H2A.Bbd histone variant nucleosomes (470, 478) as well as native oligosomes and high molecular chromatin samples (566). Note that of particular interest for studying the linker orientation are the trinucleosomes (567). With this in mind, we have reconstituted precisely positioned 601 conventional and H2AL2 trinucleosomes and have visualized them by E-CM (Figure 6).

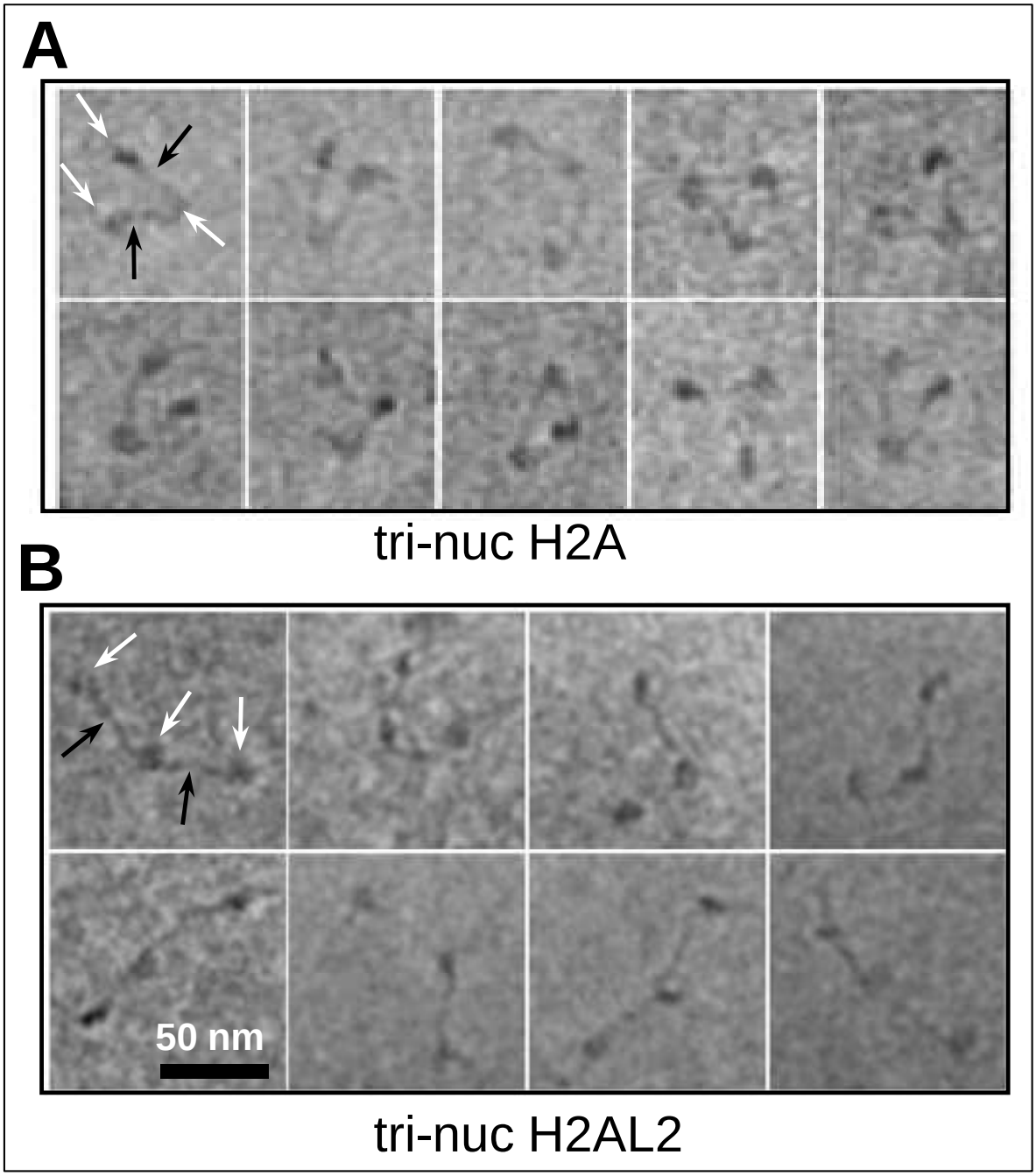

Figure 6: Electron cryo-microscopy visualization of conventional H2A and histone variant H2AL2 tri-nucleosomes. A DNA fragment containing three tandem 601 positioning sequence repeats was used to reconstitute conventional and H2AL2 tri-nucleosomes and they were visualized by E-CM. Typical micrographs for both types of particles are shown. The conventional trinucleosomes exhibit V-shaped structure with the two end-nucleosomes at both ends of the "V" and the middle-nucleosome at the center of the "V". In contrast, the majority of the H2AL2 trinucleosomes exhibit "beads on a string" structure and very few H2AL2 trinucleosomes show open "V"-type of organization. Black arrows indicate the linker DNA, while the nucleosome is designated by white arrows.

The conventional trinucleosomes exhibited a typical "V" (equilateral triangle) shape with two nucleosomes located at each end of the trinucleosomal DNA and the middle nucleosome at the "point" of the "V" (Figure 6A). The 3D organization of the H2AL2 trinucleosomes was,

however, quite different (Figure 6B). Typically, the H2AL2 trinucleosome shows “beads on a string” organization, and in some cases, a very open “V” type organization with the linkers DNA forming a very large angle (Figure 5B). We conclude that the variant H2AL2 octamer cannot properly organize the 3D conformation of the entry/exit nucleosomal DNA. We attribute this to the altered interactions of the entry/exits ends of nucleosomal DNA with the H2AL2 histone variant octamer.

III.4.7 The presence of H2AL2 affected both RSC and SWI/SNF nucleosome remodeling and mobilization

The data described above unequivocally demonstrate that the incorporation of H2AL2 in the nucleosomes results in perturbation of their structure. Perturbation in the nucleosome structure induced by the presence of the histone variant H2A.Bbd led to inhibition of both nucleosome remodeling and mobilization (474, 478). This prompted us to next ask if H2AL2, as H2A.Bbd, interferes with nucleosome remodeling and mobilization. DNase I footprinting assay was used for studying the capacity of RSC and SWI/SNF to remodel the nucleosomes. Conventional and H2AL2 end-positioned nucleosomes were reconstituted on ^{32}P-end labeled 200 bp 601 DNA sequence. Identical amounts of both samples were incubated for different times (from 2.5 to 40 minutes) at 30°C with either RSC or SWI/SNF. After arresting the remodeling reaction, the samples were treated with DNase I, the digested DNA was purified and run on 8% PAGE under denaturing conditions. SWI/SNF (Figure 7A) and RSC (Figure 7B) remodeled both conventional and H2AL2 nucleosomes. The 10 bp DNase I nucleosomal repeat was lost and many bands corresponding to the respective bands of the digestion of free DNA were observed (Figures 7A and B, compare lanes 2-7 with lanes 9-14). However, both RSC and SWI/SNF remodeled about 2.5 times more efficiently the conventional particles as determined by quantification of the intensity of some specific bands (results not shown). We conclude, that the presence of H2AL2, similarly to this of H2A.Bbd (474, 478), interferes with nucleosome remodeling.

Is H2AL2 able to affect nucleosome mobilization? To test this we have carried out a standard nucleosome mobilization assay. Centrally positioned conventional and H2AL2 nucleosomes were reconstituted by using ^{32}P-end labeled 255 bp 601 fragment and incubated for 45 minutes (in the presence of ATP) with increasing amount of either RSC or SWI/SNF (Figure 8). Treatment with the remodelers resulted, as expected, in loss of the 10 bp repeat in the DNase I digestion pattern of either one of the particles (Figure 8B).

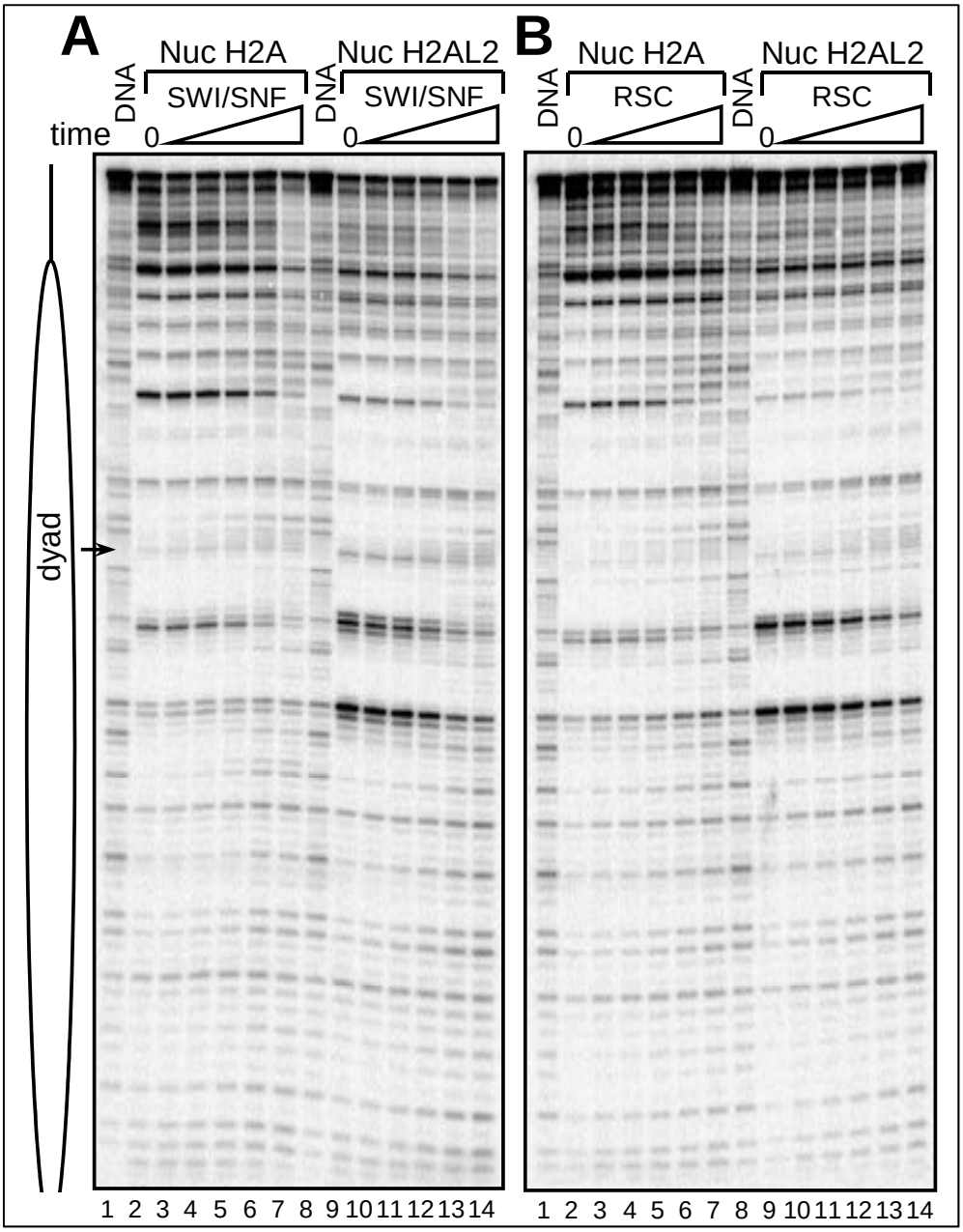

Figure 7: SWI/SNF and RSC remodeling of conventional and H2AL2 nucleosomes. End positioned conventional (lanes 2-8) and H2AL2 (lanes 10-14) nucleosomes were reconstituted on a ^{32}P-5'-labeled 200 bp 601 DNA fragment and incubated for increasing times (from 2.5 to 40 minutes) at 30°C with 2 units of either SWI/SNF (A) or RSC (B). After arresting the reactions, the samples were digested with DNase I, DNA was extracted and run on an 8% sequencing gel. The position of the dyad is indicated at the left part of the figure. Lanes 1 and 8 of each panel show the digestion pattern of free DNA.

However, careful comparison of the remodeled patterns (lanes 2 and 4 in Figure 8B) shows again some differences. Indeed, the remodeling of the conventional nucleosomes was stronger compared to this of the variant particles. In addition, some bands present in the digestion pattern of remodeled conventional nucleosomes were not detected in the digestion pattern of remodeled H2AL2 nucleosomes (Figure 8B, bands marked by stars). These results are in agreement with the data presented in Figure 7 for the 200 bp H2AL2 nucleosome and evidence for a less efficient remodeling of the variant H2AL2 255 bp particle.

Under the conditions of the experiments both remodelers induced a relocation of conventional nucleosomes (Figure 8A). Although, neither RSC nor SWI/SNF were able to relocate efficiently the H2AL2 histone variant octamer to the end of the nucleosomal DNA (Figure 8A). Quantification of the data showed that the efficiency (the initial slope of the curves, figure 8A, lower panels) of the variant H2AL2 histone octamer relocation at the end of the nucleosomal DNA by either one of the remodelers was at least 10 fold smaller than this of the conventional histone octamer. Note, however, that the upper band corresponding to the centrally positioned H2AL2 nucleosomes is becoming larger upon incubation with higher amount of either RSC or SWI/SNF (Figure 8A). This might be associated with some heterogenisation due to either histone-DNA contacts disruption and/or short range relocation of the H2AL2 particles.

We have also studied the capacity of RSC to mobilize H2AL2 nucleosomes by using an enzyme restriction assay (see schematics of the assay, Figure 9A). We have first incubated both conventional and H2AL2 nucleosomes with an amount of RSC sufficient to relocate the conventional nucleosomes at the end of the nucleosomal DNA (see Figure 8A). After arresting the reaction both types of nucleosomes were digested with Xba 1, whose restriction site is located in the linker DNA at 233 bp from the ^{32}P-laleled end of the nucleosomal DNA. If the nucleosomes were mobilized by RSC (in the presence of ATP) one should expect the yield of cleavage to drop two-fold (see figure 9A). This was really the case for conventional nucleosomes (Figures 9B and C). In contrast, essentially no change in the Xba 1 cleavage yield for the RSC incubated H2AL2 nucleosomes was detected (Figures 9B and C). These data combined with the EMSA results (Figure 8A) demonstrate that the presence of H2AL2 interferes with the chromatin remodeler induced relocation of the variant particles at the end of the nucleosomal DNA. This conclusion was further supported by studying the RSC-induced mobilization by AFM (Figure 9D). The AFM imaging showed that treatment with RSC generated conventional, but essentially not H2AL2, end-positioned nucleosomes (Figure 9D).

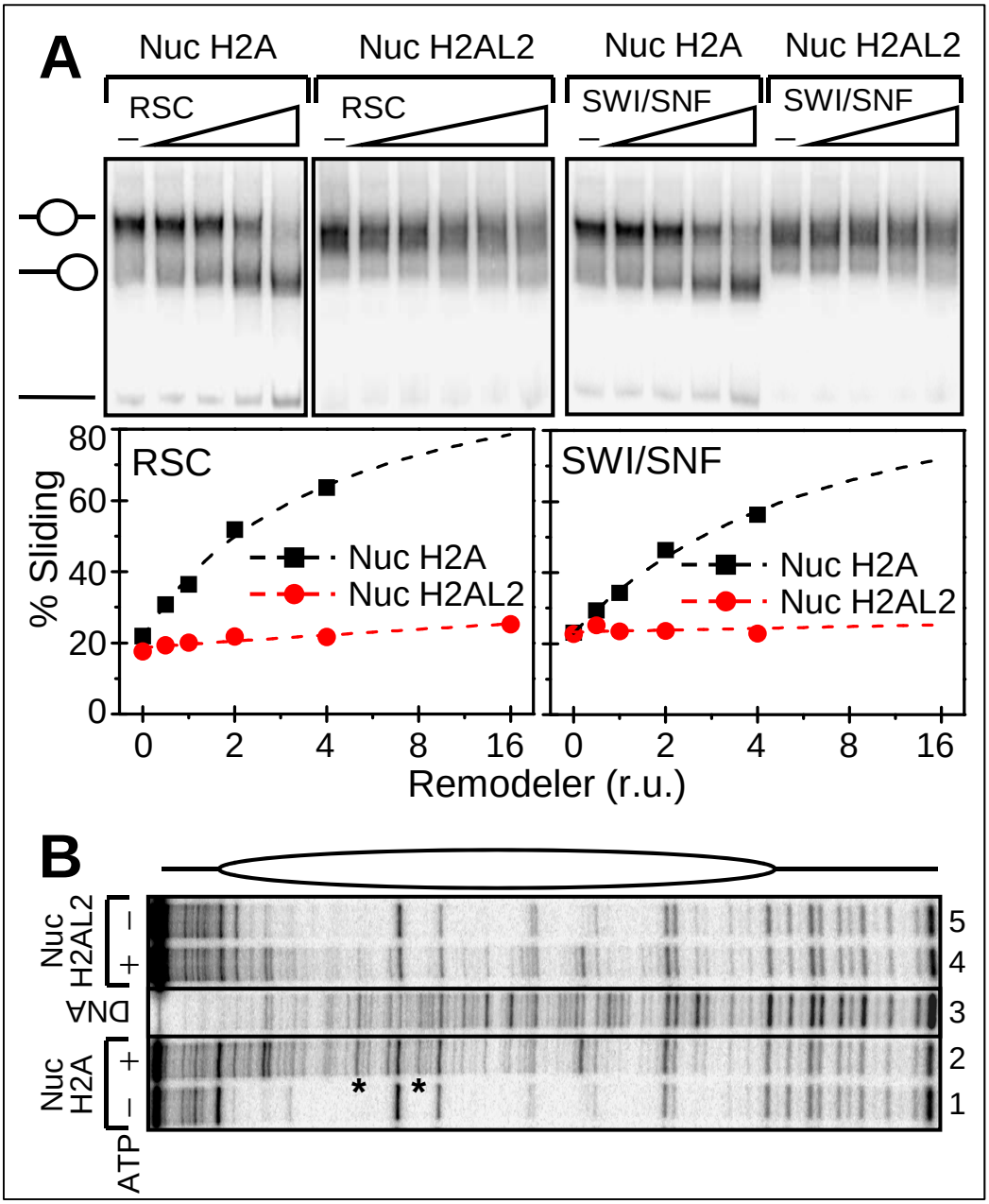

Figure 8: The presence of H2AL2 interferes with both SWI/SNF and RSC nucleosome remodeling and mobilization. (A) Nucleosome mobilization assay. Centrally positioned conventional and H2AL2 nucleosomes were reconstituted on a ^{32}P-end labeled 255 bp 601 DNA fragment and used for either RSC (left panel) or SWI/SNF (right panel) mobilization assay. Both types of reconstituted nucleosomes were incubated for 40 minutes at 30°C with increasing amounts of the respective remodeler in the presence of ATP. After arresting the reaction, the samples were run on a 5% native PAGE (the conventional and H2AL2 RSC-treated nucleosomes were run on two different gels and the data are presented in two separate panels). The center and the end-positioned (slid) nucleosomes and free DNA are indicated. The lower part of the figure shows the quantification of the data. (B) DNase I footprinting of RSC remodeled conventional and H2AL2 nucleosomes. Both centrally positioned conventional and H2AL2 particles, reconstituted on a ^{32}P-end labeled 255 bp 601 DNA fragment, were treated with the highest amount of RSC used in the mobilization reaction as described in (A). After arresting the remodeling reaction the samples were digested with DNase I, the cleaved DNA was purified and run on an 8% sequencing PAGE. A schematic of the nucleosome is shown in the upper part of the figure. Lane 3, showing the digestion of the naked DNA, was not adjacent to lanes 2 and 4 in the original gel, and was thus demarked accordingly.

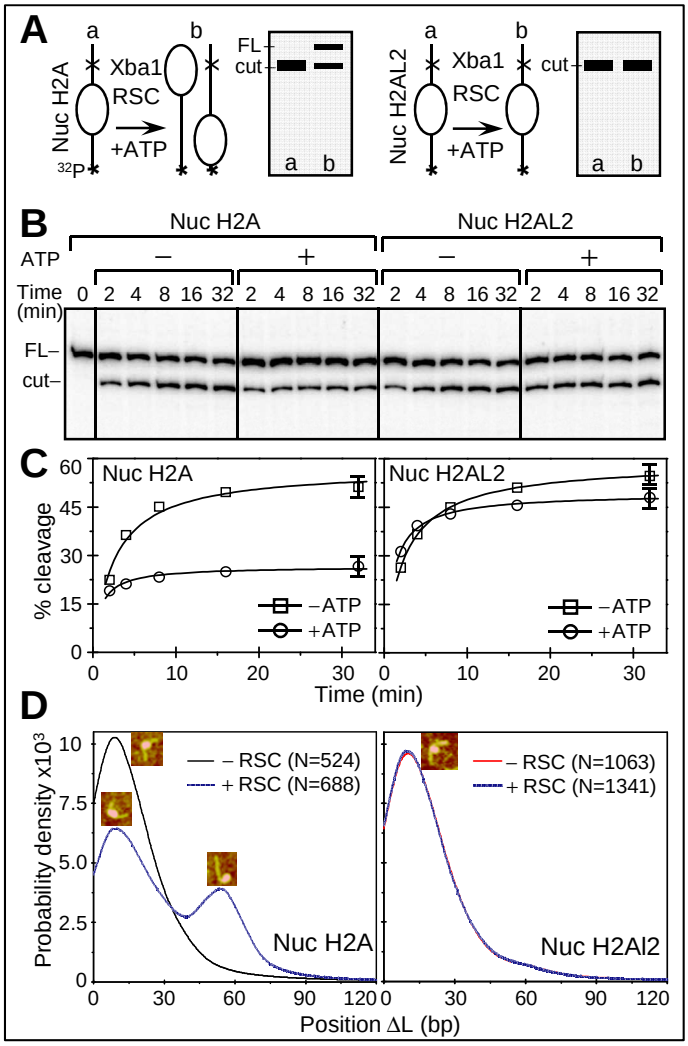

Figure 9: Xba 1 nuclease restriction and AFM analyses of the RSC-induced relocation of conventional and histone variant H2AL2 nucleosomes. (A) Schematics of the Xba 1 restriction analysis used to study the RSC induced mobilization of conventional and histone variant H2AL2 nucleosomes. The Xba 1 restriction site is located in the linker DNA of the nucleosome at 233 bases from the end of the ^{32}P-end labeled 601.2 DNA fragment. If RSC induces sliding of the nucleosome, the cut efficiency of Xba 1 is expected to decrease two-fold (the nucleosome will be mobilized to both ends of the DNA fragment, left panel). If RSC is unable to mobilize the nucleosome, no decrease of the Xba 1 cut efficiency will be observed (right panel). (B) Identical amounts (150 ng) of H2A (left panel) or H2AL2 (right panel) ^{32}P-end labeled nucleosomes were incubated with 0.04 units/µl of Xba1 either in the presence or the absence of 1 mM ATP. After digestion for the times indicated, the reaction was stopped and the digestion products were separated on the same 8% sequencing gel (the migrated products, which loading was not adjacent in the original gel, are demarked by vertical lines). The positions of the full length (FL) and cut DNA fragment are indicated on the left of the figure. (C) Quantifications of the data presented in (B). Note the two-fold decrease of cut yield for the conventional H2A nucleosomes (Nuc H2A, left panel) and the absence of effect on the cut yield in the case of H2AL2 (Nuc H2AL2, right panel) nucleosomes. The digestion with Xba 1 was carried out in remodeling buffer and under these conditions a digestion plateau was reached at ~50-60%. (D) Position distribution (ΔL) of conventional and H2AL2 histone variant nucleosomes after treatment with RSC. Either conventional or H2AL2 nucleosomes were treated with RSC in the presence of ATP and the samples were visualized by AFM. The insets indicate the centrally positioned (first peak) and the mobilized, end-positioned conventional nucleosomes (second peak). The numbers of analyzed nucleosomes are: N(H2A-RSC) = 524, N(H2A+RSC)= 688 conventional nucleosomes and N(H2AL2-RSC) = 1063 and N(H2AL2+RSC) = 1341 variant nucleosomes, respectively.

III.5 Discussion

In this work we have studied the structural and functional properties of the histone variant H2AL2 nucleosomes. We confirmed that this histone variant is testis-specific and we show that it can efficiently replace conventional H2A in the nucleosome. The variant H2AL2 nucleosome exhibited both structural and functional properties distinct from these of the conventional one. DNase I and OH° footprinting, micrococcal nuclease and exonuclease III digestion and nucleosomal DNA restriction nuclease accessibility assay demonstrated alterations in the overall H2AL2 nucleosome structure. AFM imaging showed that only ~ 130 bp of DNA were wrapped around the H2AL2 histone variant octamer. The H2AL2 trinucleosomes exhibited essentially "beads on a string" nucleosomal organization in contrast to the conventional trinucleosomes, which showed equilateral triangle shape. Finally, we found that H2AL2 nucleosomes cannot be efficiently both remodeled and relocated at the end of the nucleosomal DNA by either one of the chromatin remodelers RSC or SWI/SNF. The effect of H2AL2 on the efficiency of nucleosome relocation was, however, more pronounced than this on the efficiency of nucleosome remodeling. Note that for the reconstitution of the nucleosomal samples we have used *Xenopus laevis* core histones H2B, H3 and H4, but their mouse analogs are essentially the same and thus, the described results would not be affected.

The above summarized data indicate that the observed perturbations in the H2AL2 nucleosome structure were sufficient to induce an impediment of the remodeling of the nucleosome and the relocation of the variant histone octamer to the nucleosomal DNA end. In particular, the alterations in the wrapping of DNA around the H2AL2 variant histone octamer may not allow the proper binding of the variant particle in the nucleosome binding pocket (568-570) of both RSC and SWI/SNF.

H2AL2 is a testis-specific histone variant ((483) and this work). H2A.Bbd is also expressed mainly in testis. Common properties of the H2AL2 and H2A.Bbd particles are their altered structures and their capacity to interfere with the remodeler's function, i.e. to interfere with nucleosome remodeling and relocation. Therefore, both histones would be involved in the *in vivo* "construction" of distinct nucleosomes with specialized functions. These functions would require an easier removal of the variant dimers from the nucleosome and no nucleosome mobilization.

We have reported earlier that the docking domain of H2A.Bbd is required for nucleosome mobilization (478). Since the docking domain of H2AL2 differed considerably from this of the conventional H2A and its length is closer to this of H2A.Bbd (see Figure 1A)

this indicates that the cells in both mouse and human use very similar strategies to generate nucleosomes lacking the ability to be mobilized by chromatin remodelers.

The H2A.Bbd nucleosomes exhibited an open structure (478). The H2AL2 trinucleosomes showed also an open (beads on a string type) structure and micrococcal nuclease digestion of H2AL2 nucleosome arrays suggest a more relaxed organization of these variant arrays. This appeared to be determined by the altered interactions of the H2AL2 histone octamer with the ends of the nucleosome DNA (this work). Since the H2A.Bbd the docking domain was required for the generation of the open nucleosome structure we hypothesized that the H2AL2 altered docking domain is also involved in the generation of the open structure of the H2AL2 nucleosomes and nucleosomal arrays. This open structure of both H2A.Bbd and H2L2A chromatin filaments could play an important role during different spermiogenesis specific processes, including replacement of these histone variants.

III.6 Funding

CNRS; La Ligue Nationale Contre le Cancer (Equipe labelise´ La Ligue to S.D.) the Association pour la Recherche sur le Cancer (Grant N 4821 to D.A.); the Region Rhone-Alpes (Convention CIBLE 2008 to D.A. and S.D.); Agence Nationale de la Recherche (Grant Blanc ‘CHROREMBER’ to S.D., D.A. and J.B) and the Grant Agency of the Czech Republic (Grant #304/05/2168 to J.B.) and the Ministry of Education, Youth and Sports (Grants MSM0021620806 and LC535 to J.B.) and the Academy of Sciences of the Czech Republic (Grant #AV0Z50110509 to J.B.). Funding for open access charge: Association pour la Recherche sur le Cancer (Grant 4821).

III.7 Acknowledgements

We thank Dr. Workman for kindly providing us with the yeast strain expressing tagged RSC and SWI/SNF and Dr. Daniela Rhodes for providing the 601 chromatin template DNA. We thank Fabien Montel for setting up the automated AFM image analysis. S.D. acknowledges the Franco-Indian scientific program ARCUS for support.

III.8 Supplementary figure 1S: Northern-blot

RNA blotting was performed using a membrane First ChoiceTM Northern blots (Ambion) according to the manufacturer's protocol. The H2AL2 antisense RNA probe was generated using the Strip-EZ RNATM kit (Ambion, Inc.). The GAPHD DNA probe was labeled by random priming using the Prime-a-GeneTM Labeling System (Promega) and a DNA sequence first cloned with the primers:

5’-GCACAGTCAAGGCCGAGAATGG-3’ (forward) and

5’-TGGGGGCCGAGTTGGGATAGG-3’ (reverse).

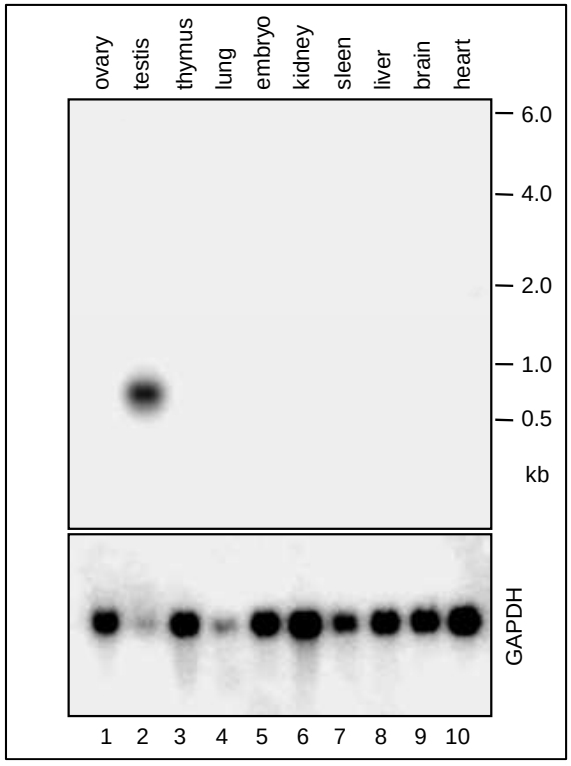

Supplementary figure 1: Northern blot analysis shows that H2AL2 is specifically expressed in testis. Total RNA was isolated from the indicated different tissues and the Northern blot was carried out by using a standard protocol. For estimation of the amount of RNA isolated from the different tissues and loaded on the gel, the membrane was also hybridized with a GAPDH RNA specific probe.

CHAPITRE IV

PUBLICATION 3

LE DOMAINE D'ENCRAGE DE H2A ET L'ANGLE D'ENTRE-SORTIE DE L'ADN DE LIAISON DETERMINE L'ASSOCIATION DE H1 AVEC LE NUCLEOSOME.

Dans ce chapitre nous apportons les preuves que l'histone H1 est incapable de s'associer correctement avec les nucleosomes variants H2AL2 et H2A.Bbd et de générer la structure en tige de l'ADN de liaison. Les expériences avec des domaines d'encrage d'histones conventionnels et variants inter-changés ont montre que cette propriété est déterminée par le domaine d'encrage « défective » de ces histones variants. Cette étude suggère un rôle de ces histones variants dans la structure supérieure de la chromatine.

CHAPTER IV: PUBLICATION 3

THE DOCKING DOMAIN OF H2A AND THE ENTRY/EXIT ANGLE OF THE LINKER DNA DETERMINE THE BINDING OF H1

(Manuscript under preparation)

Sajad Hussain Syed[1,2], Manu Shukla[1,2], Dimitar Angelov[2], Stefan Dimitrov[1]* and Jan Bednar[3,4]*

[1]Université Joseph Fourier - Grenoble 1; INSERM Institut Albert Bonniot, U823, Site Santé-BP 170, 38042 Grenoble Cedex 9, France

[2]Université de Lyon, Laboratoire de Biologie Moléculaire de la Cellule, CNRS-UMR 5239/INRA 1237/IFR128 Biosciences, Ecole Normale Supérieure de Lyon, 46 Allée d'Italie, 69364 Lyon cedex 07, France

[3]CNRS/UJF, Laboratoire de Spectrométrie Physique, UMR 5588, BP87, 140 Av. de la Physique, 38402 St. Martin d'Hères Cedex, France

[4]Institute of Cellular Biology and Pathology, First Faculty of Medicine, Charles University in Prague and Department of Cell Biology, Institute of Physiology,Academy of Sciences of the Czech Republic, Albertov 4, 128 01 Prague 2, Czech Republic

*Corresponding authors:

e-mail: stefan.dimitrov@ujf-grenoble.fr, phone: +33476549473 ; fax: +33476549595

e-mail: jbednar@spectro.ujf-grenoble.fr, phone:+ 33476514761; fax: +33476635495

Running title: Histone H1 mapping on nucleosome

Keywords: chromatin/hydroxyradical footprinting/nucleosome/cryo-EM

IV.1 Introduction

Eukaryotic genome is organized in a repeating array of nucleosome core particle (NCP) and linker DNA. NCP is an octameric disc composed two copies of each of the four core histone proteins (H3, H4, H2A and H2B) around which 146bp of DNA are wrapped in nearly 1.65 superhelical turns (571). The linker DNA is occupied in most of the eukaryotes by linker histone H1, which is essential for chromatin compaction. The nucleosomal organization of the DNA makes it inaccessible to the many proteins that must bind to it for normal cellular functions. Although this process is still not clear (572-574), but there are three suggested main mechanisms that the cell has developed to overcome the nucleosomal barrier. These processes include ATP dependent chromatin remodeling, post translational modifications of histone and incorporation of histone variants.

Linker histones consists of a folded globular domain which is flanked by less structured and highly charged N-and C- terminal tails (59, 575). Linker histones bind preferentially to the supercoiled (576-579) and four-way junction (4WJ) DNA (580) compared to linear DNA. This preferential binding of linker histones to 4WJ DNA was explained to depend on the particular angle formed between the two DNA arms or crossovers (580). In chapter 2 we have mapped at single base resolution the specific H1 linker histone binding to the nucleosome and have proposed a three binding sites model for globular domain of H1.

Histone variants are non-allelic isoforms of the conventional histones. Incorporation of a histone variant usually confered a particular structure of the nucleosome (421). More recently the histone variants of H2A family namely H2A.Bbd (478) and H2AL2 (chapter 3) have been shown to form open nucleosome structures. These variants show a high divergence in the structure of their docking domain compared to the conventional H2A. The histone octamer of both the variants is shown to wrap only ~130bp of DNA with a DNA turn less from both sides of the core particle. AFM and CryoEM images show a highly flexible structure of the variant particles where the entry exit DNA form ~ 180 angle in contrast to the “V” shape in the conventional nucleosomes. These peculiar properties of the variant nucleosomes appeared to be associated with the "defective" docking domain of both H2A.Bbd and H2AL2. Interestingly, several remodeling complexes were not capable to both remodel and mobilize H2A.Bbd (478) and H2AL2 variant (chapter 3) nucleosomes suggesting a relationship between the unusual nucleosome variant structure and the capacity of remodelers to act on these nucleosomes.

Bearing in mind how histone H1 interacts with the nucleosome, i.e. the specific requirement for the 3D organization of the entering and exiting DNA allowing H1 to bind to three nucleosomal DNA sites (see Figure 6, of chapter 2), one could expect the opened H2A.Bbd or H2AL2 nuclesome structure to also affect the H1 binding. In this work we have approached this problem by using a combination of biochemical techniques and electron cryo-microscopy (EC-M). Our data demonstrate that histone H1 was unable to bind properly to the variant nucleosomes and to generate a stem structure. Experiments with swapped docking domains of conventional histone H2A and the variant histone H2A.Bbd showed that this is determined by the "defective" docking domain of these H2A histone variants.

IV.2 Results

IV.2.1 NAP-1 mediated binding of linker histone H1 to conventional and variant nucleosomes

We have separately reconstituted conventional, H2AL2 and H2A.Bbd centrally positioned 189bp mononucleosomes on the strong positioning 601 sequence (183). We have also used H2A.ddBbd (a H2A chimera, where the H2A docking domain was replaced with the "defective" docking domain of H2A.Bbd) to reconstitute centrally positioned nucleosomes. The nucleosomes were then used for deposition of linker histone H1 with the help of linker histone chaperone Nap1. The complexes were then analyzed by the band-shift gel electrophoresis experiment. Figure 1B shows titration of H1 binding to the different nucleosomal substrates. As seen, there is a clear shift in the electrophoretic mobility of the conventional nucleosomal band upon H1 binding (compare control lane1 with lane2), which is in good agreement with reported data (92) and our data in chapter 2. In the case of H2AL2 nucleosome there was also a shift in the electrophoretic mobility of the nucleosome observed upon H1 titration, but a higher smear was observed. H2A.Bbd nucleosomes exhibited, however, different behavior upon H1 binding. Indeed, the shifted band was not well defined, rather a highly diffused smear was observed. In addition, the higher concentrations of H1 led to the formation of aggregates (not shown). These results suggest that the linker histone can bind to the variant nucleosomes, albeit more efficiently to H2AL2 than H2A.Bbd, but the binding is less specific than to the conventional nucleosomes. Interestingly, the same picture as this for H2A.Bbd, was seen for the H2A.ddBbd nucleosomes (Figure 1B, lanes 18-22), suggesting that the H2A docking domain is essential for the specific interaction of histone H1 with the nucleosome.

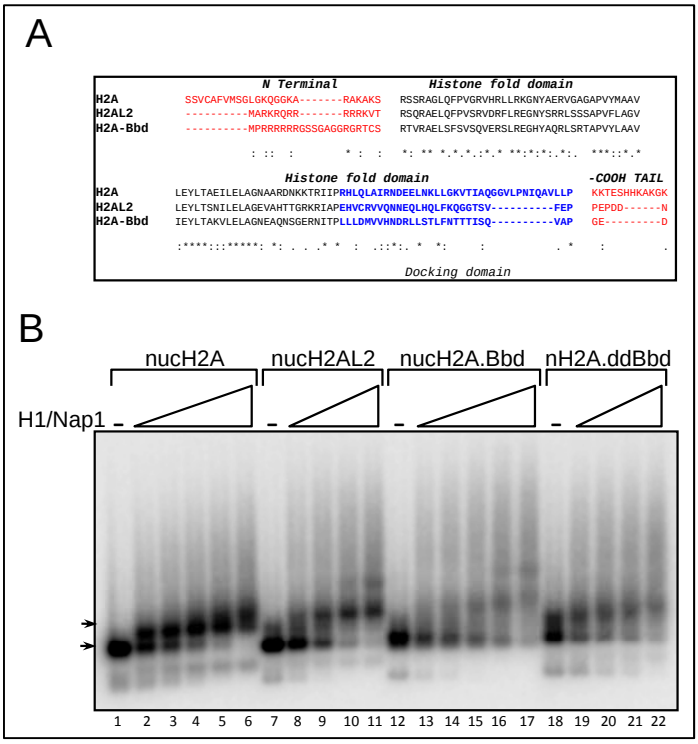

Figure 1: Nap1 facilitated deposition of linker histone H1 on different mononucleosomal substrates. (A) Sequence alignment of mouse H2A.1, H2AL2 and human H2A.Bbd. The N- and C-termini, the histone-fold domain as well as the docking domain are indicated. (B) Nucleosomes with H2A (lane 1), H2AL2 (lane 7), H2A.Bbd (lane 12) and H2A.ddBbd (lane 18) were reconstituted on a centrally positioned 189bp 601 positioning DNA. Increasing concentrations of H1/Nap1 complex, in a molar ratio of 2:1, were added to H2A (lanes 2-6), H2AL2 (lanes 8-11), H2A.Bbd (lanes 13-17) and H2A.ddBbd (lanes 19-22). The samples were then run on 2% agarose gel under native conditions. The positions of both non-associated (-H1) and associated (+H1) with linker histones dinucleosomes are indicated by arrows.

IV.2.2 Hydroxy radical mapping of H1 on H2AL2 nucleosomes

The gel shift analysis gives only some general information on the histone H1-nucleosome interactions. To study in more detail these interactions we have used hydroxyl radical footprinting, since this allowed to ascertain the nature of H1 binding and mapping the exact location of H1 on the nucleosome (see Chapter 2). Briefly, H2A, H2AL2, H2A.Bbd and H2A.ddBbd dinucleosomes were reconstituted on an end labeled 423 bp long DNA bearing two 601-nucleosomal positioning sequences. H1 was deposited by using NAP-1. Control and H1 deposited dinucleosomes were subjected to treatment with hydroxyl radicals and the cleaved DNA was purified and analysed on an 8% denaturing gel (Figures 2, 3).

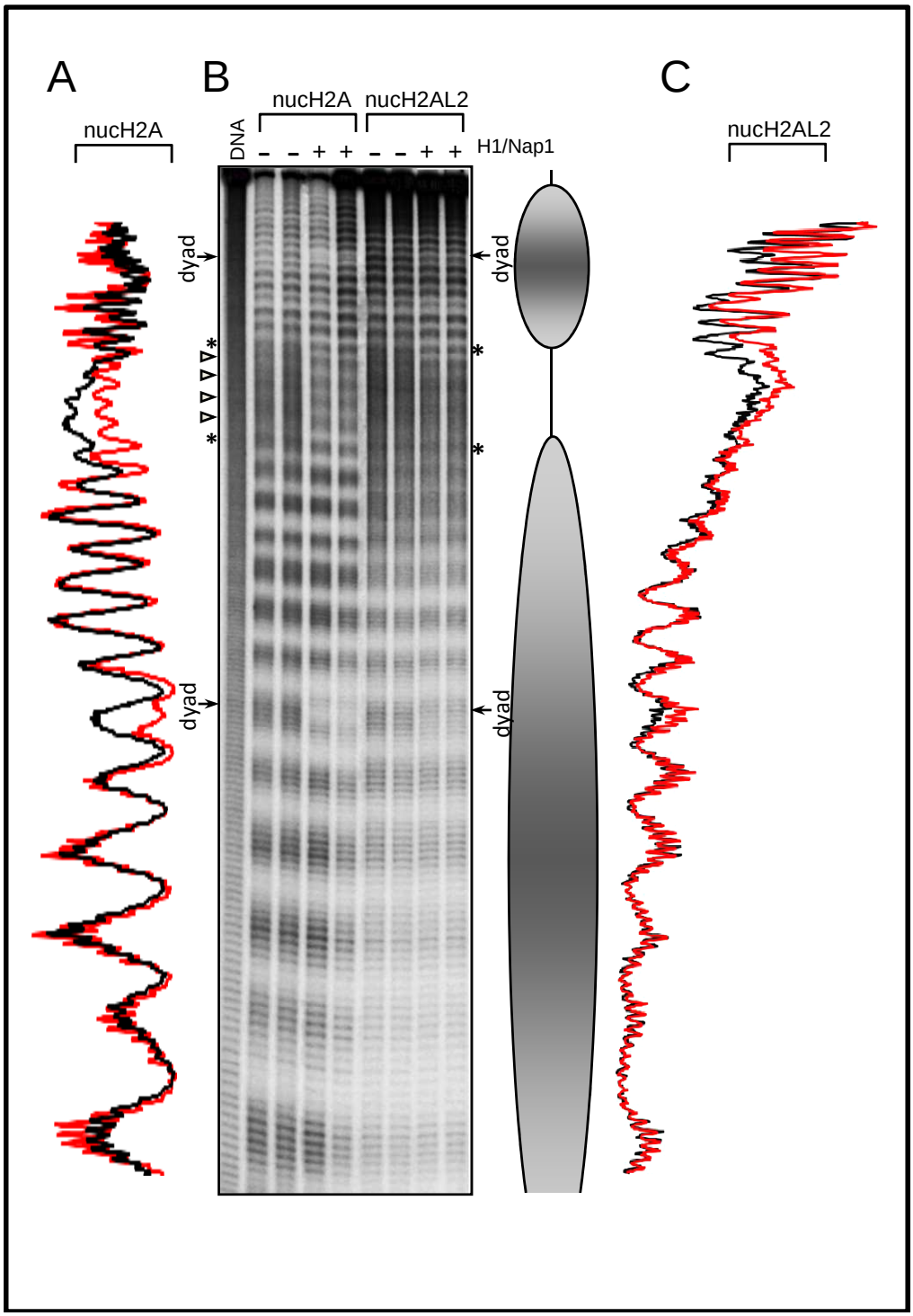

Figure 2: Hydroxyl radical footprinting analysis of conventional and H2AL2 variant dinucleosomal substrates in presence and absence of linker histone H1 show a weak H1 binding in the variant. Dinucleosome were reconstituted on 423bp 601 nucleosome positioning sequence and H1 was deposited in complex with histone chaperone Nap1. (A & C) Scans of the OH° digestion pattern of intact (black) and H1-containing (red) conventional and H2AL2 dinucleosomes respectively. (B) Hydroxyl radical cleavage pattern of H2A and H2AL2 dinucleomes, either intact or H1 deposited. DNA, OH° cleavage pattern of naked DNA. The arrowheads and the stars show the digestion products of the central part and the ends of the linker DNA, respectively. (∆) represents cleavage products corresponding to the central part of the linker DNA. Schematic drawing of the dinucleosome is also presented

As expected, in agreement with gel shift analyses and our previous data (see chapter 3), control (without H1) H2AL2 dinucleosomes showed, in contrast to conventional nucleosomes, less contrasted repeats suggesting perturbations in the histone-DNA interactions and more open structure. The binding of H1 to conventional nucleosomes induced a strong and specific footprint at the dyad and a clear 10 bp repeat in the linker DNA (Figure 2, but see also Figure 3, chapter 2). Although, the hydroxyl radical footprinting pattern of H2AL2 nucleosomes containing H1, was quite distinct. Indeed, a very weak footprinting at the dyad and no generation of the repeats at the linker DNA were detected. Note, however, that the presence of H1 induces a protection of additional 10 bp of linker DNA only at one end of the nucleosomal DNA (Figure 2).

IV.2.3 The docking domain of histone H2A is required for proper histone H1 binding to the nucleosome

The highest divergence in H2AL2 compared to conventional H2A resides in its docking domain (see Figure 1A and chapter 3), suggesting that the docking domain of H2AL2 might be determinant for the inability of H1 to properly bind to the H2AL2 nucleosome. If this was the case, histone H1 should not also interact properly with the H2A.Bbd nucleosome (the docking domain of H2A.Bbd is even more divergent than that of H2AL2, Figure 1A and (473). To approach this we have carried out a hydroxyl radical footprinting analysis of H2A.Bbd nucleosomes with or without histone H1 (Figure 3). As in the case of H2AL2 nucleosomes, the H2A.Bbd nucleosome without H1 exhibited less contrasted OH° pattern, evidencing for perturbation in its structure (compare Figure 3A with Figure 2). The NAP-1 mediated association of histone H1 with the H2A.Bbd nucleosome does not induce any changes in OH° cleavage pattern of the variant particle DNA (Figure 3A). Interestingly, the situation was identical with the nucleosome, reconstituted with the chimera H2A.ddBbd, i.e. upon binding of H1 no changes in the pattern of OH° cleavage of H2A.ddBbd chimeric particle DNA were detected (Figure 3B). We conclude that: (i) the inability of H1 to bind to the nucleosomal DNA is a common property for both H2A histone variant particles and, (ii) a defective docking domain of H2A was sufficient to confer this property to a nucleosomal particle.

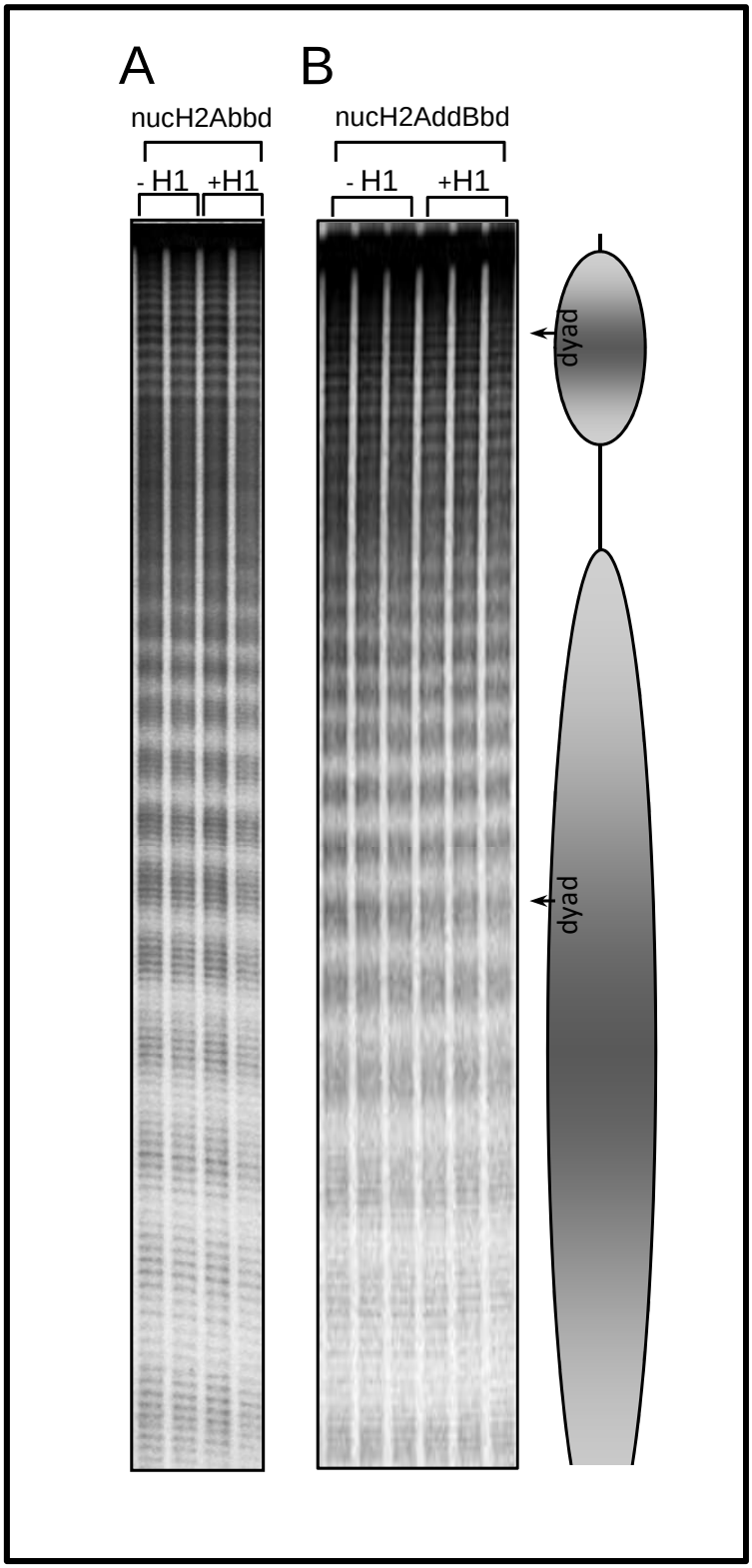

Figure 3: Hydroxyl radical footprinting show no binding of linker histone H1 to the H2A.Bbd and swapped mutant H2A.ddBbd dinucleosomal substrate. (A**) Control (lanes 2-6) and H2A.Bbd dinucleosomes in complex with linker histone (lanes 7-11) were subjected to hydroxyl radical reaction and the cleavage pattern is shown. (**B**) H2A.ddBbd dinucleosomes in presence and absence of linker histone H1 were subjected to hydroxyl radical reaction. The reaction was stopped and the purified DNA was loaded on 8% PAGE under denaturing conditions. Schematic drawing of the dinucleosome is presented. The arrowheads show the position of nucleosomal dyad.**

IV.2.4 Electron cryo-microscopy imaging reveals a "beads on a string" structure for H1 associated H2AL2, H2A.Bbd and chimeric H2A.ddBbd trinucleosomes

The OH° footprinting data show the absence of the 10 bp repeats in the linker DNA of the H2AL2, H2A.Bbd and H2A.ddBbd dinucleosomes (Figures 2 and 3). Since this repeat reflects the presence of a "stem" structure of the linker DNA (the close juxtaposition of the two linker in space induced by H1 in conventional nucleosomal samples, Figure 4A and Chapter 2, Figure 2), this suggests that no such stem structure would be generated in the variant particles. To test this we have used Electron Cryo-microscopy (EC-M) to visualize conventional, variant (H2AL2 and H2A.Bbd) and chimeric (H2A.ddBbd) trinucleosomes reconstituted on a 623bp DNA containing three repeats of positioning 601 sequence. Note that EC-M is the least invasive method for visualizing the highly dynamic structure of chromatin (538), as unlike conventional microscopy there is no fixation of the material and thus, EC-M can be used to study different chromatin conformers under "native" conditions.

Conventional trinucleosomes without H1 exhibited triangular shaped beads on the thread structure (Figure 4A). In agreement with our previous results, upon NAP-1 mediated deposition of linker histone H1 the outgoing and incoming linkers of the nucleosome were pulled together towards the axis of the nucleosome dyad, which resulted in the formation of “stem structure” of the linker DNA (arrow in the Figure 4B). EC-M visualization of both the variant and chimeric trinucleosomes without H1 show that these particles are quite different compared to their conventional counterparts. Indeed, they look like “beads on a string” filament, with linkers DNA forming an angle close to 180°C (Figure 4C-E). Remarkably, the shape of these particles remain completely unchanged upon depositing linker histone H1 (Figure 4F-H), thus demonstrating that there is no stem structure formation. We conclude that even the physiological NAP-1 mediated deposition of H1 cannot lead to a 3D reorganization of the variant and chimeric trinucleosomes and would not probably result in a *bona fide* 30 nm chromatin fiber structure if longer nucleosomal arrays were used in the experiments.

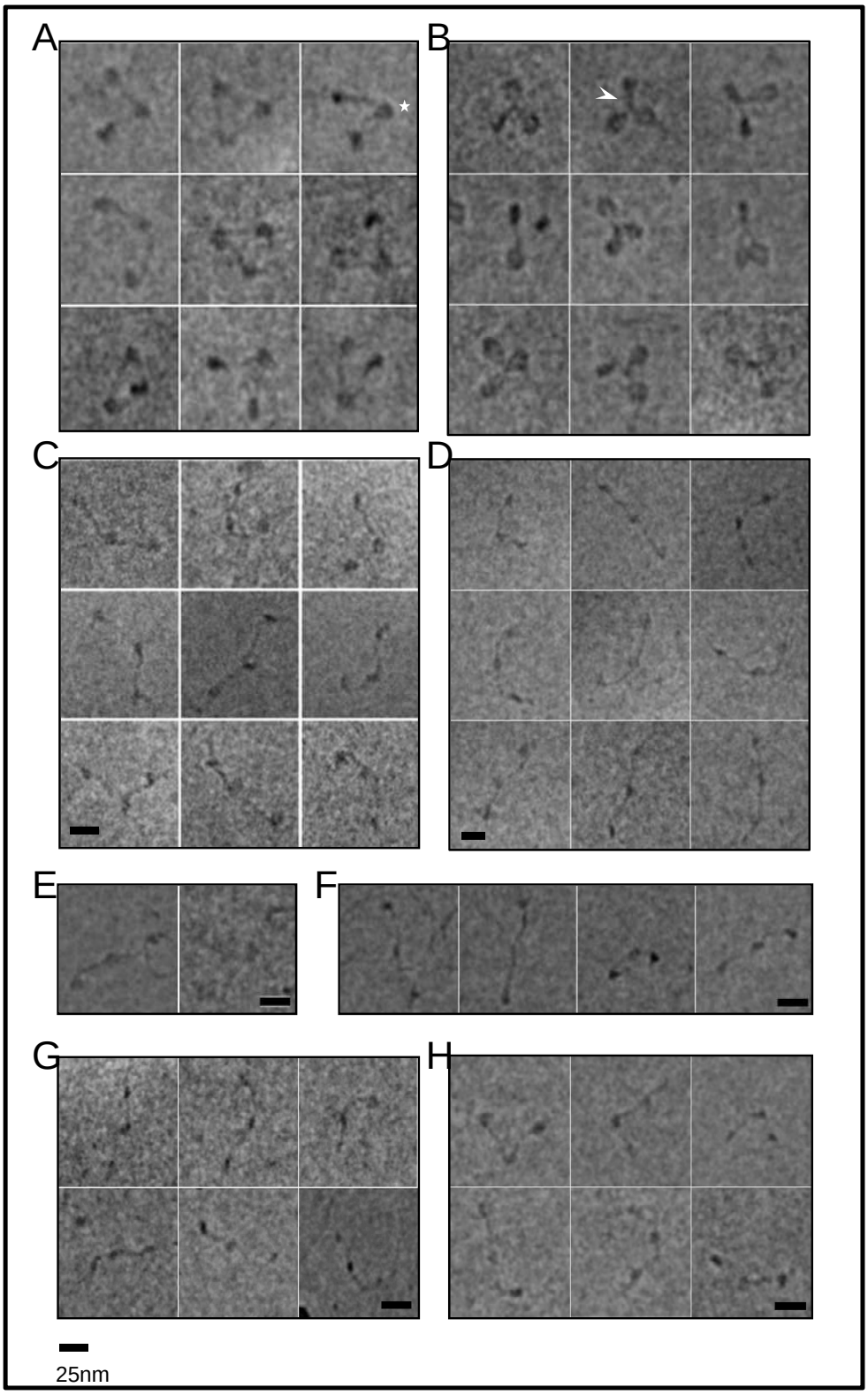

Figure 4: Electron cryo-micrographs of various control and H1 deposited H2A histone variant tri-nucleosomes don't show any detectible difference. A DNA fragment containing three tandem 601 positioning sequence repeats was used to reconstitute H2A (A),H2AL2 (C), H2A.Bbd (E) and H2A.ddBbd (G) tri-nucleosomes and were subsequently used for H1 deposition (B), (D), (F) and (H) respectively. The arrow and star shows the stem structure and nucleosome respectively. Figure A and B adapted from Chapter 2 (figure 2).

IV.3 Materials and Methods

IV.3.1 Preparation of DNA fragments

The 189bp DNA fragment containing the 601 nucleosome positioning sequence at the center was obtained by polymerase chain reaction (PCR) amplification from plasmid pGem-3Z-601 (kindly provided by B Bartholomew and J Widom). The fragment was labeled by incorporating 30μCi of [-^{32}P] CTP to the PCR reaction. DNA fragments containing the two and three 601 positioning sequences were subcloned from the 33x 200-601 chromatin array DNA (kindly provided by Daniela Rhodes) and end labeled by klenow enzyme at the EcoR I overhang as described in chapter 2.

IV.3.2 Protein purification, nucleosome reconstitution and hydroxyl radical footprinting

Recombinant *Xenopus laevis* full length histone proteins were expressed and purified as described (529). H2AL2 (chapter 3), H2A.Bbd and H2A.ddBbd (H2A domain from M1 to I80 fused to H2A.Bbd domain from T84 to D115) (474, 478) were expressed and purified from bacteria as described earlier. Full length 227 amino acid human linker histone H1.5 was purified as described in chapter 2. Nucleosome reconstitution was performed by the salt dialysis method (530). Briefly an equimolar mixture of the histones was dialyzed overnight at 4°C against histone folding buffer (10 mM Tris [pH 7.5], 5 mM β-mercaptoethanol, 1 mM EDTA) containing 2.0 M NaCl. Carrier DNA (150–200 bp, 2 μg) and 50 ng of ^{32}P-labeled DNA were mixed with equimolar amount of histone octamer in histone folding and stepwise dialyzed against decreasing concentration of NaCl down to 10 mM. Hydroxyl radical footprinting was performed exactly as reported in the chapter 2.

IV.3.3 Cryoelectron microscopy

Trinucleosome reconstitutions were performed without any carrier DNA. Control and H1 deposited trinucleosomes of H2A, H2AL2, H2A.Bbd and H2A.ddBbd were concentrated to 200ng/μl and buffer exchanged against nucleosomal buffer using 100 kDa cut off centricons. Immediately after the buffer exchange, 3 μl droplet of the solution was deposited on an electron microscopy grid with home made perforated supporting film with surface treated by successive evaporation of carbon and platinum/carbon layers. The grid was immediately plunged into liquid ethan (-183°C) after removing the excess of the solution by brief blotting using Whatman No 1 filter paper. The Grid was transferred into Tecnai G^2

Sphera 20 electron microscope using Gatan 626 cryotransfer holder. Sample was visualized at 80 kV acceleration voltage and images were recorded on Gatan Ultrascan1000 slow scan CCD camera at microscope nominal magnification either 14500x or 25000x (final pixel size 0.7 and 0.4 nm) with 2.5 µm underfocus.

IV.4 Discussion

By using a combination of hydroxyl radical footprinting and EC-M we have recently mapped at one base pair resolution the histone H1-nucleosomal DNA interactions and have shown how they reflect the 3D organization of the linker DNA (see Chapter 2). The OH° mapping demonstrated that the globular domain of histone H1 (GH1) interacts specifically with 10 bp of DNA, localized symmetrically to the nucleosome dyad. Moreover, GH1 makes additional contacts with ~10 bp of DNA from each end of the nucleosome core particle. A stretch of 15 aminoacids residues (located immediately after the end of GH1) was required for the formation of the stem structure. We have proposed a detailed model, which described at very high resolution how both histone H1 interacts with the nucleosomal DNA and maintains the structure of the chromatin fiber (see Chapter 2, Figure 6). In this model, the GH1 structure was large enough to fill the space between the exiting and entering DNA and to simultaneously interact with ~10 bp of each linker DNA as well as with the nucleosomal dyad. The binding C-terminus of H1 together with the binding of GH1 efficiently "clamped" the exiting and entering linkers and resulted in the formation of the stem structure. Note that the model requires three contacts of GH1 with nucleosomal DNA and thus, a specific orientation of the linkers.

This work shows that NAP-1 is able to deposit histone H1 on any of the studied particles, the conventional, both the variant H2AL2 and H2A.Bbd and the chimeric H2A.ddBbd ones. Although, a proper interaction of H1 with nucleosomal DNA was found with the conventional particles, no simultaneous protection of both linkers and the nucleosomal dyad against OH° was observed in either the variant or the chimeric structures containing histone H1. All these three structures exhibited, however, a common property, namely a "beads on a string" type of organization with completely perturbed mutual orientation of the entering and exiting DNA linkers. This peculiar ("beads on a string") structural organization would not allow the simultaneous contacts of GH1 with both linkers and the nucleosomal dyad.

Interestingly, the swapping of the docking domain of H2A with the "defective" one of H2A.Bbd was sufficient to create completely open H2A.ddBbd trinucleosomes. The docking domain of H2A interacts with the last helix of histone H3 and with the C-terminal region of H4 (aminoacids 95-102). Our data suggest that the alterations of these interactions would generate perturbed nucleosomal structures unable to properly interact with histone H1. The cell could achieve this by using either histone variants with "defective" H2A docking domain or probably, by modifying (in some other not identified for the moment way) the structure of the docking domain.

Immunofluorescence data showed that the histone variant H2A.Bbd colocalized with hyperacetylated chromatin (471). In agreement with this, *in vitro* experiments illustrated the higher capacity of p300 to acetylate H2A.Bbd nucleosomes (474). In addition, p300- and GAL4-VP16-activated transcription was found to be more efficient for H2A.Bbd nucleosomal arrays than for conventional arrays (194, 474, 478). All these data suggest that H2A.Bbd is involved *in vivo* in transcriptional regulation. The data presented in this work support and reinforce this hypothesis. Typically, transcribed regions in the nucleus are generally devoid of histone H1 (581). The presence of H2A.Bbd nucleosomes within these regions would not allow the stable incorporation of histone H1 and thus, could be one of the main reasons for the depletion of H1 from them. Note that both H2A.Bbd and H2AL2 are over expressed during spermatogenesis ((565); chapter 3) and similar mechanism could operate for the generation of H1 depleted chromatin domains during this process.

CHAPITRE V

PERSPECTIVES

Le développement de l'approche de déposition de H1 dans des conditions proches des conditions physiologiques et l'utilisation avec succès de EC-M a haute résolution, l'empreinte aux radicaux OH et le modèle à « gros grains » nous a mis dans une position unique dans l'étude de la structure et le rôle fonctionnel de l'histone de liaison. Dans la perspective de l'étude future, nous adressons les questions suivantes :

1. Comment H1 interagit avec un chapelet de nucleosomes de diffèrent longueurs de l'ADN de liaison
2. Rôle de la queue N-terminale de H3 dans la maintenance de la structure en tige.
3. Rôle des différents résidus de H1 de charge positive dans son association avec le nucléosome et la formation de la structure tige.
4. Les histones de liaison Hho 1p du levure et B4 du Xenope.
5. Structure du complexe H1-NAP1.
6. Exclusion mutuelle de H1 et H2A.Bbd et H2AL2 dans des cellules somatiques et pendant la spermiogenese.

CHAPTER V: PERSPECTIVES

The development of the approach for deposition of H1 at nearly physiological conditions and the successful use of high resolution EC-M, OH° radical footprinting and coarse-grain DNA mechanics put us in a unique position to study the structural and functional roles of linker histones. In future we will address the following questions:

V.1 How does H1 interact with nucleosomal array with different linker length

A recent theoretical study (582) suggested that linker DNA variation can give rise to different conformations to the fiber structure, which differ both in mechanical (583) and topological (584) properties. The study proposed that the chromatin fiber containing linker histones is a highly polymorph structure, tuned by the NRL (Nucleosome Repeat Length) and suggested different structures of the fiber which can explain the numerous experimental and theoretical models of the 30 nm chromatin fiber: solenoids (188), 2-start helix (185) (32), 3-start helix (585) and 5- start helix (586). This study can be tested experimentally, by applying the same approaches we have used here in the thesis, on the longer nucleosomal arrays with different repeat lengths. We believe there should be changes in the linker DNA protection pattern, hence the stem structure, by changing the NRL. Of particular interest would be the localization of the globular domain in these different NRL–dependent structures. The information in turn can be used to develop the NRL-dependent *in silico* models of the 30nm fiber. Topological (Linking number) variations in the different arrays upon linker histone incorporation can be studied by using appropriate approaches.

V.2 Role of histone H3 N-terminal tail in maintenance of the stem

Core histone tail domains play critical roles in regulating the structure and accessibility of nucleosomal DNA within the chromatin fiber. The N-terminal tail of H3 is of particular interest since it interacts with higher affinity with the linker DNA (540). Keeping this in mind and the fact that deleted H1 mutant 1-127 was able to generate a stem structure; we hypothesize that the N-terminus of H3 could have a role in the stem structure formation and/or stabilization. In order to test such possibility we will replace the full length H3 by tailless H3 (N terminal) in our reconstitutions and carry out the same experiments as these described in the thesis work. If the results prove the involvement of N terminal H3, we will next use a swapped mutant of H3 fused to the N-terminus of H2B. This would shed light on the specificity of "assistance" of the N-terminus of H3 in the formation of the stem structure..

V.3 Role of different positively charged residues of H1 in the binding and stem structure formation

From our studies we support the three binding site model (91) for GH1 binding to the nucleosome. The three binding sites on the globular domain bear mainly positively charged lysine and arginine residues. In addition the last seven aminoacids in the 1-127 H1 deletion mutant, which are necessary for its role in the stem structure formation, is rich in lysine residues (KPKAKKA). The next direction of the study will be to mutate these positively charged residues either singly or in combinations by either neutral or negatively or even different positively charged residues. The results will provide more detailed role of these aminoacids in the binding of GH1 and stem structure formation.

V.4 Yeast histone Hho1p and Xenopus specific B4 histone

Yeast *Saccharomyces cerevisiae* has a linker histone, Hho1p, (70) which contains two globular domains, without N and C terminal tails. It will be interesting to see if Hho1p can bind in the same way as H1 to nucleosomal arrays with 167 bp repeat (the NRL of yeast is 167).

B4 is *Xenopus laevis* oocyte-specific linker histone and like other members of the oocyte-specific family has a relatively high level of acidic amino acids, compared with somatic histones (587). It has 36 aspartic and glutamic acid residues, almost all of which are localized in the extended C-terminal tail. B4 like other linker histones binds the nucleosome *in vitro* and shown to protect internucleosomal linker DNA from digestion by nucleases (588). However B4, unike H1 allows chromatin to be remodeled by ATP dependent chromatin remodeling factors (528) and folds chromatin arrays to a lesser extent, compared to H1 (587). The current studies can be extended to study the mode of B4 interaction with the chromatin array and may suggest its role in chromatin dynamics during the development.

V.5 Structure of H1/NAP1

NAP-1 has been found in complex with histones H2A and H2B *in vivo,* suggesting a role in *de novo* chromatin assembly (589). Yeast NAP-1 binds H2A-H2B and H3-H4 and mediates nucleosome assembly *in vitro* (590, 591). yNAP-1 has been shown to exist as a stable dimer and self-associated oligomers in solution. The crystal structure reveals that yNAP-1 exhibits a fold consisting of a long α-helix that is mainly responsible for dimerization and a β-sheet which is similar to other known histone chaperone proteins (592). No structural

data on higher eukaryotic NAP-1 are available. In contrast to yNAP-1, mouse NAP-1 (and probably human NAP-1, which exhibits highly homologous structure to this of mNAP-1) is a chaperone of linker histones. With this in mind we have began collaboration with Dr. D. Panne (EMBL Outstation, Grenoble) to co-crystallize and solve the structure of mNAP-1-H1 complex.

V.6 Mutual exclusion of H1 and H2A.Bbd and H2AL2 in somatic cells and during spermatogenesis

H2A.Bbd histone variant has been shown colocalized with hyperacetylated chromatin (471) suggesting its role in transcriptional regulation. Linker histones are transcriptional repressor and usually transcribed regions are depleted of them (581, 593). With this in mind we propose to carry out genome-wide out ChIP–on-Chip and ChIP-Seq experiments to test with higher resolution if there is no, as expected, colocalization of these proteins. The same experiments could be carried out with H2AL2 but during spermatogenesis.

BIBLIOGRAPHY

1. van Holde K. 1988.
2. Luger K, Mader AW, Richmond RK, Sargent DF, Richmond TJ. 1997. *Nature* 389: 251-60
3. Davey CA, Sargent DF, Luger K, Maeder AW, Richmond TJ. 2002. *J Mol Biol* 319: 1097-113
4. W F. 1882. *Leipzig* 18
5. Paweletz N. 2001. *Nat Rev Mol Cell Biol* 2: 72-5
6. Miescher F. 1871. *Hoppe-Seyler, med. chem. Unters* 4: 441-60
7. Kossel A. 1911. *Munchener medizinische Wochenschrifte.* 58: 65-9
8. Vries HD. 1904. *Science* 20: 395-401
9. Olins DE, Olins AL. 2003. *Nat Rev Mol Cell Biol* 4: 809-14
10. Avery O.T. MCM, and McCarthy M. 1944. *Journal of Experimental Medicine* 79: 137-59
11. Mazia D. 1941. *Cold Spring Harb. Symp. Quant. Biol.* IX: 40-6
12. Watson JD, Crick FH. 1953. *Cold Spring Harb Symp Quant Biol* 18: 123-31
13. Wilkins MH, Seeds WE, Stokes AR, Wilson HR. 1953. *Nature* 172: 759-62
14. Franklin RE, Gosling RG. 1953. *Nature* 172: 156-7
15. Medawar PB, Zubay G. 1959. *Biochim Biophys Acta* 33: 244-6
16. Johns EW, Butler JA. 1962. *Biochem J* 82: 15-8
17. Johns EW. 1964. *Biochem J* 92: 55-9
18. Johns EW. 1967. *Biochem J* 104: 78-82
19. Everid AC, Small JV, Davies HG. 1970. *J Cell Sci* 7: 35-48
20. Finch JT, Klug A. 1976. *Proc Natl Acad Sci U S A* 73: 1897-901
21. Olins AL, Olins DE. 1974. *Science* 183: 330-2
22. Woodcock CL, Sweetman HE, Frado LL. 1976. *Exp Cell Res* 97: 111-9
23. Kornberg RD, Thomas JO. 1974. *Science* 184: 865-8
24. Oudet P, Gross-Bellard M, Chambon P. 1975. *Cell* 4: 281-300
25. Noll M, Kornberg RD. 1977. *J Mol Biol* 109: 393-404
26. Arents G, Burlingame RW, Wang BC, Love WE, Moudrianakis EN. 1991. *Proc Natl Acad Sci U S A* 88: 10148-52
27. Thomas JO. 1999. *Curr Opin Cell Biol* 11: 312-7
28. Brown DT, Izard T, Misteli T. 2006. *Nat Struct Mol Biol* 13: 250-5
29. Worcel A, Strogatz S, Riley D. 1981. *Proc Natl Acad Sci U S A* 78: 1461-5
30. Staynov DZ, Dunn S, Baldwin JP, Crane-Robinson C. 1983. *FEBS Lett* 157: 311-5
31. Woodcock CL, Frado LL, Rattner JB. 1984. *J Cell Biol* 99: 42-52
32. Williams SP, Athey BD, Muglia LJ, Schappe RS, Gough AH, Langmore JP. 1986. *Biophys J* 49: 233-48
33. Dorigo B, Schalch T, Bystricky K, Richmond TJ. 2003. *J Mol Biol* 327: 85-96
34. Robinson PJ, Fairall L, Huynh VA, Rhodes D. 2006. *Proc Natl Acad Sci U S A* 103: 6506-11
35. Cockell M, Gasser SM. 1999. *Curr Opin Genet Dev* 9: 199-205
36. Hansen JC. 2002. *Annu Rev Biophys Biomol Struct* 31: 361-92
37. E H. 1928. *Jb. Wiss. Bot* 69: 728
38. Williamson R. 1970. *J Mol Biol* 51: 157-68
39. Hewish DR, Burgoyne LA. 1973. *Biochem Biophys Res Commun* 52: 475-81
40. Compton JL, Hancock R, Oudet P, Chambon P. 1976. *Eur J Biochem* 70: 555-68
41. Morris NR. 1976. *Cell* 9: 627-32
42. Noll M. 1976. *Cell* 8: 349-55
43. Spadafora C, Bellard M, Compton JL, Chambon P. 1976. *FEBS Lett* 69: 281-5

44. Thomas JO, Thompson RJ. 1977. *Cell* 10: 633-40
45. Travers AA. 1990. *Cell* 60: 177-80
46. Langst G, Becker PB. 2004. *Biochim Biophys Acta* 1677: 58-63
47. Widom J. 1997. *Curr Biol* 7: R653-5
48. Simpson RT. 1978. *Biochemistry* 17: 5524-31
49. Harp JM, Hanson BL, Timm DE, Bunick GJ. 2000. *Acta Crystallogr D Biol Crystallogr* 56: 1513-34
50. Bentley GA, Lewit-Bentley A, Finch JT, Podjarny AD, Roth M. 1984. *J Mol Biol* 176: 55-75
51. Finch JT, Brown RS, Richmond T, Rushton B, Lutter LC, Klug A. 1981. *J Mol Biol* 145: 757-69
52. Richmond TJ, Finch JT, Rushton B, Rhodes D, Klug A. 1984. *Nature* 311: 532-7
53. Uberbacher EC, Bunick GJ. 1989. *J Biomol Struct Dyn* 7: 1-18
54. Luger K, Mäder AW, Richmond RK, Sargent DF, Richmond TJ. 1997. *Nature* 389: 251-60
55. Xie X, Kokubo T, Cohen SL, Mirza UA, Hoffmann A, et al. 1996. *Nature* 380: 316-22
56. Arents G, Moudrianakis EN. 1995. *Proc Natl Acad Sci U S A* 92: 11170-4
57. Ramakrishnan V. 1995. *Proc Natl Acad Sci U S A* 92: 11328-30
58. Angelov D, Vitolo JM, Mutskov V, Dimitrov S, Hayes JJ. 2001. *Proc Natl Acad Sci U S A* 98: 6599-604
59. Hartman PG, Chapman GE, Moss T, Bradbury EM. 1977. *Eur J Biochem* 77: 45-51
60. Lennox RW, Cohen LH. 1983. *J Biol Chem* 258: 262-8
61. Lennox RW, Cohen LH. 1984. *Dev Biol* 103: 80-4
62. Tanaka M, Hennebold JD, Macfarlane J, Adashi EY. 2001. *Development* 128: 655-64
63. Cole RD. 1987. *Int J Pept Protein Res* 30: 433-49
64. Sirotkin AM, Edelmann W, Cheng G, Klein-Szanto A, Kucherlapati R, Skoultchi AI. 1995. *Proc Natl Acad Sci U S A* 92: 6434-8
65. Lin Q, Sirotkin A, Skoultchi AI. 2000. *Mol Cell Biol* 20: 2122-8
66. Fan Y, Sirotkin A, Russell RG, Ayala J, Skoultchi AI. 2001. *Mol Cell Biol* 21: 7933-43
67. Alami R, Fan Y, Pack S, Sonbuchner TM, Besse A, et al. 2003. *Proc Natl Acad Sci U S A* 100: 5920-5
68. Shen X, Yu L, Weir JW, Gorovsky MA. 1995. *Cell* 82: 47-56
69. Shen X, Gorovsky MA. 1996. *Cell* 86: 475-83
70. Patterton HG, Landel CC, Landsman D, Peterson CL, Simpson RT. 1998. *J Biol Chem* 273: 7268-76
71. Schafer G, McEvoy CR, Patterton HG. 2008. *Proc Natl Acad Sci U S A* 105: 14838-43
72. Gunjan A, Sittman DB, Brown DT. 2001. *J Biol Chem* 276: 3635-40
73. Lee H, Habas R, Abate-Shen C. 2004. *Science* 304: 1675-8
74. Konishi A, Shimizu S, Hirota J, Takao T, Fan Y, et al. 2003. *Cell* 114: 673-88
75. Dimitrov SI, Russanova VR, Pashev IG. 1987. *EMBO J* 6: 2387-92
76. Russanova VR, Dimitrov SI, Makarov VL, Pashev IG. 1987. *Eur J Biochem* 167: 321-6
77. Woodcock CL, Dimitrov S. 2001. *Curr Opin Genet Dev* 11: 130-5
78. Woodcock CL, Skoultchi AI, Fan Y. 2006. *Chromosome Res* 14: 17-25
79. Travers A. 1999. *Trends Biochem Sci* 24: 4-7
80. Wolffe AP, Ura K. 1997. *Methods* 12: 10-9
81. Robinson PJ, Rhodes D. 2006. *Curr Opin Struct Biol* 16: 336-43
82. Allan J, Mitchell T, Harborne N, Bohm L, Crane-Robinson C. 1986. *J Mol Biol* 187: 591-601

83. Allan J, Hartman PG, Crane-Robinson C, Aviles FX. 1980. *Nature* 288: 675-9
84. Zhou YB, Gerchman SE, Ramakrishnan V, Travers A, Muyldermans S. 1998. *Nature* 395: 402-5
85. Hayes JJ, Wolffe AP. 1993. *Proc Natl Acad Sci U S A* 90: 6415-9
86. Staynov DZ, Crane-Robinson C. 1988. *EMBO J* 7: 3685-91
87. An W, Leuba SH, van Holde K, Zlatanova J. 1998. *Proc Natl Acad Sci U S A* 95: 3396-401
88. Travers AA, Muyldermans SV. 1996. *J Mol Biol* 257: 486-91
89. Lennard AC, Thomas JO. 1985. *EMBO J* 4: 3455-62
90. Pruss D, Bartholomew B, Persinger J, Hayes J, Arents G, et al. 1996. *Science* 274: 614-7
91. Fan L, Roberts VA. 2006. *Proc Natl Acad Sci U S A* 103: 8384-9
92. Shintomi K, Iwabuchi M, Saeki H, Ura K, Kishimoto T, Ohsumi K. 2005. *Proc Natl Acad Sci U S A* 102: 8210-5
93. Howe L, Ausio J. 1998. *Mol Cell Biol* 18: 1156-62
94. Subirana JA. 1990. *Biopolymers* 29: 1351-7
95. Lu X, Hansen JC. 2004. *J Biol Chem* 279: 8701-7
96. Khadake JR, Markose ER, Rao MR. 1994. *Indian J Biochem Biophys* 31: 335-8
97. Khadake JR, Rao MR. 1995. *Biochemistry* 34: 15792-801
98. Bradbury EM, Cary PD, Chapman GE, Crane-Robinson C, Danby SE, et al. 1975. *Eur J Biochem* 52: 605-13
99. Clark DJ, Hill CS, Martin SR, Thomas JO. 1988. *EMBO J* 7: 69-75
100. Lee Walters ETK. 1985. *Journal of the American Chemical Society* 107: 6422-4
101. Vila R, Ponte I, Collado M, Arrondo JL, Suau P. 2001. *J Biol Chem* 276: 30898-903
102. Vila R, Ponte I, Jimenez MA, Rico M, Suau P. 2000. *Protein Sci* 9: 627-36
103. Hill CS, Martin SR, Thomas JO. 1989. *EMBO J* 8: 2591-9
104. Bharath MM, Chandra NR, Rao MR. 2002. *Proteins* 49: 71-81
105. Khadake JR, Rao MR. 1997. *Biochemistry* 36: 1041-51
106. Khadake JR, Rao MR. 1997. *FEBS Lett* 400: 193-6
107. Bharath MM, Ramesh S, Chandra NR, Rao MR. 2002. *Biochemistry* 41: 7617-27
108. Mirzabekov AD, San'ko DF, Kolchinsky AM, Melnikova AF. 1977. *Eur J Biochem* 75: 379-89
109. Th'ng JP, Sung R, Ye M, Hendzel MJ. 2005. *J Biol Chem* 280: 27809-14
110. Kimura H, Cook PR. 2001. *J Cell Biol* 153: 1341-53
111. Lever MA, Th'ng JP, Sun X, Hendzel MJ. 2000. *Nature* 408: 873-6
112. Phair RD, Misteli T. 2000. *Nature* 404: 604-9
113. Raghuram N, Carrero G, Th'ng J, Hendzel MJ. 2009. *Biochem Cell Biol* 87: 189-206
114. Bharath MM, Chandra NR, Rao MR. 2003. *Nucleic Acids Res* 31: 4264-74
115. Izzo A, Kamieniarz K, Schneider R. 2008. *Biol Chem* 389: 333-43
116. Parseghian MH, Henschen AH, Krieglstein KG, Hamkalo BA. 1994. *Protein Sci* 3: 575-87
117. Parseghian MH, Hamkalo BA. 2001. *Biochem Cell Biol* 79: 289-304
118. Albig W, Doenecke D. 1997. *Hum Genet* 101: 284-94
119. Seyedin SM, Kistler WS. 1979. *Biochemistry* 18: 1371-5
120. Albig W, Drabent B, Kunz J, Kalff-Suske M, Grzeschik KH, Doenecke D. 1993. *Genomics* 16: 649-54
121. Albig W, Meergans T, Doenecke D. 1997. *Gene* 184: 141-8
122. Wang ZF, Krasikov T, Frey MR, Wang J, Matera AG, Marzluff WF. 1996. *Genome Res* 6: 688-701

123. Wang ZF, Tisovec R, Debry RW, Frey MR, Matera AG, Marzluff WF. 1996. *Genome Res* 6: 702-14
124. Walter L, Klinga-Levan K, Helou K, Albig W, Drabent B, et al. 1996. *Cytogenet Cell Genet* 75: 136-9
125. Pina B, Martinez P, Suau P. 1987. *Eur J Biochem* 164: 71-6
126. Pina B, Suau P. 1987. *FEBS Lett* 210: 161-4
127. Meergans T, Albig W, Doenecke D. 1997. *DNA Cell Biol* 16: 1041-9
128. Parseghian MH, Newcomb RL, Winokur ST, Hamkalo BA. 2000. *Chromosome Res* 8: 405-24
129. Kim K, Choi J, Heo K, Kim H, Levens D, et al. 2008. *J Biol Chem* 283: 9113-26
130. Parseghian MH, Clark RF, Hauser LJ, Dvorkin N, Harris DA, Hamkalo BA. 1993. *Chromosome Res* 1: 127-39
131. Zlatanova J, Doenecke D. 1994. *FASEB J* 8: 1260-8
132. Panyim S, Chalkley R. 1969. *Biochem Biophys Res Commun* 37: 1042-9
133. Gabrielli F, Aden DP, Carrel SC, von Bahr C, Rane A, et al. 1984. *Mol Cell Biochem* 65: 57-66
134. Doenecke D, Tonjes R. 1986. *J Mol Biol* 187: 461-4
135. Happel N, Schulze E, Doenecke D. 2005. *Biol Chem* 386: 541-51
136. Drabent B, Bode C, Bramlage B, Doenecke D. 1996. *Histochem Cell Biol* 106: 247-51
137. Steger K, Klonisch T, Gavenis K, Drabent B, Doenecke D, Bergmann M. 1998. *Mol Hum Reprod* 4: 939-45
138. De Lucia F, Faraone-Mennella MR, D'Erme M, Quesada P, Caiafa P, Farina B. 1994. *Biochem Biophys Res Commun* 198: 32-9
139. Oko RJ, Jando V, Wagner CL, Kistler WS, Hermo LS. 1996. *Biol Reprod* 54: 1141-57
140. Drabent B, Saftig P, Bode C, Doenecke D. 2000. *Histochem Cell Biol* 113: 433-42
141. Fantz DA, Hatfield WR, Horvath G, Kistler MK, Kistler WS. 2001. *Biol Reprod* 64: 425-31
142. Iguchi N, Tanaka H, Yomogida K, Nishimune Y. 2003. *Int J Androl* 26: 354-65
143. Yan W, Ma L, Burns KH, Matzuk MM. 2003. *Proc Natl Acad Sci U S A* 100: 10546-51
144. Wisniewski JR, Zougman A, Kruger S, Mann M. 2007. *Mol Cell Proteomics* 6: 72-87
145. Jenuwein T, Allis CD. 2001. *Science* 293: 1074-80
146. Pham AD, Sauer F. 2000. *Science* 289: 2357-60
147. Jiang T, Zhou X, Taghizadeh K, Dong M, Dedon PC. 2007. *Proc Natl Acad Sci U S A* 104: 60-5
148. Strahl BD, Allis CD. 2000. *Nature* 403: 41-5
149. Guo CY, Mizzen C, Wang Y, Larner JM. 2000. *Cancer Res* 60: 5667-72
150. Talasz H, Helliger W, Sarg B, Debbage PL, Puschendorf B, Lindner H. 2002. *Cell Death Differ* 9: 27-39
151. Horn PJ, Carruthers LM, Logie C, Hill DA, Solomon MJ, et al. 2002. *Nat Struct Biol* 9: 263-7
152. Guo XW, Th'ng JP, Swank RA, Anderson HJ, Tudan C, et al. 1995. *EMBO J* 14: 976-85
153. Ajiro K, Yoda K, Utsumi K, Nishikawa Y. 1996. *J Biol Chem* 271: 13197-201
154. Ohsumi K, Katagiri C, Kishimoto T. 1993. *Science* 262: 2033-5
155. Th'ng JP, Guo XW, Swank RA, Crissman HA, Bradbury EM. 1994. *J Biol Chem* 269: 9568-73
156. Gurley LR, Walters RA, Tobey RA. 1975. *J Biol Chem* 250: 3936-44
157. Yasuda H, Matsumoto Y, Mita S, Marunouchi T, Yamada M. 1981. *Biochemistry* 20: 4414-9

158. Halmer L, Gruss C. 1996. *Nucleic Acids Res* 24: 1420-7
159. Bradbury EM, Inglis RJ, Matthews HR, Sarner N. 1973. *Eur J Biochem* 33: 131-9
160. Bradbury EM, Inglis RJ, Matthews HR. 1974. *Nature* 247: 257-61
161. Hohmann P, Tobey RA, Gurley LR. 1976. *J Biol Chem* 251: 3685-92
162. Gurley LR, D'Anna JA, Barham SS, Deaven LL, Tobey RA. 1978. *Eur J Biochem* 84: 1-15
163. Langan TA, Gautier J, Lohka M, Hollingsworth R, Moreno S, et al. 1989. *Mol Cell Biol* 9: 3860-8
164. Boggs BA, Allis CD, Chinault AC. 2000. *Chromosoma* 108: 485-90
165. Alexandrow MG, Hamlin JL. 2005. *J Cell Biol* 168: 875-86
166. Lu MJ, Mpoke SS, Dadd CA, Allis CD. 1995. *Mol Biol Cell* 6: 1077-87
167. Chadee DN, Taylor WR, Hurta RA, Allis CD, Wright JA, Davie JR. 1995. *J Biol Chem* 270: 20098-105
168. Roque A, Ponte I, Arrondo JL, Suau P. 2008. *Nucleic Acids Res* 36: 4719-26
169. Lever MA, Th'ng JPH, Sun X, Hendzel MJ. 2000. *Nature* 408: 873-6
170. Dou Y, Bowen J, Liu Y, Gorovsky MA. 2002. *J Cell Biol* 158: 1161-70
171. Contreras A, Hale TK, Stenoien DL, Rosen JM, Mancini MA, Herrera RE. 2003. *Mol Cell Biol* 23: 8626-36
172. Green GR, Lee HJ, Poccia DL. 1993. *J Biol Chem* 268: 11247-55
173. Hendzel MJ, Lever MA, Crawford E, Th'ng JP. 2004. *J Biol Chem* 279: 20028-34
174. Goytisolo FA, Gerchman SE, Yu X, Rees C, Graziano V, et al. 1996. *EMBO J* 15: 3421-9
175. Vaquero A, Scher M, Lee D, Erdjument-Bromage H, Tempst P, Reinberg D. 2004. *Mol Cell* 16: 93-105
176. Daujat S, Zeissler U, Waldmann T, Happel N, Schneider R. 2005. *J Biol Chem* 280: 38090-5
177. Kasinsky HE, Lewis JD, Dacks JB, Ausio J. 2001. *FASEB J* 15: 34-42
178. Happel N, Doenecke D. 2009. *Gene* 431: 1-12
179. Thoma F, Koller T. 1977. *Cell* 12: 101-7
180. Thoma F, Koller T, Klug A. 1979. *J Cell Biol* 83: 403-27
181. Bednar J, Horowitz RA, Grigoryev SA, Carruthers LM, Hansen JC, et al. 1998. *Proc Natl Acad Sci U S A* 95: 14173-8
182. Smith MF, Athey BD, Williams SP, Langmore JP. 1990. *J Cell Biol* 110: 245-54
183. Lowary PT, Widom J. 1998. *J Mol Biol* 276: 19-42
184. Huynh VA, Robinson PJ, Rhodes D. 2005. *J Mol Biol* 345: 957-68
185. Dorigo B, Schalch T, Kulangara A, Duda S, Schroeder RR, Richmond TJ. 2004. *Science* 306: 1571-3
186. Wu C, Bassett A, Travers A. 2007. *EMBO Rep* 8: 1129-34
187. Thomas JO, Butler PJ. 1980. *J Mol Biol* 144: 89-93.
188. Widom J, Klug A. 1985. *Cell* 43: 207-13
189. Gerchman SE, Ramakrishnan V. 1987. *Proc Natl Acad Sci U S A* 84: 7802-6
190. Athey BD, Smith MF, Rankert DA, Williams SP, Langmore JP. 1990. *J Cell Biol* 111: 795-806
191. Sun J, Zhang Q, Schlick T. 2005. *Proc Natl Acad Sci U S A* 102: 8180-5
192. Fan JY, Rangasamy D, Luger K, Tremethick DJ. 2004. *Mol Cell* 16: 655-61
193. Shogren-Knaak M, Ishii H, Sun JM, Pazin MJ, Davie JR, Peterson CL. 2006. *Science* 311: 844-7
194. Zhou J, Fan JY, Rangasamy D, Tremethick DJ. 2007. *Nat Struct Mol Biol* 14: 1070-6
195. Montel F, Menoni H, Castelnovo M, Bednar J, Dimitrov S, et al. 2009. *Biophys J* 97: 544-53

196. Maresca TJ, Freedman BS, Heald R. 2005. *J Cell Biol* 169: 859-69
197. Fan Y, Nikitina T, Zhao J, Fleury TJ, Bhattacharyya R, et al. 2005. *Cell* 123: 1199-212
198. Yao J, Lowary PT, Widom J. 1993. *Proc Natl Acad Sci U S A* 90: 9364-8
199. Routh A, Sandin S, Rhodes D. 2008. *Proc Natl Acad Sci U S A* 105: 8872-7
200. McBryant SJ, Adams VH, Hansen JC. 2006. *Chromosome Res* 14: 39-51
201. Tremethick DJ. 2007. *Cell* 128: 651-4
202. Bassett A, Cooper S, Wu C, Travers A. 2009. *Curr Opin Genet Dev* 19: 159-65
203. Paulson JR, Laemmli UK. 1977. *Cell* 12: 817-28
204. Belmont AS, Bruce K. 1994. *J Cell Biol* 127: 287-302
205. Rattner JB, Lin CC. 1985. *Cell* 42: 291-6
206. Frenster JH, Allfrey VG, Mirsky AE. 1963. *Proc Natl Acad Sci U S A* 50: 1026-32
207. Grewal SI, Elgin SC. 2002. *Curr Opin Genet Dev* 12: 178-87
208. Sun FL, Cuaycong MH, Elgin SC. 2001. *Mol Cell Biol* 21: 2867-79
209. Sugiyama T, Cam HP, Sugiyama R, Noma K, Zofall M, et al. 2007. *Cell* 128: 491-504
210. Grewal SI, Elgin SC. 2007. *Nature* 447: 399-406
211. Hovsepian JHFaJA. 44th Annual Meeting of the American Society for Cell Biology, Washington Convention Center, Washington, D.C and-www.euchromatin.com/Frenster08.htm
212. Santos-Rosa H, Schneider R, Bannister AJ, Sherriff J, Bernstein BE, et al. 2002. *Nature* 419: 407-11
213. Bernstein BE, Kamal M, Lindblad-Toh K, Bekiranov S, Bailey DK, et al. 2005. *Cell* 120: 169-81
214. Grunstein M. 1997. *Nature* 389: 349-52
215. Fahrner JA, Baylin SB. 2003. *Genes Dev* 17: 1805-12
216. Fisher AG, Merkenschlager M. 2002. *Curr Opin Genet Dev* 12: 193-7
217. Grewal SI, Moazed D. 2003. *Science* 301: 798-802
218. White SA, Allshire RC. 2004. *Nat Cell Biol* 6: 696-7
219. Filipowicz W. 2005. *Cell* 122: 17-20
220. Taddei A, Maison C, Roche D, Almouzni G. 2001. *Nat Cell Biol* 3: 114-20
221. Mochizuki K, Fine NA, Fujisawa T, Gorovsky MA. 2002. *Cell* 110: 689-99
222. Volpe TA, Kidner C, Hall IM, Teng G, Grewal SI, Martienssen RA. 2002. *Science* 297: 1833-7
223. Craig JM. 2005. *Bioessays* 27: 17-28
224. Swaminathan J, Baxter EM, Corces VG. 2005. *Genes Dev* 19: 65-76
225. Talbert PB, Henikoff S. 2006. *Nat Rev Genet* 7: 793-803
226. Babu A, Verma RS. 1987. *Int Rev Cytol* 108: 1-60
227. Horn PJ, Peterson CL. 2002. *Science* 297: 1824-7
228. Phillips DM. 1963. *Biochem J* 87: 258-63
229. Allfrey VG, Faulkner R, Mirsky AE. 1964. *Proc Natl Acad Sci U S A* 51: 786-94
230. Kouzarides T. 2007. *Cell* 128: 693-705
231. Hyland EM, Cosgrove MS, Molina H, Wang D, Pandey A, et al. 2005. *Mol Cell Biol* 25: 10060-70
232. Latham JA, Dent SY. 2007. *Nat Struct Mol Biol* 14: 1017-24
233. Dhalluin C, Carlson JE, Zeng L, He C, Aggarwal AK, Zhou MM. 1999. *Nature* 399: 491-6
234. Jacobs SA, Khorasanizadeh S. 2002. *Science* 295: 2080-3
235. Min J, Zhang Y, Xu RM. 2003. *Genes Dev* 17: 1823-8
236. Sterner DE, Berger SL. 2000. *Microbiol Mol Biol Rev* 64: 435-59
237. Zhang Y, Reinberg D. 2001. *Genes Dev* 15: 2343-60
238. Nowak SJ, Corces VG. 2004. *Trends Genet* 20: 214-20

239. Shilatifard A. 2006. *Annu Rev Biochem* 75: 243-69
240. Nathan D, Ingvarsdottir K, Sterner DE, Bylebyl GR, Dokmanovic M, et al. 2006. *Genes Dev* 20: 966-76
241. Hassa PO, Haenni SS, Elser M, Hottiger MO. 2006. *Microbiol Mol Biol Rev* 70: 789-829
242. Cuthbert GL, Daujat S, Snowden AW, Erdjument-Bromage H, Hagiwara T, et al. 2004. *Cell* 118: 545-53
243. Wang Y, Wysocka J, Sayegh J, Lee YH, Perlin JR, et al. 2004. *Science* 306: 279-83
244. Nelson CJ, Santos-Rosa H, Kouzarides T. 2006. *Cell* 126: 905-16
245. Fischle W, Wang Y, Allis CD. 2003. *Curr Opin Cell Biol* 15: 172-83
246. Iizuka M, Matsui T, Takisawa H, Smith MM. 2006. *Mol Cell Biol* 26: 1098-108
247. Khorasanizadeh S. 2004. *Cell* 116: 259-72
248. Xu F, Zhang K, Grunstein M. 2005. *Cell* 121: 375-85
249. Kurdistani SK, Grunstein M. 2003. *Nat Rev Mol Cell Biol* 4: 276-84
250. Robyr D, Suka Y, Xenarios I, Kurdistani SK, Wang A, et al. 2002. *Cell* 109: 437-46
251. Wang A, Kurdistani SK, Grunstein M. 2002. *Science* 298: 1412-4
252. Iizuka M, Smith MM. 2003. *Curr Opin Genet Dev* 13: 154-60
253. Gu W, Roeder RG. 1997. *Cell* 90: 595-606
254. Pelletier G, Stefanovsky VY, Faubladier M, Hirschler-Laszkiewicz I, Savard J, et al. 2000. *Mol Cell* 6: 1059-66
255. Kouzarides T. 2002. *Curr Opin Genet Dev* 12: 198-209
256. Murray K. 1964. *Biochemistry* 3: 10-5
257. Shi Y, Lan F, Matson C, Mulligan P, Whetstine JR, et al. 2004. *Cell* 119: 941-53
258. Metzger E, Wissmann M, Yin N, Muller JM, Schneider R, et al. 2005. *Nature* 437: 436-9
259. Tsukada Y, Fang J, Erdjument-Bromage H, Warren ME, Borchers CH, et al. 2006. *Nature* 439: 811-6
260. Beisel C, Imhof A, Greene J, Kremmer E, Sauer F. 2002. *Nature* 419: 857-62
261. Ng HH, Ciccone DN, Morshead KB, Oettinger MA, Struhl K. 2003. *Proc Natl Acad Sci U S A* 100: 1820-5
262. Bannister AJ, Zegerman P, Partridge JF, Miska EA, Thomas JO, et al. 2001. *Nature* 410: 120-4
263. Cao R, Wang L, Wang H, Xia L, Erdjument-Bromage H, et al. 2002. *Science* 298: 1039-43
264. Czermin B, Melfi R, McCabe D, Seitz V, Imhof A, Pirrotta V. 2002. *Cell* 111: 185-96
265. Lachner M, O'Carroll D, Rea S, Mechtler K, Jenuwein T. 2001. *Nature* 410: 116-20
266. Peters AH, Kubicek S, Mechtler K, O'Sullivan RJ, Derijck AA, et al. 2003. *Mol Cell* 12: 1577-89
267. Schotta G, Lachner M, Sarma K, Ebert A, Sengupta R, et al. 2004. *Genes Dev* 18: 1251-62
268. Brehm A, Tufteland KR, Aasland R, Becker PB. 2004. *Bioessays* 26: 133-40
269. Grant PA. 2001. *Genome Biol* 2: REVIEWS0003
270. Cheung P, Allis CD, Sassone-Corsi P. 2000. *Cell* 103: 263-71
271. Goto H, Tomono Y, Ajiro K, Kosako H, Fujita M, et al. 1999. *J Biol Chem* 274: 25543-9
272. Downs JA, Lowndes NF, Jackson SP. 2000. *Nature* 408: 1001-4
273. Rogakou EP, Boon C, Redon C, Bonner WM. 1999. *J Cell Biol* 146: 905-16
274. Hsu JY, Sun ZW, Li X, Reuben M, Tatchell K, et al. 2000. *Cell* 102: 279-91
275. Wang H, Zhai L, Xu J, Joo HY, Jackson S, et al. 2006. *Mol Cell* 22: 383-94

276. Bergink S, Salomons FA, Hoogstraten D, Groothuis TA, de Waard H, et al. 2006. *Genes Dev* 20: 1343-52
277. Wang H, Wang L, Erdjument-Bromage H, Vidal M, Tempst P, et al. 2004. *Nature* 431: 873-8
278. Clapier CR, Cairns BR. 2009. *Annu Rev Biochem* 78: 273-304
279. Eisen JA, Sweder KS, Hanawalt PC. 1995. *Nucleic Acids Res* 23: 2715-23
280. Bao Y, Shen X. 2007. *Cell* 129: 632
281. Cairns BR. 2007. *Nat Struct Mol Biol* 14: 989-96
282. Durr H, Flaus A, Owen-Hughes T, Hopfner KP. 2006. *Nucleic Acids Res* 34: 4160-7
283. Gangaraju VK, Bartholomew B. 2007. *Mutat Res* 618: 3-17
284. Gangaraju VK, Prasad P, Srour A, Kagalwala MN, Bartholomew B. 2009. *Mol Cell* 35: 58-69
285. Mohrmann L, Verrijzer CP. 2005. *Biochim Biophys Acta* 1681: 59-73
286. Cairns BR, Erdjument-Bromage H, Tempst P, Winston F, Kornberg RD. 1998. *Mol Cell* 2: 639-51
287. Lessard J, Wu JI, Ranish JA, Wan M, Winslow MM, et al. 2007. *Neuron* 55: 201-15
288. Narlikar GJ, Fan HY, Kingston RE. 2002. *Cell* 108: 475-87
289. Cairns BR. 2005. *Curr Opin Genet Dev* 15: 185-90
290. Tsukiyama T, Wu C. 1995. *Cell* 83: 1011-20.
291. Tsukiyama T, Daniel C, Tamkun J, Wu C. 1995. *Cell* 83: 1021-6
292. Varga-Weisz PD, Wilm M, Bonte E, Dumas K, Mann M, Becker PB. 1997. *Nature* 388: 598-602.
293. Ito T, Bulger M, Pazin MJ, Kobayashi R, Kadonaga JT. 1997. *Cell* 90: 145-55.
294. Corona DF, Tamkun JW. 2004. *Biochim Biophys Acta* 1677: 113-9
295. Boyer LA, Latek RR, Peterson CL. 2004. *Nat Rev Mol Cell Biol* 5: 158-63
296. Ferreira H, Flaus A, Owen-Hughes T. 2007. *J Mol Biol* 374: 563-79
297. Carey M, Li B, Workman JL. 2006. *Mol Cell* 24: 481-7
298. Hassan AH, Prochasson P, Neely KE, Galasinski SC, Chandy M, et al. 2002. *Cell* 111: 369-79
299. Goldmark JP, Fazzio TG, Estep PW, Church GM, Tsukiyama T. 2000. *Cell* 103: 423-33
300. Deuring R, Fanti L, Armstrong JA, Sarte M, Papoulas O, et al. 2000. *Mol Cell* 5: 355-65
301. Badenhorst P, Voas M, Rebay I, Wu C. 2002. *Genes Dev* 16: 3186-98
302. Delmas V, Stokes DG, Perry RP. 1993. *Proc Natl Acad Sci U S A* 90: 2414-8
303. Woodage T, Basrai MA, Baxevanis AD, Hieter P, Collins FS. 1997. *Proc Natl Acad Sci U S A* 94: 11472-7
304. Eissenberg JC. 2001. *Gene* 275: 19-29
305. Jones DO, Cowell IG, Singh PB. 2000. *Bioessays* 22: 124-37
306. Koonin EV, Zhou S, Lucchesi JC. 1995. *Nucleic Acids Res* 23: 4229-33
307. Denslow SA, Wade PA. 2007. *Oncogene* 26: 5433-8
308. Bao Y, Shen X. 2007. *Mutat Res* 618: 18-29
309. Flanagan JF, Peterson CL. 1999. *Nucleic Acids Res* 27: 2022-8
310. Chai B, Huang J, Cairns BR, Laurent BC. 2005. *Genes Dev* 19: 1656-61
311. Hirschhorn JN, Brown SA, Clark CD, Winston F. 1992. *Genes Dev* 6: 2288-98
312. Sudarsanam P, Iyer VR, Brown PO, Winston F. 2000. *Proc Natl Acad Sci U S A* 97: 3364-9
313. Davie JK, Kane CM. 2000. *Mol Cell Biol* 20: 5960-73
314. Yudkovsky N, Logie C, Hahn S, Peterson CL. 1999. *Genes Dev* 13: 2369-74
315. Cosma MP, Tanaka T, Nasmyth K. 1999. *Cell* 97: 299-311

316. Natarajan K, Jackson BM, Zhou H, Winston F, Hinnebusch AG. 1999. *Mol Cell* 4: 657-64
317. Dimova D, Nackerdien Z, Furgeson S, Eguchi S, Osley MA. 1999. *Mol Cell* 4: 75-83
318. Krebs JE, Fry CJ, Samuels ML, Peterson CL. 2000. *Cell* 102: 587-98
319. Shim EY, Hong SJ, Oum JH, Yanez Y, Zhang Y, Lee SE. 2007. *Mol Cell Biol* 27: 1602-13
320. Neely KE, Hassan AH, Brown CE, Howe L, Workman JL. 2002. *Mol Cell Biol* 22: 1615-25
321. Nagaich AK, Walker DA, Wolford R, Hager GL. 2004. *Mol Cell* 14: 163-74
322. Ng HH, Robert F, Young RA, Struhl K. 2002. *Genes Dev* 16: 806-19
323. Angus-Hill ML, Schlichter A, Roberts D, Erdjument-Bromage H, Tempst P, Cairns BR. 2001. *Mol Cell* 7: 741-51
324. Moreira JM, Holmberg S. 1999. *EMBO J* 18: 2836-44
325. Damelin M, Simon I, Moy TI, Wilson B, Komili S, et al. 2002. *Mol Cell* 9: 563-73
326. Hakimi MA, Bochar DA, Schmiesing JA, Dong Y, Barak OG, et al. 2002. *Nature* 418: 994-8
327. Hsu JM, Huang J, Meluh PB, Laurent BC. 2003. *Mol Cell Biol* 23: 3202-15
328. Huang J, Hsu JM, Laurent BC. 2004. *Mol Cell* 13: 739-50
329. Cao Y, Cairns BR, Kornberg RD, Laurent BC. 1997. *Mol Cell Biol* 17: 3323-34
330. Armstrong JA, Papoulas O, Daubresse G, Sperling AS, Lis JT, et al. 2002. *EMBO J* 21: 5245-54
331. Srinivasan S, Armstrong JA, Deuring R, Dahlsveen IK, McNeill H, Tamkun JW. 2005. *Development* 132: 1623-35
332. Carrera I, Zavadil J, Treisman JE. 2008. *Mol Cell Biol* 28: 5238-50
333. Kwon H, Imbalzano AN, Khavari PA, Kingston RE, Green MR. 1994. *Nature* 370: 477-81
334. Kitagawa H, Fujiki R, Yoshimura K, Mezaki Y, Uematsu Y, et al. 2003. *Cell* 113: 905-17
335. Hsiao PW, Fryer CJ, Trotter KW, Wang W, Archer TK. 2003. *Mol Cell Biol* 23: 6210-20
336. Brown SA, Imbalzano AN, Kingston RE. 1996. *Genes Dev* 10: 1479-90
337. Treand C, du Chene I, Bres V, Kiernan R, Benarous R, et al. 2006. *EMBO J* 25: 1690-9
338. Corey LL, Weirich CS, Benjamin IJ, Kingston RE. 2003. *Genes Dev* 17: 1392-401
339. Zhao K, Wang W, Rando OJ, Xue Y, Swiderek K, et al. 1998. *Cell* 95: 625-36
340. de la Serna IL, Carlson KA, Imbalzano AN. 2001. *Nat Genet* 27: 187-90
341. Wang Z, Zhai W, Richardson JA, Olson EN, Meneses JJ, et al. 2004. *Genes Dev* 18: 3106-16
342. Lickert H, Takeuchi JK, Von Both I, Walls JR, McAuliffe F, et al. 2004. *Nature* 432: 107-12
343. Gresh L, Bourachot B, Reimann A, Guigas B, Fiette L, et al. 2005. *EMBO J* 24: 3313-24
344. Vradii D, Wagner S, Doan DN, Nickerson JA, Montecino M, et al. 2006. *J Cell Physiol* 206: 112-8
345. Huang X, Gao X, Diaz-Trelles R, Ruiz-Lozano P, Wang Z. 2008. *Dev Biol* 319: 258-66
346. Versteege I, Sevenet N, Lange J, Rousseau-Merck MF, Ambros P, et al. 1998. *Nature* 394: 203-6
347. Roberts CW, Galusha SA, McMenamin ME, Fletcher CD, Orkin SH. 2000. *Proc Natl Acad Sci U S A* 97: 13796-800

348. Wong AK, Shanahan F, Chen Y, Lian L, Ha P, et al. 2000. *Cancer Res* 60: 6171-7
349. Hendricks KB, Shanahan F, Lees E. 2004. *Mol Cell Biol* 24: 362-76
350. Kalpana GV, Marmon S, Wang W, Crabtree GR, Goff SP. 1994. *Science* 266: 2002-6
351. Alen C, Kent NA, Jones HS, O'Sullivan J, Aranda A, Proudfoot NJ. 2002. *Mol Cell* 10: 1441-52
352. Moreau JL, Lee M, Mahachi N, Vary J, Mellor J, et al. 2003. *Mol Cell* 11: 1609-20
353. Morillon A, Karabetsou N, O'Sullivan J, Kent N, Proudfoot N, Mellor J. 2003. *Cell* 115: 425-35
354. Vincent JA, Kwong TJ, Tsukiyama T. 2008. *Nat Struct Mol Biol* 15: 477-84
355. Whitehouse I, Rando OJ, Delrow J, Tsukiyama T. 2007. *Nature* 450: 1031-5
356. Fazzio TG, Kooperberg C, Goldmark JP, Neal C, Basom R, et al. 2001. *Mol Cell Biol* 21: 6450-60
357. Corona DF, Siriaco G, Armstrong JA, Snarskaya N, McClymont SA, et al. 2007. *PLoS Biol* 5: e232
358. Corona DF, Clapier CR, Becker PB, Tamkun JW. 2002. *EMBO Rep* 3: 242-7
359. Lusser A, Urwin DL, Kadonaga JT. 2005. *Nat Struct Mol Biol* 12: 160-6
360. Maier VK, Chioda M, Rhodes D, Becker PB. 2008. *EMBO J* 27: 817-26
361. Fyodorov DV, Kadonaga JT. 2002. *Nature* 418: 897-900
362. Ito T, Levenstein ME, Fyodorov DV, Kutach AK, Kobayashi R, Kadonaga JT. 1999. *Genes Dev* 13: 1529-39
363. Collins N, Poot RA, Kukimoto I, Garcia-Jimenez C, Dellaire G, Varga-Weisz PD. 2002. *Nat Genet* 32: 627-32
364. Poot RA, Bozhenok L, van den Berg DL, Steffensen S, Ferreira F, et al. 2004. *Nat Cell Biol* 6: 1236-44
365. Kwon SY, Xiao H, Glover BP, Tjian R, Wu C, Badenhorst P. 2008. *Dev Biol* 316: 538-47
366. Hochheimer A, Zhou S, Zheng S, Holmes MC, Tjian R. 2002. *Nature* 420: 439-45
367. Isogai Y, Keles S, Prestel M, Hochheimer A, Tjian R. 2007. *Genes Dev* 21: 2936-49
368. Hanai K, Furuhashi H, Yamamoto T, Akasaka K, Hirose S. 2008. *PLoS Genet* 4: e1000011
369. Bozhenok L, Wade PA, Varga-Weisz P. 2002. *EMBO J* 21: 2231-41
370. Percipalle P, Fomproix N, Cavellan E, Voit R, Reimer G, et al. 2006. *EMBO Rep* 7: 525-30
371. Li J, Santoro R, Koberna K, Grummt I. 2005. *EMBO J* 24: 120-7
372. Strohner R, Nemeth A, Nightingale KP, Grummt I, Becker PB, Langst G. 2004. *Mol Cell Biol* 24: 1791-8
373. Li J, Langst G, Grummt I. 2006. *EMBO J* 25: 5735-41
374. Strohner R, Nemeth A, Jansa P, Hofmann-Rohrer U, Santoro R, et al. 2001. *EMBO J* 20: 4892-900
375. Konev AY, Tribus M, Park SY, Podhraski V, Lim CY, et al. 2007. *Science* 317: 1087-90
376. Walfridsson J, Khorosjutina O, Matikainen P, Gustafsson CM, Ekwall K. 2007. *EMBO J* 26: 2868-79
377. Simic R, Lindstrom DL, Tran HG, Roinick KL, Costa PJ, et al. 2003. *EMBO J* 22: 1846-56
378. Marfella CG, Ohkawa Y, Coles AH, Garlick DS, Jones SN, Imbalzano AN. 2006. *J Cell Physiol* 209: 162-71
379. Ogas J, Kaufmann S, Henderson J, Somerville C. 1999. *Proc Natl Acad Sci U S A* 96: 13839-44

380. Murawska M, Kunert N, van Vugt J, Langst G, Kremmer E, et al. 2008. *Mol Cell Biol* 28: 2745-57
381. Linder B, Mentele E, Mansperger K, Straub T, Kremmer E, Rupp RA. 2007. *Genes Dev* 21: 973-83
382. Bagchi A, Papazoglu C, Wu Y, Capurso D, Brodt M, et al. 2007. *Cell* 128: 459-75
383. Ishihara K, Oshimura M, Nakao M. 2006. *Mol Cell* 23: 733-42
384. Thompson BA, Tremblay V, Lin G, Bochar DA. 2008. *Mol Cell Biol* 28: 3894-904
385. Wade PA, Gegonne A, Jones PL, Ballestar E, Aubry F, Wolffe AP. 1999. *Nat Genet* 23: 62-6
386. Unhavaithaya Y, Shin TH, Miliaras N, Lee J, Oyama T, Mello CC. 2002. *Cell* 111: 991-1002
387. von Zelewsky T, Palladino F, Brunschwig K, Tobler H, Hajnal A, Muller F. 2000. *Development* 127: 5277-84
388. Fujita N, Jaye DL, Geigerman C, Akyildiz A, Mooney MR, et al. 2004. *Cell* 119: 75-86
389. Kaji K, Caballero IM, MacLeod R, Nichols J, Wilson VA, Hendrich B. 2006. *Nat Cell Biol* 8: 285-92
390. Yoshida T, Hazan I, Zhang J, Ng SY, Naito T, et al. 2008. *Genes Dev* 22: 1174-89
391. Papamichos-Chronakis M, Krebs JE, Peterson CL. 2006. *Genes Dev* 20: 2437-49
392. van Attikum H, Fritsch O, Gasser SM. 2007. *EMBO J* 26: 4113-25
393. Mizuguchi G, Shen X, Landry J, Wu WH, Sen S, Wu C. 2004. *Science* 303: 343-8
394. Krogan NJ, Keogh MC, Datta N, Sawa C, Ryan OW, et al. 2003. *Mol Cell* 12: 1565-76
395. Kobor MS, Venkatasubrahmanyam S, Meneghini MD, Gin JW, Jennings JL, et al. 2004. *PLoS Biol* 2: E131
396. Choi K, Park C, Lee J, Oh M, Noh B, Lee I. 2007. *Development* 134: 1931-41
397. Deal RB, Topp CN, McKinney EC, Meagher RB. 2007. *Plant Cell* 19: 74-83
398. Shimada K, Oma Y, Schleker T, Kugou K, Ohta K, et al. 2008. *Curr Biol* 18: 566-75
399. Papamichos-Chronakis M, Peterson CL. 2008. *Nat Struct Mol Biol* 15: 338-45
400. Morrison AJ, Highland J, Krogan NJ, Arbel-Eden A, Greenblatt JF, et al. 2004. *Cell* 119: 767-75
401. van Attikum H, Fritsch O, Hohn B, Gasser SM. 2004. *Cell* 119: 777-88
402. Wu S, Shi Y, Mulligan P, Gay F, Landry J, et al. 2007. *Nat Struct Mol Biol* 14: 1165-72
403. Huang J, Laurent BC. 2004. *Cell Cycle* 3: 973-5
404. Cai Y, Jin J, Yao T, Gottschalk AJ, Swanson SK, et al. 2007. *Nat Struct Mol Biol* 14: 872-4
405. Jonsson ZO, Jha S, Wohlschlegel JA, Dutta A. 2004. *Mol Cell* 16: 465-77
406. Fritsch O, Benvenuto G, Bowler C, Molinier J, Hohn B. 2004. *Mol Cell* 16: 479-85
407. Osley MA, Tsukuda T, Nickoloff JA. 2007. *Mutat Res* 618: 65-80
408. Clapier CR, Langst G, Corona DF, Becker PB, Nightingale KP. 2001. *Mol Cell Biol* 21: 875-83
409. Corona DF, Langst G, Clapier CR, Bonte EJ, Ferrari S, et al. 1999. *Mol Cell* 3: 239-45
410. van Holde K, Yager T. 2003. *Biochem Cell Biol* 81: 169-72
411. Edayathumangalam RS, Weyermann P, Dervan PB, Gottesfeld JM, Luger K. 2005. *J Mol Biol* 345: 103-14
412. Langst G, Becker PB. 2001. *Mol Cell* 8: 1085-92
413. Lorch Y, Davis B, Kornberg RD. 2005. *Proc Natl Acad Sci U S A* 102: 1329-32
414. Strohner R, Wachsmuth M, Dachauer K, Mazurkiewicz J, Hochstatter J, et al. 2005. *Nat Struct Mol Biol* 12: 683-90

415. Aoyagi S, Hayes JJ. 2002. *Mol Cell Biol* 22: 7484-90
416. Aoyagi S, Wade PA, Hayes JJ. 2003. *J Biol Chem* 278: 30562-8
417. Saha A, Wittmeyer J, Cairns BR. 2006. *Nat Rev Mol Cell Biol* 7: 437-47
418. Zofall M, Persinger J, Kassabov SR, Bartholomew B. 2006. *Nat Struct Mol Biol* 13: 339-46
419. Fitzgerald DJ, DeLuca C, Berger I, Gaillard H, Sigrist R, et al. 2004. *EMBO J* 23: 3836-43
420. Saha A, Wittmeyer J, Cairns BR. 2002. *Genes Dev* 16: 2120-34
421. Boulard M, Bouvet P, Kundu TK, Dimitrov S. 2007. *Subcell Biochem* 41: 71-89
422. Tsanev R, Russev G, Pashev I, Zlatanova J. 1993. *CRC Press, Boca Raton, FI*
423. Ahmad K, Henikoff S. 2002. *Cell* 111: 281-4
424. Henikoff S, Furuyama T, Ahmad K. 2004. *Trends Genet* 20: 320-6
425. Ausio J, Abbott DW. 2002. *Biochemistry* 41: 5945-9
426. Kamakaka RT, Biggins S. 2005. *Genes Dev* 19: 295-310
427. Sarma K, Reinberg D. 2005. *Nat Rev Mol Cell Biol* 6: 139-49
428. Smith MM. 2002. *Curr Opin Cell Biol* 14: 279-85
429. Moss SB, Challoner PB, Groudine M. 1989. *Dev Biol* 133: 83-92
430. Malik HS, Henikoff S. 2003. *Nat Struct Biol* 10: 882-91
431. Redon C, Pilch D, Rogakou E, Sedelnikova O, Newrock K, Bonner W. 2002. *Curr Opin Genet Dev* 12: 162-9
432. Fernandez-Capetillo O, Lee A, Nussenzweig M, Nussenzweig A. 2004. *DNA Repair (Amst)* 3: 959-67
433. Clarkson MJ, Wells JR, Gibson F, Saint R, Tremethick DJ. 1999. *Nature* 399: 694-7
434. Dhillon N, Kamakaka RT. 2000. *Mol. Cell* 6: 769-80
435. Faast R, Thonglairoam V, Schulz TC, Beall J, Wells JR, et al. 2001. *Curr Biol* 11: 1183-7
436. Santisteban MS, Kalashnikova T, Smith MM. 2000. *Cell* 103: 411-22
437. Abbott DW, Ivanova VS, Wang X, Bonner WM, Ausio J. 2001. *J Biol Chem* 276: 41945-9.
438. Rangasamy D, Greaves I, Tremethick DJ. 2004. *Nat Struct Mol Biol* 11: 650-5
439. Greaves IK, Rangasamy D, Devoy M, Marshall Graves JA, Tremethick DJ. 2006. *Mol Cell Biol* 26: 5394-405
440. Rangasamy D, Berven L, Ridgway P, Tremethick DJ. 2003. *EMBO J* 22: 1599-607
441. Adams RR, Carmena M, Earnshaw WC. 2001. *Trends Cell Biol* 11: 49-54
442. Meneghini MD, Wu M, Madhani HD. 2003. *Cell* 112: 725-36
443. Guillemette B, Bataille AR, Gevry N, Adam M, Blanchette M, et al. 2005. *PLoS Biol* 3: e384
444. Li B, Pattenden SG, Lee D, Gutierrez J, Chen J, et al. 2005. *Proc Natl Acad Sci U S A* 102: 18385-90
445. Raisner RM, Hartley PD, Meneghini MD, Bao MZ, Liu CL, et al. 2005. *Cell* 123: 233-48
446. Zhang R, Poustovoitov MV, Ye X, Santos HA, Chen W, et al. 2005. *Dev Cell* 8: 19-30
447. Zhang H, Roberts DN, Cairns BR. 2005. *Cell* 123: 219-31
448. Siino JS, Nazarov IB, Svetlova MP, Solovjeva LV, Adamson RH, et al. 2002. *Biochem Biophys Res Commun* 297: 1318-23
449. Rogakou EP, Pilch DR, Orr AH, Ivanova VS, Bonner WM. 1998. *J Biol Chem* 273: 5858-68
450. Stiff T, Shtivelman E, Jeggo P, Kysela B. 2004. *DNA Repair (Amst)* 3: 245-56
451. Downs JA, Allard S, Jobin-Robitaille O, Javaheri A, Auger A, et al. 2004. *Mol Cell* 16: 979-90

452. Fernandez-Capetillo O, Mahadevaiah SK, Celeste A, Romanienko PJ, Camerini-Otero RD, et al. 2003. *Dev Cell* 4: 497-508
453. Pehrson JR, Fried VA. 1992. *Science* 257: 1398-400
454. Allen MD, Buckle AM, Cordell SC, Lowe J, Bycroft M. 2003. *J Mol Biol* 330: 503-11
455. Chadwick BP, Willard HF. 2001. *Hum Mol Genet* 10: 1101-13
456. Costanzi C, Pehrson JR. 2001. *J. Biol. Chem.* 276: 21776-84
457. Pehrson J, Fuji RN. 1998. *Nucl. Acids Res.* 26: 2837-42
458. Costanzi C, Pehrson JR. 1998. *Nature* 393: 599-601
459. Rasmussen TP, Mastrangelo MA, Eden A, Pehrson JR, Jaenisch R. 2000. *J Cell Biol* 150: 1189-98
460. Chadwick BP, Willard HF. 2002. *J Cell Biol* 157: 1113-23
461. Grigoryev SA, Nikitina T, Pehrson JR, Singh PB, Woodcock CL. 2004. *J Cell Sci* 117: 6153-62
462. Agelopoulos M, Thanos D. 2006. *EMBO J* 25: 4843-53
463. Costanzi C, Stein P, Worrad DM, Schultz RM, Pehrson JR. 2000. *Development* 127: 2283-9
464. Perche P, Vourch C, Souchier C, Robert-Nicoud M, Dimitrov S, Khochbin C. 2000. *Curr. Biol.* 10: 1531-4
465. Rasmussen TP, Huang T, Mastrangelo MA, Loring J, Panning B, Jaenisch R. 1999. *Nucleic Acids Res* 27: 3685-9
466. Mietton F, Sengupta AK, Molla A, Picchi G, Barral S, et al. 2009. *Mol Cell Biol* 29: 150-6
467. Ouararhni K, Hadj-Slimane R, Ait-Si-Ali S, Robin P, Mietton F, et al. 2006. *Genes Dev* 20: 3324-36
468. Karras GI, Kustatscher G, Buhecha HR, Allen MD, Pugieux C, et al. 2005. *EMBO J* 24: 1911-20
469. Angelov D, Molla A, Perche P-Y, Hans F, Côté J, et al. 2003. *Mol. Cell* 11: 1033-41
470. Doyen CM, An W, Angelov D, Bondarenko V, Mietton F, et al. 2006. *Mol Cell Biol* 26: 1156-64
471. Chadwick BP, Willard HF. 2001. *J. Cell. Biol.* 152: 375-84
472. Eirin-Lopez JM, Ishibashi T, Ausio J. 2008. *Faseb J* 22: 316-26
473. Bao Y, Konesky K, Park YJ, Rosu S, Dyer PN, et al. 2004. *EMBO J* 23: 3314-24
474. Angelov D, Verdel A, An W, Bondarenko V, Hans F, et al. 2004. *EMBO J* 23: 3815-24
475. Gautier T, Abbott DW, Molla A, Verdel A, Ausio J, Dimitrov S. 2004. *EMBO Rep* 5: 715-20
476. Okuwaki M, Kato K, Shimahara H, Tate S, Nagata K. 2005. *Mol Cell Biol* 25: 10639-51
477. Angelov D, Bondarenko VA, Almagro S, Menoni H, Mongelard F, et al. 2006. *EMBO J* 25: 1669-79
478. Doyen CM, Montel F, Gautier T, Menoni H, Claudet C, et al. 2006. *EMBO J* 25: 4234-44
479. Menoni H, Gasparutto D, Hamiche A, Cadet J, Dimitrov S, et al. 2007. *Mol Cell Biol* 27: 5949-56
480. Rao BJ, Brahmachari SK, Rao MR. 1983. *J Biol Chem* 258: 13478-85
481. Trostle-Weige PK, Meistrich ML, Brock WA, Nishioka K, Bremer JW. 1982. *J Biol Chem* 257: 5560-7
482. Caron C, Govin J, Rousseaux S, Khochbin S. 2005. *Prog Mol Subcell Biol* 38: 65-89
483. Govin J, Escoffier E, Rousseaux S, Kuhn L, Ferro M, et al. 2007. *J Cell Biol* 176: 283-94

484. Wu F, Caron C, De Robertis C, Khochbin S, Rousseaux S. 2008. *J Reprod Dev* 54: 413-7
485. Hwang I, Chae CB. 1989. *Mol Cell Biol* 9: 1005-13
486. Churikov D, Zalenskaya IA, Zalensky AO. 2004. *Cytogenet Genome Res* 105: 203-14
487. Gineitis AA, Zalenskaya IA, Yau PM, Bradbury EM, Zalensky AO. 2000. *J Cell Biol* 151: 1591-8
488. Li A, Maffey AH, Abbott WD, Conde e Silva N, Prunell A, et al. 2005. *Biochemistry* 44: 2529-35
489. Tanphaichitr N, Sobhon P, Taluppeth N, Chalermisarachai P. 1978. *Exp Cell Res* 117: 347-56
490. van Roijen HJ, Ooms MP, Spaargaren MC, Baarends WM, Weber RF, et al. 1998. *Hum Reprod* 13: 1559-66
491. Wattanaseree J, Svasti J. 1983. *Arch Biochem Biophys* 225: 892-7
492. Zalensky AO, Siino JS, Gineitis AA, Zalenskaya IA, Tomilin NV, et al. 2002. *J Biol Chem* 277: 43474-80
493. Choi YC, Gu W, Hecht NB, Feinberg AP, Chae CB. 1996. *DNA Cell Biol* 15: 495-504
494. Churikov D, Siino J, Svetlova M, Zhang K, Gineitis A, et al. 2004. *Genomics* 84: 745-56
495. Boulard M, Gautier T, Mbele GO, Gerson V, Hamiche A, et al. 2006. *Mol Cell Biol* 26: 1518-26
496. Loyola A, Almouzni G. 2007. *Trends Biochem Sci* 32: 425-33
497. Govin J, Caron C, Rousseaux S, Khochbin S. 2005. *Trends Biochem Sci* 30: 357-9
498. Howman EV, Fowler KJ, Newson AJ, Redward S, MacDonald AC, et al. 2000. *Proc Natl Acad Sci U S A* 97: 1148-53
499. Palmer DK, O'Day K, Margolis RL. 1989. *Prog Clin Biol Res* 318: 61-72
500. Palmer DK, O'Day K, Margolis RL. 1990. *Chromosoma* 100: 32-6
501. Yoda K, Ando S, Morishita S, Houmura K, Hashimoto K, et al. 2000. *Proc Natl Acad Sci U S A* 97: 7266-71
502. Van Hooser AA, Ouspenski, II, Gregson HC, Starr DA, Yen TJ, et al. 2001. *J Cell Sci* 114: 3529-42
503. Blower MD, Karpen GH. 2001. *Nat Cell Biol* 3: 730-9
504. Sullivan KF, Hechenberger M, Masri K. 1994. *J Cell Biol* 127: 581-92
505. Shelby RD, Vafa O, Sullivan KF. 1997. *J Cell Biol* 136: 501-13
506. Keith KC, Baker RE, Chen Y, Harris K, Stoler S, Fitzgerald-Hayes M. 1999. *Mol Cell Biol* 19: 6130-9
507. Furuyama T, Dalal Y, Henikoff S. 2006. *Proc Natl Acad Sci U S A* 103: 6172-7
508. Okada M, Cheeseman IM, Hori T, Okawa K, McLeod IX, et al. 2006. *Nat Cell Biol* 8: 446-57
509. Foltz DR, Jansen LE, Black BE, Bailey AO, Yates JR, 3rd, Cleveland DW. 2006. *Nat Cell Biol* 8: 458-69
510. Dalal Y, Wang H, Lindsay S, Henikoff S. 2007. *PLoS Biol* 5: e218
511. Frank D, Doenecke D, Albig W. 2003. *Gene* 312: 135-43
512. Wu RS, Tsai S, Bonner WM. 1982. *Cell* 31: 367-74
513. Ahmad K, Henikoff S. 2002. *Mol Cell* 9: 1191-200.
514. Bosch A, Suau P. 1995. *Eur J Cell Biol* 68: 220-5
515. Shahbazian M, Young J, Yuva-Paylor L, Spencer C, Antalffy B, et al. 2002. *Neuron* 35: 243-54
516. Jin C, Felsenfeld G. 2007. *Genes Dev* 21: 1519-29
517. Hake SB, Garcia BA, Kauer M, Baker SP, Shabanowitz J, et al. 2005. *Proc Natl Acad Sci U S A* 102: 6344-9

518. Mito Y, Henikoff JG, Henikoff S. 2005. *Nat Genet* 37: 1090-7
519. Jin C, Zang C, Wei G, Cui K, Peng W, et al. 2009. *Nat Genet* 41: 941-5
520. Tagami H, Ray-Gallet D, Almouzni G, Nakatani Y. 2004. *Cell* 116: 51-61
521. Hamiche A, Schultz P, Ramakrishnan V, Oudet P, Prunell A. 1996. *J Mol Biol* 257: 30-42
522. Woodcock CL, Dimitrov S. 2001. *Curr Opin Genet Dev* 11: 130-5.
523. Wolffe AP, Khochbin S, Dimitrov S. 1997. *Bioessays* 19: 249-55
524. Zlatanova J, Seebart C, Tomschik M. 2008. *Trends Biochem Sci* 33: 247-53
525. de la Barre AE, Angelov D, Molla A, Dimitrov S. 2001. *EMBO J* 20: 6383-93.
526. Smirnov IV, Dimitrov SI, Makarov VL. 1988. *J Biomol Struct Dyn* 5: 1149-61
527. Scrittori L, Hans F, Angelov D, Charra M, Prigent C, Dimitrov S. 2001. *J Biol Chem* 276: 30002-10.
528. Saeki H, Ohsumi K, Aihara H, Ito T, Hirose S, et al. 2005. *Proc Natl Acad Sci U S A* 102: 5697-702
529. Luger K, Rechsteiner TJ, Richmond TJ. 1999. *Methods Mol. Biol.* 119: 1-16
530. Mutskov V, Gerber D, Angelov D, Ausio J, Workman J, Dimitrov S. 1998. *Mol. Cell. Biol.* 18: 6293-304
531. Angelov D, Molla A, Perche PY, Hans F, Cote J, et al. 2003. *Mol Cell* 11: 1033-41
532. Pettersen EF, Goddard TD, Huang CC, Couch GS, Greenblatt DM, et al. 2004. *J Comput Chem* 25: 1605-12
533. Balasubramanian B, Pogozelski WK, Tullius TD. 1998. *Proc Natl Acad Sci U S A* 95: 9738-43
534. Sanner MF, Olson AJ, Spehner JC. 1996. *Biopolymers* 38: 305-20
535. Cerf C, Lippens G, Ramakrishnan V, Muyldermans S, Segers A, et al. 1994. *Biochemistry* 33: 11079-86
536. Becker NB, Everaers R. 2007. *Phys Rev E Stat Nonlin Soft Matter Phys* 76: 021923
537. Becker NB, Wolff L, Everaers R. 2006. *Nucleic Acids Res* 34: 5638-49
538. Bednar J, Woodcock CL. 1999. *Methods Enzymol* 304: 191-213
539. Stefanovsky V, Dimitrov SI, Russanova VR, Angelov D, Pashev IG. 1989. *Nucleic Acids Res* 17: 10069-81.
540. Angelov D, Vitolo JM, Mutskov V, Dimitrov S, Hayes JJ. 2001. *Proc Natl Acad Sci U S A* 98: 6599-604.
541. Steger DJ, Eberharter A, John S, Grant PA, Workman JL. 1998. *Proc Natl Acad Sci U S A* 95: 12924-9.
542. Mathematica. 2005. *Wolfram Research, Inc. Mathematica. Champaign, Illinois, 2005. Version*
7
543. Lu XJ, Olson WK. 2003. *Nucleic Acids Res* 31: 5108-21
544. Ramakrishnan V, Finch JT, Graziano V, Lee PL, Sweet RM. 1993. *Nature* 362: 219-23
545. Ou-Yang. 1998. *Physical Review E* 58: 4816–9
546. Pastor N, Weinstein H, Jamison E, Brenowitz M. 2000. *J Mol Biol* 304: 55-68
547. Strahs D, Barash D, Qian X, Schlick T. 2003. *Biopolymers* 69: 216-43
548. Lee B, Richards FM. 1971. *J Mol Biol* 55: 379-400
549. Tsai J, Taylor R, Chothia C, Gerstein M. 1999. *J Mol Biol* 290: 253-66
550. Calladine CR, Drew HR. 1984. *J Mol Biol* 178: 773-82
551. Robinson PJ, An W, Routh A, Martino F, Chapman L, et al. 2008. *J Mol Biol* 381: 816-25
552. Smirnov IV, Dimitrov SI, Makarov VL. 1988. *J Biomol Struct Dyn* 5: 1127-34
553. Ausio J, Dong F, van Holde KE. 1989. *J Mol Biol* 206: 451-63

554. Gordon F, Luger K, Hansen JC. 2005. *J Biol Chem* 280: 33701-6
555. Wang GG, Allis CD, Chi P. 2007. *Trends Mol Med* 13: 363-72
556. Ausio J, van Holde KE. 1986. *Biochemistry* 25: 1421-8
557. Garcia-Ramirez M, Rocchini C, Ausio J. 1995. *J Biol Chem* 270: 17923-8
558. Côté J, Peterson CL, Workman JL. 1998. *Proc. Natl. Acad. Sci. USA* 95: 4947-52
559. Lorch Y, Zhang M, Kornberg RD. 1999. *Cell* 96: 389-92.
560. Wu C, Travers A. 2004. *Nucleic Acids Res* 32: e122
561. Li B, Howe L, Anderson S, Yates JR, 3rd, Workman JL. 2003. *J Biol Chem* 278: 8897-903
562. Hayes JJ, Lee KM. 1997. *Methods* 12: 2-9
563. Montel F, Fontaine E, St-Jean P, Castelnovo M, Faivre-Moskalenko C. 2007. *Biophys J* 93: 566-78
564. Dubochet J, Adrian M, Chang JJ, Homo JC, Lepault J, et al. 1988. *Q Rev Biophys* 21: 129-228
565. Gonzalez-Romero R, Mendez J, Ausio J, Eirin-Lopez JM. 2008. *Gene* 413: 1-7
566. Claudet C, Angelov D, Bouvet P, Dimitrov S, Bednar J. 2005. *J Biol Chem* 280: 19958-65
567. Bednar J, Horowitz RA, Dubochet J, Woodcock CL. 1995. *J Cell Biol* 131: 1365-76
568. Chaban Y, Ezeokonkwo C, Chung WH, Zhang F, Kornberg RD, et al. 2008. *Nat Struct Mol Biol* 15: 1272-7
569. Leschziner AE, Saha A, Wittmeyer J, Zhang Y, Bustamante C, et al. 2007. *Proc Natl Acad Sci U S A* 104: 4913-8
570. Smith CL, Horowitz-Scherer R, Flanagan JF, Woodcock CL, Peterson CL. 2003. *Nat Struct Biol* 10: 141-5
571. Richmond TJ, Davey CA. 2003. *Nature* 423: 145-50
572. Kornberg RD, Lorch Y. 1999. *Cell* 98: 285-94
573. Felsenfeld G, Groudine M. 2003. *Nature* 421: 448-53
574. Felsenfeld G. 1996. *Cell* 86: 13-9
575. Cary PD, Hines ML, Bradbury EM, Smith BJ, Johns EW. 1981. *Eur J Biochem* 120: 371-7
576. Vogel T, Singer MF. 1975. *Proc Natl Acad Sci U S A* 72: 2597-600
577. Vogel T, Singer MF. 1976. *J Biol Chem* 251: 2334-8
578. Singer DS, Singer MF. 1976. *Nucleic Acids Res* 3: 2531-47
579. Krylov D, Leuba S, van Holde K, Zlatanova J. 1993. *Proc Natl Acad Sci U S A* 90: 5052-6
580. Varga-Weisz P, Zlatanova J, Leuba SH, Schroth GP, van Holde K. 1994. *Proc Natl Acad Sci U S A* 91: 3525-9
581. Crane-Robinson C. 1999. *Bioessays* 21: 367-71
582. Wong H, Victor JM, Mozziconacci J. 2007. *PLoS One* 2: e877
583. Ben-Haim E, Lesne A, Victor JM. 2001. *Phys Rev E Stat Nonlin Soft Matter Phys* 64: 051921
584. Barbi M, Mozziconacci J, Victor JM. 2005. *Phys Rev E Stat Nonlin Soft Matter Phys* 71: 031910
585. Makarov V, Dimitrov S, Smirnov V, Pashev I. 1985. *FEBS Lett* 181: 357-61
586. Daban JR, Bermudez A. 1998. *Biochemistry* 37: 4299-304
587. Godde JS, Ura K. 2009. *Int J Dev Biol* 53: 215-24
588. Ura K, Nightingale K, Wolffe AP. 1996. *EMBO J* 15: 4959-69
589. Chang L, Loranger SS, Mizzen C, Ernst SG, Allis CD, Annunziato AT. 1997. *Biochemistry* 36: 469-80
590. Ishimi Y, Yasuda H, Hirosumi J, Hanaoka F, Yamada M. 1983. *J Biochem* 94: 735-44

591. McBryant SJ, Park YJ, Abernathy SM, Laybourn PJ, Nyborg JK, Luger K. 2003. *J Biol Chem* 278: 44574-83
592. Park YJ, Luger K. 2006. *Proc Natl Acad Sci U S A* 103: 1248-53
593. Laybourn PJ, Kadonaga JT. 1991. *Science* 254: 238-45